MOLECULAR GENETIC DISSECTION OF BUNDLE SHEATH SUBERIZATION IN *ZEA MAYS* AND *SETARIA VIRIDIS*, TWO MODEL NADP-ME C_4 GRASSES

A Dissertation
Presented to the Faculty of the Graduate School
of Cornell University
in Partial Fulfillment of the Requirements for the Degree of
Doctor of Philosophy

by
Rachel Anne Mertz
May 2016

MOLECULAR GENETIC DISSECTION OF BUNDLE SHEATH SUBERIZATION IN *ZEA MAYS* AND *SETARIA VIRIDIS*, TWO MODEL NADP-ME C_4 GRASSES

Rachel Anne Mertz, Ph.D.

Cornell University 2016

C_4 grasses often outperform C_3 species under hot, arid conditions due to superior water and nitrogen use efficiencies and lower rates of photorespiration. A method of concentrating CO_2 around the site of carbon fixation in the bundle sheath (BS) is required to realize these gains. In NADP-malic enzyme (NADP-ME)-type C_4 grasses such as maize (*Zea mays*), suberin deposition in the BS cell wall is hypothesized to act as a diffusion barrier to CO_2 escape and O_2 entry from surrounding mesophyll cells. Suberin is a heteropolyester comprised of acyl-lipid-derived aliphatic and phenylpropanoid-derived aromatic components. Suberin is synthesized by a large network of biosynthetic and regulatory genes, none of which have been characterized in C_4 grasses to date.

A set of candidate genes expressed concurrently with BS suberization were identified in maize, rice (*Oryza sativa*), and *Setaria viridis* and a putative biosynthetic pathway was assembled based on functional characterizations from model dicots. To disrupt aromatic suberin synthesis, two paralogously duplicated maize homologues of Arabidopsis *ALIPHATIC SUBERIN FERULOYL TRANSFERASE*, Zm*Asft1* and Zm*Asft2*, were mutated using tightly linked *Dissociation* transposons. Loss-of-function double mutants exhibited a significant reduction in suberin-specific aliphatic monomers in both leaves and roots without a stoichiometric decrease in aromatic monomers. There was no

evidence that increased esterification to arabinoxylan, the major polymer sink for ferulic acid in maize leaves, masked the aromatic defect. Reduced staining of osmiophilic material and attenuated cohesion between the BS suberin lamellae and polysaccharides were observed by TEM, indirectly implicating aromatic monomers in the ultrastructural defect. Cell wall elasticity, transpiration, and stomatal conductance significantly increased without pleiotropic changes in cuticular permeability, suggesting that the mutation facilitated water movement through the BS apoplast. However, there were no morphological phenotypes under ambient conditions. Likewise, net CO_2 assimilation and ^{13}C isotope discrimination were indistinguishable from wild type, indicating no difference in BS leakiness between genotypes. Thus, Zm*Asft* expression has a minor effect on leaf water movement but is not required for the CO_2 concentrating mechanism. A more severe disruption to the suberin lamella is necessary to determine whether these structures are essential for CO_2 concentration in NADP-ME-type C_4 grasses.

BIOGRAPHICAL SKETCH

Rachel Anne Mertz was born and raised in West Lafayette, Indiana. She was fascinated by plants from an early age, and upon completing high school, she joined the Department of Botany and Plant Pathology at Purdue University as an undergraduate Plant Biology major. In her first semester, she met Dr. Nicholas Carpita in an introductory course and joined his laboratory as an undergraduate research assistant at the beginning of the following semester. Despite an inauspicious start to her research career in which she shattered a piece of glassware that she was assigned to clean, Rachel developed a deep and abiding interest in the intricate polysaccharide linkage structures of the plant cell wall. The major focus of her research during her four years of study in Dr. Carpita's laboratory was the forward genetic mapping and biochemical characterization of two arabinose-deficient cell wall mutants, *murus5* and *murus6*.

After graduating from Purdue University with a Bachelors of Science With Highest Distinction in Plant Biology in 2008, Rachel enrolled in the Graduate School at Cornell University and joined the Field of Plant Biology. Her objective was to pursue a dissertation project that would enable her to expand and deepen her knowledge of cell wall biochemistry, and so she completed her first rotation in the lab of Dr. Jocelyn Rose, where she developed an interest in the cutin research ongoing in his lab. She met her advisor, Dr. Thomas Brutnell, during a networking seminar for first year students and faculty, where he was presenting a summary of his lab's work on the molecular genetic dissection of C_4 photosynthesis in maize. She engaged him in conversation after the seminar, and upon learning of her background in cell wall biology, he said that he had always wondered why the bundle sheath cell walls of C_4 grasses contained suberin. Rachel was intrigued by the question and made it the focus of her dissertation research as a member Dr. Brutnell's laboratory.

This dissertation is dedicated in memory of my maternal grandmother, Doris Fix. My grandmother valued scholarship immensely, and encouraged my educational pursuits from the earliest years of my life until she passed away in 2013. One of the great regrets of my grandmother's life was that as a young woman coming of age in rural Indiana in the heart of the Great Depression, she was unable to attend college. I am honoured by the opportunity to become the first woman in my family to earn a Ph.D., and to dedicate this dissertation to her. I would also like to acknowledge the enduring support of my mother, Susan Bever, and my younger sister, Dorie Mertz.

ACKNOWLEDGEMENTS

I would like to thank my advisor, Dr. Thomas Brutnell, for his support and guidance during my time as a member of his lab. Bundle sheath suberization has been a fascinating problem to work on, and my time in the Brutnell Lab has broadened my horizons considerably. I am also grateful for the mentorship of Dr. E. Robert Turgeon and Dr. Jocelyn Rose, who served on my dissertation committee. During my time at Cornell, Dr. Trevor Yeats and Dr. Greg Buda provided significant guidance as I learned to analyse suberin polyesters. After the Brutnell Lab relocated to the Danforth Center, Dr. Jan Jaworski and Ms. Jia Li provided invaluable assistance and as I continued my suberin analyses. I also wish to thank my collaborators Dr. R. Howard Berg, Dr. Asaph Cousins, Dr. Susanne von Caemmerer, Mr. Lwanga Nsubuga, and Dr. Patricia Ellsworth for their invaluable contributions toward characterizing my suberin mutant. Within the Brutnell Lab, I was fortunate to work closely with Mr. Kevin Ahern, Dr. Anthony Studer, Dr. Lin Wang, and Dr. Sarit Weissmann. I am also grateful to Dr. Nicholas Carpita, Ms. Anna Olek, and Dr. Maureen McCann for their continued guidance and support.

The work presented in this dissertation was funded by the National Science Foundation via a grant (IOS- 1127017) to TPB.

TABLE OF CONTENTS

LIST OF FIGURES

LIST OF TABLES

LIST OF ABBREVIATIONS

ABCG, ATP-binding cassette subfamily G

Ac/Ds, *Activator*/*Dissociation* (elements)

ASFT, aliphatic suberin feruloyl transferase

BS, bundle sheath

Cas9, CRISPR-associated endonuclease 9

CASP, CASPARIAN STRIP MEMBRANE DOMAIN PROTEIN

CC, companion cell

p-coumaric acid, *para*-coumaric acid

CRISPR, Clustered, randomly interspersed, short palindromic repeats

CS, Casparian Strips

CUS1, CUTIN SYNTHASE1

CYP, CYTOCHROME P450

DCA, dicarboxylic acid

di-OH, di-hydroxy [fatty acid]

ER, endoplasmic reticulum

ECR, enoyl-CoA reductase

ESB1, *ENHANCED SUBERIN1*

FA, fatty acid

FAE, fatty acid elongase

GAX, glucuronoarabinoxylan

GDSL, GDSL-like lipase/acylhydrolase

G3P, glycerol-3-phosphate

HACD, hydroxyacyl-CoA dehydrase

HCA, hydroxycinnamic acid

In muro, In the cell wall

ITW, inner tangential wall

KCS, ketoacyl-CoA synthase

KCR, ketoacyl-CoA reductase

LACS, long chain acyl-CoA synthetase

LCFA, long chain fatty acid

M, mesophyll

2-MAG, *sn*-2 monoacylglycerol

MS, mestome sheath

MX, metaxylem vessel

NAD-ME, NAD-malic enzyme

NADP-ME, NADP-malic enzyme

ω-OH, omega hydroxy [fatty acid]

OTW, outer tangential wall

PAM, protospacer adjacent motif

PCK, phosphoenolpyruvate carboxykinase

PCW, primary cell wall

PD, plasmodesmata

PM, plasma membrane

PER64, PEROXIDASE64

RBOHF, Respiratory Burst Oxidase Homologue Family F

RNAi, RNA Interference

RW, radial wall

SCR, *SCARECROW*

sgRNA, small guide RNA

SHR, *SHORT-ROOT*

SL, suberin lamellae

ST, sieve tube

Suc, sucrose

tracrRNA, trans-encoded CRISPR RNA

TCW, tertiary cell wall

TF, transcription factor

VLCFA, very long chain fatty acid

VP, vascular parenchyma

WT, wild type

CHAPTER ONE

BUNDLE SHEATH SUBERIZATION IN GRASS LEAVES: MULTIPLE BARRIERS TO CHARACTERIZATION[1]

ABSTRACT

High yielding, stress tolerant grass crops are essential to meeting future food and energy demands. Efforts are underway to engineer improved varieties of the C_3 cereal crop rice by introducing NADP-ME C_4 photosynthesis using maize as a model system. However, several modifications to the rice leaf vasculature are potentially necessary, including the introduction of suberin lamellae into the bundle sheath cell walls. Suberized cell walls are ubiquitous in the root endodermis of all grasses, and developmental similarities are apparent between endodermis and bundle sheath cell walls. Nonetheless, there is considerable heterogeneity in sheath cell development and suberin composition both within and between grass taxa. The effect of this variation on physiological function remains ambiguous over forty years after suberin lamellae were initially proposed to regulate solute and photoassimilate fluxes and C_4 gas exchange. Interspecies variation has confounded efforts to ascribe physiological differences specifically to the presence or absence of suberin lamellae. Thus, specific perturbation of suberization within a uniform genetic background is needed, but until recently, sufficient genetic resources were largely unavailable. The recent dissection of the suberin biosynthesis pathway in model dicots and the identification of several promising candidate genes in model grasses will facilitate the characterization of the first suberin biosynthesis genes in a monocot. Much remains to be learned

[1] Originally published in Mertz RA and Brutnell TPB (2015) *J Exp Bot* **65** (13): 3371-3380.

about the role of bundle sheath suberization in leaf physiology, but the stage is set for significant advances in the near future.

INTRODUCTION

Increased yield and stress tolerance under marginal growing conditions are urgently needed to keep pace with food and biofuel needs (Ray *et al*., 2013). C4 grasses are well suited to this task, as they have greater water and nitrogen use efficiencies than their C_3 counterparts, and perform better under hot, dry conditions (Sage, 2004; Taylor *et al*., 2010). C_4 species comprise the most productive cereal crops and are promising biomass feedstocks for next-generation biofuels (Taylor *et al*., 2010; Byrt *et al*., 2011). Given the high productivity associated with C4 plants, efforts are currently underway to engineer C_4 photosynthesis into the C_3 crop rice (*Oryza sativa*), with the NADP-malic enzyme (NADP-ME) subtype serving as a prototype for engineering efforts. If successful, it is predicted that C_4 rice will increase yields by 50% and require significantly less fertilizer than existing varieties (Hibberd *et al*., 2008; Sage and Zhu, 2011). However, successful engineering of NADP-ME C_4 photosynthesis into rice may require a suite of anatomical modifications, including increased vein density, a photosynthetic bundle sheath (reviewed in Nelson, 2011), and deposition of the lipophilic heteropolyester suberin into the parenchymatous bundle sheath cell wall (Hattersley and Browning, 1981).

Lipophilic cell wall deposits are common to all land plant lineages, and are thought to have been essential to the transition from aquatic life (Rensing *et al*., 2008). In grass roots, suberin is ubiquitously deposited beneath the primary cell wall in the endodermis (Esau, 1965), and variably in the root exodermis (Perumalla *et al*., 1990). In grass leaves, the vasculature is sheathed by one or two cell layers; the innermost layer, the mestome sheath (MS) is ubiquitously

suberized (Hattersley and Perry, 1984). Suberin deposition in the outermost layer, the bundle sheath (BS), occurs primarily in classical phosphoenolpyruvate carboxykinase (PCK) and NADP-ME-type C_4 grasses, with the MS generally absent from the latter (Hattersley and Browning, 1981; Eastman *et al*., 1988a). Grasses with classical NAD-malic enzyme (NAD-ME) C_4 anatomy lack a suberized BS, but non-classical species with large BS surface areas contacting mesophyll (M) may be suberized (Prendergast *et al*., 1987). Despite this correlation, BS surface area and cell wall suberization appear genetically unlinked (Ohsugi *et al*., 1997). Variation in the structure and development of suberized walls occurs both within and between species.

Suberized vascular sheaths have several putative physiological functions. For example, suberized cell walls potentially mediate vascular fluxes of solutes and photoassimilates in all grasses, and have also been implicated in abiotic stress tolerance (Kuo *et al*., 1974; Griffith *et al*., 1985). In C_4 species, BS suberization may restrict exchange of gases and photosynthetic intermediates across the BS/M interface (Laetsch, 1971). However, extensive suberization may also reduce biomass quality or digestibility due to its enrichment in phenylpropanoid precursors (Akin *et al*., 1983; Schreiber et al., 1999). Thus, suberized walls are promising targets for biomass improvement in all grasses, and may be required to engineer PCK or NADP-ME C_4 photosynthesis into C_3 species. Selective manipulation of suberization at the organ or tissue level is desirable to maximize stress tolerance and digestibility. Recent studies have indicated an intriguing molecular link between root endodermal differentiation and bundle sheath differentiation (Slewinski *et al*., 2012). Thus, a deeper understanding of suberin biosynthesis and regulation in leaf tissues may provide an entry into engineering the pathway in roots as well.

However, efforts to dissect vascular sheath suberization have been confounded by interspecies variation and a lack of genetic resources in model grasses. Despite over forty years

of research, sheath suberization remains functionally ambiguous. In this review, the development, chemical composition, physiology, and biosynthesis of suberized cell walls in vascular sheaths of grass leaves are discussed.

Bundle sheath suberization shares common features with root development

In an early review of root development, van Fleet (1961) described four states of endodermal cell wall differentiation common to monocots, including grasses (Vanfleet, 1961). State I occurs early in development, when osmiophilic Casparian Strips (CS) are deposited in the radial primary cell walls. CS are tightly associated with the plasmalemma (Esau, 1965) and are comprised predominately of lignin. Suberin is absent (Naseer et al., 2012) or a minor component (Zeier et al., 1999; Zeier and Schreiber, 1998). The majority of endodermal suberization occurs during State II, when suberin lamellae (SL) form beneath the primary cell wall and surround the symplast (Zeier *et al*., 1999; Robards and Robb, 1972). SL are thin (25-40 μm), lamellar, osmiophilic deposits except near plasmodesmata (PD), where thickened lamellae constrict the aperture of the pore (Haas and Carothers, 1975). Following SL development, a tertiary wall forms asymmetrically (State III). The tertiary wall is then enriched with lignin with the thickest region lying on the inner tangential wall in a characteristic "U-shape" (State IV; van Fleet, 1961). To date, maize (*Zea mays*) is the only grass for which tertiary wall composition has been analyzed. The tertiary wall is entirely lignocellulosic, and additional suberin deposition does not occur at this state (Zeier *et al*., 1999). Likewise, in both maize and non-graminaceous monocots, lipophilic Sudan III staining is limited to the state I CS and state II SL, suggesting that tertiary walls are exclusively lignocellulosic across broad taxa (Zeier and Schreiber, 1998; Zeier *et al*., 1999).

Although not strictly analogous, grass leaf BS and root endodermal development share several common features. A grass leaf sampled at the proper developmental state encompasses a complete sink-to source gradient, which matures basipetally (Evert *et al*., 1996a; Li *et al*., 2010). States II-IV of root endodermal maturation are common to the leaf vascular sheaths surrounding large, intermediate, and minor veins (Figure 1.1A-B, Figure 1.2A). Although CS form ubiquitously within millimeters of the apex in grass roots (Robards and Robb, 1972; Haas and Carothers, 1975; Clark and Harris, 1981), they are absent from both BS and MS (Eastman *et al*., 1988a). As in roots, State II SL are 25-40 μm thick, constrict plasmodesmata, and can surround all or part of the symplast (Eastman *et al*., 1988a; Evert *et al*., 1977; Robinson-Beers and Evert, 1991a, b). In both BS and MS, SL may be continuous around the cell periphery, as in major vein MS cells of rice, oat (*Avena byzantia*), and barley (*Hordeum vulgare*) (O'Brien and Carr, 1970; Chonan *et al*., 1981; Evert *et al*., 1996b). Alternatively, they may be discontinuous or absent in the inner tangential wall as in maize BS (Evert *et al*., 1977). Suberization may also vary within a single vascular bundle. For example, in sugarcane (*Saccharum* hybrid), BS cell walls have a continuous SL when adjacent to xylem and are limited to the outer tangential and radial walls when adjacent to phloem (Robinson-Beers and Evert, 1991a). In the majority of grasses sampled to date, suberization was assayed at a single time point, and comparatively little is known about suberization in the context of leaf development.

Vascular sheath suberization follows cell elongation and may either be synchronous in all vein orders and cell positions within a bundle as in maize BS (Evert *et al*., 1996a) or asynchronous as in wheat (*Triticum aestivum*) MS (O'Brien and Kuo, 1975). In juvenile maize leaves, BS cells suberize concurrently with metaxylem lignification and chloroplast

Figure 1.1. Ultrastructure of the bundle sheath cell wall.

A. A bundle sheath cell from a small vascular bundle of the NADP-ME C_4 grass maize. A State II suberin lamella (SL; solid blue line) is deposited in the outer tangential wall (OTW) and radial wall (RW) along the bundle sheath/mesophyll interface, but is absent from the inner tangential wall (ITW). State I Casparian Strips (CS) are present in the root endodermis (not pictured) but absent from the equivalent positions in the RW (dashed blue box). Chloroplasts are centrifugally positioned along the OTW. The area enlarged in Figure 1.1B is enclosed by a solid blue box.
B. Fine structure of the bundle sheath cell wall. The outermost layer is a polysaccharide primary cell wall (PCW). A State II suberin lamella (SL) is deposited beneath the primary wall, followed by a State III/IV lignocellulosic tertiary cell wall (TCW). The plasma membrane (PM) is immediately adjacent to the TCW. Scale bars denote 10 μm in A. and 1 μm in B.

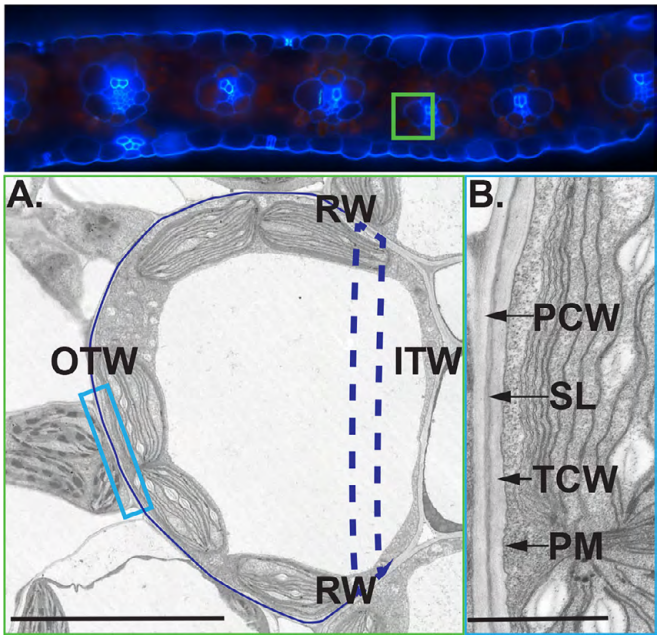
A.
RW
OTW
ITW
RW
B.
PCW
SL
TCW
PM

Figure 1.2 Proposed functions of suberized cell walls in C_4 grasses.

A. Organization of suberized cell layers around large veins of C_3 and C_4 grasses. In classical NADP-ME and PCK C_4 species, suberin lamellae (black lines) are continuous in outer tangential and radial walls and variable in inner tangential walls of both vascular sheaths. Both NAD-ME and C_3 grasses possess a suberized MS and an unsuberized BS. The MS is absent in all veins of NADP-ME species and in intermediate and small veins of other subtypes. Chloroplasts in the BS are centrifugally oriented only in suberized C_4 species. Bundle sheath areas are not drawn to scale.
B. Large veins of classical PEPCK and non-classical NAD-ME C_4 grasses. Diffusion of C_4 acids (C_4; green line) and sucrose (Suc; purple line) synthesized in mesophyll (M) cells into the vascular bundle is symplastic; ovals indicate passage through plasmodesmata. Apoplastic diffusion of released CO_2 and Suc is prevented at suberized walls (bent arrows). Likewise, O_2 (black line) can diffuse into M but not BS cells (bent arrow). In this model, sucrose travels symplastically to the vascular parenchyma (VP), enters the apoplast (dashed purple line), and is loaded into the sieve tube-companion cell complex (CC & ST). Water and dissolved solutes (blue line) exit the metaxylem vessel (MX) wall and travel apoplastically through radial walls between suberin lamellae of adjacent BS and MS cells. Dashed lines crossing cell walls indicate that a metabolite crosses the plasma membrane.
C. Intermediate and small veins of classical PEPCK and non-classical NAD-ME C_4 grasses, and all veins of classical NADP-ME C_4 grasses. Cell wall ultrastructure and metabolite transport occur as described in A., but the mestome sheath is discontinuous (not pictured) or absent.

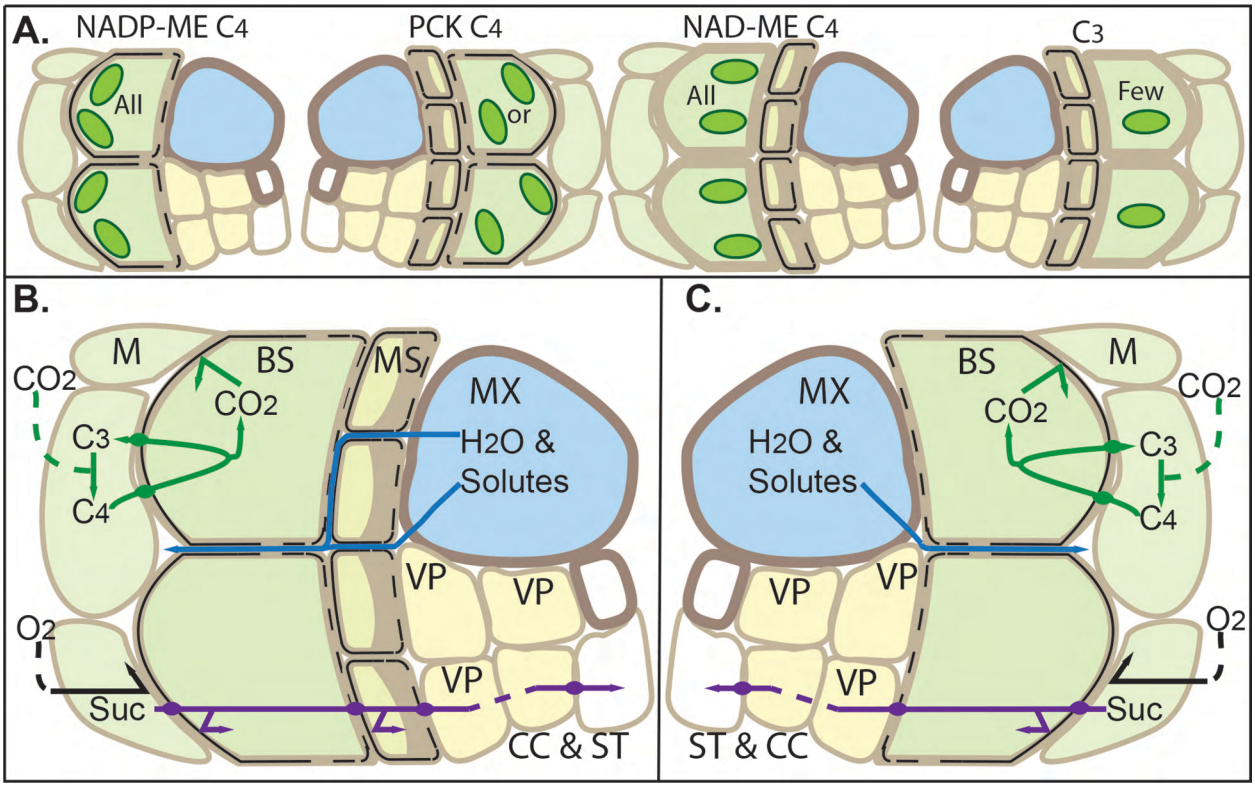
A.
NADP-ME C4
PCK C4
NAD-ME C4
C3
All
or
All
Few
B.
M
BS
MS
MX
CO2
CO2
C3
C4
H2O &
Solutes
VP
VP
VP
O2
Suc
CC & ST
C.
MX
BS
M
H2O &
Solutes
CO2
CO2
C3
C4
VP
VP
VP
O2
Suc
ST & CC

differentiation after thin-walled sieve tube maturation is complete (Evert *et al*., 1996a; Li *et al*., 2010). Conversely, wheat MS cells suberize concurrently with adjacent vascular tissue, and phloem-adjacent cells mature prior to xylem-adjacent neighbors (O'Brien and Kuo, 1975). In agreement with these data, candidate suberin biosynthesis genes reach maximum expression at the rice leaf base, (Wang *et al*., 2014), whereas maize homologues peak in the transitional zone concurrently with lignin biosynthesis (Li *et al*., 2010). Leaf developmental profiles from non-NADP-ME Panicoideae species are needed to determine whether asynchronous suberization is a general feature of MS versus BS development, or is specific to members of the BEP clade.

Vascular sheath cell wall development is not strictly analogous to the endodermis

Compared to both root suberization and leaf cuticle formation, which shares common monomer constituents with suberin synthesis (Pollard *et al*., 2008), little is known about the developmental plasticity of vascular sheath suberization. Root suberization is highly plastic. For instance, maize State II SL are developmentally delayed in both endo- and exodermis in hydroponically grown roots relative to aeroponics and vermiculite (Zimmermann *et al*., 2000; Enstone and Peterson, 2005). Likewise, cuticular wax deposition initiates prior to the emergence of a developing leaf from the ligule of its predecessor, and can be induced in younger, elongating cells near the leaf base by manual peeling of the ligule (Richardson *et al*., 2005). Conversely, cutin biosynthesis occurs constitutively in the region of cell elongation at the emerging leaf base and deposition does not continually increase in parallel with wax synthesis (Richardson *et al*., 2007). At least in maize, BS suberization also appears to be constitutive; despite variation in growth conditions (irradiance, temperature, and photoperiod), plant age, leaf sampled, and

degree of leaf emergence from the ligule, suberization occurred at identical developmental states in diverse inbreds B73 and W273 (Evert *et al*., 1996a; Li *et al*., 2010).

As discussed above for State II SL, the rate of State III/IV tertiary wall maturation varies greatly by root order and environment (Robards and Robb, 1972; Enstone and Peterson, 2005), but is not well characterized in leaves. Both BS and MS possess lignocellulosic tertiary walls, but endodermis-like asymmetrical thickenings are present only in the MS (Eastman *et al*., 1988a; Evert *et al*., 1977; O'Brien and Kuo, 1975). However, in maize, cell identity of both endodermis and BS are regulated by a common Scarecrow (ZmScr) homologue (Slewinski *et al*., 2012). Thus, divergent wall architectures can occur downstream of cell identity regulators. The molecular mechanism of asymmetric cell wall deposition is unknown for both SL and tertiary walls. For tertiary walls, cellulose deposition regulated by localized microtubule depolymerization may lead to patterns of asymmetrical thickening, as demonstrated for xylem vessels (Oda *et al*., 2010; Pesquet *et al*., 2010). Similarly, localized lignin polymerization domains, as recently reported for Arabidopsis (Arabidopsis thaliana) endodermal CS (Roppolo *et al*., 2011; Lee *et al*., 2013) might define sites of lignification. Whether a similar system occurs in monocots remains an open question.

Suberin composition varies qualitatively and quantitatively between species and organs

The developmental heterogeneity of suberin biosynthesis described above is accompanied by considerable compositional variation within the SL themselves. Suberin is a heterogeneous polyester matrix comprised of acyl lipid-derived aliphatic and phenylpropanoid-derived aromatic components (reviewed in Pollard *et al*., 2008). Suberin shares many common

Figure 1.3. A simplified pathway of grass aliphatic suberin biosynthesis modeled on *Arabidopsis thaliana*.
Following de novo fatty acid synthesis in the plastid, long chain fatty acid (LCFA) precursors are converted to acyl-CoA thioesters by a long chain acyl-CoA synthetase (LACS). Within the endoplasmic reticulum (ER), LCFA are oxidized to omega-hydroxy or di-hydroxy acids (ω-OH, di-OH) by cytochrome P450s (CYP). ω-OH LCFA may be oxidized by an unknown enzyme to produce dicarboxylic acids (DCA). Prior to oxidation, LCFA may be elongated to very long chain fatty acids (VLCFA) by the fatty acid elongase (FAE) complex. The FAE is comprised of a ketoacyl-CoA synthase (KCS), a ketoacyl-CoA reductase (KCR), a hydroxyacyl-CoA dehydrase, and an enoyl-CoA reductase (ECR). Both LCFA and VLCFA can be reduced to primary alcohols by fatty acyl-CoA reductase (FAR) or esterified to glycerol-3-phosphate (G3P) by glycerol-3-phosphate acyltransferase (GPAT) to produce sn-2 monoacylglycerol (2-MAG). In the cytosol, aliphatic suberin feruloyl transferase (ASFT) can esterify the monolignol precursor ferulic acid to ω-OH fatty acids and primary alcohols of various chain lengths to form alkyl ferulates. Monomers reach the plasma membrane by an unknown mechanism and are putatively exported by ATP-binding cassette subfamily G (AGCG) members. Polyesters may be synthesized by a GDSL-like lipase/acylhydrolase (GDSL). Enzymes denoted with an asterisk (*) are inferred from cutin synthesis. Grass suberin candidates discussed in the text are highlighted in red. Green frames denote monomers abundant in both suberin and cutin, while blue frames denote monomers that are suberin-enriched. Values in parentheses denote numbers of putative maize homologues for each Arabidopsis protein (Wang *et al*., 2014). The two groups of ABCG candidates denote half and whole transporters, respectively (Verrier *et al*., 2008). Putative GPAT5 substrate specificities were inferred from (Yang *et al*., 2012).

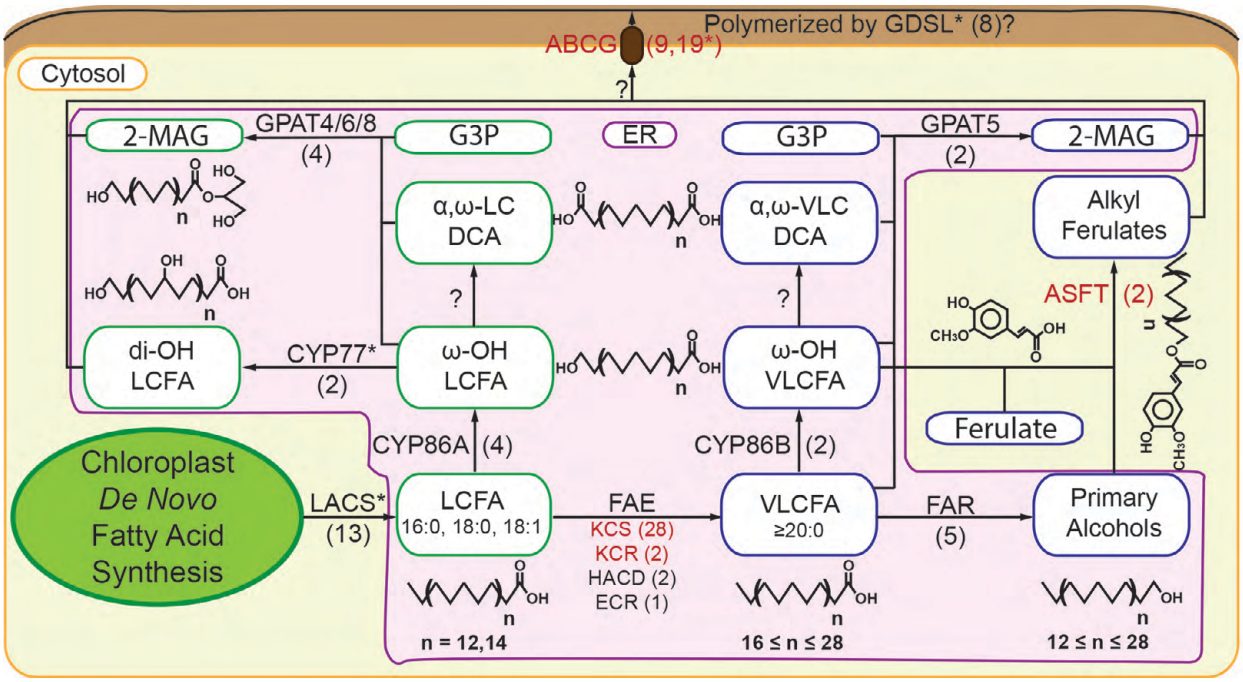
Polymerized by GDSL* (8)?
ABCG (9,19*)
?
Cytosol
2-MAG
GPAT4/6/8
(4)
G3P
ER
G3P
GPAT5
(2)
2-MAG
α,ω-LC DCA
α,ω-VLC DCA
Alkyl Ferulates
ASFT (2)
?
?
di-OH LCFA
CYP77*
(2)
ω-OH LCFA
ω-OH VLCFA
Ferulate
CYP86A (4)
CYP86B (2)
Chloroplast De Novo Fatty Acid Synthesis
LACS*
(13)
LCFA
16:0, 18:0, 18:1
FAE
KCS (28)
KCR (2)
HACD (2)
ECR (1)
VLCFA
≥20:0
FAR
(5)
Primary Alcohols
n = 12,14
16 ≤ n ≤ 28
12 ≤ n ≤ 28

monomers with epidermal cutin (Figure 1.3); both are lipophilic cell wall matrices of glycerol and oxidized long chain (16:0, 18:0, and 18:1) fatty acids (LCFA), but suberin is enriched in aromatics and very long chain (≥20:0) aliphatic monomers (VLCFA; reviewed by Pollard *et al*., 2008).

Much remains to be learned about the variation in grass suberin composition between species and organs, particularly in the vascular sheaths. In roots, suberin varies both qualitativelyand quantitatively between species. For instance, maize endodermal suberin is 34 times less abundant per unit area than rice, but is synthesized from a more diverse array of VLCFA (Schreiber *et al*., 2005a). Aliphatic composition also varies within a species by tissue type and developmental age. In State I CS, LCFA predominate in both sorghum (*Sorghum bicolor*) and maize (Zeier *et al*., 1999; Espelie and Kolattukudy, 1979a), whereas omega-hydroxy fatty acids predominate in State II SL (Zeier *et al*., 1999; Schreiber *et al*., 2005a; Soukup *et al*., 2007). Generally, VLCFA content increases proportionally with tissue age (Zeier *et al*., 1999; Soukup *et al*., 2007).

To date, vascular sheath suberin content has been profiled only in maize BS and rye (*Secale cereale*) MS (Griffith *et al*., 1985; Espelie and Kolattukudy, 1979b). As expected for State II SL, both tissues contain significant amounts of omega-hydroxy fatty acids. In the maize BS, LCFA predominate over VLCFA; thus, mature SL in BS and endodermis have similar chain length distributions of monomers (Zeier *et al*., 1999; Espelie and Kolattukudy, 1979b). However, polyhydroxy and epoxy fatty acids are the dominant constituent of BS and MS, respectively (Griffith *et al*., 1985; Espelie and Kolattukudy, 1979b). Polyhydroxy fatty acids are a major constituent of leaf cutin in many species (reviewed by Pollard *et al*., 2008). Both monomers are also major components of leaf cutin in these grasses; thus, vascular sheath suberin composition

shares similarities with epidermal cutin as well as root suberin. The functional implications of variable suberin composition are unclear.

Like aliphatic suberin, aromatic suberin varies quantitatively between species and generally increases with tissue age (Schreiber *et al*., 2005a; Soukup *et al*., 2007). The monolignol precursors coumarate and ferulate comprise the majority of aromatic suberin in all grasses studied to date (Zeier *et al*., 1999; Schreiber *et al*., 2005a; Soukup *et al*., 2007). However, accurate quantification of aromatic suberin in grasses is complicated by extensive esterification of ferulate and coumarate to arabinoxylans in the polysaccharide cell wall (Schreiber *et al*., 2005a; Harris and Hartley, 1976; Mueller-Harvey *et al*., 1986). These ferulate monomers, like monolignols, can undergo oxidative coupling to form covalent crosslinks to each other and to lignin (reviewed by Ralph *et al*., 2004; Ralph, 2010). Although coumarate does not dimerize *in planta* (Ralph *et al*., 1994), it is thought to function as a nucleation site for polymerization of other monolignols (reviewed in Ralph, 2010). Thus, phenolic suberin in vascular sheath cell walls is ideally positioned to crosslink with both hemicellulose and lignin and thus may contribute to biomass recalcitrance. This is especially true for C_4 species, where veins occupy the largest proportion of leaf tissue area (Hattersley, 1984). Accordingly, suberized portions of the BS and MS cell walls are recalcitrant to degradation in rumen fluid relative to parenchymatous C_3 BS cells with polysaccharide primary walls (Akin *et al*., 1983). However, unsuberized C_4 NAD-ME BS cells are the least digestible, suggesting that suberized cell walls are less recalcitrant than lignocellulosic walls (Wilson and Hattersley, 1983). As discussed above, although aromatic suberin is necessary for barrier function in model dicots, (see Ranathunge *et al*., 2011, and references therein), the precise relationship between monomer content and physiological function remains an open question.

Vascular sheath suberization may affect multiple aspects of leaf physiology

Although vascular sheath suberization has been correlated with multiple facets of leaf physiology (Figure 1.2B-C), causal relationships have not been established. O'Brien and Carr proposed that suberin lamellae restrict passive loss of water and solutes from the vasculature in both BS and MS cells (O'Brien and Carr, 1970). BS cells resist plasmolysis when exposed to concentrated (1.5M) sucrose (Evert *et al*., 1978) and desiccation stress (Giles *et al*., 1974; Giles *et al*., 1976), indicating low apoplastic permeability. Accordingly, ions dissolved in the transpiration stream can enter the tertiary walls of BS cells but cannot diffuse across the SL to the primary cell wall (Figure 1.1B, Figure 1.2B-C; Botha *et al*., 1982; Evert *et al*., 1985). SL in radial walls of adjacent MS/BS cells do not fuse; thus, water and solutes diffuse through the radial walls of all vein orders in both C_3 and C_4 grasses (Evert *et al*., 1985; Peterson *et al*., 1985; Canny, 1986; Eastman *et al*., 1988b). As the CS are the major endodermal permeability barriers in radial walls, the absence of these structures in vascular sheaths may explain their permeability to ions (Peterson *et al*., 1993).

Likewise, BS and MS suberization may restrict apoplastic backflow of sucrose out of the vascular bundle, facilitating spatial separation of transpirational efflux and phloem loading (Kuo *et al*., 1974; Canny, 1986). In the majority of grasses studied to date, sucrose synthesized in M cells travels via PD to vascular parenchyma cells, where it enters the apoplast for uptake by companion cells (Figure 1.2B-C) (reviewed in Braun and Slewinski, 2009). Accordingly, PD density in these species is highest along a symplastic pathway leading from M cells through BS, MS (if present), and into vascular parenchyma (VP) cells, the site of sucrose entry into the apoplast (Robinson-Beers and Evert, 1991b; Evert *et al*., 1996b; Evert *et al*., 1978; Botha, 1992).

PD frequency is highest in small veins and lowest in large veins, consistent with functional specialization for phloem loading by small veins (Fritz *et al*., 1989). Patterns of suberization are consistent with a role for SL in restricting sucrose diffusion to a symplastic route. During tissue maturation, vascular sheath suberization is completed prior to the sink-source transition (Evert *et al*., 1996a). Likewise, when MS suberization is asynchronous within individual bundles, complete SL appear first adjacent to phloem cells (O'Brien and Kuo, 1975). Furthermore, although SL are discontinuous in the inner tangential walls bordering phloem-associated vascular parenchyma in many PCK and NADP-ME C_4 species, they are present near PD (Evert *et al*., 1977; Robinson-Beers and Evert, 1991a). The absence of SL in portions of these walls may provide an apoplastic route into the vasculature. However, the bypass does not occur in the maize *sucrose export defective1* (*sxd1*) mutant, in which BS/VP PD are occluded by callose (Russin *et al*., 1996; Botha et al., 2000). This suggests that other cell wall components, potentially lignin, may also contribute significantly to diffusion resistance.

In addition to the proposed roles for SL in all grasses, specialized functions may occur in PCK or NADP-ME C_4 species. For example, suberization along the entire C_4 BS/M interface is hypothesized to restrict photosynthetic intermediates to a symplastic route (Evert *et al*., 1977). As PD are the primary limiting factor for metabolite diffusion, their abundance correlates with net C_4 photosynthetic rate, and PD frequency at the BS/M interface is significantly higher in all C_4 subtypes relative to C_3 species (Botha, 1992). Accordingly, although isolated BS strands accumulate metabolites, neither plasmolysed BS strands nor protoplasts can do so (Weiner *et al*., 1988). Although recent models of C4 metabolite exchange include suberized PD constrictions as a limiting factor (Sowinski *et al*., 2008), the functional impact of these structures remains unclear. For instance, the molecular weight size exclusion limit of BS PD is comparable between

classical PCK and NAD-ME species; thus, the plasmodesmatal neck constriction common to both groups, and not the SL may be the primary determinant of size exclusion (Botha, 1992). Likewise, PD abundance per unit vein at the BS/M interface is highest in the NAD-ME type (Botha, 1992). This suggests that metabolite flux is mostly or entirely symplastic even in the absence of SL.

Laetsch (1971) proposed that BS SL are barriers which prevent apoplastic diffusion of CO_2 and O_2 across the BS/M interface (Figure 1.2; Laetsch, 1971). Suberized tissues have low diffusional O_2 permeability (Ranathunge *et al*., 2003) and regulate gas exchange in root exodermis, periderm and lenticels, and root nodules of legumes (Jacobsen *et al*., 1998; Lendzian, 2006; Kotula *et al*., 2009). Likewise, the CO_2 permeability of C_4 BS cells is over 100-fold lower than C_3 M cells (Furbank *et al*., 1989). Unsuberized NAD-ME species also exhibit low permeability; thus, BS permeability results from a combination of apoplastic modifications and cellular metabolism, and SL are not obligatory for CO_2 concentration (Jenkins *et al*., 1989; von Caemmerer and Furbank, 2003). However, NAD-ME grasses exhibit a suite of anatomical modifications including lignocellulosic secondary walls, centripetal chloroplast orientation, and a decreased BS surface area:volume ratio that may limit gas exchange (Hattersley and Browning, 1981). Centrifugally oriented chloroplasts tightly associated with the BS/M interface are common only in species with a suberized BS (Hattersley and Browning, 1981; Hatch, 1975). Interestingly, BS suberization and chloroplast orientation segregate independently in interspecific Panicum hybrids (Ohsugi *et al*., 1997). Hybrid plants were suberized with variable BS chloroplast orientation. Dry matter carbon isotope ratios ($\delta^{13}C$) were identical in the hybrid lines and higher than in classical NAD-ME species, suggesting that SL contribute to a lower (more C_4-like) degree of carbon isotope discrimination in closely related species (Ohsugi et al.,

1997). However, the validity of dry matter carbon isotope ratios as a measure of CO_2 leakage from BS strands remains tenuous due to confounding variation from plant metabolism (von Caemmerer and Furbank, 2003, and references therein).

Stress physiology of suberized vascular sheaths is largely uncharacterized. Both total MS suberization and the proportion of epoxy fatty acids increased during cold acclimation of rye (Griffith *et al*., 1985), but the molecular mechanism by which MS suberization promotes cold tolerance remains ambiguous. Conversely, short-term ultrastructural changes in BS suberization were not reported during drought stress and subsequent rehydration of either maize or sorghum (Giles *et al*., 1974; Giles *et al*., 1976). Additional studies of vascular sheath suberization under both biotic and abiotic stress are needed in grasses, both to expand existing knowledge of barrier function, and to facilitate candidate gene identification. For example, two candidate suberin biosynthesis genes were recently identified in rice roots undergoing salt-induced suberin deposition (Krishnamurthy *et al*., 2009).

Molecular genetic dissection of biosynthesis and regulation

Mutants with altered suberization are necessary to assess the functions of SL in a uniform genetic background with minimal confounding variation. Despite substantial progress toward elucidating the molecular genetic basis of both suberin and cutin biosynthesis in the C_3 dicots Arabidopsis and potato (*Solanum tuberosum*; reviewed by Ranathunge *et al*., 2011; Beisson *et al*., 2012; Yeats and Rose, 2013), no suberin biosynthesis genes have been characterized in any grass species. However, biochemical and forward genetics approaches have identified several candidate genes potentially involved in suberin biosynthesis (Figure 1.3). Although these candidates have been studied exclusively in roots, tissue specific transcript profiling indicates

that many putative suberin biosynthesis genes are expressed in both roots and leaves (Sekhon *et al*., 2011).

cDNA isolation from maize roots yielded *a 3-ketoacyl-CoA synthase* (*KCS*) homologous to *AtKCS1* (Todd et al., 1999; Schreiber, 2000) and a putative suberin-associated O-methyltransferase, *Zea Root Preferential 4* (*ZmZPR4*) (Held et al., 1993). Biochemical evidence of anionic peroxidase and Fatty Acid Elongase (FAE) complex activity in maize seminal roots undergoing endo- and exodermal suberization was also reported (Pozuelo *et al*., 1984; Schreiber *et al*., 2005b). In the latter case, the chain-length specificity was consistent with aliphatic suberin monomer content, supporting the role of the KCS in suberin biosynthesis (Schreiber *et al*., 2005b). KCS is associated with a Fatty Acid Elongase complex involved in sequential acyl chain elongation (Joubes *et al*., 2008). The cuticular wax-associated 3-ketoacyl-CoA reductases (KCRs) Glossy8a and 8b are also components of the maize Fatty Acid Elongase complex and thus may contribute to suberin biosynthesis (Xu *et al*., 1997; Xu *et al*., 2002; Dietrich *et al*., 2005). Therefore, a detailed evaluation of wax biosynthesis mutants for pleiotropic suberin phenotypes may identify suberin biosynthesis genes.

Bi-functional Arabidopsis KCS that contribute to both suberin and wax biosynthesis exist (Franke *et al*., 2009; Lee *et al*., 2009), as do ATP-binding cassette subfamily G transporters involved in monomer secretion to the apoplast (Bird *et al*., 2007; Panikashvili *et al*., 2010). Recently, a rice KCS with cuticular wax defects and ubiquitous expression was characterized and proposed to contribute to multiple cellular processes requiring Fatty Acid Elongase, including suberin biosynthesis (Yu *et al*., 2008). Likewise, two homologous ATP-binding cassette subfamily G transporters from rice and barley exhibit cuticular wax defects and impaired transpiration barrier function, and are expressed throughout the leaf elongation zone, including

the MS (Chen *et al*., 2011). Thus, multifunctional wax biosynthesis genes likely exist in grasses as well. However, a second rice KCS shows an epidermal localization consistent with a specific function in cuticular wax biosynthesis (Ito *et al*., 2011). Therefore, tissue-specific expression data is needed to refine the selection of suberin biosynthesis candidates, particularly for large, redundant gene families.

Delineating suberin-associated KCS genes is also of interest because these enzymes are thought to be rate limiting for VLCFA biosynthesis (Millar and Kunst, 1997). Thus, mining their promoter regions for *cis*-regulatory elements may elucidate transcriptional regulators of suberin biosynthesis, which are uncharacterized in any species.

It was recently reported that in oat addition lines containing maize chromosome 3, lipophilic material is ectopically deposited in C_3 BS cell walls (Tolley *et al*., 2012). The deposition pattern resembles the maize BS; however, SL are absent, and the authors conclude that additional loci are required for their biosynthesis (Tolley *et al*., 2012). A homologue of the secondary cell wall regulator *SECONDARY WALL-ASSOCIATED NAC DOMAIN 2* (*AtSND2*) is among the candidate loci on chromosome 3 (Li *et al*., 2010; Tolley *et al*., 2012). Recently, a homologue of the Arabidopsis *SCARECROW* (*AtSCR*) transcription factor was also shown to affect endodermal CS formation and BS suberization in maize (Slewinski *et al*., 2012; DiLaurenzio *et al*., 1996). This study supports developmental similarities of vascular sheaths between organs, but the precise effect of SCR on suberin biosynthesis remains unclear.

CONCLUSIONS AND FUTURE DIRECTIONS

Suberized cell layers surrounding the vasculature are a ubiquitous feature of grass leaves. However, variation in development and monomer content exists both within and between

species, with unclear effects on barrier function. Sheath suberization has been implicated in numerous physiological processes, but interspecies variation has complicated efforts to dissect barrier function. Mutants with altered suberization are needed to characterize BS function within a uniform genetic background. The genomic resources (Draper *et al*., 2001; Matsumoto *et al*., 2005; Paterson *et al*., 2009; Schnable *et al*., 2009; Bennetzen *et al*., 2012), and expression data (Li *et al*., 2010; Sekhon *et al*., 2011; Wang *et al*., 2014) needed to facilitate candidate identification are available, and a putative biosynthesis pathway has been partially delineated (Figure 1.3; Li *et al*., 2010; Wang *et al*., 2014). Both stable mutants and transgenic lines can now be generated in both C_3 and C_4 model grasses (Draper *et al*., 2001; An *et al*., 2005; Brutnell *et al*., 2010; Vollbrecht *et al*., 2010; Bragg *et al*., 2012).

At the outset of this research, no biosynthesis or regulatory genes underlying suberin biosynthesis were characterized in any grass species. Furthermore, the only transcripts attributed specifically to suberin biosynthesis, the *ZmKcs* and *ZmZrp4* cDNA clones described above, exhibited root-specific expression (Schreiber, 2000; Held *et al*., 1993). Thus, the first priority was to delineate a putative pathway for maize leaf suberin biosynthesis populated with candidate genes expressed in close spatiotemporal proximity to bundle sheath suberin lamella formation (Chapter 2). A major challenge of interpreting the transcriptome data was the lack of cell type specificity along the developmental gradient. Because cutin, cuticular wax, and suberin share many common monomer components, ascribing candidate genes to specific polyester biosynthetic pathways was not possible in most cases. For the Panicoid grasses maize and green millet (*Setaria viridis*), a spatiotemporal separation was observed between likely cutin biosynthesis candidates and a small cohort of genes homologous to suberin-specific VLCFA-modifying genes of Arabidopsis (Chapter 2). The tightly delimited expression domain of these

suberin biosynthesis candidates facilitated the identification a candidate suberin synthase of the GDSL lipase/acylhydrolase family as well as several MYB and WRKY transcription factors putatively involved in regulation (Chapter 2). In order to dissect the physiological functions of BS suberization, particularly whether SL form an essential gas exchange barrier for NADP-ME C_4 photosynthesis, two putative maize homologues of Arabidopsis *ALIPHATIC SUBERIN FERULOYL TRANSFERASE* (*AtASFT*; Gou *et al*., 2009, Molina *et al*., 2009) were mutated using *Dissociation* transposons (Chapter 3). The chemical phenotype, ultrastructure, and barrier properties of *Zmasft1*; *asft2* double mutants differed significantly from previously characterized dicot homologues. In particular, a significant attenuation of ω-OH VLCFA was observed without a stoichiometric decrease in any aromatic monomer, whereas cell wall ferulate was reduced by 50-90% in *Atasft* and potato (*Solanum tuberosum*) *StFHT*-RNAi lines (Molina *et al*., 2009; Serra *et al*., 2010). The cell wall architecture was indistinguishable from wild type in dicot *asft* mutants, but *Zmasft* double mutants exhibited fragile BS cells with reduced cohesion between polyester and polysaccharide wall domains. Despite these alterations, the *Zmasft* double mutant had no effect on C_4 gas exchange and only a minor increase in leaf transpirational flux (Chapter 3). Taken together with previous studies, these results suggest that the cell wall context within which SL occur has a significant impact on their barrier properties. At least in the Type II cell walls of maize, ester linkages between aromatic and aliphatic monomer species appear to be crucial for the cohesion of suberized cell walls in general, but not for the interior architecture of the lamella in particular (Chapter 3). Therefore, it was concluded that a stronger disruption to the aliphatic suberin polyester was necessary to disrupt barrier function. A targeted reverse genetic mutagenesis of the suberin synthase candidate *SvGDSL1* was initiated using RNA interference (RNAi) in green millet (Chapter 4). Chapter 4 concludes with a discussion of promising new

approaches to generate more severe suberin mutants in green millet using the emerging CRISPR/Cas9 technology.

The extent to which the physiological functions of vascular sheath suberin are shared between taxa with differing vein anatomies and C_4 archetypes remains to be determined. Genetic resources for PCK C_4 grasses are currently limited, but a targeted reverse genetics approach is presently feasible for both NAD-ME C_4 (Switchgrass [*Panicum virgatum*]) and C_3 (rice, *Brachypodium distachyon*) model grasses. Thus, after forty years of ambiguity, the stage is now set for a rapid expansion of our understanding of sheath suberization in grasses.

REFERENCES

Akin DE, Wilson JR, Windham WR. (1983) Site and rate of tissue digestion in leaves of C3, C4, and C3/C4 intermediate Panicum species. *Crop Science* **23**: 147-155.

An G, Lee S, Kim SH, Kim SR. (2005) Molecular Genetics Using T-DNA in Rice. *Plant and Cell Physiology* **46**: 14-22.

Beisson F, Li-Beisson Y, Pollard M. (2012) Solving the puzzles of cutin and suberin polymer biosynthesis. Current Opinion in Plant Biology 15, 329-337.

Bennetzen JL, Schmutz J, Wang H, *et al*. (2012) Reference genome sequence of the model plant Setaria. *Nature Biotechnology* **30**: 555-561.

Bird D, Beisson F, Brigham A, Shin J, Greer S, Jetter R, Kunst L, Wu X, Yephremov A, Samuels L. (2007) Characterization of Arabidopsis ABCG11/WBC11, an ATP binding cassette (ABC) transporter that is required for cuticular lipid secretion. *The Plant Journal* **52**: 485-498.

Botha CEJ. (1992) Plasmodesmatal distribution, structure and frequency in relation to assimilation in C3 and C4 grasses in Southern Africa. Planta 187, 348-358.

Botha CEJ, Cross RHM, van Bel AJE, Peter CI. (2000) Phloem loading in the sucrose-export-defective (SXD-1) mutant maize is limited by callose deposition at plasmodesmata in bundle sheath-vascular parenchyma interface. *Protoplasma* **214**: 65-72.

Bragg JN, Wu J, Gordon SP, Guttman ME, Thilmony R, Lazo GR, Gu YQ, Vogel JP. (2012) Generation and Characterization of the Western Regional Research Center Brachypodium T-DNA Insertional Mutant Collection. *PLOS One* **9**: e41916. doi:10.1371/journal.pone.0041916.

Braun DM, Slewinski TL. (2009) Genetic Control of Carbon Partitioning in Grasses: Roles of Sucrose Transporters and Tie-dyed Loci in Phloem Loading. *Plant Physiology* **149**: 71-81.

Brutnell TP, Wang L, Swartwood K, Goldschmidt A, Jackson D, Zhu XG, Kellogg E, Van Eck J. (2010) *Setaria viridis*: a model for C4 photosynthesis. *The Plant Cell* **22**: 2537-2544.

Byrt CS, Grof CP, Furbank RT. (2011) C4 plants as biofuel feedstocks: optimising biomass production and feedstock quality from a lignocellulosic perspective. *Journal of Integrative Plant Biology* **53**: 120-135.

Canny MJ. (1986) Water pathways in wheat leaves. 3. The passage of the mestome sheath and the function of the suberized lamellae. *Physiologia Plantarum* **66**: 637-647.

Chonan N, Kaneko M, Kawahara H, Matsuda T. (1981) Ultrastructure of the large vascular bundles in the leaves of rice plant. *Japanese Journal of Crop Science* **50**: 323-331.

Clark LH, Harris WH. (1981) Observations on the root anatomy of rice (*Oryza-sativa*-L). *American Journal of Botany* **68**: 154-161.

Dietrich CR, Perera MA, M DY-N, Meeley RB, Nikolau BJ, Schnable PS. (2005) Characterization of two GL8 paralogs reveals that the 3-ketoacyl reductase component of fatty acid elongase is essential for maize (*Zea mays* L.) development. *The Plant Journal* **42**: 844-861.

Di Laurenzio L, WysockaDiller J, Malamy JE, Pysh L, Helariutta Y, Freshour G, Hahn MG, Feldmann KA, Benfey PN. (1996) The *SCARECROW* gene regulates an asymmetric cell division that is essential for generating the radial organization of the Arabidopsis root. *Cell* **86**: 423-433.

Domergue F, Lessire R. (2008) The VLCFA elongase gene family in Arabidopsis thaliana: phylogenetic analysis, 3D modelling and expression profiling. *Plant Molecular Biology* **67**: 547-566.

Draper J, Mur LAJ, Jenkins G, *et al*. (2001) *Brachypodium distachyon*. A new model system for functional genomics in grasses. *Plant Physiology* **127**: 1539-1555.

Eastman PAK, Dengler NG, Peterson CA. (1988a) Suberized Bundle Sheaths in Grasses (Poaceae) of Different Photosynthetic Types .1. Anatomy, Ultrastructure and Histochemistry. *Protoplasma* **142**: 92-111.

Eastman PAK, Peterson CA, Dengler NG. (1988b) Suberized bundle sheaths in grasses (Poaceae) of different photosynthetic types. 2. Apoplastic permeability. *Protoplasma* **142**: 112-126.

Enstone DE, Peterson CA. (2005) Suberin lamella development in maize seedling roots grown in aerated and stagnant conditions. *Plant Cell and Environment* **28**: 444-455.

Esau K. (1965) *Plant Anatomy*: New York, Wiley.

Espelie KE, Kolattukudy PE. (1979a) Composition of the Aliphatic Components of Suberin of the Endodermal Fraction from the 1st Internode of Etiolated Sorghum Seedlings. *Plant Physiology* **63**: 433-435.

Espelie KE, Kolattukudy PE. 1979b. Composition of the Aliphatic Components of Suberin from the Bundle Sheaths of Zea-Mays Leaves. *Plant Science Letters* **15**: 225-230.

Evert RF, Botha CEJ, Mierzwa RJ. (1985) Free-space marker studies on the leaf of *Zea-mays*-L. *Protoplasma* 126, 62-73.

Evert RF, Eschrich W, Heyser W. (1977) Distribution and structure of plasmodesmata in mesophyll and bundle-sheath cells of *Zea-mays*-L. *Planta* **136**: 77-89.

Evert RF, Eschrich W, Heyser W. (1978) Leaf structure in relation to solute transport and phloem loading in *Zea-mays*-L. *Planta* **138**: 279-294.

Evert RF, Russin WA, Bosabalidis AM. (1996a) Anatomical and ultrastructural changes associated with sink-to-source transition in developing maize leaves. *International Journal of Plant Sciences* **157**: 247-261.

Evert RF, Russin WA, Botha CEJ. (1996b) Distribution and frequency of plasmodesmata in relation to photoassimilate pathways and phloem loading in the barley leaf. *Planta* **198**: 572-579.

Franke R, Hofer R, Briesen I, Emsermann M, Efremova N, Yephremov A, Schreiber L. (2009) The *DAISY* gene from Arabidopsis encodes a fatty acid elongase condensing enzyme involved in the biosynthesis of aliphatic suberin in roots and the chalaza-micropyle region of seeds. *The Plant Journal* **57**: 80-95.

Fritz E, Evert RF, Nasse H. (1989) Loading and transport of assimilates in different maize leaf bundles - digital image-analysis of C-14 microautoradiographs. *Planta* **178**: 1-9.

Furbank RT, Jenkins CL, Hatch MD. (1989) CO2 Concentrating Mechanism of C4 Photosynthesis: Permeability of Isolated Bundle Sheath Cells to Inorganic Carbon. *Plant Physiology* **91**: 1364-1371.

Giles KL, Beardsel.Mf, Cohen D. (1974) Cellular and ultrastructural changes in mesophyll and bundle sheath-cells of maize in response to water stress. *Plant Physiology* **54**: 208-212.

Giles KL, Cohen D, Beardsell MF. (1976) Effects of water stress on ultrastructure of leaf cells of *Sorghum-bicolor*. *Plant Physiology* **57**: 11-14.

Gou JY, Yu XH, Liu CJ. (2009) A hydroxycinnamoyltransferase responsible for synthesizing suberin aromatics in Arabidopsis. *Proceedings of the National Academy of Sciences of the United States of America* **106**: 18855-18860.

Griffith M, Huner NPA, Espelie KE, Kolattukudy PE. (1985) Lipid polymers accumulate in the epidermis and mestome sheath cell-walls during low-temperature development of winter rye leaves. *Protoplasma* 125: 53-64.

Haas DL, Carothers ZB. (1975) Some ultrastructural observations on endodermal cell development in *Zea-mays* roots. *American Journal of Botany* **62**: 336-348.

Harris PJ, Hartley RD. (1976) Detection of bound ferulic acid in cell-walls of Gramineae by ultraviolet fluoresence microscopy. *Nature* **259**: 508-510.

Hatch MD, Kagawa T, and Craig, S. (1975) Subdivision of C4-pathway Species based on Differing C4 Acid Decarboxylating Systems and Ultrastructural Features. *Australian Journal of Plant Physiology* **2**: 111-128.

Hattersley PW. (1984) Characterization of C4 type leaf anatomy in grasses (Poaceae), mesophyll - bundle sheath area ratios. *Annals of Botany* **53**: 163-179.

Hattersley PW, Browning AJ. (1981) Occurence of the suberized lamella in leaves of grasses of different photosynthetic types.1. In parenchymatous bundle sheaths and PCR (Kranz) sheaths. *Protoplasma* **109**: 371-401.

Hattersley PW, Perry S. (1984) Occurrence of the suberized lamella in leaves of grasses of different photosynthetic types. 2. In herbarium material. *Australian Journal of Botany* **32**: 465-473.

Held BM, Wang H, John I, Wurtele ES, Colbert JT. (1993) An mRNA putatively coding for an O-methyltransferase accumulates preferentially in maize roots and is located predominantly in the region of the endodermis. *Plant Physiology* **102**: 1001-1008.

Hibberd JM, Sheehy JE, Langdale JA. 2008. Using C4 photosynthesis to increase the yield of rice-rationale and feasibility. *Current Opinion in Plant Biology* **11**: 228-231.

Ito Y, Kimura F, Hirakata K, Tsuda K, Takasugi T, Eiguchi M, Nakagawa K, Jacobsen KR, Rousseau RA, Denison RF. (1998) Tracing the path of oxygen into birdsfoot trefoil and alfalfa nodules using iodine vapor. *Botanica Acta* **111**: 193-203.

Jenkins CLD, Furbank RT, Hatch MD. (1989) Inorganic carbon diffusion between C4 mesophyll and bundle sheath-cells - direct bundle sheath CO2 assimilation in intact leaves in the presence of an inhibitor of the C4 pathway. *Plant Physiology* **91**: 1356-1363.

Joubes J, Raffaele S, Bourdenx B, Garcia C, Laroche-Traineau J, Moreau P, Kotula L, Ranathunge K, Steudle E. (2009) Apoplastic barriers effectively block oxygen permeability across outer cell layers of rice roots under deoxygenated conditions: roles of apoplastic pores and of respiration. *New Phytologist* **184**: 909-917.

Krishnamurthy P, Ranathunge K, Franke R, Prakash HS, Schreiber L, Mathew MK. (2009) The role of root apoplastic transport barriers in salt tolerance of rice (*Oryza sativa* L.). *Planta* **230**: 119-134.

Kuo J, Canny MJ, O'Brien TP. 1974. Pit-field distribution, plasmodesmatal frequency, and assimilate flux in mestome sheath-cells of wheat leaves. *Planta* **121**: 97-118.

Ito Y, Kimura F, Hirakata K, Tsuda K, Takasugi T, Eiguchi M, Nakagawa K, Kurata N. (2011) Fatty acid elongase is required for shoot development in rice. *The Plant Journal* **66**: 680-688.

Laetsch WM. (1971) Chloroplast structural relationships in leaves of C4 plants. In: Hatch MD, Osmond CB, Slayter CO, eds. *Photosynthesis and photorespiration*. New York: Wiley Interscience, 323-349.

Lee SB, Jung SJ, Go YS, Kim HU, Kim JK, Cho HJ, Park OK, Suh MC. 2009. Two Arabidopsis 3-ketoacyl CoA synthase genes, KCS20 and KCS2/DAISY, are functionally redundant in cuticular wax and root suberin biosynthesis, but differentially controlled by osmotic stress. *The Plant Journal* **60**:462-475.

Lee Y, Rubio MC, Alassimone J, Geldner N. (2013) A Mechanism for Localized Lignin Deposition in the Endodermis. *Cell* **153**: 402-412.

Lendzian KJ. (2006) Survival strategies of plants during secondary growth: barrier properties of phellems and lenticels towards water, oxygen, and carbon dioxide. *Journal of Experimental Botany* **57**: 2535-2546.

Li P, Ponnala L, Gandotra N, *et al*. (2010) The developmental dynamics of the maize leaf transcriptome. *Nature Genetics* **42**: 1060-1067.

Matsumoto T, Wu JZ, Kanamori H *et al*. (2005) The map-based sequence of the rice genome. *Nature* **436**: 793-800.

Millar AA, Kunst L. (1997) Very-long-chain fatty acid biosynthesis is controlled through the expression and specificity of the condensing enzyme. *The Plant Journal* **12**: 121-131.

Molina I, Li-Beisson Y, Beisson F, Ohlrogge JB, Pollard, M. (2009) Identification of an Arabidopsis Feruloyl-Coenzyme A transferase required for suberin synthesis. *Plant Physiology* **151**: 1317-1328.

Mueller-Harvey I, Hartley RD, Harris PJ, Curzon EH. (1986) Linkage of para-coumaroyl and feruloyl groups to cell-wall polysaccharides of barley straw. *Carbohydrate Research* **148**: 71-85.

Naseer S, Lee Y, Lapierre C, Franke R, Nawrath C, Geldner N. (2012) Casparian strip diffusion barrier in Arabidopsis is made of a lignin polymer without suberin. *Proceedings of the National Academy of Sciences of the United States of America* **109**: 10101–10106.

Nelson T. (2011) Development of Leaves in C4 Plants: Anatomical Features That Support C4 Metabolism. In: Raghavendra AS, Sage RF, eds. C4 *Photosynthesis and Related CO2 Concentrating Mechanisms*, Vol. 32: Springer, Po Box 17, 3300 Aa Dordrecht, Netherlands, 147-159.

O'Brien TP, Carr DJ. (1970) A suberized layer in the cell walls of the bundle sheath of grasses. *Australian Journal of Biological Sciences* **23**: 275-283.

O'Brien TP, Kuo J. (1975) Development of the Suberized Lamella in the Mestome Sheath of Wheat Leaves. *Australian Journal of Botany* **23**: 783-794.

Oda Y, Iida Y, Kondo Y, Fukuda H. (2010) Wood Cell-Wall Structure Requires Local 2D-Microtubule Disassembly by a Novel Plasma Membrane-Anchored Protein. *Current Biology* **20**: 1197-1202.

Ohsugi R, Ueno O, Komatsu T, Sasaki H, Murata T. (1997) Leaf anatomy and carbon discrimination in NAD-malic enzyme Panicum species and their hybrids differing in bundle sheath cell ultrastructure. *Annals of Botany* **79**: 179-184.

Paterson AH, Bowers JE, Bruggmann R, *et al*. (2009) The *Sorghum bicolor* genome and the diversification of grasses. *Nature* **457**: 551-556.

Panikashvili D, Shi JX, Bocobza S, Franke RB, Schreiber L, Aharoni A. (2010) The Arabidopsis DSO/ABCG11 transporter affects cutin metabolism in reproductive organs and suberin in roots. *Molecular Plant* **3**: 563-575.

Perumalla CJ, Peterson CA, Enstone DE. (1990) A survey of angiosperm species to detect hypodermal Casparian bands. 1. Roots with a uniseriate hypodermis and epidermis. *Botanical Journal of the Linnean Society* **103**: 93-112.

Pesquet E, Korolev AV, Calder G, Lloyd CW. (2010) The Microtubule-Associated Protein AtMAP70-5 Regulates Secondary Wall Patterning in Arabidopsis Wood Cells. *Current Biology* **20**: 744-749.

Peterson CA, Griffith M, Huner NPA. (1985) Permeability of the suberized mestome sheath in winter rye. *Plant Physiology* **77**: 157-161.

Peterson CA, Murrmann M, Steudle E. (1993) Location of the major barriers to water and ion movement in young roots of *Zea-mays* L. *Planta* **190**: 127-136.

Pollard M, Beisson F, Li Y, Ohlrogge JB. (2008) Building lipid barriers: biosynthesis of cutin and suberin. *Trends in Plant Science* **13**: 236-246.

Pozuelo JM, Espelie KE, Kolattukudy PE. (1984) Magnesium-deficiency results in increased suberization in endodermis and hypodermis of corn roots. *Plant Physiology* **74**: 256-260.

Prendergast HDV, Hattersley PW, Stone NE. (1987) New structural biochemical associations in leaf blades of C4 grasses (Poaceae). *Australian Journal of Plant Physiology* **14**: 403-420.

Ralph J. (2010) Hydroxycinnamates in lignification. *Phytochemistry Reviews* **9**: 65-83.

Ralph J, Bunzel M, Marita J, Hatfield R, Lu F, Kim H, Schatz P, Grabber J, Steinhart H. (2004) Peroxidase-dependent cross-linking reactions of p-hydroxycinnamates in plant cell walls. *Phytochemistry Reviews* **3**: 79-96.

Ralph J, Quideau S, Grabber JH, Hatfield RD. (1994) Identification and synthesis of new ferulic acid dehydrodimers present in grass cell-walls. *Journal of the Chemical Society-Perkin Transactions* **1**: 3485-3498.

Ranathunge K, Schreiber L, Franke R. (2011) Suberin research in the genomics era-New interest for an old polymer. *Plant Science* **180**: 399-413.

Ranathunge K, Steudle E, Lafitte R. (2003) Control of water uptake by rice (*Oryza sativa* L.): role of the outer part of the root. *Planta* **217**: 193-205.

Ray DK, Mueller ND, West PC, Foley, JA. (2013) Yield trends are insufficient to double total crop production by 2050. *PLoS One* doi:10.1371/journal.pone0066248

Rensing SA, Lang D, Zimmer AD, *et al*. (2008). The *Physcomitrella* genome reveals evolutionary insights into the conquest of land by plants. *Science* **319**: 64-69.

Richardson A, Franke R, Kerstiens G, Jarvis M, Schreiber L, Fricke W. (2005) Cuticular wax deposition in growing barley (*Hordeum vulgare*) leaves commences in relation to the point of emergence of epidermal cells from the sheaths of older leaves. *Planta* **222**: 472-483.

Richardson A, Wojciechowski T, Franke R, Schreiber L, Kerstiens G, Jarvis M, Fricke W. (2007) Cuticular permeance in relation to wax and cutin development along the growing barley (*Hordeum vulgare*) leaf. *Planta* **225**: 1471-1481.

Robards AW, Robb ME. (1972) Uptake and binding of uranyl ions by barley roots. *Science* **178**: 980-982.

Robinson-Beers K, Evert RF. (1991a) Fine-structure of plasmodesmata in mature leaves of sugarcane. *Planta* **184**: 307-318.

Robinson-Beers K, Evert RF. (1991b) Ultrastructure of and plasmodesmatal frequency in mature leaves of sugarcane. *Planta* **184**: 291-306.

Roppolo D, De Rybel B, Tendon VD, Pfister A, Alassimone J, Vermeer JE, Yamazaki M, Stierhof YD, Beeckman T, Geldner N. (2011) A novel protein family mediates Casparian strip formation in the endodermis. *Nature* **473**: 380-383.

Russin WA, Evert RF, Vanderveer PJ, Sharkey TD, Briggs SP. (1996) Modification of a Specific Class of Plasmodesmata and Loss of Sucrose Export Ability in the *sucrose export defective1* Maize Mutant. *The Plant Cell* **8**: 645-658.

Sage RF. (2004) The evolution of C4 photosynthesis. *New Phytologist* **161**: 341-370.

Sage RF, Zhu XG. (2011) Exploiting the engine of C4 photosynthesis. *Journal of Experimental Botany* **62**: 2989-3000.

Schnable PS, Ware D, Fulton RS, *et al*. (2009) The B73 Maize Genome: Complexity, Diversity, and Dynamics. *Science* **326**: 1112-1115.

Schreiber L, Franke R, Hartmann KD, Ranathunge K, Steudle E. (2005a) The chemical composition of suberin in apoplastic barriers affects radial hydraulic conductivity differently in the roots of rice (*Oryza sativa* L. cv. IR64) and corn (*Zea mays* L. cv. Helix). *Journal of Experimental Botany* **56**: 1427-1436.

Schreiber L, Franke R, Lessire R. (2005b) Biochemical characterization of elongase activity in corn (*Zea mays* L.) roots. *Phytochemistry* **66**: 131-138.

Schreiber L, Hartmann K, Skrabs M, Zeier J. (1999) Apoplastic barriers in roots: chemical composition of endodermal and hypodermal cell walls. *Journal of Experimental Botany* **50**, 1267-1280.

Schreiber L, Skrabs, M., Hartmann, K., Becker, D., Cassagnet, C., and Lessiret, R. (2000) Biochemical and molecular characterization of corn (*Zea mays* L.) root elongases. *Biochemical Society Transactions* **28**: 647-649.

Sekhon RS, Lin HN, Childs KL, Hansey CN, Buell CR, de Leon N, Kaeppler SM. (2011) Genome-wide atlas of transcription during maize development. *The Plant Journal* **66**: 553-563.

Serra O, Hohn C, Franke R, Prat S, Molinas M, & Figueras M. (2010). A feruloyl transferase involved in the biosynthesis of suberin and suberin-associated wax is required for maturation and sealing properties of potato periderm. *The Plant Journal* **62**: 277-290.

Slewinski TL, Anderson AA, Zhang CK, Turgeon R. (2012) Scarecrow Plays a Role in Establishing Kranz Anatomy in Maize Leaves. *Plant and Cell Physiology* **53**: 2030-2037.

Soukup A, Armstrong W, Schreiber L, Franke R, Votrubova O. (2007) Apoplastic barriers to radial oxygen loss and solute penetration: a chemical and functional comparison of the exodermis of two wetland species, *Phragmites australis* and *Glyceria maxima*. *New Phytologist* **173**: 264-278.

Sowinski P, Szczepanik J, Minchin PEH. (2008) On the mechanism of C4 photosynthesis intermediate exchange between Kranz mesophyll and bundle sheath cells in grasses. *Journal of Experimental Botany* **59**: 1137-1147.

Taylor SH, Hulme SP, Rees M, Ripley BS, Woodward FI, Osborne CP. (2010) Ecophysiological traits in C-3 and C-4 grasses: a phylogenetically controlled screening experiment. *New Phytologist* **185**: 780-791.

Todd J, Post-Beittenmiller D, Jaworski JG. (1999) KCS1 encodes a fatty acid elongase 3-ketoacyl-CoA synthase affecting wax biosynthesis in *Arabidopsis thaliana*. *The Plant Journal* **17**: 119-130.

Tolley BJ, Sage TL, Langdale JA, Hibberd JM. (2012) Individual Maize Chromosomes in the C-3 Plant Oat Can Increase Bundle Sheath Cell Size and Vein Density. *Plant Physiology* **159**: 1418-1427.

Van Fleet DS. 1961. Histochemistry and function of the endodermis. *Botanical Review* **27**: 165-220.

Verrier PJ, Bird D, Burla B, *et al*. (2008) Plant ABC proteins - a unified nomenclature and updated inventory. *Trends in Plant Science* **13**: 151-159.

Vollbrecht E, Duvick J, Schares JP, *et al*. (2010) Genome-wide distribution of transposed *Dissociation* elements in maize. *The Plant Cell* **22**: 1667-1685.

von Caemmerer S, Furbank RT. (2003) The C4 pathway: an efficient CO2 pump. *Photosynthesis Research* **77**: 191-207.

Wang L, Czedik-Eysenberg A, Mertz RA, *et al*. (2014) Comparative analysis of C4 and C3 photosynthesis in developing leaves of maize and rice. *Nature Biotechnology* **32(11)**: 1158-1165.

Weiner H, Burnell JN, Woodrow IE, Heldt HW, Hatch MD. (1988) Metabolite diffusion into bundle sheath-cells from C4 plants - relation to C4 photosynthesis and plasmodesmatal function. *Plant Physiology* **88**: 815-822.

Wilson JR, Hattersley PW. (1983) *In vitro* digestion of bundle sheath-cells in rumen fluid and its relation to the suberized lamella and C4 photosynthetic type in *Panicum* species. *Grass and Forage Science* **38**: 219-223.

Xu X, Dietrich CR, Delledonne M, Xia Y, Wen TJ, Robertson DS, Nikolau BJ, Schnable PS. (1997) Sequence analysis of the cloned *glossy8* gene of maize suggests that it may code for a beta-ketoacyl reductase required for the biosynthesis of cuticular waxes. *Plant Physiology* **115**: 501-510.

Xu X, Dietrich CR, Lessire R, Nikolau BJ, Schnable PS. (2002) The Endoplasmic reticulum-associated maize GL8 protein is a component of the acyl-coenzyme A elongase ivolved in the production of cuticular waxes. *Plant Physiology* **128**: 924-934.

Yang W, Simpson JP, Li-Beisson Y, Beisson F, Pollard MR, Ohlrogge JB. (2012) A Land Plant-Specific Glycerol-3-Phosphate Acyltransferase Family in Arabidopsis: Substrate Specificity, *sn*-2 Preference and Evolution. *Plant Physiology* **160**: 638-652.

Yeats TH, Rose JKC. (2013) The Formation and Function of Plant Cuticles. *Plant Physiology* **163**: 5-20.

Yu DM, Ranathunge K, Huang H, Pei ZY, Franke R, Schreiber L, He CZ. (2008) *Wax Crystal-Sparse Leaf1* encodes a beta-ketoacyl CoA synthase involved in biosynthesis of cuticular waxes on rice leaf. *Planta* **228**: 675-685.

Zeier J, Ruel K, Ryser U, Schreiber L. (1999) Chemical analysis and immunolocalisation of lignin and suberin in endodermal and hypodermal/rhizodermal cell walls of developing maize (*Zea mays* L.) primary roots. *Planta* **209**: 1-12.

Zeier J, Schreiber L. (1998) Comparative investigation of primary and tertiary endodermal cell walls isolated from the roots of five monocotyledoneous species: chemical composition in relation to fine structure. *Planta* **206**: 349-361.

Zimmermann HM, Hartmann K, Schreiber L, Steudle E. (2000) Chemical composition of apoplastic transport barriers in relation to radial hydraulic conductivity of corn roots (*Zea mays* L.). *Planta* **210**: 302-311.

CHAPTER TWO

IDENTIFICATION OF SUBERIN BIOSYNTHESIS AND REGULATORY CANDIDATES IN MODEL GRASSES[2]

ABSTRACT

Ten-day-old leaves of maize, rice, and green millet (*Setaria viridis*) mature basipetally and encompass a complete sink-to-source gradient of gene expression. The bundle sheath cell wall also exhibits a developmental gradient, beginning with a primary cell wall at the leaf base and forming a suberized endodermoid wall as the leaf transitions to maturity. To identify suberin biosynthesis candidates for targeted mutagenesis, a putative biosynthetic pathway comprised of monomers from the maize root endodermis was generated. Homologues of previously characterized polyester biosynthesis genes from Arabidopsis were identified, indicating that the pathway is well conserved between monocots and dicots. A subset of candidate genes involved in very long chain fatty acid modification was co-expressed in a spatiotemporal pattern concurrent with bundle sheath suberization in all three grasses. This tightly delimited expression pattern was utilized to identify candidates for uncharacterized steps of suberin synthesis, including polymerization and transcriptional regulation. The very long chain fatty acid modifying genes and transcription factors were selected as promising candidates for targeted mutagenesis in maize and *Setaria viridis*.

INTRODUCTION

[2] Modified from Wang L, Czedik-Eysenberg A, Mertz, RA *et al.* (2014) *Nat Biotech* **32(11)**: 1158-1165.

A developing grass leaf matures basipetally, and, if sampled at the proper time point, forms a complete sink-to-source gradient (Evert *et al*., 1996; Li *et al*., 2010). A developmental gradient is also apparent in leaf tissues that undergo specialized secondary cell wall modifications, in particular deposition of the polyesters cutin and suberin. Cutin is deposited constitutively on the primary cell walls of expanding epidermal cells at the leaf base (Richardson *et al*., 2005). As cell expansion ceases and the tissue is displaced into drier air beyond the sheath of the preceding leaf, the cutin scaffold is augmented with a variety of hydrophobic waxes (Richardson *et al*., 2007). Likewise, both the bundle sheath (BS) and mestome sheath (MS) layers surrounding leaf veins begin their development with a thin polysaccharide primary cell wall, which is modified by the sequential deposition of a polyester suberin lamella and a lignocellulosic tertiary wall beneath the primary cell wall (Chapter 1, Figure 1.1; Evert *et al*., 1996).

Suberin is a heterogeneous polyester matrix with aliphatic and aromatic components (Bernards, 2002). Aliphatic suberin is comprised principally of fatty acids and their oxidized or reduced derivatives esterified to glycerol; major derivatives include ω-hydroxy fatty acids, mid-chain oxidized fatty acids, α,ω-dicarboxylic acids, and primary alcohols (Figure 2.1A; Pollard *et al*., 2008). Aromatic suberin is comprised of hydroxycinnamic acids, principally the monolignol precursors ferulic and *p*-coumaric acid (Figure 2.1B; Bernards & Lewis, 1998). Although suberin shares many common monomer components with cutin, the latter is enriched in very long chain ω-OH FAs ($>C_{20}$) and hydroxycinnamic acids across multiple plant taxa (Pollard *et al*., 2008). Maize (*Zea mays*) suberin monomer content has been profiled in both roots (Zeier *et al*., 1999; Schreiber *et al*., 2005) and bundle sheath strands (Espelie and Kolattukudy, 1979). In all tissues examined, omega-hydroxy fatty acids (ω-OH FAs) were the most abundant monomer class. In

Figure 2.1. Aliphatic and aromatic monomers of suberin and cutin.

A. Aliphatic monomer species.
B. Aromatic monomer species.

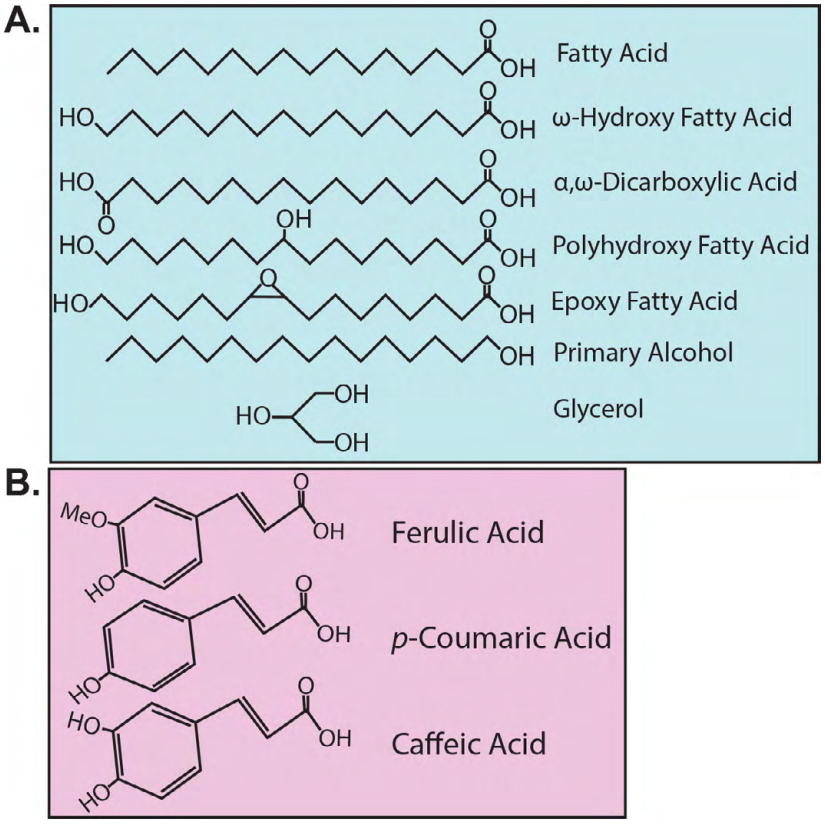
A.
Fatty Acid
ω-Hydroxy Fatty Acid
α,ω-Dicarboxylic Acid
Polyhydroxy Fatty Acid
Epoxy Fatty Acid
Primary Alcohol
Glycerol
B.
Ferulic Acid
p-Coumaric Acid
Caffeic Acid

both the BS and the root endodermis, long chain ω-OH FAs (ω-OH LCFA; $<C_{20}$) were most abundant, although significant quantities of very long chain ω-OH FAs (ω-OH VLCFA; $>C_{20}$) also accumulated. These monomers are also present in Arabidopsis (*Arabidopsis thaliana*) suberin (Franke *et al*., 2005). Thus, a similar biochemical pathway is likely required to synthesize suberin in grasses and Arabidopsis, and putative suberin biosynthesis genes can be predicted based on homology to characterized genes from model dicots.

Several suberin biosynthesis genes were recently characterized in the C_3 model plants Arabidopsis and potato (*Solanum tuberosum*; reviewed in Ranathunge *et al*., 2011). Comparatively little is known about the regulatory elements underlying suberin biosynthesis. At the outset of this research, no suberin biosynthesis or regulatory genes were characterized in any monocot. To identify promising candidates for mutagenesis, a putative biosynthesis pathway was generated using published monomer profiles of maize and rice root suberin. Biosynthesis genes were well conserved between model dicots and maize, rice (*Oryza sativa*), and green millet (*Setaria viridis*). Tightly delimited spatiotemporal expression of a subset of suberin biosynthesis candidates facilitated the identification of additional uncharacterized genes, including a candidate suberin synthase and several putative transcriptional regulators. Most candidates are expressed in both leaf and root tissues, suggesting that bundle sheath and endodermal cell wall differentiation proceeds similarly. The Casparian Strip genes are a notable exception, and are not expressed in leaves. There is also genetic overlap between suberin and cutin biosynthetic pathways within leaves. The implications for targeted mutagenesis to generate a suberin-specific phenotype are discussed.

RESULTS

Delineation of a putative suberin and cutin biosynthesis pathway in maize and rice leaves

In order to identify candidates for targeted mutagenesis, a putative suberin biosynthesis pathway was constructed for maize and rice using published root endodermal monomer profiles (Zeier *et al*., 1999; Schreiber *et al*., 2005). The inferred steps of polyester biosynthesis are comparable to the pathway described for model dicots (Ranathunge *et al*., 2011), and are presented in Figure 2.2. Following *de novo* fatty acid synthesis in the plastid, long chain fatty acid (LCFA; $C_{16:0}$-$C_{18:0}$; $C_{18:1}$) precursors are converted to acyl-CoA thioesters by a long chain acyl-CoA synthetase (LACS). Within the endoplasmic reticulum, LCFA are oxidized to ω-OH LCFA by cytochrome P450s from the CYP86A subfamily. ω-OH LCFA may be oxidized by an unknown enzyme to produce α,ω-dicarboxylic acids (DCA). A subset of ω-OH LCFA undergo additional mid-chain oxidation events to produce poly-hydroxy and epoxy species (Figure 2.1; refer to Chapter 1, Figure 1.3).

Alternatively, LCFA may be elongated to very long chain fatty acids (VLCFA; $C_{22:0}$-$C_{30:0}$) by the fatty acid elongase complex. The FAE is comprised of a ketoacyl-CoA synthase (KCS), a ketoacyl-CoA reductase (KCR), a hydroxyacyl-CoA dehydrase (HACD), and an enoyl-CoA reductase (ECR). Both LCFA and VLCFA derivatives can be reduced to primary alcohols by fatty acyl-CoA reductase (FAR) or esterified to glycerol-3-phosphate (G3P) by glycerol-3-phosphate acyltransferase (GPAT) to produce *sn*-2 monoacylglycerol (2-MAG). In the cytosol, aliphatic suberin feruloyl transferase (ASFT) can esterify the monolignol precursor ferulic acid to ω-OH FA and primary alcohols of various chain lengths to form acyl ferulates. Monomers reach the plasma membrane by an unknown mechanism and are

Figure 2.2. A putative pathway for maize and rice suberin biosynthesis.

Green text denotes suberin monomers detected in both maize and rice; monomers listed in black are found exclusively in maize (Zeier *et al*., 1999; Schreiber *et al*., 2005). The blue line denotes the biochemical pathway of the very long chain fatty acid modifying genes presented in Figure 2.5. Red and violet numbers indicate maize and rice genes, respectively, with peak expression at leaf base. Blue numbers indicate maize genes with peak expression proximal to the point of emergence, which are predicted to contribute to suberin or wax biosynthesis. Teal numbers indicate rice genes with peak expression proximal to the point of emergence. Purple and navy numbers designate all other expression patterns, including those not expressed in leaf tissues. The picture on the right shows an electron-microscopic image of maize BS/ME interface with a suberized BS (indicated by arrow). Gene nomenclature is based on Arabidopsis conventions. ω-OH, omega-hydroxy fatty acid; DCA, alpha-omega dicarboxylic acid; -OH, primary fatty alcohol; ACP, acyl carrier protein; ASFT, aliphatic suberin feruloyl transferase; CYP, cytochrome P450 hydroxylase/monooxygenase; ECR, enoyl-CoA reductase; FAR, fatty acid reductase; GDSL, glycine-aspartic acid-serine-leucine motif lipase/hydrolase; GPAT, glycerol-3-phosphate acyltransferase; HACD, hydroxyacyl-CoA dehydrase; KCS, ketoacyl-CoA synthase; KCR, ketoacyl-CoA reductase; LACS, long chain acyl-CoA synthetase; MAG, monoacylglycerol.

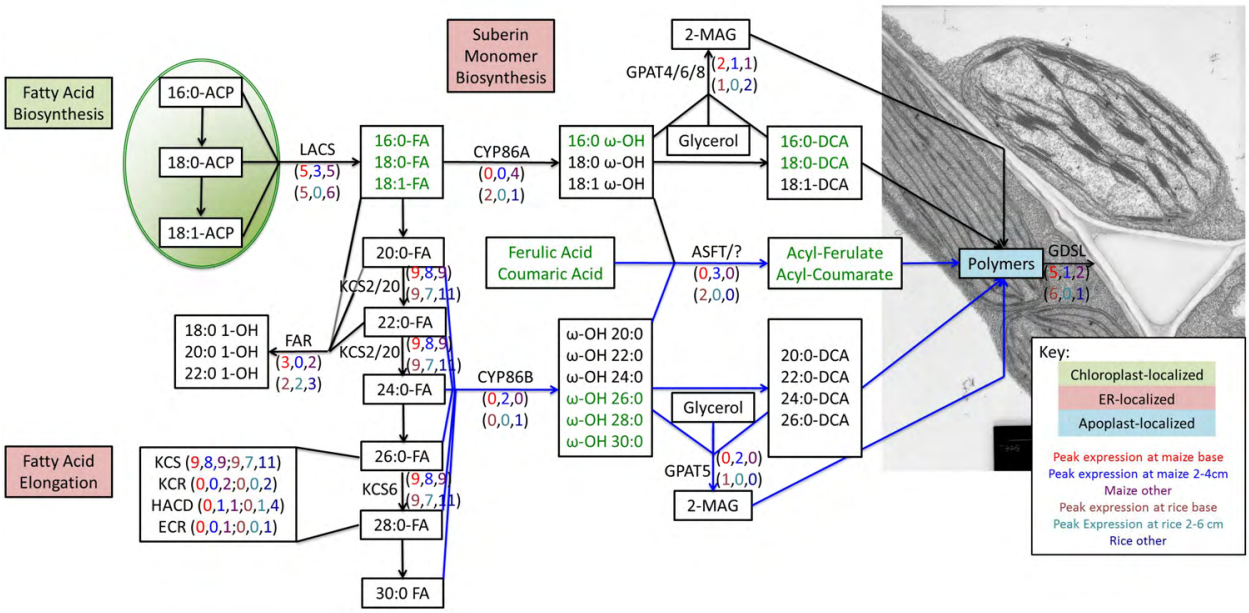
Fatty Acid Biosynthesis
16:0-ACP
18:0-ACP
18:1-ACP
LACS
(5,3,5)
(5,0,6)
16:0-FA
18:0-FA
18:1-FA
Suberin Monomer Biosynthesis
CYP86A
(0,0,4)
(2,0,1)
16:0 ω-OH
18:0 ω-OH
18:1 ω-OH
2-MAG
GPAT4/6/8
(2,1,1)
(1,0,2)
Glycerol
16:0-DCA
18:0-DCA
18:1-DCA
20:0-FA
KCS2/20
(9,8,9)
(9,7,11)
22:0-FA
24:0-FA
18:0 1-OH
20:0 1-OH
22:0 1-OH
FAR
(3,0,2)
(2,2,3)
Ferulic Acid
Coumaric Acid
ASFT/?
(0,3,0)
(2,0,0)
Acyl-Ferulate
Acyl-Coumarate
Polymers
GDSL
(5,1,2)
(6,0,1)
CYP86B
(0,2,0)
(0,0,1)
ω-OH 20:0
ω-OH 22:0
ω-OH 24:0
ω-OH 26:0
ω-OH 28:0
ω-OH 30:0
Glycerol
20:0-DCA
22:0-DCA
24:0-DCA
26:0-DCA
GPAT5
(0,2,0)
(1,0,0)
2-MAG
Fatty Acid Elongation
KCS (9,8,9;9,7,11)
KCR (0,0,2;0,0,2)
HACD (0,1,1;0,1,4)
ECR (0,0,1;0,0,1)
26:0-FA
KCS6
(9,8,9)
(9,7,11)
28:0-FA
30:0 FA
Key:
Chloroplast-localized
ER-localized
Apoplast-localized
Peak expression at maize base
Peak expression at maize 2-4cm
Maize other
Peak expression at rice base
Peak Expression at rice 2-6 cm
Rice other

putatively exported by ATP-binding cassette subfamily G (ABCG) members. Polyesters may be synthesized by a GDSL-like lipase/acylhydrolase (GDSL) similar to tomato (*Solanum lycopersicum*) CUTIN SYNTHASE1 (SlCUS1).

As the objective was to identify candidates that would yield a severe but specific defect in suberin polyester synthesis, a subset of candidate gene families encoding fatty acid ω-hydroxylases (*CYP86A* and *CYP86B*), glycerol-3-phosphate acyltransferases (*GPAT4/6/8* and *GPAT5*), and aliphatic suberin feruloyl transferases (*ASFT*) were selected for further analysis. The putative dicot homologues of these genes are specifically involved in suberin or cutin monomer biosynthesis, with no reported pleiotropic effects on other aspects of acyl lipid metabolism (Ranathunge *et al*., 2011). In maize, rice, and millet these candidates form small, monophyletic gene families with low degrees of paralogous duplication (Figure 2.3-2.4; Chapter 3, Figure 3.1A). Thus, disruption of these candidates by targeted reverse genetics is much more practical than for the large, redundant KCS gene family.

Suberin and cutin-specific fatty acid modification genes are well conserved between grasses and model dicots

Candidate fatty acid ω-hydroxylase genes

Fatty acids destined for polyester synthesis frequently undergo oxidation events following export from the plastid or, in the case of very long chain species, release from the fatty acid elongase complex. Members of the Cytochrome P450 (CYP450) monooxygenase superfamily catalyze the ω-hydroxylation of fatty acids destined for incorporation into suberin and cutin polyesters (reviewed in Pinot *et al.*, 2011). ω-OH FA, which bear a hydroxyl group on the terminal methyl residue of the acyl chain opposite the carboxyl terminus (Figure 2.1), are the

most abundant aliphatic monomer component of most suberins, including maize and rice, and are the putative precursor of α,ω-DCA, the second most abundant aliphatic component (Schreiber *et al*., 2005; Pollard *et al*., 2008; Beisson *et al*., 2012). In vegetative organs, all suberin and cutin fatty acid ω-hydroxylases characterized to date are members of the CYP86 subfamily; CYP86A members exhibit a substrate preference for long chain fatty acids ($> C_{20}$), whereas CYP86B proteins preferentially hydroxylate very long chain species ($\leq C_{20}$; reviewed in Beisson *et al*., 2012).

In model dicots, CYP86A proteins can be grouped into two phylogenetically distinct sub-clades (Pinot & Beisson, 2011). Members of the first sub-clade are expressed in aerial tissues and contribute to cuticle biosynthesis (*AtCYP86A2*, *AtCYP86A4*, and *AtCYP86A8*), whereas the second, smaller sub-clade contains genes that contribute to suberin synthesis and are expressed in subterranean organs (*AtCYP86A1* and its potato orthologue *StCYP86A33*; Hofer *et al*., 2008; Serra *et al*., 2009; Figure 2.3A). A Neighbor-Joining tree populated by the characterized dicot genes plus putative homologues from maize, rice, *Setaria italica*, and *Setaria viridis* was constructed (Figure 2.3A). The structure of the CYP86A subfamily is well conserved between monocots and dicots. One sub-clade, containing the paralogues *ZmCyp86A34* and *ZmCyp86A36*, *OsCYP86A9, SiCYP86A39,* and *SvCYP86A42*, contains likely orthologues of the suberin-specific *CYP86A* genes from model dicots (Figure 2.3A). Interestingly, none of the maize or millet genes in this sub-clade are expressed during leaf development; the expression data from the maize gene atlas suggests that they are expressed exclusively in roots during vegetative development (Figure 2.3B,D; Sekhon *et al*., 2011; Stelpflug *et al*., 2015). The single rice orthologue, *OsCYP86A9*, is expressed strongly near the leaf base (Figure 2.3C). For the three Panicoid grass species, all

Figure 2.3. Putative fatty acid ω-hydroxylases of model grasses.

A. Rooted Neighbor-Joining phylogeny of CYP86 subfamily members from maize, rice, millet, and model dicots (Saitou & Nei, 1987). OsCYP704B2, a rice CYP450 involved in anther cutin biosynthesis (Li *et al*., 2010), serves as an outgroup. Bootstrap support (1000 replicates) is shown next to the corresponding branches (Felsenstein, 1985). The tree is drawn to scale, with branch lengths in the same units as those of the evolutionary distances used to infer the phylogenetic tree. The evolutionary distances were computed using the Poisson correction method (Zuckerkandl & Pauling, 1965) and are presented as the number of amino acid substitutions per site. Evolutionary analyses were conducted in MEGA6 (Tamura *et al*., 2013). Gene names marked with an asterisk are provisional names not yet curated by the CYP450 Nomenclature Committee.
B. Expression of *CYP86A* and *CYP86B* genes in maize during third leaf development. *CYP86A* sub-family members are red, *CYP86B* sub-family members are blue. Expression is presented in reads per kilobase per million reads (RPKM).
C. Expression of *CYP86A* and *CYP86B* genes in rice during third leaf development.
D. Expression of *CYP86A* and *CYP86B* genes in *Setaria viridis* during third leaf development.

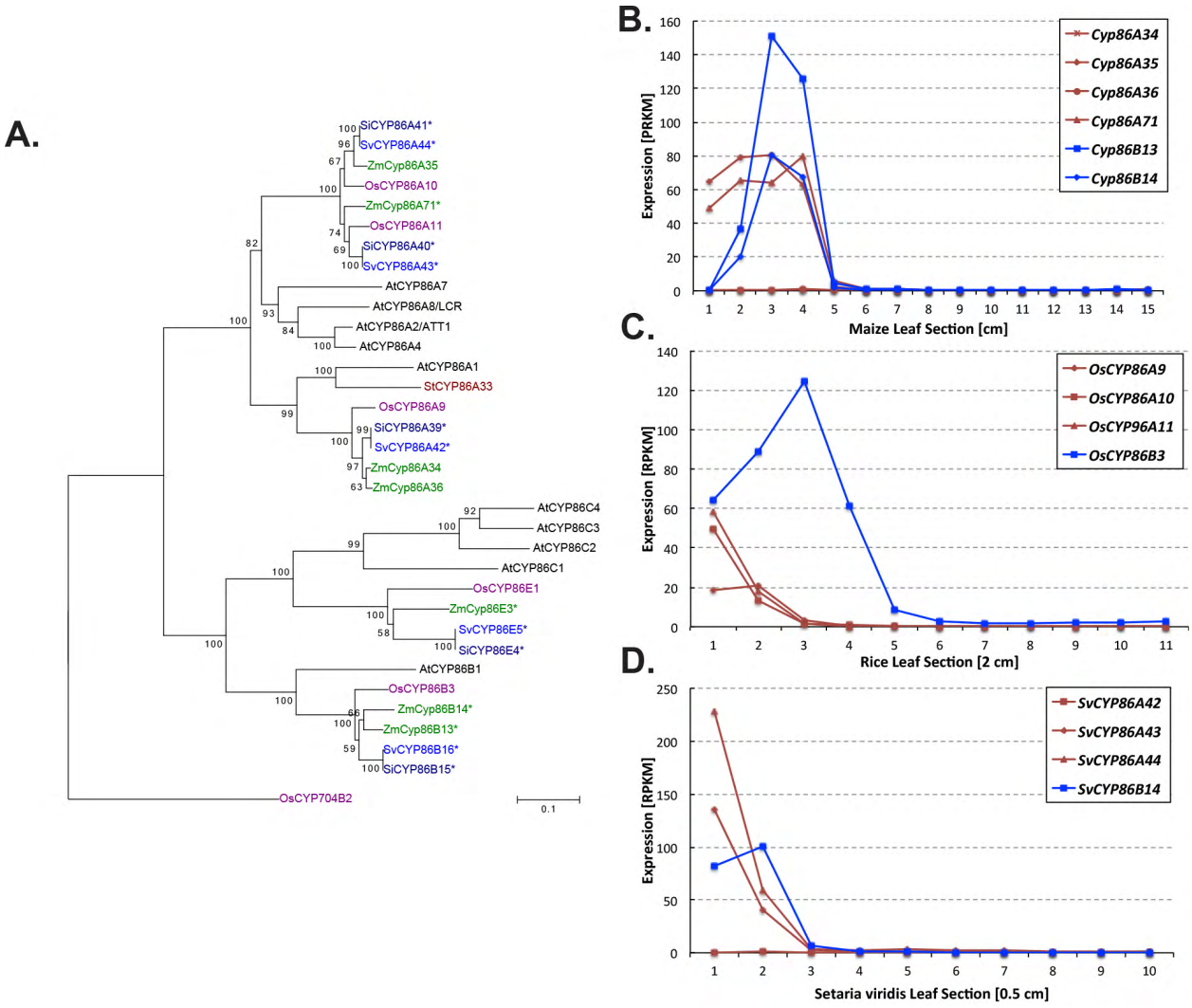
A.
SiCYP86A41*
SvCYP86A44*
ZmCyp86A35
OsCYP86A10
ZmCyp86A71*
OsCYP86A11
SiCYP86A40*
SvCYP86A43*
AtCYP86A7
AtCYP86A8/LCR
AtCYP86A2/ATT1
AtCYP86A4
AtCYP86A1
StCYP86A33
OsCYP86A9
SiCYP86A39*
SvCYP86A42*
ZmCyp86A34
ZmCyp86A36
AtCYP86C4
AtCYP86C3
AtCYP86C2
AtCYP86C1
OsCYP86E1
ZmCyp86E3*
SvCYP86E5*
SiCYP86E4*
AtCYP86B1
OsCYP86B3
ZmCyp86B14*
ZmCyp86B13*
SvCYP86B16*
SiCYP86B15*
OsCYP704B2
0.1
B.
Expression [PRKM]
Maize Leaf Section [cm]
Cyp86A34
Cyp86A35
Cyp86A36
Cyp86A71
Cyp86B13
Cyp86B14
C.
Expression [RPKM]
Rice Leaf Section [2 cm]
OsCYP86A9
OsCYP86A10
OsCYP96A11
OsCYP86B3
D.
Expression [RPKM]
Setaria viridis Leaf Section [0.5 cm]
SvCYP86A42
SvCYP86A43
SvCYP86A44
SvCYP86B14

CYP86A genes with significant leaf expression are members of the second sub-clade containing putative orthologues of the cutin-related Arabidopsis CYP86A proteins (Figure 2.3A). This clade contains two genes from each grass species; in rice and the two millet species, both genes are strongly expressed at the leaf base, whereas the maize orthologues are broadly expressed throughout the entire region from the leaf base to the transition zone 3-4 cm above the leaf base where nascent suberin lamellae first appear (Li *et al*., 2010).

The CYP86B subfamily contains a single candidate gene in rice, *Setaria viridis*, and *Setaria italica*, and is paralogously duplicated in maize (Figure 2.3A). Both maize paralogues are strongly and specifically expressed 2-4 cm above the leaf base immediately preceding the transition zone, as is their *Setaria viridis* orthologue, which peaks 0.5-1 cm from the leaf base (Figure 2.3B,D). The single rice orthologue is strongly expressed throughout the transition zone, suggesting that it may have additional functions in addition to suberin biosynthesis (Figure 2.3C). None of the dicot-specific CYP86C or monocot-specific CYP86E sub-family members have been characterized to date. Expression data from the maize transcriptome atlas suggests that *ZmCyp86E3* is expressed exclusively in tassels and developing seeds (Sekhon *et al*., 2011; Stelpflug *et al*., 2015).

Candidate glycerol-3-phosphate acyltransferases

Following synthesis by CYP86 proteins, ω-OH FA can undergo additional acylation reactions to form various esterified oligomers. In Arabidopsis, both CYP86A1 and CYP86B1 can provide ω-OH fatty acyl-CoA substrates to *sn*-glycerol-3-phosphate 2-acyltransferase (GPAT), which generates 2-monoacylglycerol (2-MAG) precursors for polymer biosynthesis (Li *et al*., 2007; Molina *et al*., 2009). The eight Arabidopsis GPATs exhibiting *sn2*-acyltransferase

activity group into three phylogenetic clades: a cutin-specific clade (*AtGPAT4*, *GPAT6*, and *GPAT8*), a suberin-specific clade (*AtGPAT5* and *GPAT7*), and a third clade of unknown biochemical function (*AtGPAT1-3*; Yang *et al*., 2012; Figure 2.4). Suberin-related GPATs are not expressed in the epidermis, exhibit a unique substrate preference for VLCFA derivatives, and are well conserved across all clades of vascular plants sampled to date (Beisson *et al*., 2007; Yang *et al*., 2012). Thus, the maize and millet *GPAT5* orthologues are ideal mutagenesis candidates with which to generate a BS-specific suberin defect. Putative maize, rice, and millet homologues of AtGPAT5 and AtGPAT6 proteins were identified and their phylogenetic relationship to was evaluated using a Neighbor-Joining tree (Figure 2.4). The results were in good agreement with a previously published phylogeny of the GPATs (Yang *et al*., 2012). The cutin-specific clade (GPAT4/6/8 Clade, Figure 2.4) formed a monophyletic group containing three genes from each species. All grass proteins belonging to this group contain the diagnostic phosphatase motifs required to convert 2-lysophosphatidic acid to 2-MAG, which are specific to the cutin-related GPAT subfamily (**D**X**D**X[T/V][L/V][D/S] and **K**-[G/S][**D**/S]XXX[**D**/N]; Yang *et al*., 2010; Yang *et al*., 2012). All three putative homologues of *AtGPAT6* are strongly expressed at the leaf base concurrently with cutin biosynthesis (Figure 2.5A-C).

The suberin-specific clade (GPAT5/7 Clade, Figure 2.4) forms a small, monophyletic group containing no more than two proteins per species. The suberin clade also contains a diagnostic sequence motif; the essential aspartate and lysine residues of the phosphatase domain are mutated, facilitating unambiguous identification of the grass GPAT5 orthologues (**E**X**E**X[T/V][L/V][D/S] and [**L**/**V**-[G/S][**K**/G/R]XXX[**T**/A]; Yang *et al*., 2010).

Figure 2.4. Putative glycerol-3-phosphate acyltransferases of model grasses.

Unrooted Neighbor-Joining phylogeny of suberin and cutin-related GPAT subfamily members from maize, rice, millet, and model dicots (Saitou & Nei, 1987). The tree was generated using MEGA6 (Tamura *et al*., 2013) as described in Figure 2.2.

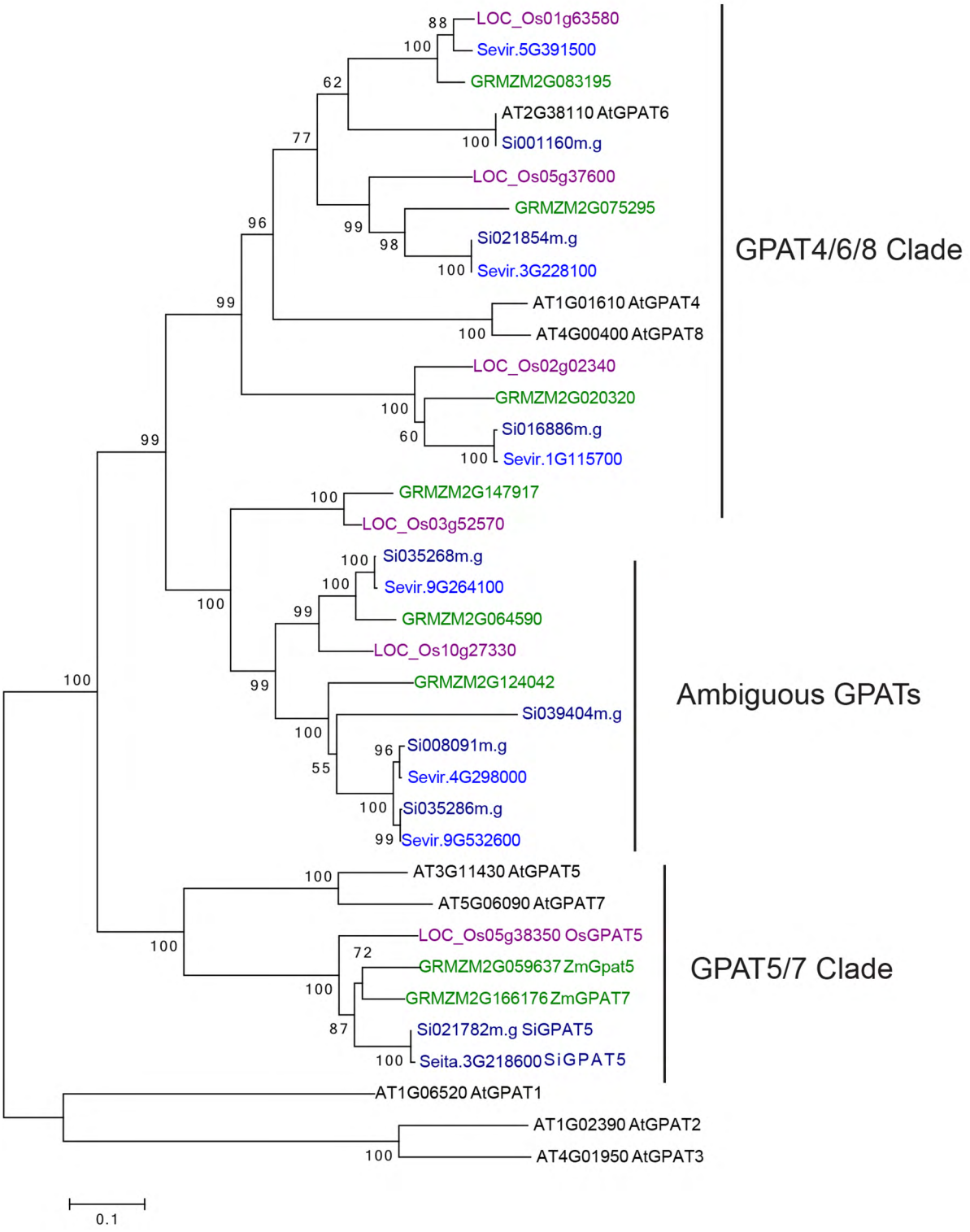
LOC_Os01g63580
Sevir.5G391500
GRMZM2G083195
AT2G38110 AtGPAT6
Si001160m.g
LOC_Os05g37600
GRMZM2G075295
Si021854m.g
Sevir.3G228100
AT1G01610 AtGPAT4
AT4G00400 AtGPAT8
LOC_Os02g02340
GRMZM2G020320
Si016886m.g
Sevir.1G115700
GPAT4/6/8 Clade
GRMZM2G147917
LOC_Os03g52570
Si035268m.g
Sevir.9G264100
GRMZM2G064590
LOC_Os10g27330
GRMZM2G124042
Si039404m.g
Si008091m.g
Sevir.4G298000
Si035286m.g
Sevir.9G532600
Ambiguous GPATs
AT3G11430 AtGPAT5
AT5G06090 AtGPAT7
LOC_Os05g38350 OsGPAT5
GRMZM2G059637 ZmGpat5
GRMZM2G166176 ZmGPAT7
Si021782m.g SiGPAT5
Seita.3G218600 SiGPAT5
GPAT5/7 Clade
AT1G06520 AtGPAT1
AT1G02390 AtGPAT2
AT4G01950 AtGPAT3
0.1

Figure 2.5 Cutin biosynthesis candidates are strongly expressed near the leaf base in model grasses.

A. Expression of cutin biosynthesis candidates in maize during third leaf development. Gene names are as described in Figure 2.2. Expression is presented in reads per kilobase per million reads (RPKM).
B. Expression of cutin biosynthesis candidates in rice during third leaf development.
C. Expression of cutin biosynthesis candidates in *Setaria viridis* during third leaf development.
D. Maize and rice cutin candidates are both expressed near the leaf base. Gene expression [RPKM] is plotted against a Unified Developmental Gradient (Wang *et al*., 2014) that accounts for variation between developmental time-points in maize and rice.

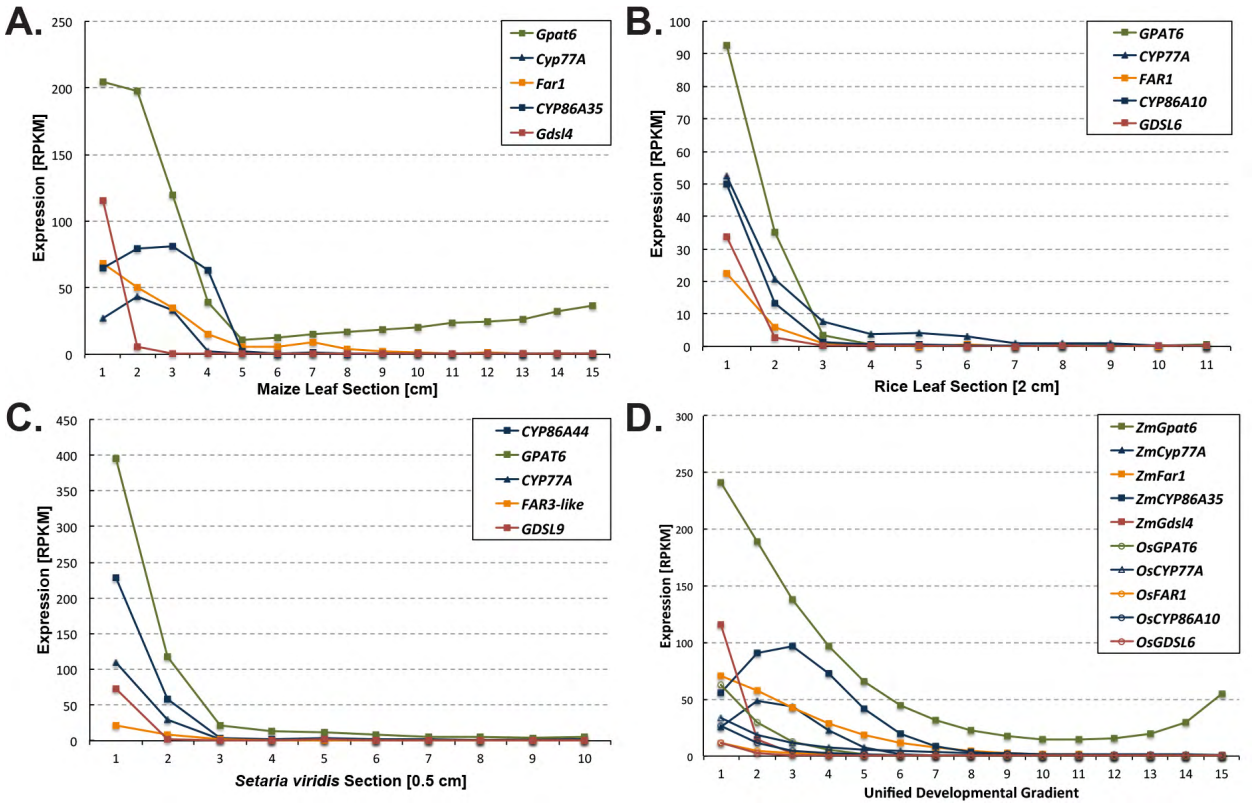
A.
Expression [RPKM]
Maize Leaf Section [cm]
Gpat6
Cyp77A
Far1
CYP86A35
Gdsl4
B.
Expression [RPKM]
Rice Leaf Section [2 cm]
GPAT6
CYP77A
FAR1
CYP86A10
GDSL6
C.
Expression [RPKM]
Setaria viridis Section [0.5 cm]
CYP86A44
GPAT6
CYP77A
FAR3-like
GDSL9
D.
Expression [RPKM]
Unified Developmental Gradient
ZmGpat6
ZmCyp77A
ZmFar1
ZmCYP86A35
ZmGdsl4
OsGPAT6
OsCYP77A
OsFAR1
OsCYP86A10
OsGDSL6

All maize, rice, and millet genes of the suberin clade are expressed concurrently with vascular sheath suberization (Figure 2.6A-C).

We also observed a grass-specific clade sister to the GPAT4/6/8 Clade (Ambiguous GPATs, Figure 3.4). Although the first conserved phosphatase motif was present in the Ambiguous GPATs, the critical lysine and aspartate residues of the second conserved phosphatase motif were mutated (data not shown). Members of this clade were broadly expressed in leaves, but there was no obvious pattern of transcript accumulation within the group (data not shown). Although the Arabidopsis GPAT1-3 Clade also contains a partially mutated phosphatase domain (Yang *et al*., 2012), the Ambiguous GPATs were clearly resolved from the AtGPAT1-3 Clade in the Neighbor-Joining tree (Figure 2.4). The function of these genes is not apparent from the expression data.

Candidate Hydroxycinnamoyl-CoA acyltransferases

The ω-hydroxyl group of ω-OH FA can also act as an acyl acceptor to various hydroxycinnamoyl-CoA donors. These reactions are catalyzed by BAHD acyltransferases, which utilize CoA-thioesters of hydroxycinnamic acids to generate acyl ferulates, coumarates, or caffeates (reviewed by Molina and Kosma, 2015). The maize *Aliphatic suberin feruloyl transferase* genes are the focus of Chapter 3, and further analysis of these genes is presented therein. Although the Arabidopsis genome contains separate genes encoding cutin and suberin feruloyl transferases (Molina *et al*., 2009; Rautengarten *et al*., 2012), all of the grass genes belonging to the *ASFT* sub-clade are expressed concurrently with BS suberization (Figure 2.6).

Figure 2.6. A subset of VLCFA-modifying genes are expressed concurrently with BS suberization.

A. Expression of suberin biosynthesis candidates in maize during third leaf development. Gene names are as described in Figure 2.2. Expression is presented in reads per kilobase per million reads (RPKM).
B. Expression of suberin biosynthesis candidates in rice during third leaf development.
C. Expression of suberin biosynthesis candidates in *Setaria viridis* during third leaf development.
D. Maize and rice suberin candidates are differentially expressed. Gene expression [RPKM] is plotted against a Unified Developmental Gradient (Wang *et al*., 2014) that accounts for variation between developmental time-points in maize and rice.

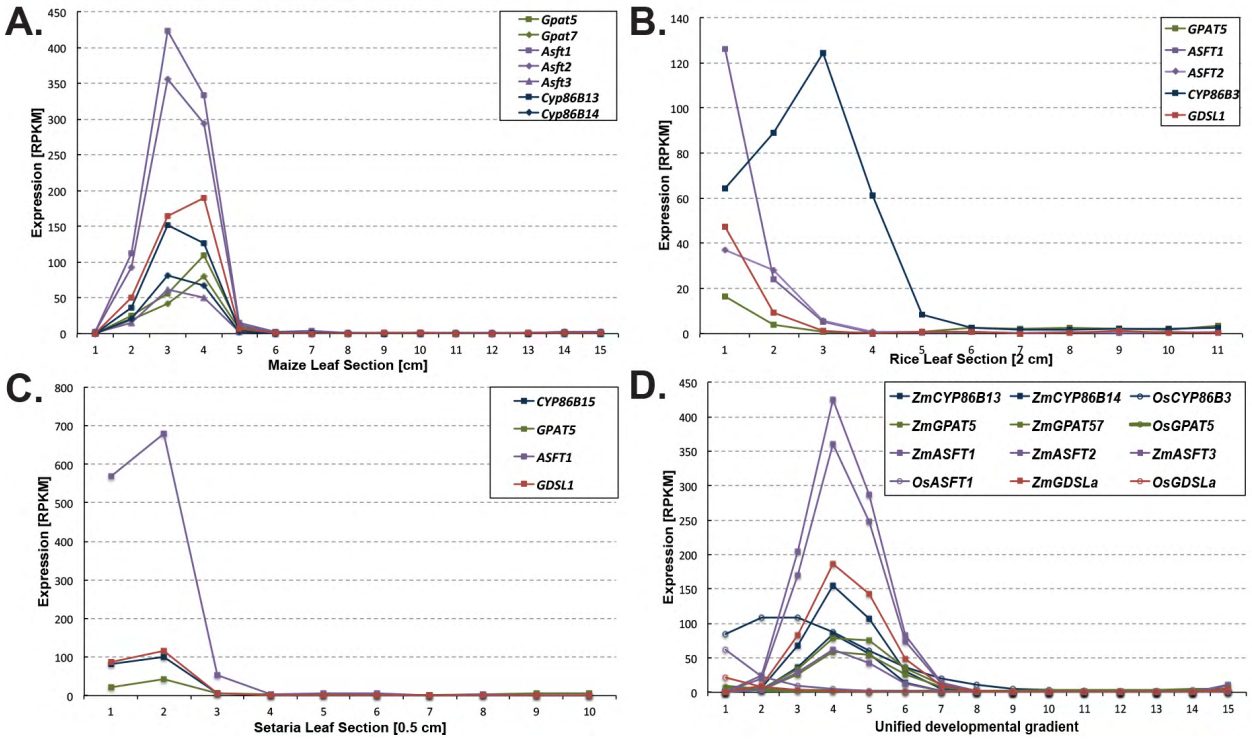
A.
Expression [RPKM]
Maize Leaf Section [cm]
Gpat5
Gpat7
Asft1
Asft2
Asft3
Cyp86B13
Cyp86B14
B.
Expression [RPKM]
Rice Leaf Section [2 cm]
GPAT5
ASFT1
ASFT2
CYP86B3
GDSL1
C.
Expression [RPKM]
Setaria Leaf Section [0.5 cm]
CYP86B15
GPAT5
ASFT1
GDSL1
D.
Expression [RPKM]
Unified developmental gradient
ZmCYP86B13
ZmCYP86B14
OsCYP86B3
ZmGPAT5
ZmGPAT57
OsGPAT5
ZmASFT1
ZmASFT2
ZmASFT3
OsASFT1
ZmGDSLa
OsGDSLa

A suite of very long chain fatty acid modifying genes are co-expressed concurrently with sheath suberization in maize, rice, and *Setaria viridis*

Putative grass homologues of the glycerol-3-phosphate acyltransferase At*GPAT5*, the fatty acid ω-hydroxylase At*CYP86B1*, and the ω-hydroxyacid O-feruloyl transferase At*ASFT/HHT* were identified as the most likely mutagenesis candidates to generate a suberin-specific polymer defect. All three genes were identified as essential components of suberin biosynthesis as loss of function alleles and show suberin-specific mutant phenotypes in Arabidopsis (Beisson *et al*., 2007; Compagnon *et al*., 2009; Gou *et al*., 2009; Molina *et al*., 2009). Furthermore, VLCFA derivatives ($\geq C_{20}$) and hydroxycinnamic acids are specifically enriched in suberin relative to cutin across broad plant taxa, whereas LCFA derivatives (C_{16}-C_{18}) are abundant in both polymers (reviewed in Pollard *et al*., 2008). In maize, two paralogously duplicated, unlinked loci show strong homology to each Arabidopsis gene (Figure 2.6A). Transcripts for these genes peak in abundance in the transition zone 2-4 cm above the leaf base, and then decline sharply (Figure 2.6A). Peak expression of the *ZmAsft* and *ZmCyb86B* genes occurs prior to *ZmGpat5* and *ZmGpat7,* and suggests aromatic suberin is synthesized prior to aliphatics, as previously suggested (Lulai & Morgan, 1992; Naseer *et al*., 2011). The developmental gradients of rice and green millet are shifted toward greater maturity at the leaf base and do not have sufficient resolution to determine whether *ASFT* expression precedes *GPAT5* across multiple grass taxa. However, the suberin biosynthesis candidates are co-expressed within a tight spatiotemporal window across all three grass species (Figure 2.6B-C). In rice, the suberin biosynthesis candidates reached peak expression at the leaf base rather than in the transition zone (Figure 2.6B). When a cluster analysis of maize and rice expression values was carried out and plotted against a unified developmental gradient that accounted for variation

in tissue age, suberin biosynthesis candidates were differentially expressed between species (Figure 2.6D; Wang *et al*., 2014). These results suggest that developmental trajectories may differ for bundle and mestome sheaths.

The tight spatiotemporal association of putative suberin biosynthetic genes facilitated the identification of additional candidates via a "guilt by association" approach. One of the co-expressed genes identified by cluster analysis encoded a putative GDSL lipase/acylhydrolase related to the recently characterized tomato cutin synthase *SlCD1*/*CUS1* that polymerizes cutin monomers in the apoplast (Isaacson *et al*., 2009; Yeats *et al*., 2012). This gene, tentatively named *GDSL1*, was co-expressed with the suberin biosynthesis candidates in all three species (Figure 2.6A-C). In order to evaluate the phylogenetic relationship between the monocot GDSL proteins and previously characterized dicot homologues, a Neighbor-Joining tree was generated using a set of published Arabidopsis and tomato CUS proteins as a scaffold (Yeats *et al*., 2014). The *GDSL1* sub-clade is a monophyletic group containing a single sequence from maize, rice, and millet (Figure 2.7). The monocot *GDSL1* sub-clade is sister to a group of three uncharacterized dicot sequences (At3g50400, At2g23540, and Solyc02g090210). The GDSL1 sub-clade is clearly resolved from the CUS Clade, which contains four to seven putative homologues of *SlCUS1* in maize, rice, and millet (Figure 2.7). With the exception of *ZmGdsl3* and *OsGDSL3*, which are constitutively expressed at low levels throughout leaf development (data not shown), all members of the *CUS* Clade are strongly expressed at the leaf base concurrently with other candidate genes of cutin biosynthesis (Figure 2.6A-D).

Figure 2.7. Putative suberin and cutin synthases of model grasses.

Unrooted Neighbor-Joining phylogeny of the Cutin Synthase-like (CUS) Clade (Yeats et al., 2014) and related proteins from maize, rice, millet, and model dicots (Saitou & Nei, 1987). The CUS Clade and putative suberin synthase proteins (GDSL1 clade) are annotated. Bootstrap support (1000 replicates) is shown next to the corresponding branches (Felsenstein, 1985). Evolutionary analyses were conducted in MEGA6 (Tamura *et al*., 2013) as described in Figure 2.3.

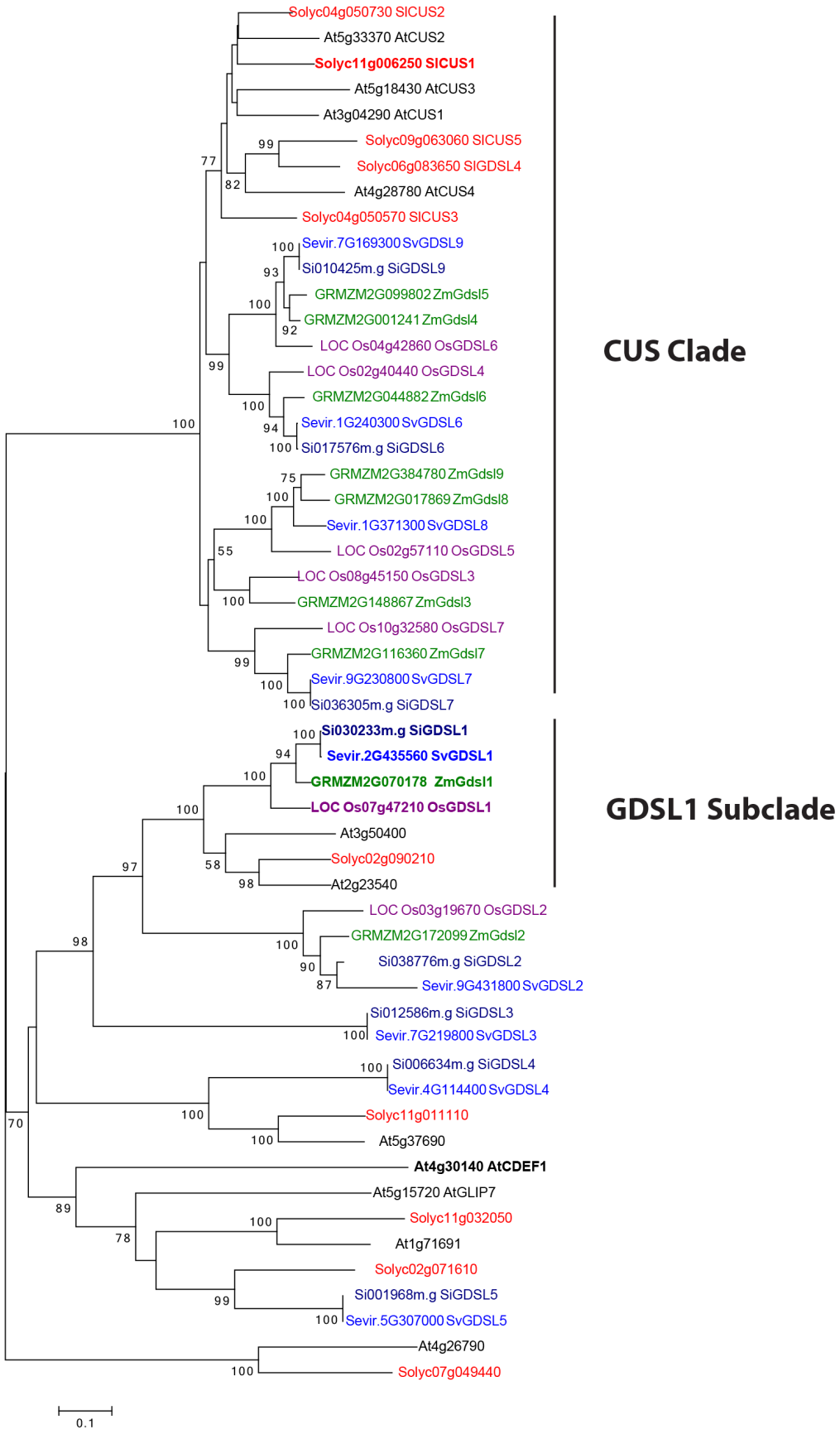
Solyc04g050730 SlCUS2
At5g33370 AtCUS2
Solyc11g006250 SlCUS1
At5g18430 AtCUS3
At3g04290 AtCUS1
Solyc09g063060 SlCUS5
Solyc06g083650 SlGDSL4
At4g28780 AtCUS4
Solyc04g050570 SlCUS3
Sevir.7G169300 SvGDSL9
Si010425m.g SiGDSL9
GRMZM2G099802 ZmGdsl5
GRMZM2G001241 ZmGdsl4
LOC Os04g42860 OsGDSL6
LOC Os02g40440 OsGDSL4
GRMZM2G044882 ZmGdsl6
Sevir.1G240300 SvGDSL6
Si017576m.g SiGDSL6
GRMZM2G384780 ZmGdsl9
GRMZM2G017869 ZmGdsl8
Sevir.1G371300 SvGDSL8
LOC Os02g57110 OsGDSL5
LOC Os08g45150 OsGDSL3
GRMZM2G148867 ZmGdsl3
LOC Os10g32580 OsGDSL7
GRMZM2G116360 ZmGdsl7
Sevir.9G230800 SvGDSL7
Si036305m.g SiGDSL7
Si030233m.g SiGDSL1
Sevir.2G435560 SvGDSL1
GRMZM2G070178 ZmGdsl1
LOC Os07g47210 OsGDSL1
At3g50400
Solyc02g090210
At2g23540
LOC Os03g19670 OsGDSL2
GRMZM2G172099 ZmGdsl2
Si038776m.g SiGDSL2
Sevir.9G431800 SvGDSL2
Si012586m.g SiGDSL3
Sevir.7G219800 SvGDSL3
Si006634m.g SiGDSL4
Sevir.4G114400 SvGDSL4
Solyc11g011110
At5g37690
At4g30140 AtCDEF1
At5g15720 AtGLIP7
Solyc11g032050
At1g71691
Solyc02g071610
Si001968m.g SiGDSL5
Sevir.5G307000 SvGDSL5
At4g26790
Solyc07g049440
0.1
CUS Clade
GDSL1 Subclade

Transcriptional regulators of lignin and cuticle biosynthesis were utilized to define a putative expression pattern for suberin regulatory candidates

At the outset of this study, no transcription factors (TFs) specifically involved in the regulation of suberin biosynthesis had been characterized in any species. Thus, the identification of candidate TFs in maize and rice was predicated on several assumptions. First, because maize and rice have qualitatively similar suberin monomer compositions to Arabidopsis and at least one putative homologue per species for each of the biosynthetic steps defined to date (Figure 2.2), transcriptional regulators were considered likely to be homologous between grasses and model dicots. The majority of the suberin biosynthetic genes characterized to date are exclusively expressed in the endodermis and periderm during root development (Beisson *et al*., 2007; Hofer *et al*., 2008; Compagnon *et al*., 2009; Molina *et al*., 2009; Domergue *et al*., 2010; Kosma *et al*., 2012). Thus, it was assumed that any positive regulators of suberin biosynthesis were also likely to be specifically expressed at the sites of suberin synthesis. Thus, an initial list of vascular sheath suberin regulatory candidates was defined by protein homology to a set of endodermis-enriched Arabidopsis transcription factors (Mustroph *et al*., 2009).

A putative spatiotemporal relationship between TF and suberin biosynthesis candidate expression in developing grass leaves could not be inferred from the Arabidopsis translatome data. Both the narrow spatiotemporal region of suberin deposition and the tightly delimited expression pattern of biosynthesis candidates indicate that BS suberization is likely under tight regulatory control. Thus, other cell wall biosynthetic processes with distinct spatiotemporal expression patterns in developing grass leaves were identified. Leaf cuticle biosynthesis was recently shown to occur at the base of developing barley leaves (Richardson *et al*., 2007), and an HD-ZIP IV transcription factor required for maize cuticle biosynthesis, Zm*OCL1* and several of

its putative targets were characterized (Javelle *et al*., 2010). *OUTER CELL LAYER1* was strongly expressed at the maize leaf base, as expected for a positive transcriptional regulator of cuticle biosynthesis (Figure 2.8A). Seven of the fourteen putative target genes reported by Javelle and colleagues were significantly expressed in developing third leaves. Interestingly, the two positively regulated targets with the highest expression values, the lipid transfer protein *LptII.12* and the fatty acid reductase Zm*FAR1*, peaked in expression concurrently with *OCL1* at the leaf base. Conversely, three negatively regulated targets, an indol-3-glycerol phosphate lyase (*IGL*), a SWEET family transporter (*Mtn3*/*SALIVA*), and a proline-rich protein (*PRP*) were minimally expressed at the leaf base; transcript abundance increased in older tissue after *OCL1* transcript abundance declined (Figure 2.8A). These results suggest that transcription factors and their positively regulated targets are tightly co-expressed in the third leaf developmental gradient. However, *OCL1* is also present in leaf primordia, and so these data capture only later stages of *OCL1* expression (Ingram *et al*., 1999). Candidate genes involved in metaxylem lignification, which occurs concurrently with BS suberization in the transition zone (Evert *et al*., 1996) were evaluated as a secondary test. Putative maize homologues were identified for At*MYB58* and At*MYB63*, two Arabidopsis MYB transcription factors that positively regulate core monolignol biosynthesis genes (Zm*Myb13* and Zm*Myb152*; Figure 2.8B; Zhou *et al*., 2009). Several families of monolignol biosynthetic genes are expanded in maize relative to Arabidopsis (Penning *et al*., 2009). At least one maize family member for each of the putative target genes described by Zhou and colleagues (2009) was strongly expressed concurrently with *ZmMyb13* and *ZmMyb152* in the transition zone 2-4 cm above the leaf base (Figure 2.8B; Zhou et al., 2009). It was concluded that putative positive regulators of both cutin and lignin monomer biosynthesis were co-expressed with their targets in developing third leaves.

Figure 2.8 Suberin regulatory candidates are co-expressed with their putative targets.

A. The maize HD-ZIP IV transcription factor *OUTER CELL LAYER1* (*OCL1)* and a subset of its positively regulated targets are co-expressed at the leaf base. Transcript accumulation of negatively regulated targets of *OCL1* increases at later developmental time points where *OCL1* is no longer expressed. Ltp, lipid transfer protein; FAR, fatty acid reductase; IGL, indole-3-glycerol phosphate lyase; Mtn3/SALIVA, SWEET efflux transporter; PRP, proline-rich protein.
B. Putative maize homologues of the positive lignin regulators *AtMYB58* and *AtMYB63* are co-expressed with a subset of their putative targets. PAL, phenylalanine ammonia lyase; C4H, cinnamate-4-hydroxylase; C3′H, coumaroyl shikimate 3′-hydroxylase; 4CL, 4-coumarate CoA ligase; CCR, cinnamoyl-CoA reductase; CCoAOMT, caffeoyl-CoA O-methyltransferase.
C. Maize suberin regulatory candidates from the MYB (blue) and WRKY (red) transcription factor families are co-expressed with putative suberin biosynthesis genes in the transition zone. *ZmGpat5* (gray) transcript expression is shown as a reference. Expression is presented in reads per kilobase per million reads (RPKM).
D. Rice suberin regulatory candidates from the MYB (blue) and WRKY (red) transcription factor families are co-expressed with putative suberin biosynthesis genes at the leaf base. *OsGPAT5* (gray) transcript expression is shown as a reference. Expression is presented in reads per kilobase per million reads (RPKM).
E. *Setaria viridis* suberin regulatory candidates from the MYB (blue) and WRKY (red) transcription factor families are co-expressed with putative suberin biosynthesis genes in the transition zone. *SvGpat5* (gray) transcript expression is shown as a reference. Expression is presented in reads per kilobase per million reads (RPKM).

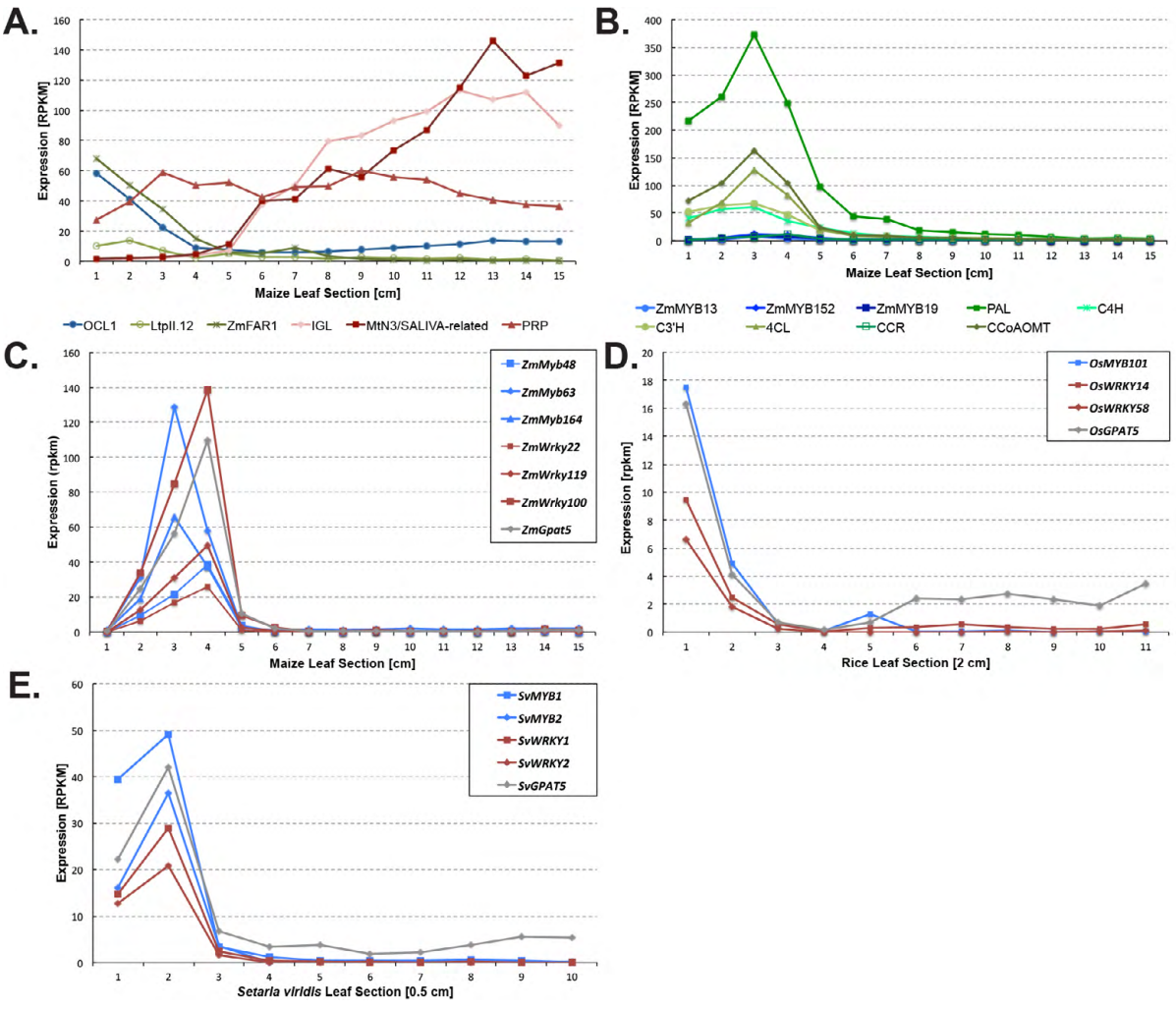
A.
Expression [RPKM]
Maize Leaf Section [cm]
OCL1
LtpII.12
ZmFAR1
IGL
MtN3/SALIVA-related
PRP
B.
Expression [RPKM]
Maize Leaf Section [cm]
ZmMYB13
ZmMYB152
ZmMYB19
PAL
C4H
C3'H
4CL
CCR
CCoAOMT
C.
Expression (rpkm)
Maize Leaf Section [cm]
ZmMyb48
ZmMyb63
ZmMyb164
ZmWrky22
ZmWrky119
ZmWrky100
ZmGpat5
D.
Expression [rpkm]
Rice Leaf Section [2 cm]
OsMYB101
OsWRKY14
OsWRKY58
OsGPAT5
E.
Expression [RPKM]
Setaria viridis Leaf Section [0.5 cm]
SvMYB1
SvMYB2
SvWRKY1
SvWRKY2
SvGPAT5

Thus, the transcript accumulation profiles of the transcription factor candidates were evaluated relative to the putative suberin biosynthesis genes described above. The initial list of maize TFs homologous to the endodermis-enriched Arabidopsis TF set was refined to a group of 3 MYB (Zm*Myb48*, Zm*Myb63*, and Zm*Myb164*) and 3 WRKY (Zm*Wrky119*, Zm*Wrky22*, and Zm*Wrky100*) TF candidates that were expressed concurrently with the VLCFA-modifying gene candidates (Figure 2.8C). Only this group of TFs had homologues that were also co-expressed with suberin biosynthesis candidates in both rice and green millet (Figure 2.8D-E). Furthermore, canonical AtMYB4 (Lois *et al*., 1989) and W-Box (Rushton *et al*., 1996) binding motifs were identified in the proximal promoters of the maize suberin biosynthesis candidates and their Arabidopsis homologues (Davilury *et al*., 2003; Palaniswarmy *et al*., 2006). Therefore, this small subset of homologous MYB and WRKY TFs were determined to be the strongest suberin regulatory candidates in all three model grasses.

Genes of the Casparian Strip biosynthesis pathway are not expressed in leaf vascular sheaths

As discussed in Chapter 1, bundle sheaths of grasses share many common anatomical features with the root endodermis. However, multiple histochemical surveys of bundle and mestome sheaths from diverse grass taxa show that leaf vascular sheaths lack Casparian Strips (CS; Eastman et al., 1988). In developing maize leaves, the BS primary cell wall is in an undifferentiated state from 0-1 cm from the leaf base, with suberin lamellae (analogous to State II endodermal cell wall development) becoming apparent by 3-4 cm above the leaf base (Evert *et al*., 1996; Li *et al*., 2010). Thus, genes involved in CS development, if these structures are present, should be expressed in leaf sections between 1 and 4 cm from the leaf base. Until

recently, the genes underlying CS biosynthesis were uncharacterized in any species. Multiple genes encoding regulatory and biosynthetic proteins essential for CS formation were recently characterized in the model dicot *Arabidopsis thaliana* (Kamiya *et al*., 2015 and references therein; Figure 2.9). Putative homologues of *AtMYB36*, *SGN3*, *CASP1*, *ESB1*, *SGN4*/*RBOHF*, and *PER64* were identified in maize, rice, and *Setaria viridis*, and their transcript accumulation profiles in developing leaves were evaluated.

The earliest characterized step of CS formation is activation of downstream targets by *AtMYB36*, which was among the endodermis-enriched transcription factors we evaluated above in our initial survey of potential suberin regulators (Mustroph *et al*., 2009; Kamiya *et al*., 2015; Liberman *et al*., 2015). *AtMYB36* is a direct target of the endodermal master regulator *AtSCR* (Kamiya *et al*., 2015; Liberman *et al*., 2015). *ZmScr1* is essential to establish both endodermal and BS cell identity in maize (Slewinski *et al.*, 2012), and reaches maximum transcript accumulation from 0-1 cm above the maize leaf base. Of particular interest, *Zmscr* mutants fail to establish a CS at a normal frequency (Slewinski *et al*., 2012). The closest maize homolog of *AtMYB36*, *ZmMyb12*, belongs to Clade S10 of the maize R2R3 MYB family (Du *et al.*, 2012; the gene is called *ZmMYB084* by the authors). *ZmMyb12* and the five additional genes belonging to the same sub-clade (*ZmMyb16*, *ZmMyb108*, *ZmMyb113, ZmMyb140,* and *ZmMyb111*) are predominately expressed in developing maize roots rather than aerial tissues (Sekhon *et al.*, 2010; Stelpflug *et al.*, 2015). Of the six genes, only *ZmMyb140* shows significant (RPKM > 2) transcript accumulation in leaves. However, its expression maximum occurs 3-4 cm above the leaf base, concurrently with the first appearance of suberin lamellae. Thus, *Myb140* is likely expressed too late in leaf development to facilitate CS formation in advance of BS suberization.

Figure 2.9 Casparian Strip biosynthetic genes are present in grasses, but not expressed in leaves.

Schematic of the Casparian Strip biosynthetic and regulatory pathway in Arabidopsis. The transmembrane protein, CASPARIAN STRIP MEMBRANE DOMAIN PROTEIN (CASP), in concert with the dirigent protein ENHANCED SUBERIN 1 (ESB1), selectively admits an NADP-dependent oxidase, RBOHF, and a peroxidase, PER64, to the Casparian Strip Domain (CSD) of the plasma membrane (PM). These proteins facilitate localized lignin polymerization in the primary cell wall (PCW), forming a Casparian Strip (CS). The receptor-like kinase *SCHENGEN3* (*SGN3*) maintains the boundaries of the CSD through an unknown mechanism. All CASP pathway genes except for *SGN3* are direct targets of *MYB36*, which is itself a direct target of the endodermal master regulator *SCARECROW* (*SCR*). Relevant citations are available within the main text.

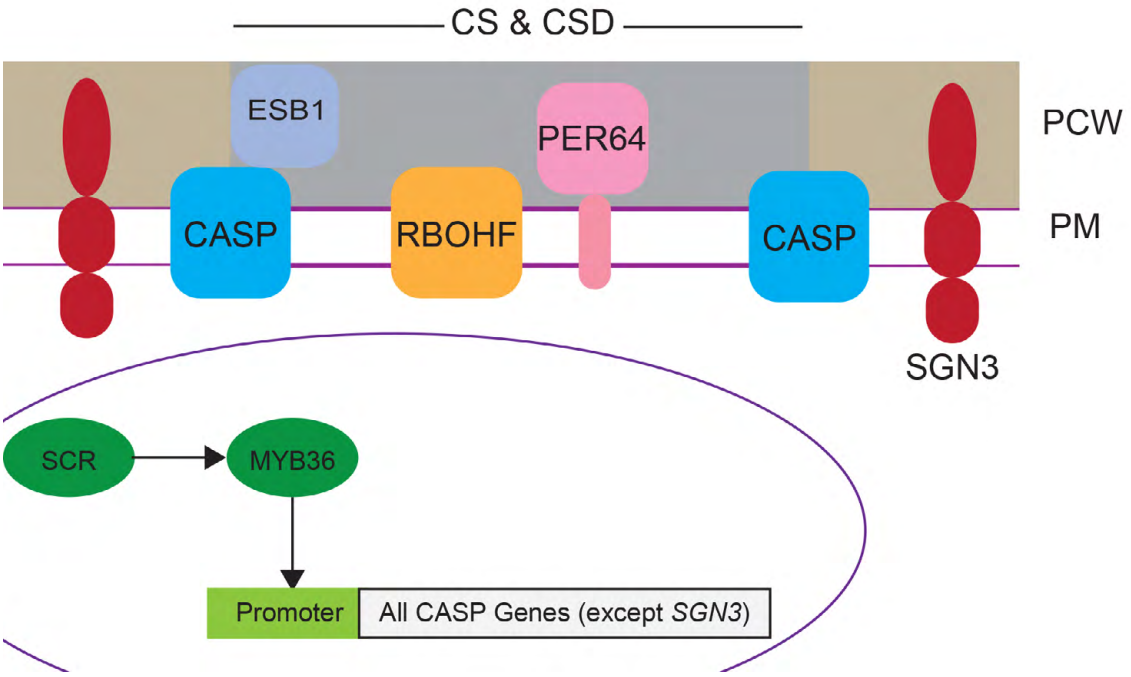
CS & CSD
ESB1
PER64
CASP
RBOHF
CASP
PCW
PM
SGN3
SCR
MYB36
Promoter
All CASP Genes (except SGN3)

Additional genetic evidence that the CS is absent from BS cell walls is provided by expression profiles of putative Arabidopsis *CASPARIAN STRIP MEMBRANE PROTEIN* (*AtCASP)* homologues. CASPs are transmembrane proteins that act in concert with the apoplastic dirigent protein ENHANCED SUBERIN1 (ESB1) to form a localized membrane scaffold essential for normal CS positioning, termed the Casparian Strip Domain (Roppolo *et al.*, 2011; Hosmani *et al.*, 2013). Both the *CASP*s and *ESB1* are putative targets of *MYB36* (Kamiya *et al.*, 2015). All four of the putative maize *Casp* genes, identified by a diagnostic "E/QSLPFFTQF" motif within the first extracellular loop (Roppolo *et al*., 2014), are expressed exclusively in roots in the maize transcriptome atlas (Sekhon *et al*., 2010; Stelpflug *et al*., 2015). Likewise, all three of the maize dirigent proteins with the highest sequence similarity to *AtESB1* are also expressed only in roots (Sekhon *et al*., 2011; Stelpflug *et al*., 2015). The *CASP* genes are conserved in all land plants characterized to date that share a common origin of roots (Roppolo *et al*., 2014). Thus, these results strongly suggest that the CS pathway is conserved between maize and Arabidopsis roots, and that the CS is missing from the leaf BS. As the BS lacks other features of the endodermal cell wall, particularly asymmetrically thickened tertiary walls, rice CASP homologues were identified to determine whether these results extend to the mestome sheath (MS). Rice also contains four canonical *CASP* genes, none of which are significantly expressed in leaves (data not shown).

The Casparian Strip Domain selectively admits two transmembrane proteins essential for localized lignin polymerization, an NADP-dependent oxidase, RBOHF, and a peroxidase, PER64 (Figure 2.9; Lee *et al.*, 2014). Unlike the putative regulatory and structural genes described above, transcripts of the putative maize *RBOHF* homologues are constitutively expressed throughout the maize leaf developmental gradient, and are broadly expressed in nearly

all tissues of the maize plant (Sekhon *et al*., 2011; Stelpflug *et al*., 2015). Likewise, the putative *PER64* homologue, *ZmPrx58* (Wang *et al*., 2015) is strongly expressed at the leaf base in addition to the maturation zone of primary roots, coleoptiles, and developing embryos (Sekhon *et al*., 2011; Stelpflug *et al*., 2015). However, in Arabidopsis, neither RBOHF nor PER64 are capable of synthesizing a normal CS in the absence of CASP expression (Lee *et al*., 2014). Thus, these candidates are unlikely to contribute to CS biosynthesis in leaf vascular sheaths in the absence of CASP expression. Both the RBOH and Class III Peroxidase families are large and highly redundant, and the specific residues or post-translational modifications that enable RBOHF and PER64 to enter the CSD have yet to be identified. To identify candidate RBOHF and PER64 functional homologues that were not apparent from BLASTp searches, we queried the co-expression network of the rice CASPs described above using RiceNet v.2 (Lee *et al.*, 2015). The network analysis yielded two additional apoplastic peroxidases, neither of which is significantly expressed in leaves (data not shown).

Thus, despite ultrastructural and developmental similarities with the root endodermis, neither the BS nor the MS cell wall is formed by a wholesale adoption of the endodermal regulatory network governed by Short-Root and Scarecrow. Both prior ultrastructural studies and this transcript profiling approach support the conclusion that leaf vascular sheaths are devoid of CS.

DISCUSSION

The polyester biosynthesis pathway is well conserved between grasses and model dicots

Cutin evolved concurrently with the first land plants approximately 450 million years ago, and suberin is thought to have originated with the first vascular plants (Rensing *et al*., 2008;

Yang *et al*., 2012). Orthologues of multiple cuticle biosynthesis genes from higher plants, including ABCG subfamily transporters, glycerol-3-phosphate acyltransferases, and cutin synthase-like proteins are present in the moss *Physcomitrella patens*, which suggests that the polyester biosynthesis pathway was already well-established prior to the monocot/dicot split 200 million years ago (Nelson *et al*., 2004; Buda *et al*., 2013; Yang *et al*., 2012; Yeats *et al*., 2014). These genetic similarities are reflected in the qualitatively similar suberin monomer distributions between model dicots and grasses (reviewed in Pollard *et al*., 2008). The candidate gene approach presented above is in good agreement with existing phylogenetic and chemical data. At least one putative gene from maize, rice, and millet was identified for each known step of intercellular monomer biosynthesis based on homology to Arabidopsis proteins previously implicated in polyester biosynthesis (Figure 2.1). Unlike many gene families of the monolignol biosynthetic pathway, which have undergone considerable expansion in grasses since the monocot/dicot split (Penning *et al*., 2009), most of the families involved in aliphatic suberin and cutin synthesis contain similar numbers of candidate genes in grasses relative to Arabidopsis (Figure 2.2-2.4; Figure 2.6). This will greatly expedite the functional dissection of candidate genes.

Although the process is less well characterized, the export and polymerization of monomers in the apoplast also appears to be well conserved between model dicots and grasses. Several putative homologues of the tomato cutin synthase *SlCUS1* belonging to the CUS Clade were identified (Figure 2.6; Yeats *et al*., 2014). Aliphatic substrates are thought to reach the site of CUS polymerization in the apoplast by several mechanisms, including active transport by ABC subfamily G transporters and chaperoning by membrane-anchored or apoplastic lipid transfer proteins (reviewed in Yeats and Rose, 2013). Although ABCG is a large subfamily

comprising over 40 members in both Arabidopsis and rice (Verrier *et al*., 2008), Waßmann (2014) correctly predicted a rice ABCG protein involved in suberin biosynthesis by phylogenetic grouping with a set of Arabidopsis transporters co-regulated with suberin biosynthesis genes. Three of these Arabidopsis genes were subsequently shown to be essential for root suberin biosynthesis (Yadav *et al*., 2014). A rice ABCG transporter, *OsABCG5*/*RCN1* (LOC_Os03g07150), was the first suberin biosynthesis gene to be functionally dissected in any monocot (Shiono *et al*., 2014a). Therefore, polyester synthesis pathways are largely conserved between Arabidopsis and the grasses, and identification of candidates by homology to characterized dicot genes is likely to yield genuine suberin biosynthesis genes.

Leaf vascular sheaths are not strictly analogous to the root endodermis

The suberin biosynthesis pathway appears to be broadly conserved between organs as well as between taxa. The majority of the candidate genes were strongly expressed in maize leaves and roots (Sekhon *et al*., 2010; Stelpflug *et al*., 2015). Furthermore, the chain length distribution of ω-OH fatty acids is similar between the maize root endodermis and the leaf BS across multiple growth stages and genetic backgrounds (Espelie and Kolattukudy, 1979; Zeier *et al*., 1999; Chapter 3). Both BS and endodermal progenitors require the expression of maize *Short-Root1* (*ZmShr1*) and *Scarecrow* (*ZmScr*) to acquire cell identity markers, including a differentiated cell wall (Slewinski *et al*., 2012; Slewinski *et al*., 2014). However, BS cell wall differentiation does not appear to involve a simple transposition of the endodermal development program into an aerial tissue. The CS is a ubiquitous feature of endodermal cell walls in all extant vascular plants (Roppolo *et al.*, 2014), but CS regulatory and biosynthesis candidates were not expressed in leaves of either maize or green millet. Although the mestome sheath of C_3

grasses retains endodermoid cell wall traits such as thickened inner tangential walls (O'Brien & Carr, 1970), the CS biosynthetic machinery was not expressed in rice leaves either. Thus, the leaf vascular sheath cell wall identity program selectively retains the suberin lamellae and thickened tertiary walls of the endodermis, but not the pathway leading to CS formation. The first confirmed step of the CS pathway, *Scr* expression, is common to both tissues, at least in maize. Thus, the regulatory checkpoint where the endodermal and vascular sheath cell wall programs diverge potentially lies between *SCR* and its direct target, the uncharacterized grass orthologue of *AtMYB36*. Recent ectopic expression studies in Arabidopsis and tobacco (*Nicotiana benthamiana*) with both *AtMYB36* and the suberin master regulator *AtMYB41* indicate that these transcription factors are necessary and sufficient to induce CS and suberin lamellae, respectively, in all cell types (Kosma *et al*., 2014; Kamiya *et al*., 2015). Thus, vascular sheath cells are likely competent to synthesize CS under the influence of the appropriate transcriptional regulator. Interestingly, the suberin lamellae in the radial walls of the rice mestome sheath are interrupted by a small gap at the approximate position of the CS of endodermal cells (Figure 3 of Chonan *et al*., 1981). The suberin lamella is also discontinuous in the endodermal radial wall parallel to the CS of maize roots (Chapter 3, Figure 3.10A-B). Thus, it is possible that components of the Casparian Strip Membrane Domain (CSD), possibly CASP-like proteins, are present in the rice mestome sheath and are sufficient to prevent suberin polymerization in the adjoining cell wall. Characterization of a grass *MYB36* orthologue would yield considerable insight into cell-type specific regulation of cell wall developmental regulators.

In the endodermis, CS are required to prevent unrestricted apoplastic diffusion of ions into the transpiration stream, and to restrict the backflow of ions during times of low water potential when the plant is not transpiring (reviewed in Enstone *et al*., 2003). In the BS, ions

dissolved in the transpiration stream readily diffused into tertiary cell walls, but were unable to diffuse through the SL and remained trapped in the tertiary wall (Botha *et al*., 1982; Evert *et al*., 1985). The radial walls between adjacent BS cells were the only apoplastic path between the vasculature and leaf mesophyll accessible to dissolved ions (Botha *et al*., 1982; Evert *et al*., 1985). Thus, the absence of CS in leaf vascular sheaths may be essential for normal partitioning of mineral nutrients to distal tissues via the transpiration stream. The functional implications of restoring a CS to the vascular sheath could be evaluated by ectopic *MYB36* expression under a BS-specific promoter.

Cutin and suberin biosynthesis pathways overlap in leaves

Although the expression profiles of most suberin biosynthesis candidates are similar between the roots and leaves, the suberin lamella biosynthesis pathway does not appear to be a simple projection of the endodermal program either, at least in maize. In particular, members of the suberin-related *CYP86A1* sub-clade are expressed exclusively in maize roots, and all leaf polyesters appear to be synthesized by genes from the cutin-related sub-clade (Figure 2.3). One possible interpretation is that maize BS suberin is comprised predominately of very long chain fatty acid-derived monomers, presumably synthesized by the two *CYP86B* paralogues. However, this is inconsistent with previous reports of BS suberin composition (Espelie and Kolattukudy, 1979) as well as measurements of BS-enriched leaf macerates conducted in this study (refer to Chapter 3, Figure 3.3C). A more likely explanation is that members of the cutin-related clade were recruited to provide monomers for polyester synthesis in suberizing bundle sheaths in addition to their ancestral function in cuticle biosynthesis. In accordance with this theory, both *ZmCyp86A35* and the putative mid-chain monooxygenase *ZmCyp77A* have a broad transcript

accumulation pattern that encompasses probable regions of both cutin and suberin biosynthesis (Figure 2.6). *ZmCyp77A* is a putative homologue of *AtCYP77A4* and *AtCYP77A6*, two monooxygenases required for the synthesis of 9/10,16-dihydroxy hexadecanoate and 9,10-epoxy octadecanoate, respectively (Li-Beisson *et al*., 2009; Sauveplane *et al*., 2009). Di-hydroxy fatty acids are generally enriched in cutin relative to suberin across multiple plant taxa (Pollard *et al*., 2008). Espelie and Kolattukudy (1979) reported that 9/10,16-dihydroxy hexadecanoate is a major component of BS suberin. Conversely, di-hydroxy fatty acids were reported as a minor (< 10%) component of endodermal suberin by Pozuelo and colleagues (1984), and were not reported in either maize or rice in subsequent experiments (Zeier *et al*., 1999; Schreiber *et al*., 2005). These disparities could be attributed to differences in suberin composition between genetic backgrounds. However, root and leaf polyester profiles from the maize W22 inbred line are in agreement with these results (Chapter 3). Taken together, these biochemical data and transcript profiles suggest that BS suberin composition is intermediate in character between conventional endodermal suberin and leaf cutin.

Cell-type specific transcript profiles for the bundle sheath and epidermis are needed to determine the tissue localization underlying the expression patterns presented in this study. Several maize genes with epidermis-specific expression have been described (Nakazono *et al*., 2003; Javelle *et al*., 2011). Promoter dissection of these genes may yield a suitable candidate to drive cell-type specific expression of an epitope-tagged ribosomal construct for translatome profiling (Mustroph *et al*., 2009).

Spatiotemporal separation of cutin and suberin biosynthesis facilitates candidate gene selection for targeted mutagenesis

A strong, suberin-specific mutant in a uniform genetic background is required to unambiguously attribute physiological defects to the suberized BS. The genetic overlap between polyester biosynthesis pathways within leaves significantly confounds efforts to identify candidate genes likely to yield a suberin-specific biochemical phenotype. Fortunately, the finely resolved developmental gradient of juvenile maize leaves facilitated the identification of a small cohort of genes encoding putative homologues of proteins specifically involved in suberin biosynthesis. Interestingly, these VLCFA-related candidates are expressed concurrently with or immediately prior to the first histochemical detection of the suberin lamellae 3-4 cm above the leaf base (Figure 2.5A,C; Li *et al*., 2010), whereas the LCFA-related homologues are maximally expressed earlier in leaf development (Figure 2.6). It is not likely that the VLCFA-related genes alone are sufficient for BS suberin biosynthesis. In Arabidopsis, VLCFA monomers are specifically attenuated in in *cyp86b1* and *gpat5* mutants, and GPAT5 exhibits a strong *in vitro* substrate preference for VLCFA (Beisson *et al*., 2007; Compagnon *et al*., 2009; Yang et al., 2010). Likewise, the *gpat5* mutation is not sufficient to abolish LCFA accumulation in root suberin, and another GPAT with a strong preference for LCFA, GPAT4, is also strongly expressed in roots (Beisson *et al*., 2007; Yang *et al*., 2012). Interestingly, all of the suberin biosynthesis candidates in the VLCFA-related group catalyze late steps in the biosynthetic pathway. Taken together, these biochemical and genetic data suggest that VLCFA derivatives are a minor component of BS suberin deposited late in the process of lamella formation. Thus, the LCFA-modifying candidates may generate a stronger mutant phenotype. As discussed above, cell type-specific transcriptomes or translatomes of the BS and leaf epidermis are needed to identify the LCFA-modifying *GPAT* and *CYP86A* candidates most likely to contribute to BS suberization. Although null mutants would facilitate the initial functional characterization, BS-

specific RNAi constructs would likely be necessary to elucidate the physiological function of BS suberization without a confounding cuticle defect.

The tightly delimited expression of the suberin biosynthesis candidates facilitated the identification of several candidate genes for uncharacterized steps of suberin biosynthesis and regulation. A suberin synthase candidate, tentatively named *GDSL1*, was co-expressed with the suberin biosynthesis candidates across all three grass species. Although the biochemical function of the *GDSL1* proteins remains to be determined, several lines of evidence implicate them as potential suberin synthases. In addition to the putative cutin synthases of the CUS Clade, they are closely related to Arabidopsis *CUTICLE DESTRUCTING FACTOR 1* (*AtCDEF1*; Takahashi *et al*., 2010; Figure 3.6). Although the native function of CDEF1 appears to be depolymerization of stigmatic polyesters during pollen tube penetration, it is capable of depolymerizing both epidermal cutin and endodermal suberin lamellae when heterologously expressed (Takahashi *et al*., 2010; Roppolo *et al*., 2011). This suggests that the CUS Clade and its close relatives contain multiple groups of GDSL lipases capable of acting on polyesters. Likewise, *OsGDSL1* is co-expressed with *OsCYP86B3*, which was recently shown to be essential for incorporation of ω-OH VLCFA into rice root suberin (Waßmann, 2014). The author did not report compositional data for the mestome sheath or leaf cuticle; nonetheless, these data provide strong evidence that the VLCFA-related candidates are required for suberin biosynthesis in grasses as well as model dicots.

A putative master regulator of suberin biosynthesis, *AtMYB41*, was recently characterized in Arabidopsis (Kosma *et al*., 2014). *AtMYB41* was among the endodermis-enriched TFs described by Mustroph and colleagues (2009) that were evaluated as potential regulators of BS suberization in this study. The closest maize homologue, *ZmMyb141*, was expressed exclusively

in roots and internodes (Sekhon *et al*., 2010; Stelpflug *et al*., 2015). The closest maize homologue with significant expression in developing leaves was *ZmMyb48*, one of the high priority transcription factor candidates co-expressed with the suberin biosynthesis candidates (Figure 2.8C). To date, no homologues of the WRKY candidates have been characterized. However, *OsWRKY14* (Figure 2.8D) was recently shown to be up-regulated concurrently with two suberin biosynthesis candidates, *OsCYP86B3* and *OsGPAT5*, in the root exodermis during hypoxia stress (Shiono *et al*., 2014b). Thus, putative suberin transcriptional regulators are also conserved between model dicots and grasses, the candidate gene approach described above successfully yielded several promising transcription factor candidates.

CONCLUSION

The characterized steps of the cutin and suberin polyester biosynthesis pathways are largely conserved between monocots and dicots. Cutin and suberin share many common monomer constituents, and there appears to be considerable overlap between their respective biosynthetic pathways. However, suberin is enriched in very long chain fatty acids relative to cutin, and so identified a subset of very long chain fatty acid-modifying genes and transcription factors that may contribute significantly or exclusively to suberin biosynthesis was identified. Subsequent chapters will focus on the functional dissection of these candidate genes through targeted reverse genetics in maize and *Setaria viridis*.

MATERIALS AND METHODS

Identification of candidate genes

Arabidopsis thaliana protein sequences involved in suberin, cutin, or cuticular wax biosynthesis were identified from the literature and queried against the maize (*Zea mays*; B73 RefGen v2) and rice (*Oryza Sativa* Nipponbare/*japonica*; Os-Nipponbare-Reference-IRGSP-1.0; MSU Release 7.0) reference proteomes at Phytozome 6.0 (http://www.phytozome.com) using BLASTP searches under the default parameters. Putative homologues were evaluated for leaf transcript expression using previously published RNA-Sequencing data described in (Li *et al*., 2010 and Wang *et al*., 2014). A genomic sequence was not available for *Setaria viridis*, so the reference genome of its domesticated relative *Setaria italica* (*Setaria italica* v2.1) was queried, and candidate genes were matched to *Setaria viridis* RNA-Sequencing data assuming a 1:1 orthology between *S. viridis* and *S. italica* gene models. This assumption was validated for each candidate upon the release of the first *Setaria viridis* draft genome (*Setaria viridis* A10.1, v1.1) in 2015. For suberin biosynthesis candidates, co-expression analysis was carried out according to Wang *et al*., (2014). All phylogenetic trees were generated using MEGA6 (Tamura *et al*., 2013). Amino acid sequences were aligned within the MEGA environment using MUSCLE under the default parameters. Neighbor-Joining trees were generated from the alignments using a Jones-Taylor-Thornton model assuming uniform substitution rates, and pairwise deletion of gaps. Branch support was estimated with 1000 bootstrap replications.

REFERENCES

Beisson F, Li Y, Bonaventure G, Pollard M, & Ohrogge JB. (2007) The acyltransferase GPAT5 is required for the synthesis of suberin in seed coat and root of *Arabidopsis*. *The Plant Cell* **19**: 351-368.

Beisson F, Li-Beisson Y, & Pollard M. (2012) Solving the puzzles of cutin and suberin polymer biosynthesis. *Current Opinion in Plant Biology* **15**: 329-337.

Bernards MA. (2002) Demistifying suberin. *Canadian Journal of Botany* **80**: 227.

Bernards MA & Lewis NG. (1998) The macromolecular aromatic domain in suberized tissue: a changing paradigm. *Phytochemistry* **47**: 915-933.

Botha CEJ, Evert RF, Cross RHM, & Marshall DM. The suberin lamella, a possible barrier to water movement from the veins to the mesophyll of *Themeda triandra* Forsk. *Protoplasma* **112**: 1-8.

Buda GJ, Barnes WJ, Fich EA, Park S, Yeats TH, Zhao L, Domozych DS, & Rose JKC. (2013) An ATP Binding Cassette Transporter is required for cuticular wax deposition and dessication tolerance in the moss *Physcomitrella patens*. *The Plant Cell* **25**: 4000-4013.

Chonan N, Kaneko M, Kawahara H, Matsuda T. (1981) Ultrastructure of the large vascular bundles in the leaves of rice plant. *Japanese Journal of Crop Science* **50**: 323-331.

Christin P-A, Osborne CP, Chatelet DS, Columbus JT, Besnard G, Hodkinson TR, Garrison LM, Vorontsova MS, & Edwards EJ. (2014) Anatomical enablers and the evolution of C_4 photosynthesis in grasses. *Proceedings of the National Academy of Sciences USA* **110**(4): 1381-1386.

Compagnon V, Diehl P, Benveniste I, Meyer D, Schaller H, Schreiber L, Franke R, & Pinot F. (2009). *CYP86B1* is required for very long chain ω-hydroxyacid and α,ω-dicarboxylic acid synthesis in root and seed suberin polyester. *Plant Physiology* **150**: 1831-1843.

Davuluri RV *et al.* (2003) AGRIS: Arabidopsis Gene Regulatory Information Server, an information resource of Arabidopsis *cis*-regulatory elements and transcription factors. *BMC Bioinformatics* **4**: 25.

Domergue F, Vishwanath SJ, Joubès J, Ono J, Lee JA, Bourdon M, Alhattab R, Lowe C, Pascal S, Lessire R, & Rowland O. (2010). The Arabidopsis Fatty Acyl-Coenzyme A Reductases, FAR1, FAR4, and FAR5, generate primary fatty alcohols associated with suberin deposition. *Plant Physiology* **153**: 1539-1554.

Du H, Feng B-R, Yang S-S, Huang Y-B, & Tang Y-X. (2012) The R2R3-MYB transcription factor family in maize. *PLoS ONE* **7**(6): e37463. doi:10.1371/journal.pone.0037463.

Eastman PAK, Dengler NG, & Peterson CA. (1988)**.** Suberized Bundle Sheaths in Grasses (Poaceae) of Different Photosynthetic Types .1. Anatomy, Ultrastructure and Histochemistry. *Protoplasma* **142**: 92-111**.**

Enstone DE, Peterson CA, & Ma F. (2003) Root endodermis and exodermis: structure, function, and responses to the environment. *Journal of Plant Growth Regulation* **21**: 335-351.

Espelie KE & Kolattukudy PE. (1979) Composition of the aliphatic components of 'suberin' from the bundle sheaths of *Zea mays* leaves. *Plant Science Letters* **15**: 225-230.

Evert RF, Botha CEJ, & Mierzwa RJ. (1985) Free-Space Marker Studies on the Leaf of *Zea mays* L. *Protoplasma* **126**: 62-73.

Evert RF, Russin WA, Bosabalidis AM. (1996) Anatomical and ultrastructural changes associated with sink-to-source transition in developing maize leaves. *International Journal of Plant Sciences* **157**: 247-261.

Felsenstein J. (1985) Confidence limits on phylogenies: An approach using the bootstrap. *Evolution* **39**:783-791.

Franke R, Briesen I, Wojciechowski T, Faust A, Yephremov A, Nawrath C, & Schreiber L. (2005) Apoplastic polymers in Arabidopsis surface tissues – A typical suberin and a particular cutin. *Phytochemistry* **66**: 2643-2658.

Gou JY, Yu XH, & Liu CJ. (2009) A hydroxycinnamoyltransferase responsible for synthesizing suberin aromatics in Arabidopsis. *Proceedings of the National Academy of Sciences, USA* **106**: 18855-18860.

Hofer R, Briesen I, Beck M, Pinot F, Schreiber L, & Franke R. (2008). The *Arabidopsis* cytochrome P450 CYP86A1 encodes a fatty acid ω-hydroxylase involved in suberin monomer synthesis. *Journal of Experimental Botany* **59**: 2347-2360.

Hosmani PS, Kamiya T, Danku J, Naseer S, Geldner N, Guerinot ML, & Salt DE. (2013) Dirigent domain-containing protein is part of the machinery required for formation of the lignin-based Casparian strip in the root. *Proceedings of the National Academy of Sciences, USA* **110**(35): 14498-14503.

Ingram GC, Magnard J-L, Vergne P, Dumas C, & Rogowsky PM. (1999) *ZmOCL1*, an HDGL2 family homeobox gene, is expressed in the outer cell layer throughout maize development. *Plant Molecular Biology* **40**: 343-354.

Isaacson, T., Kosma, D.K., Matas, A.J., Buda, G.J., He, Y., Yu, B., Pravitasari, A., Batteas, J.D., Stark, R.E., Jenks, M.A., Rose, J.K.C. (2009) Cutin deficiency in the tomato fruit cuticle consistently affects resistance to microbial infection and biomechanical properties, but not transpirational water loss. *The Plant Journal* **60**: 363-377.

Javelle M, Vernoud V, Depège-Fargeix N, Arnould C, Oursel D, Domergue F, Sarda X, and Rogowsky PM. (2010) Overexpression of the epidermis-specific Homeodomain-Leucine Zipper IV transcription factor OUTER CELL LAYER1 in maize identifies target genes involved in lipid metabolism and cuticle biosynthesis. *Plant Physiology* **154**: 273-286.

Kamiya T, Borghi M, Wang P, Danku JMC, Kalmbach L, Hosmani PS, Naseer S, Fujiwara T, Geldner N, & Salt DE. (2015) The MYB36 transcription factor orchestrates Casparian Strip formation. *Proceedings of the National Academy of Sciences, USA* **112**(33): 10533-10538.

Kosma DK, Molina I, Ohlrogge JB, & Pollard M. (2012). Identification of an Arabidopsis Fatty Alcohol: Caffeoyl-Coenzyme A Acyltransferase required for the synthesis of alkyl hydroxycinnamates in root waxes. *Plant Physiology* **160**: 237-248.

Kosma DK, Murmu J, Razeq FM, Santos P, Borgault R, Molina I, & Rowland O. (2014) AtMYB41 activates ectopic suberin synthesis and assembly in multiple plant species and cell types. *The Plant Journal* **80**: 216-229.

Lee T, Oh T, Yang S, Shin J, Hwang S, Kim CY, Kim H, Shim H, Shim JE, Ronald PC, & Lee I. (2015) RiceNet v2: an improved network prioritization server for rice genes. *Nucleic Acids Research* doi: 10.1093/nar/gkv253.

Lee Y, Rubio MC, Alassimone J, & Geldner N. (2014) A mechanism for localized lignin deposition in the epidermis. *Cell* **153**: 402-412.

Li H, Pinot F, Sauveplane V, Werck-Reichhart D, Diehl P, Schreiber L, Franke R, Zhang P, Chen L, Gao Y, Liang W, & Zhang D. (2010) Cytochrome P450 Family member CYP704B2 catalyzes the ω-hydroxylation of fatty acids and is required for anther cutin biosynthesis and pollen exine formation in rice. *The Plant Cell* **22**: 173-190.

Li P, Ponnala L, Gandotra N, *et al*. (2010) The developmental dynamics of the maize leaf transcriptome. *Nature Genetics* **42**: 1060-1067.

Li Y, Beisson F, Koo AJK, Molina I, Pollard M, & Ohlrogge J. (2007) Identification of acyltransferases required for cutin biosynthesis and production of cutin with suberin-like monomers. *Proceedings of the National Academy of Sciences, USA* **104**(46): 18339-18344.

Li-Beisson Y, Pollard M, Sauveplane V, Pinot F, Ohlrogge J, & Beisson F. (2009) Nanoridges that characterize the surface morphology of flowers require the synthesis of cutin polyester. *Proceedings of the National Academy of Sciences, USA* 106(51): 22008-22013.

Lois R, Dietrich A, Hahlbrock K, & Schulz W. (1989) A phenylalanine ammonia-lyase gene from parsley: structure, regulation and identification of elicitor and light responsive cis-acting elements. *EMBO Journal* **8**: 1641-1648.

Lulai, E. C., Morgan, W. C. (1992). Histochemical probing of potato periderm with neutral red: a sensitive cytofluorochrome for the hydrophobic domain of suberin. *Biotechnic and Histochemistry* **67**, 185-195.

Molina I, Li-Beisson Y, Beisson F, Ohlrogge JB, Pollard, M. (2009). Identification of an Arabidopsis Feruloyl-Coenzyme A transferase required for suberin synthesis. *Plant Physiology* **151**: 1317-1328.

Molina I & Kosma DK. (2015) Role of HXXXD-motif/BAHD acyltransferases in the biosynthesis of extracellular lipids. Plant Cell Reports 34: 587-601.

Mustroph A, Zanetti ME, Jang CJH *et al*. (2009) Profiling translatomes of discrete cell populations resolves altered cellular priorities during hypoxia in *Arabidopsis*. *Proceedings of the National Academy of Sciences U S A* **106**: 18843-18848.

Naseer, S., Lee, Y., Lapierre, C., Franke, R., Nawrath, C., and Geldner, N. (2012). Casparian strip diffusion barrier in Arabidopsis is made of a lignin polymer without suberin. *Proceedings of the National Academy of Sciences, USA* **109**: 10101-10106.

Nakazono M, Qiu F, Borsuk LA, Schnable PS. (2003) Laser-Capture Microdissection, a tool for the global analysis of gene expression in specific plant cell types: identification of genes expressed differentially in epidermal cells or vascular tissues of maize. *The Plant Cell* **15**: 583-596.

Nelson DR, Schuler MA, Paquette SM, Werck-Reichhart D, & Bak S. (2004) Comparative genomics of rice and Arabidopsis. Analysis of 727 Cytochrome P450 genes and pseudogenes from a monocot and a dicot. *Plant Physiology* **135**: 756-772.

O'Brien TP, Carr DJ. (1970) A suberized layer in the cell walls of the bundle sheath of grasses. *Australian Journal of Biological Sciences* **23**: 275-283.

Palaniswamy SK *et al*. (2006) AGRIS and AtRegNet, a platform to link *cis*-regulatory elements and transcription factors into regulatory networks. *Plant Physiology* **140**: 818-829.

Penning BW, Hunter CT, Tayengwa R, Eveland AL, Dugard CK, Olek AT, Vermerris W, Koch KE, McCarty DR, Davis MF, Thomas SR, McCann MC, & Carpita NC. (2009) Genetic resources for maize cell wall biology. *Plant Physiology* **151**: 1703-1728.

Pinot F & Beisson F. (2011) Cytochrome P450 metabolizing fatty acids in plants: characterization and physiological roles. *The FEBS Journal* **278**: 195-205.

Pollard M, Beisson F, Li Y, & Ohlrogge JB. (2008) Building lipid barriers: biosynthesis of cutin and suberin. *Trends in Plant Science* **13**: 236-246.

Pozuelo JM, Espelie KE, & Kolattukudy PE. (1984) Magnesium deficiency results in increased suberization in endodermis and hypodermis of corn roots. *Plant Physiology* **74**(2): 256-260.

Rautengarten C, Ebert B, Ouellet M, Nafisi M, Baidoo EEK, Benke P, Stranne M, Mukhopadhyay A, Keasling JD, Sakuragi Y, & Scheller HV. (2012) Arabidopsis *Deficient in Cutin Ferulate* encodes a transferase required for feruloylation of ω-hydroxy fatty acids in cutin polyester. *Plant Physiology* **158**: 654-665.

Richardson A, Wojciechowski T, Franke R, Schreiber L, Kerstiens G, Jarvis M, & Fricke W. (2007) Cuticular permeance in relation to wax and cutin development along the growing barley (*Hordeum vulgare*) leaf. *Planta* **225**: 1471-1481.

Rushton PJ *et al*. (1996) Interaction of elicitor-induced DNA-binding proteins with elicitor response elements in the promoters of parsley *PR1* genes. *EMBO Journal* **15**: 5690-5700.

Roppolo D, Boeckmann B, Pfister A, Boutet E, Rubio MC, Dénervaud-Tendon V, Vermeer JEM, Gheyselinck J, Xenarios I, & Geldner N. (2014) Functional and evolutionary analysis of the CASPARIAN STRIP MEMBRANE DOMAIN PROTEIN Family. *Plant Physiology* **165**: 1709-1722.

Saitou N & Nei M. (1987) The neighbor-joining method: A new method for reconstructing phylogenetic trees. *Molecular Biology and Evolution* **4**:406-425.

Sauveplane V, Kandel S, Kastner P-E, Ehlting J, Compagnon V, Werck-Reichhart D, & Pinot F. (2009) *Arabidopsis thaliana* CYP77A4 is the first cytochrome P450 able to catalyze the epoxidation of free fatty acids in plants. *The FEBS Journal* **276**: 719-735.

Schreiber L, Franke F, Hartmann K-D, Ranathunge K, & Steudle E. (2005) The chemical composition of suberin in apoplastic barriers affects radial hydrualic conductivity differently in the roots of rice (*Oryza sativa* L. cv. IR64) and corn (*Zea mays* L. cv. Helix). *Journal of Experimental Botany* **56**(415): 1427-1436.

Sekhon RS, Lin HN, Childs KL, Hansey CN, Buell CR, de Leon N, Kaeppler SM. (2011). Genome-wide atlas of transcription during maize development. *The Plant Journal* **66**: 553-563.

Serra O, Soler M, Hohn C, Sauveplane V, Pinot F, Franke R, Schreiber L, Prat S, Molinas M, & Figueras M. (2009) *CYP86A33*-targeted gene silencing in potato tuber alters suberin composition, distorts suberin lamellae, and impairs the periderm's water barrier function. *Plant Physiology* **149**: 1050-1060.

Shiono K, Ando M, Nishiuchi S, *et al*. (2014a) RCN1/OsABCG5, an ATP-binding cassete (ABC) transporter, is required for hypodermal suberization of roots in rice. *The Plant Journal* **80**: 40-51.

Shiono K, Yamaguchi T, Yamazaki S, Mohanti B, Malik AI, Nagamura Y, Nishizawa NK, Tsutsumi N, Colmer T, & Nakazono M. (2014b) Microarray analysis of laser-microdissected tissues indicates the biosynthesis of suberin in the outer part of roots during formation of a barrier to radial oxygen loss in rice (*Oryza sativa*). *Journal of Experimental Botany* **65**(17): 4795-4806.

Slewinski TL, Anderson AA, Zhang C, & Turgeon R. (2012) Scarecrow plays a role in establishing Kranz anatomy in maize leaves. *Plant and Cell Physiology* **53**(12): 2030-2037.

Slewinski TL, Anderson AA, Price S, Withee JR, Gallagher K, and Turgeon R. (2014) Short-Root1 plays a role in the development of vascular tissue and Kranz anatomy in maize leaves. *Molecular Plant* **7**(8): 1388-1392.

Stelpflug SC, Sekhon RS, Vaillancourt B, Hirsch CN, Buell CR, de Leon N, & Kaeppler SM. (2015) An expanded maize gene expression atlas based on RNA-sequencing and its use to explore root development. *The Plant Genome* doi:10.3835/plantgenome2015.04.0025.

Takahashi K, Shimada T, Kondo M, Tamai A, Mori M, Nishimura M, & Hara-Nishimura I. (2010) Ectopic expression of an esterase, which is a candidate for the unidentified plant cutinase, causes cuticular defects in *Arabidopsis thaliana*. *Plant and Cell Physiology* **51**(1): 123-131.

Tamura K, Stecher G, Peterson D, Filipski A, & Kumar S. (2013) MEGA6: Molecular Evolutionary Genetics Analysis version 6.0. *Molecular Biology and Evolution* **30**: 2725-2729.

Verrier PJ, Bird D, Burla B, *et al*. (2008) Plant ABC proteins – a unified nomenclature and updated inventory. *Trends in Plant Science* **13**(4): 151-159.

Wang L, Czedik-Eysenberg A, Mertz RA, *et al*. (2014) Comparative analysis of C4 and C3 photosynthesis in developing leaves of maize and rice. *Nature Biotechnology* **32(11)**: 1158-1165.

Waßmann FFM. (2014) Suberin biosynthesis in *O. sativa*: Characterisation of a cytochrome P450 monooxygenase. PhD Dissertation, University of Bonn.

Yadav V, Molina I, Ranathunge K, Castillo IQ, Rothstein SJ, & Reed JW. (2014) ABCG transporters are required for suberin and pollen wall extracellular barriers in *Arabidopsis*. *The Plant Cell* **26**: 3569-3588.

Yang W, Pollard M, Li-Beisson Y, Beisson F, Feig M, and Ohlrogge JB. (2010) A distinct type of glycerol-3-phosphate acyltransferase with *sn*-2 preference and phosphatase activity producing 2-monoacylglycerol. *Proceedings of the National Academy of Sciences, USA* **107**(26): 12040-12045.

Yang W, Simpson JP, Li-Beisson Y, Beisson F, Pollard M, & Ohlrogge JB. (2012) A land-plant-specific Glycerol-3-Phosphate Acyltransferase family in Arabidopsis: substrate specificity, *sn*-2 preference, and evolution. *Plant Physiology* **160**: 638-652.

Yeats TH, Martin LBB, Viart HMF, Isaacson T, He Y, Zhao L, Matas AJ, Buda GJ, Domozych, DS, Clausen MH, Rose JKC. (2012) The identification of cutin synthase: formation of the plant polyester cutin. *Nature Chemical Biology* **8**, 609-611.

Yeats TH & Rose JKC. (2013) The formation and function of plant cuticles. *Plant Physiology* **163**: 5-20.

Yeats TH, Huang W, Chatterjee S, Viart HM-F, Clausen MH, Stark RE & Rose JKC. (2014) Tomato Cutin Deficient 1 (CD1) and putative orthologs comprise an ancient family of cutin synthase-like (CUS) proteins that are conserved among land plants. *The Plant Journal* **77**: 667-675.

Zeier J, Ruel K, Ryser U, & Schreiber L. (1999) Chemical analysis and immunolocalisation of lignin and suberin in endodermal and hypodermal/rhizodermal cell walls of developing maize (*Zea mays* L.) primary roots. *Planta* **209**, 1-12.

Zhou J, Lee C, Zhong R & Ye Z-H. (2009) MYB58 and MYB63 are transcriptional activators of the lignin biosynthetic pathway during secondary cell wall formation in *Arabidopsis*. *The Plant Cell* **21**: 248-266.

Zuckerkandl E & Pauling L. (1965) Evolutionary divergence and convergence in proteins. Edited in *Evolving Genes and Proteins* by V. Bryson and H.J. Vogel, pp. 97-166. Academic Press, New York.

CHAPTER THREE

THE MAIZE *ALIPHATIC SUBERIN FERULOYL TRANSFERASE* GENES ARE ESSENTIAL FOR BUNDLE SHEATH SUBERIN ULTRASTRUCTURE BUT DISPENSABLE FOR BARRIER FUNCTION

ABSTRACT

C_4 grasses often outperform C_3 species under hot, arid conditions due to superior water and nitrogen use efficiencies and lower rates of photorespiration. A method of concentrating CO_2 around the site of carbon fixation in the bundle sheath (BS) is required to realize these gains. In NADP-malic enzyme (NADP-ME)-type C_4 grasses such as maize, suberin deposition in the BS cell wall is hypothesized to act as a diffusion barrier to CO_2 escape and O_2 entry from surrounding mesophyll cells. Suberin is a heteropolyester comprised of acyl-lipid-derived aliphatic and phenylpropanoid-derived aromatic components. Suberin is synthesized by a large network of biosynthesis and regulatory genes, none of which have been characterized in maize.

To disrupt aromatic suberin synthesis, two paralogously duplicated, unlinked maize orthologues of *Arabidopsis thaliana ALIPHATIC SUBERIN FERULOYL TRANSFERASE*, *ZmAsft1* and *ZmAsft2*, were mutated using closely linked *Dissociation* transposons. Loss-of-function double mutants revealed a 97% reduction in suberin-specific omega-hydroxy fatty acids without a stoichiometric decrease in ferulic acid. However, bundle suberin lamellae were deficient in electron opaque material, and cohesion between the suberin lamellae and polysaccharide cell walls was attenuated in double mutants. There were no other morphological phenotypes under ambient conditions. Furthermore, there was no significant effect on net CO_2 assimilation at any intercellular CO_2 concentration, and no effect on ^{13}C isotope discrimination

relative to wild type. Thus, *ZmAsft* expression is not required to establish a functional CO_2 concentrating mechanism in in maize. Double mutant leaves exhibit elevated cell wall elasticity, transpirational flux, and stomatal conductance relative to WT. Thus, the ZmAsft genes are dispensable for gas exchange barrier function but may be involved in regulation of leaf water movement.

INTRODUCTION

Cereal crops are among our most productive sources of food, feed, and fuel. Just three staple cereals, rice (*Oryza sativa*), wheat (*Triticum aesetivum*), and maize (*Zea mays*) are estimated to provide 42.5% of dietary calories consumed directly by humans and 30% of dietary protein (FAO, 2015). Global food demand is forecasted to increase significantly over the coming decades, and will be double the current level by 2050 (Tillman *et al*., 2011). However, at their current rate of growth, maize, rice, and wheat yields are forecasted to increase by only 67%, 42%, and 38%, respectively, far short of the level required to keep pace with population growth (Ray *et al*., 2013). It was estimated that a 50% yield increase on existing acreage without additional fertilizer inputs could be generated in the C_3 cereal crop rice by engineering novel cultivars utilizing the C_4 photosynthetic pathway (Mitchell and Sheehy, 2006).

In grasses utilizing C_4 photosynthesis, CO_2 is incorporated into a 4-carbon organic acid in the leaf mesophyll (M) cells and released proximal to the active site of the Rubisco carboxylase in an internal cell layer, the bundle sheath (BS), located proximal to the leaf vasculature (termed Kranz Anatomy; reviewed in Sage, 2004). This carbon concentrating mechanism protects the plant from photorespiration under hot, arid conditions and significantly increases the water and nitrogen use efficiencies relative to C_3 species (Sage, 2004; Taylor *et al*., 2010). C_4 species are

broadly grouped into three classes, termed NAD-ME, PEPCK, and NADP-ME-type, based on the primary decarboxylase used to release CO_2 within the BS, although most species can utilize multiple decarboxylases (reviewed in Furbank, 2011). Efforts are now underway to functionally dissect and reverse engineer the NADP-ME-type C_4 pathway utilized by maize, sorghum (*Sorghum bicolor*), and sugarcane (*Saccharum officinarum*) into rice (Langdale, 2011; von Caemmerer *et al.*, 2012). In addition to cell-type specific expression of key carbon concentrating genes, multiple anatomical modifications may be required, including greater vein density, increased plasmodesmatal connections between BS and M, and the introduction of suberin lamellae (SL) into the BS cell walls at the BS/M interface (reviewed in Nelson, 2011).

Over forty years ago, SL were proposed to act as gas diffusion barriers, facilitating CO_2 concentration within the BS while blocking penetration of atmospheric O_2, thereby reducing photorespiration (Laetsch, 1971). Suberized BS cells are not uniformly distributed across the grasses. Although they are generally present in NADP-ME and PEPCK-type C_4 species, both NAD-ME-type C_4 and C_3 grasses have an unsuberized outer BS and a non-photosynthetic, suberized tissue termed the mestome sheath proximal to the vasculature (Hattersley & Browning, 1981; Eastman *et al*., 1988a). Carbon isotope discrimination ratios and estimates of BS leakiness are comparable between suberized and unsuberized C_4 grasses (Henderson *et al*., 1992; von Caemmerer *et al*., 2014; Kromdijk *et al*., 2014). This implies either that the thickened lignocellulosic walls and elongated diffusion path of NAD-ME species constitutes an equally effective gas exchange barrier (Hattersley and Browning, 1981), or that SL are not essential for the CO_2 concentrating mechanism. Thus, their function within NADP-ME-type grasses must be tested before engineering these structures into C_4 rice. However, BS suberization has not been

characterized in a uniform genetic background due to a lack of candidate genes and targeted mutagenesis tools in C_4 grasses (Chapter 1).

Suberin is a heteropolyester comprised of both aliphatic and aromatic components. In maize, the principal aliphatic monomers are C_{16}-C_{28} fatty acids and several classes of oxidized and reduced derivatives, including primary alcohols, 2-hydroxy fatty acids, omega-hydroxy fatty acids, and alpha, omega-dicarboxylic acids (Espelie and Kolattukudy, 1979; Pozuelo *et al*., 1984; Zeier *et al*., 1999; Zimmermann et al., 2000; Schreiber *et al*., 2005a). The same aliphatic monomer classes are present in the epidermal cuticle (Espelie and Kolattukudy, 1979); however, suberin is consistently enriched in very long chain ($\geq C_{20}$) aliphatic species and aromatic monomers relative to cutin across multiple taxa (Pollard *et al*., 2008). The predominant aromatic monomers are the hydroxycinnamic acids *p*-coumaric and ferulic acid (Zeier *et al*., 1999). Hydroxycinnamic acids are not specifically associated with suberin in maize leaves. Maize has a Type II primary cell wall with extensive esterification of ferulic acid to the arabinosyl side chains of the hemicellulose glucuronoarabinoxylan (GAX; reviewed in Carpita and Gibeaut, 1993). Likewise, substantial quantities of *p*-coumaric acid are present in maize lignin as esterified side groups of sinapyl alcohol residues (Hatfield *et al*., 2008b). Although the suberin, GAX, and lignin-related hydroxycinnamoyl transferases are thought to be phylogenetically distinct enzymes belonging to the BAHD acyltransferase super-family (Mitchell *et al*., 2007; Tuominen *et al*., 2011; Bartley *et al*., 2013), no aliphatic suberin O-hydroxycinnamoyl transferases have been characterized to date in any monocot.

Recently, multiple hydroxycinnamoyl transferases involved in cutin, suberin, and suberin-associated wax biosynthesis have been characterized in the model dicots Arabidopsis (*Arabidopsis thaliana*), potato (*Solanum tuberosum*) and poplar (*Populus trichocarpa*; reviewed

in Molina and Kosma, 2015). Arabidopsis *ALIPHATIC SUBERIN FEULOYL TRANSFERASE* (*AtASFT*; Gou *et al*., 2009; Molina *et al*. 2009) and potato *ω-Hydroxy fatty acid/fatty alcohol hydroxycinnamoyl transferase* (*StFHT*; Serra *et al*., 2010a) are required for normal incorporation of ferulic acid and hydroxylated acyl lipids into the suberin polyester in an apparent 1:1 stoichiometry (Molina et al., 2009). Expression of *AtASFT* and *StFHT* is dispensable for normal suberin ultrastructure but required to form functional barriers to the unrestricted diffusion of salts and water across the seed coat and tuber periderm, respectively (Gou et al., 2009; Molina et al., 2009; Serra et al., 2010a). Conversely, mutants of the cutin feruloyl transferase *DEFICIENT IN CUTIN FERULATE* (*AtDCF*) and the wax-related *FATTY ALCOHOL:CAFFEOYL-CoA CAFFEOYL TRANSFERASE* (*AtFACT*) have negligible effects on barrier function (Rautengarten et al., 2012; Kosma et al., 2012). Thus, the maize *ASFT* homologues are promising targets with which to disrupt BS suberization without significantly compromising cutin barrier function.

Previously, a putative suberin biosynthetic pathway was delineated and a subset of genes expressed concurrently with vascular sheath suberization was identified in both maize and rice (Li *et al*., 2010; Wang *et al*., 2014; Chapter 2). This subset contained putative maize homologues of several genes specifically involved in suberin biosynthesis in Arabidopsis, including *CYTOCHROME P450 86B1* (*AtCYP86B1*; Compagnon et al., 2009), *GLYCEROL-3-PHOSPHATE ACYLTRANSFERASE 5* (*AtGPAT5;* Beisson *et al*., 2007), and three putative maize homologues of *AtASFT,* hereafter called *ZmAsft1*, *ZmAsft2*, and *ZmAsft3*. Of the candidate genes in this cluster, only the *ZmAsft* genes had one or more *Dissociation* transposons from the maize *Activator*/*Dissociation* collection in sufficiently tight genetic linkage to generate targeted insertion mutants (Table 3.1; Ahern *et al*., 2009; Vollbrecht *et al*., 2010). To investigate whether the suberized BS cell wall acts as an apoplastic diffusion barrier for the C_4 carbon concentrating

mechanism, an allelic series of mutations in *ZmAsft1* and *ZmAsft2* was generated by targeted insertional mutagenesis using *Dissociation* elements. *ZmAsft1* and *ZmAsft2* were found to be redundantly essential for normal accumulation of very long chain omega-hydroxy fatty acids in leaf polyesters, and the ultrastructure of the BS cell wall was compromised in double mutants. However, the *ZmAsft* genes were not required for normal CO_2 assimilation at any measured intercellular CO_2 level, nor was carbon-13 isotopic discrimination affected. Likewise, double mutants maintained wild type levels of growth during waterlogging stress. Transpirational flux and stomatal conductance were elevated under high irradiance in double mutant leaves relative to WT, and the elastic modulus of the cell wall was elevated, suggesting that the ultrastructure of the mutant cell wall was more permissive toward water efflux from the veins. Thus, the *ZmAsft* genes are dispensable for the establishment of the carbon concentrating mechanism but have a minor effect on normal leaf water movement. The implications of the ultrastructure and barrier properties of the *Zmasft* mutants toward current models of suberin structure are discussed.

RESULTS

Asfta1 and *Asfta2* are expressed concurrently with suberin synthesis in maize leaves.

Asft1 (GRMZM2G034360; Chr. 8) and *Asft2* (AC155610.2_FG007; Chr. 3) are syntenic paralogues resulting from an ancestral polyploidy event in the maize lineage after it diverged from *Sorghum* (Figure 3.1A; Schnable *et al*., 2009). *Asft3* (GRMZM2G168499; Chr. 10) is an unlinked paralogue of *Asft2* (Figure 3.1A). Although the protein encoded by the predicted *Asft3* gene model contains the HXXXD and DFGWG motifs of a canonical BAHD acyltransferase (D'Auria, 2006), it lacks the N-terminal amino acids encoded by Exons 1 and 2 of *Asft1* and *Asft2*, and is not transcribed in either B73 or W22 leaves (Figure 3.2A-B). Thus, it was

Figure 3.1. Identification and mutagenesis of two putative maize *Aliphatic Suberin Feruloyl Transferase* genes.

- **A.** Rooted Neighbor-Joining phylogeny of ASFT sub-clade proteins from grasses and model dicots (Saitou & Nei, 1987). AtHCT, a BAHD acyltransferase involved in lignin biosynthesis (Hoffmann *et al*., 2004), serves as the outgroup. Bootstrap support (1000 replicates) is shown next to the corresponding branches (Felsenstein, 1985). Evolutionary distances were computed using the Poisson correction method (Zuckerkandl & Pauling, 1965) and branch lengths are scaled to the number of amino acid substitutions per site. Evolutionary analyses were conducted in MEGA6 (Tamura *et al*., 2013).
- **B.** Expression profile of *ZmAsft1* and *ZmAsft2* during leaf development. Developing third leaves of 10-day-old T43 were divided into 1 cm increments relative to the leaf base. For both genes, expression is strongest in the transition zone proximal to the point of emergence (dashed green line), with minimal expression at the base or in emergent tissue. Gene expression is presented as a normalized relative quantity (NRQ). Relative expression values ($E^{\Delta CT}$ method) were calculated for *ZmAsft1*, *ZmAsft2*, and three references (*ZmUbq*, *Zm18S*, and *ZmTub*) and NRQs were calculated by dividing *ZmAsft* by the geometric mean of the references. Data are presented as means plus standard deviations of duplicate cDNA preparations from 3 biological replicates.
- **C.** Mutagenesis of the *ZmAsft* genes using *Dissociation* transposons. *Dissociation* (*Ds*) donor lines I.S07.2991, B.W06.0682, I.S07.1288, and *asft2-m2:Ds*, each containing an unlinked copy of *Activator-immobilized* (*Ac-im*) as a source of transposase, were testcrossed to T43. Four novel *Ds* insertion alleles of *ZmAsft1* (*asft1-m1:Ds-asft1-m4:Ds*) and five alleles of *ZmAsft2* (*asft2-m1:Ds-asft2-m5:Ds*) were identified. *Ac-im* was segregated away in subsequent generations to stabilize the insertions, and single mutants were crossed to generate double mutants. Triangles denote *Ds* transposons; the black corner indicates the 5' end of the non-functional transposase gene that introduces a premature transcription terminator when inserted in the same orientation as *ZmAsft*. Blue and purple boxes denote exons of *ZmAsft1* and *ZmAsft2*, respectively, and gray boxes denote UTRs. Gene models are drawn to scale.
- **D.** qPCR analysis of *ZmAsft* single and double mutants. Gene expression of *ZmAsft1* and *ZmAsft2* was analyzed in the transition zone of 10-day-old third leaves as described in Figure 1.1B. Expression was attenuated by approximately 99% for both *Asft1* and *Asft2* in double and corresponding single mutants (one-way ANOVA, $p < 0.001$). Different letters indicate significant differences between genotypes by a Tukey-Kramer post-hoc test ($p < 0.05$).

A.

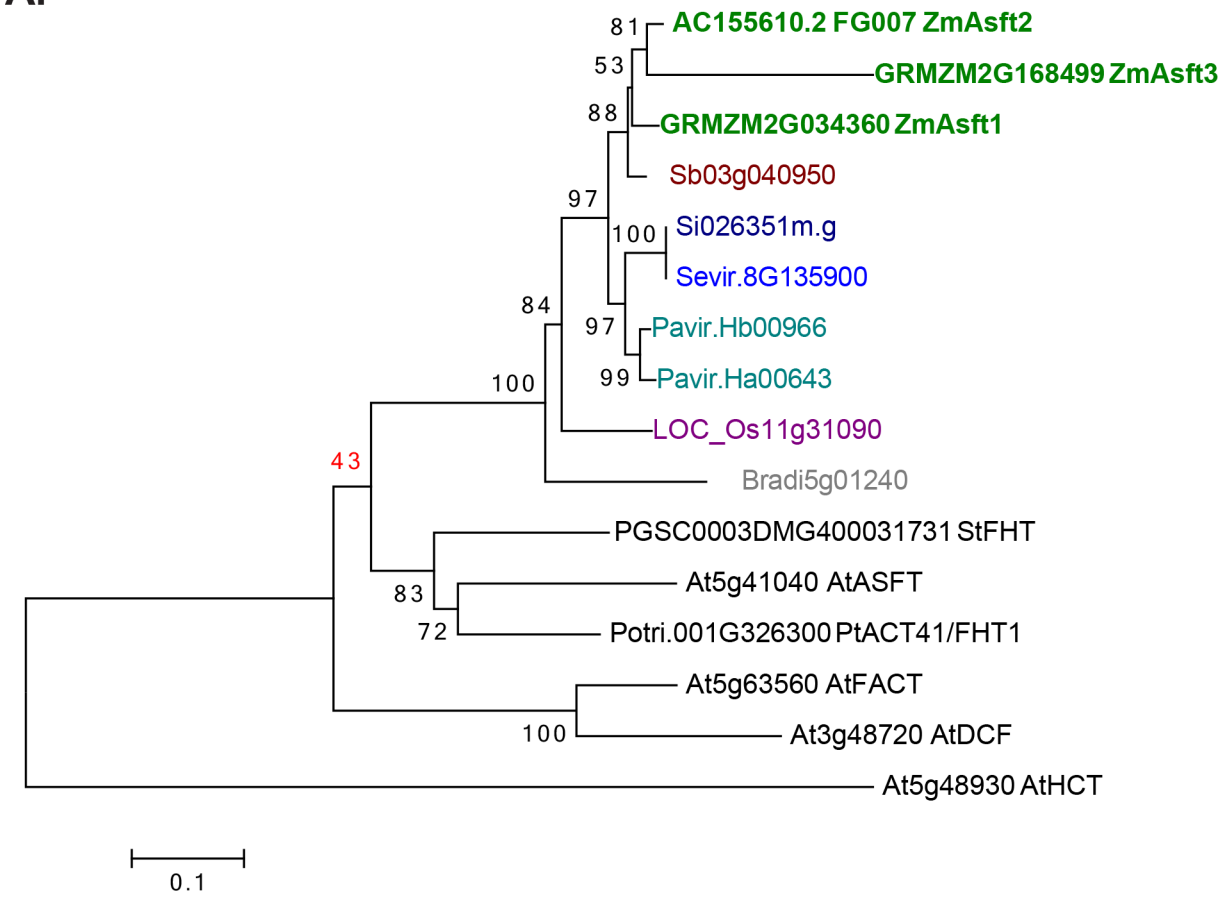
81
AC155610.2 FG007 ZmAsft2
53
GRMZM2G168499 ZmAsft3
88
GRMZM2G034360 ZmAsft1
Sb03g040950
97
100
Si026351m.g
Sevir.8G135900
84
97
Pavir.Hb00966
99
Pavir.Ha00643
100
LOC_Os11g31090
43
Bradi5g01240
PGSC0003DMG400031731 StFHT
83
At5g41040 AtASFT
72
Potri.001G326300 PtACT41/FHT1
At5g63560 AtFACT
100
At3g48720 AtDCF
At5g48930 AtHCT
0.1

B.

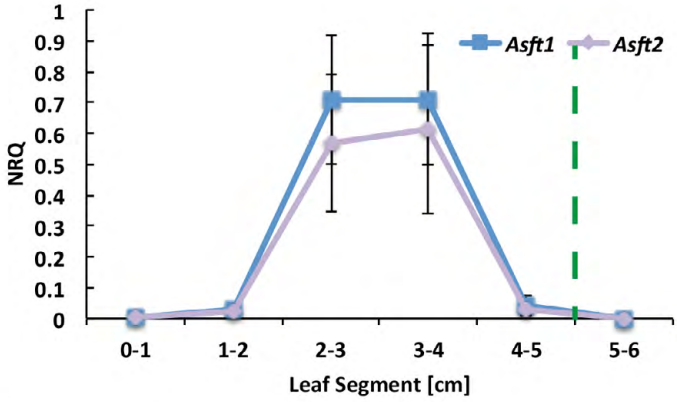
1
0.9
0.8
0.7
0.6
0.5
0.4
0.3
0.2
0.1
0
NRQ
Asft1
Asft2
0-1
1-2
2-3
3-4
4-5
5-6
Leaf Segment [cm]

C.

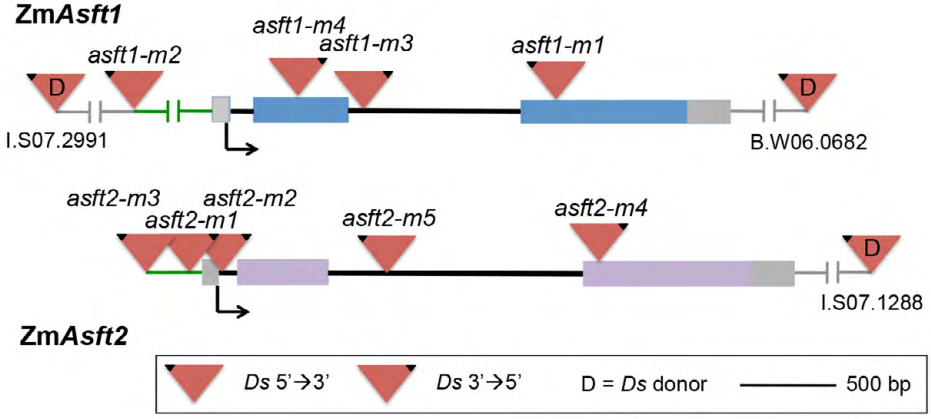
ZmAsft1
asft1-m2
asft1-m4
asft1-m3
asft1-m1
D
D
I.S07.2991
B.W06.0682
asft2-m3
asft2-m2
asft2-m1
asft2-m5
asft2-m4
D
I.S07.1288
ZmAsft2
Ds 5'→3'
Ds 3'→5'
D = Ds donor
500 bp

D.

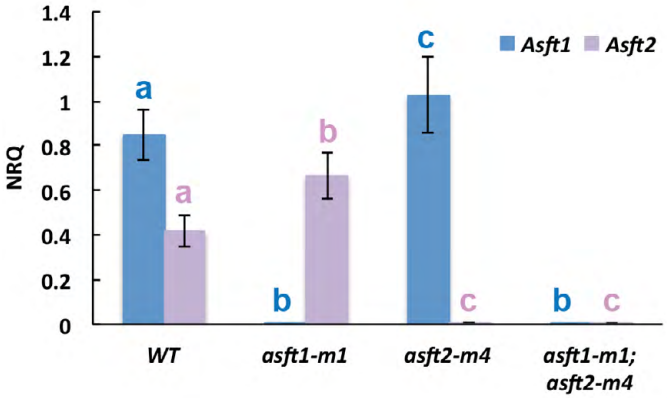
1.4
1.2
1
0.8
0.6
0.4
0.2
0
NRQ
Asft1
Asft2
a
a
b
b
c
c
b
c
WT
asft1-m1
asft2-m4
asft1-m1;
asft2-m4

Figure 3.2. *ZmAsft3* is a putative pseudogene.

A. Multiple sequence alignment of *ZmAsft* amino acid sequences with *AtASFT*. *ZmAsft3* aligns with sequences present in the second and third exons of *ZmAsft1* and *ZmAsft2*. Although it contains the canonical HXXXD and DFGWG motifs characteristic of BAHD acyltransferases (green boxes), it lacks the N-terminal sequences present in *ZmAsft1*, *ZmAsft2*, and *AtASFT*. Sequences were aligned with MultAlin (http://multalin.toulouse.inra.fr/multalin/) using the default parameters.
B. Analysis of *ZmASFT* gene expression in developing leaves by RT-PCR. Primers specific to *ZmAsft1* and *ZmAsft2* generate amplicons in both gDNA and cDNA samples, but not in cDNA samples prepared without reverse transcriptase ("No RT"), indicating that these genes are transcribed in both inbred backgrounds (B73 and T43). Conversely, *ZmAsft3* primers generate multiple non-specific amplicons, and the band corresponding to the 3'UTR of the gene (red arrow) is absent from cDNA preparations, indicating that this gene is not transcribed in developing leaves in either genetic background. Estimated amplicon sizes are 65 bp, 118 bp, and 66 bp, respectively. Samples were run on a 4% agarose gel containing 1% (v/v) ethidium bromide, and amplicon sizes were confirmed using a 25 bp DNA ladder (Invitrogen).

A.

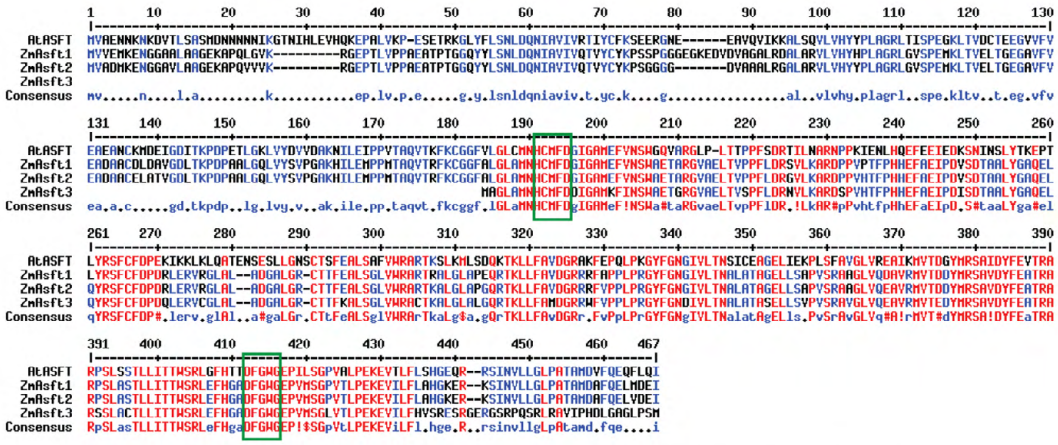
AtASFT
ZmAsft1
ZmAsft2
ZmAsft3
Consensus

B.

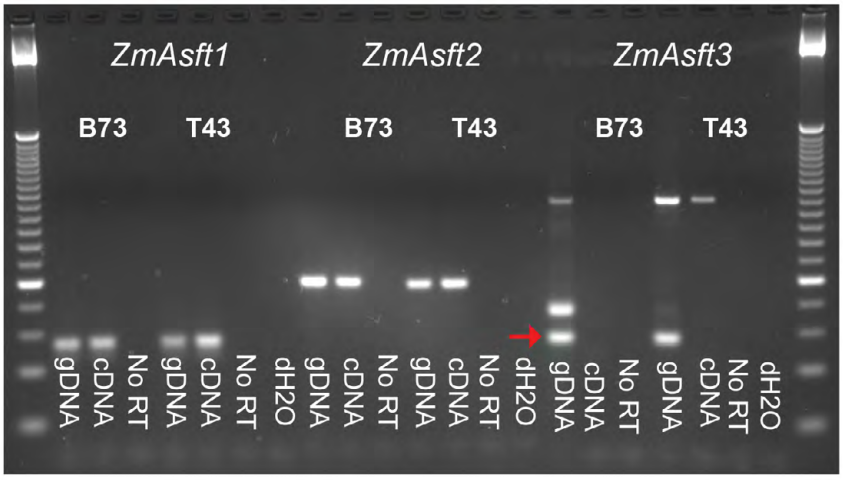
ZmAsft1
ZmAsft2
ZmAsft3
B73
T43
B73
T43
B73
T43
gDNA
cDNA
No RT
gDNA
cDNA
No RT
dH2O
gDNA
cDNA
No RT
gDNA
cDNA
No RT
dH2O
gDNA
cDNA
No RT
gDNA
cDNA
No RT
dH2O

concluded that *Asft3* is likely a pseudogene and *ZmAsft1* and *ZmAsft2* were selected for further characterization.

Asft1 and *Asft2* are expressed in multiple vegetative tissues, including seedling primary and seminal roots, developing juvenile and adult leaves, and husks (Figure 3.3A-B; Sekhon *et al*., 2011; Stelpflug *et al*., 2015). In developing leaves of the inbred B73, the parental line of the maize reference genome, expression is restricted to a narrow spatiotemporal region concurrent with maturation of metaxylem vessels (Li *et al*., 2009; Wang *et al*., 2014; Chapter 2). To determine whether *Asft1* and *Asft2* are expressed in a similar pattern in developing leaves of T43, a near isogenic line of the W22 inbred which is the parental line of the *Ac*/*Ds* collection, qRT-PCR was performed with gene-specific primers. The expression pattern in T43 was similar to B73; both paralogues were strongly expressed in the transition zone proximal to the point of emergence, with negligible expression at the leaf base or in emerging source tissue proximal to the second leaf ligule (Figure 3.1B). Thus *Asft1* and *Asft2* are likely to play similar roles during leaf maturation in both genetic backgrounds.

In Arabidopsis, feruloylation of root suberin and leaf cutin are performed by two separate but closely related acyltransferases, ASFT and DEFICIENT IN CUTIN FERULATE (DCF; Gou *et al*., 2009; Molina *et al*., 2009; Rautengarten *et al*., 2012). However, phylogenetic analysis of the ASFT sub-clade did not reveal a clear maize orthologue of AtDCF (Figure 3.1A). To investigate whether the *ZmAsft* genes are expressed in both suberized and cutinized leaf tissues, laser capture microdissection was performed on third leaf laminae to capture bundle sheath and epidermal cells from the region of maximal *Asft1* and *Asft2* expression. *Asft1* and *Asft2* are expressed in both bundle sheath and epidermal cells, suggesting that the tissue-specific pattern of hydroxycinnamoyl transferase expression observed for Arabidopsis *ASFT* and *DCT* is not

conserved in maize (Figure 3.3B). The ASFT sub-clade contains a single candidate from Sorghum (*Sorghum bicolor*), foxtail millet (*Setaria italica*), green millet (*Setaria viridis*), and rice (*Oryza sativa*), as well as two paralogous duplicates from the tetraploid switchgrass (*Panicum virgatum*; Figure 3.1A). AtDCF is clearly resolved from the putative grass ASFT homologues. Therefore, broad expression of single or redundantly duplicated *AtASFT* orthologues may be a general feature of Graminaceous monocots.

In addition to developing leaves, *Asft1* and *Asft2* expression was also analyzed in seedling primary roots. Unlike the narrow spatiotemporal region of expression observed in developing leaves, both paralogues were abundantly expressed throughout the entire length of the seedling primary root (Figure 3.3C). Further work is necessary to determine whether gene expression is specific to the suberized endo- and exodermal layers, and whether a similar pattern of expression also occurs in the nodal roots which comprise the majority of the root system at maturity (Esau, 1965). Nonetheless, the general pattern of gene expression is consistent with a role in suberin polyester synthesis. Thus, both paralogues were mutagenized by targeted reverse genetics using *Dissociation* transposons.

The A*sft* genes are amenable to mutagenesis with *Dissociation* transposons

The high degree of sequence similarity (94% identity of coding sequence; Figure 3.2A) and similar patterns of expression indicated that *Asft1* and *Asft2* were likely functionally redundant. Thus, *Dissociation* (*Ds*) transposon donors in tight linkage to *Asft1* (I.S07.2991; 71.9 kb upstream) and *Asft2* (I.S07.1288; 29.3 kb downstream) were selected from the *Activator*/*Dissociation* (*Ac*/*Ds*) collection and targeted reverse genetic screens were carried out for both paralogues.

Figure 3.3. Organ and tissue-specific expression analysis of *ZmAsft* genes.

A. RNA-Sequencing expression atlas of *ZmAsft1* and *ZmAsft2*. Gene records for *ZmAsft1* (GRMZM034360) and *ZmAsft2* (AC155610.2_FG007) were queried at Maize GDB (http://www.maizegdb.org), and the RNA-Seq expression atlases for each gene were downloaded for comparison. The expression patterns for both genes were largely identical. Both genes are most strongly expressed in differentiating primary roots (brown) and in developing leaves (green). Expression is limited in tassels (orange) and developing seeds (yellow).

B. RT-PCR of Laser Capture Microdissected leaf tissues. Tissue samples from the transition zone of 10-day-old third leaves were harvested, sectioned, and fixed in ice cold acetone prior to laser capture microdissection of bundle sheath (BS) and epidermal cells (Epi). Triplicate samples were evaluated for *ZmAsft1*, *ZmAsft2*, and *ZmUbq1* expression, with pooled cDNA prepared from undissected sibling tissue serving as a control (+). The rightmost lane immediately proximal to the 25 bp ladder contains a dH_2O blank as a negative control. Samples were run on a 4% agarose gel containing 1% (v/v) ethidium bromide.

C. RT-PCR of developing seedling primary roots. Primary roots of 10-day-old wild type seedlings were excised at the base of the kernel and divided into portions of equal length (Root 1-5; Section 1 is apical and Section 5 is basal). The base and transition zones of developing leaves from the same plants were divided into 2 cm increments and collected as a positive control (Leaf 1-3). Duplicate samples were evaluated for *ZmAsft1*, *ZmAsft2*, and *ZmUbq* expression as described in Figure 3.2. Both *ZmAsft* genes were strongly expressed along the entire developmental gradient of the seedling primary root.

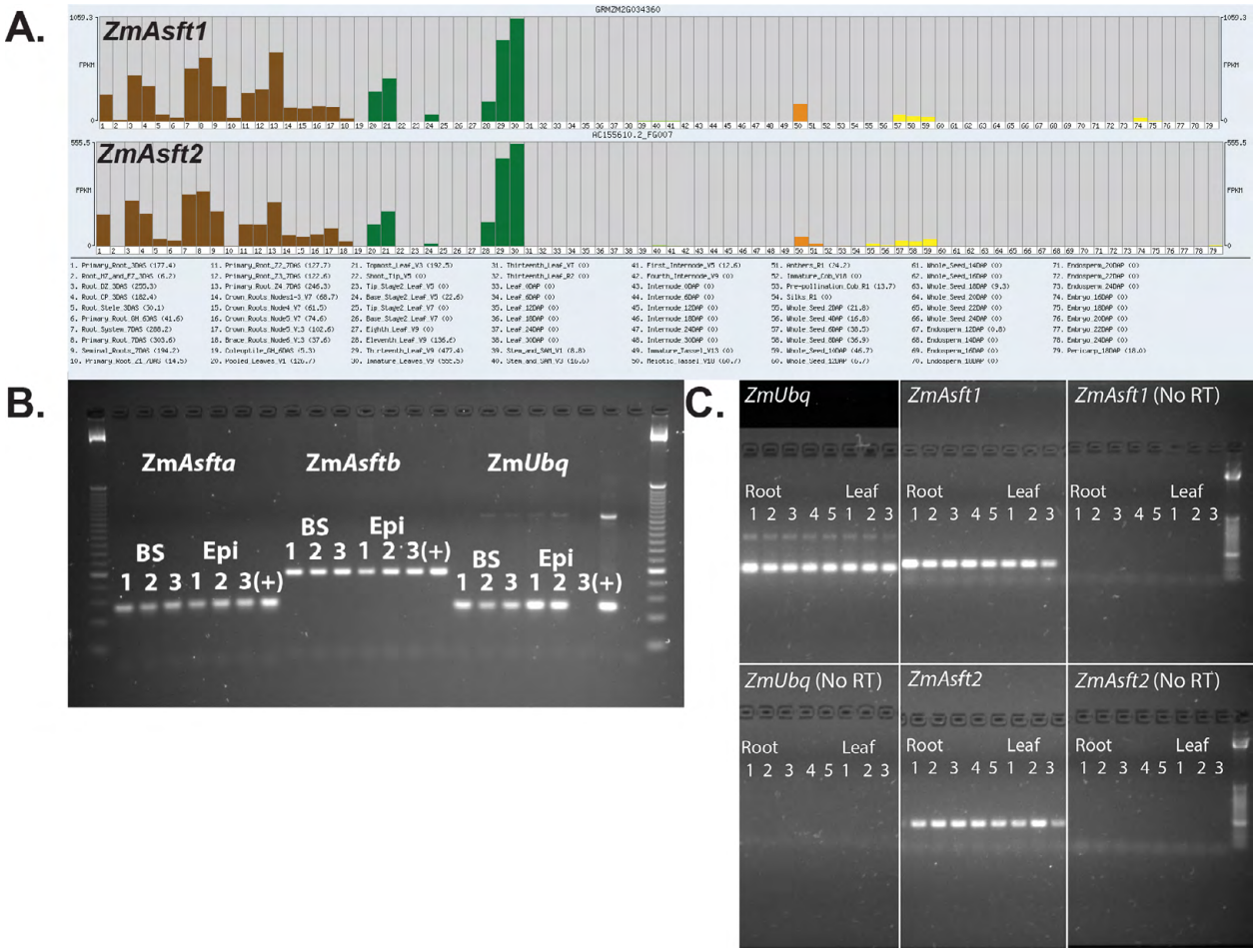
A.
ZmAsft1
ZmAsft2
B.
ZmAsfta
ZmAsftb
ZmUbq
BS
Epi
1 2 3 1 2 3(+)
C.
ZmUbq
ZmAsft1
ZmAsft1 (No RT)
ZmUbq (No RT)
ZmAsft2
ZmAsft2 (No RT)
Root
Leaf
1 2 3 4 5 1 2 3

In total, 5,400 testcross progeny of the I.S07.2991 donor were screened and a single insertion allele was recovered in Exon 3 of *Asft1* (*asft1-m1::Ds*; Figure 3.1C; Table 3.1). The low germinal insertion frequency (0.019%) of this initial screen prompted the selection of a second, more tightly linked *Ds* donor, B.W06.0682 (68.8 kb downstream of *Asft1*), which was utilized to generate a second testcross population. 1,800 progeny were screened to generate three additional independent insertion alleles, *asft1-m2::Ds*, *asft1-m3::Ds*, and *asft1-m4::Ds* (Figure 3.1C). The insertion frequency of this screen, 0.17%, was comparable to the figure previously reported for intergenic transposition events (Studer *et al*., 2014 and unpublished observations). *Asft1-m1::Ds* was confirmed to be a null allele by qRT-PCR (one-way ANOVA $p < 0.001$; Figure 3.1D). The Exon 2 insertion event *asft1-m4::Ds* also significantly attenuated transcript accumulation (one-way ANOVA $p < 0.001$; Figure 3.4A). As there was some degree of residual transcript accumulation, the codon sequence at the insertion site of *asft1-m4::Ds* was analyzed by Sanger sequencing. The transposon insertion occurred in frame within Exon 2 but caused a premature stop codon only 3 codons into the terminal inverted repeat sequence of the *Ds* transposon (data not shown). As the insertion occurred upstream of the critical HXXXD and DFGWG motifs of Exon 3, it was concluded that any residual transcripts present in *asft1-m4::Ds* mutants were likely to encode a non-functional protein.

Despite very tight linkage between *Asft2* and donor I.S08.1288, only three insertion alleles (*asft2-m1::Ds*, *asft2-m2::Ds*, and *asft2-m3::Ds*) were recovered in a screen of 3,650 testcross progeny (0.082%; Figure 3.1C and Table 3.1). Furthermore, neither *asft2-m2::Ds* nor *asft2-m3::Ds* were null alleles (Figure 3.4B). An intragenic remobilization of *asft2-m2::Ds* was performed to generate two stronger alleles, *asft2-m4::Ds* in Exon 3 and *asft2-m5::Ds* in Intron 2, each of which retained a duplicate copy of *asftb-m2::Ds* in Intron 1 (Figure 3.1C-D; Figure

Table 3.1. Targeted mutagenesis of suberin biosynthesis candidates using *Dissociator* (*Ds*) transposons.

Name	GRMZM	Location[a]	Donor *Ds*	*Ds* insertion site[b]	Physical Distance [kb; 5' or 3']	Total Genes[c]	EST distance [kb][d]	Population size [kernels]	Total insertions	Frequency [%]
Zm*Cyp86B1*	GRMZM2G013082	Chr5: 27800485-27802660	B.W06.0068	Chr5:28,471,679	669.1 (3')	11	78.7	3,240	0	0.0
			I.W06.0248	Chr5:28,622,577	819.9 (3')	14	88.2	ND	ND	ND
Zm*Cyp86B2*	GRMZM2G162758	Chr1: 239898947-239902388	I.S06.0503	Chr1:240,759,424	857.0 (3')	ND	ND	ND	ND	ND
Zm*Gpat5*	GRMZM2G059637	Chr6: 156403083-156405661	B.S05.0681	Chr6: 155927253	475.8 (5')	ND	ND	ND	ND	ND
Zm*Gpat7*	GRMZM2G166176	Chr8: 122592799-122594763	B.S08.0052A	Chr8: 123647970	1053.2(3')	ND	ND	ND	ND	ND
Zm*Asft1*	GRMZM2G034360	Chr8: 177836697-177840044	I.S07.2991	Chr8: 177764834	71.9 (5')	8	25.5	5,400	1	0.019
			B.W06.0682	Chr8:177908795	68.8 (3')	2	9.0	1,800	3	0.17
Zm*Asft2*	AC155610.2_FG007	Chr3: 184981041-184991279	I.S07.1288	Chr3: 185020576	29.3 (3')	0	0	3,650	3	0.082
			asft2-m2:Ds		0 (Intron 1)	0	0	1,350	3[c]	0.22

Table 3.1 (continued)

Name	GRMZM	Location[a]	Donor *Ds*	*Ds* insertion site[b]	Physical Distance [kb; 5' or 3']	Total Genes[c]	EST distance [kb][d]	Population size [kernels]	Total insertions	Frequency [%]
Zm*Asft3*	GRMZM2G168499	Chr10: 95253533-95254363	I.S07.0762	Chr10:95551119	296.8 (3')	ND	ND	ND	ND	ND
Zm*Gdsl1*	GRMZM2G070178	Chr7: 181152004-181153761	I.W06.0862	Chr7:180952081	199.9 (3')	ND	ND	ND	ND	ND

a. **W22 inbred (EVlab W22 v3 Browser)**
b. **W22 inbred (SGN BLAST server)**
c. **B73 Refgen v3 (http://www.plantgdb.org)**
d. **Sum of all base pairs for intervening gene models between the *Ds* donor locus and the target gene with detectable transcript accumulation by RNA-Seq in at least one tissue of the Maize Expression Atlas (Sekhon *et al.*, 2011).**

Event *asft2-m4:Ds* originated as a clonal event in the pollen donor tassel and was recovered twice.

Figure 3.4. Expression analysis of additional single and double mutant alleles.

A. qPCR analysis of *asft1-m4*; *asft2-m5* single and double mutants. Gene expression of *ZmAsft1* and *ZmAsft2* was analyzed in the transition zone of ten day old third leaves as described in Figure 3.1B. Expression was significantly attenuated by 82-89% and 94-96%, respectively, for *Asft1* and *Asft2* in double and corresponding single mutants (one-way ANOVA, $p < 0.001$). Different letters indicate significant differences between genotypes determined by a Tukey-Kramer post-hoc test at a 95% significance level.
B. qPCR analysis of *asft2-m2* and *asft2-m3* single mutants. Gene expression of *ZmAsft1* and *ZmAsft2* was analyzed in the transition zone of ten day old third leaves as described in Figure 3.1B. *Asft1* expression did not differ significantly between genotypes. *Asft2* was reduced by approximately 88% in *asft2-m2::Ds* and by 30% in *asft2-m3::Ds* relative to WT (one-way ANOVA, $p < 0.001$). Different letters indicate significant differences between genotypes determined by a Tukey-Kramer post-hoc test at a 95% significance level.

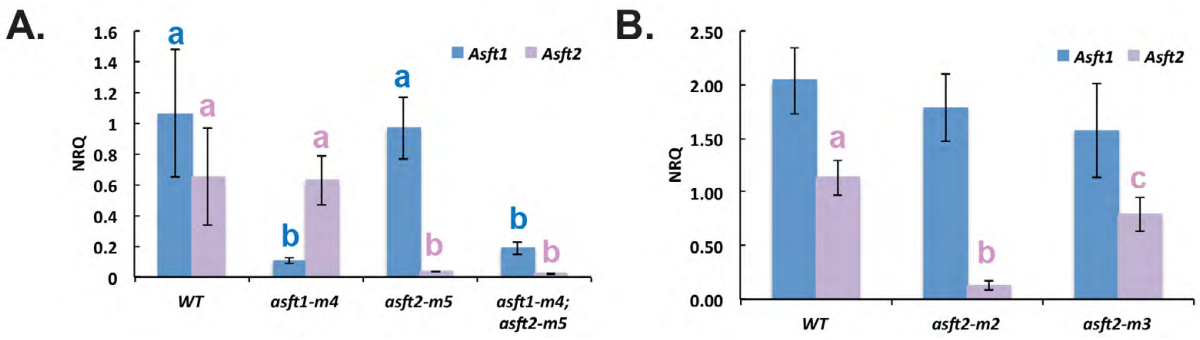
A.
NRQ
1.6
1.4
1.2
1
0.8
0.6
0.4
0.2
0
Asft1
Asft2
a
a
b
a
b
a
b
b
WT
asft1-m4
asft2-m5
asft1-m4;
asft2-m5
B.
NRQ
2.50
2.00
1.50
1.00
0.50
0.00
Asft1
Asft2
a
b
c
WT
asft2-m2
asft2-m3

3.4A). The observed insertion frequency of 0.22% of 1,350 total kernels was comparable to previous reports of intragenic remobilization (Studer *et al*., 2014 and unpublished observations).

The single mutants *asft1-m1::Ds* and *asft1-m4::Ds* were crossed to *asft2-m4::Ds* and *asft2-m5::Ds* single mutants to generate double mutants. There were no obvious morphological differences in any allelic combination of double mutants compared to their isogenic WT siblings under ambient conditions. This is typical for many of the suberin biosynthesis mutants characterized to date, including *AtASFT* (Molina *et al*., 2009). In the absence of a stress stimulus, chemical profiling of cell wall polyesters was necessary to differentiate suberin mutants from wild type siblings.

The *Asft* genes are redundantly essential for normal accumulation of very long chain omega-hydroxy fatty acids in leaf polyesters

To analyze the leaf polyester composition, the insoluble cell wall polyesters were depolymerized by base-catalyzed transmethylation, the hydroxyl groups of the solubilized monomers were converted to trimethylsilyl ethers, and derivatized monomers were quantified by GC-FID. For an initial survey of leaf polyester composition, *asft1-m1::Ds*; *asft2-m4::Ds* double mutants (referred to hereafter as *asft1-m1*; *asft2-m4*), the corresponding single mutants, and isogenic wild-type (WT) siblings were identified from a segregating population by genotyping. Fully expanded third leaf laminae were sampled at 28 days after sowing. BS strands were not separated from the leaf epidermis prior to tissue homogenization, and so these preparations contained a mixture of cell wall polyesters originating from the epidermal cuticle in addition to BS strands. The majority of the monomers recovered were hydroxycinnamic acids (HCA) in both mutant and WT samples (68% for single mutants and WT, 73% for double mutants; Figure

3.5A). Among aliphatic monomers, the distribution of primary alcohols, fatty acids, α,ω-dicarboxylic acids, and poly-hydroxy fatty acids were comparable between all four genotypes (Figure 3.5A). However, omega-hydroxy fatty acids (ω-OH FA), the most abundant aliphatic component, were significantly reduced in double mutant leaves relative to single mutants and WT (one-way ANOVA, $p < 0.01$; Figure 3.5A). When the individual ω-OH FA species were partitioned by chain length, $C_{22:0}$-$C_{30:0}$ very long chain omega-hydroxy fatty acids (ω-OH VLCFA) were strongly and specifically attenuated in double mutants, whereas long chain species (ω-OH LCFA) were unaffected (one-way ANOVA, $p < 0.001$ for all five ω-OH VLCFA species; Figure 3.5B). The two single mutants each showed minor deficiencies in $C_{22:0}$-$C_{30:0}$ ω-OH VLCFA relative to WT. Similar results were observed from single and double mutants of the *asft1-m4* and *asft2-m5* alleles, although single mutants of these lines had indistinguishable $C_{22:0}$-$C_{30:0}$ ω-OH VLCFA content from WT (Figure 3.6A-C). Thus, *ZmAsft1* and *ZmAsft2* are redundantly essential for normal accumulation of $C_{22:0}$-$C_{30:0}$ ω-OH VLCFA in leaf polyesters.

Total ferulic acid was reduced by 50-90% in the dicot ASFT mutants Arabidopsis *asft* and potato *FHT*-RNAi lines (Gou *et al.*, 2009; Molina *et al.*, 2009; Serra *et al.*, 2010a). Unlike Arabidopsis and potato, maize has a type II primary cell wall with significant quantities of ferulic acid esterified to the arabinose side chains of the cross-linking glycan glucuronoarabinoxylan (GAX; Kato and Nevins, 1985). Therefore, a less severe reduction in total ester-linked HCA content was expected in maize relative to the model dicots. However, there was no stoichiometric decrease in *p*-coumaric, ferulic, or caffeic acid concurrent with the reduction in ω-OH VLCFA in the double mutant (Figure 3.5C; Figure 3.6B). On average, the total amount of $C_{22:0}$-$C_{30:0}$ ω-OH VLCFA was reduced by 670 pmol/mg dry weight in double mutants relative to WT (Figure 3.5B). Only trace

Figure 3.5. Whole leaf polyester composition of *asft* mutants and WT siblings.

- **A.** Overview of the major monomer classes present in fully expanded third leaf laminae. Blue bars denote *asft1-m1*; *asft2-m4* double mutants, red and purple bars denote *asft1-m1* and *asft2-m4* single mutants, respectively, and orange bars denote wild type (WT). Monomers were quantified by total GC-FID peak area normalized to ω-pentadecalactone and methyl heptadecanoate internal standards, and are presented as nmoles per mg dry weight. Asterisks denote significant differences between genotypes determined by a one-way ANOVA (**, $p < 0.01$) with a Tukey-Kramer post-hoc comparison (different letters denote significant differences at $p < 0.05$). Values are averages with standard deviations of three biological replicates. HCA, hydroxycinnamic acid; PA, primary alcohol; FA, fatty acid; DCA: α,ω-dicarboxylic acid; ωOH FA, ω-hydroxy fatty acid; polyOH FA, poly-hydroxy fatty acid.
- **B.** Chain length distribution of ω-OH FAs. Double mutants are significantly deficient in $C_{22:0}$-$C_{30:0}$ very long chain ω-OH FAs relative to single mutants and WT (one-way ANOVA, $p < 0.001$). Different letters denote significant differences between genotypes as determined by a Tukey-Kramer post-hoc test ($p < 0.05$). Horizontal axis labels denote acyl chain lengths (16-30 carbons) and number of double bonds (0,1) of monomers.
- **C.** Hydroxycinnamic acid content of whole leaves. Neither *p*-coumaric nor ferulic acid are significantly different between genotypes (one-way ANOVA, $p > 0.05$).

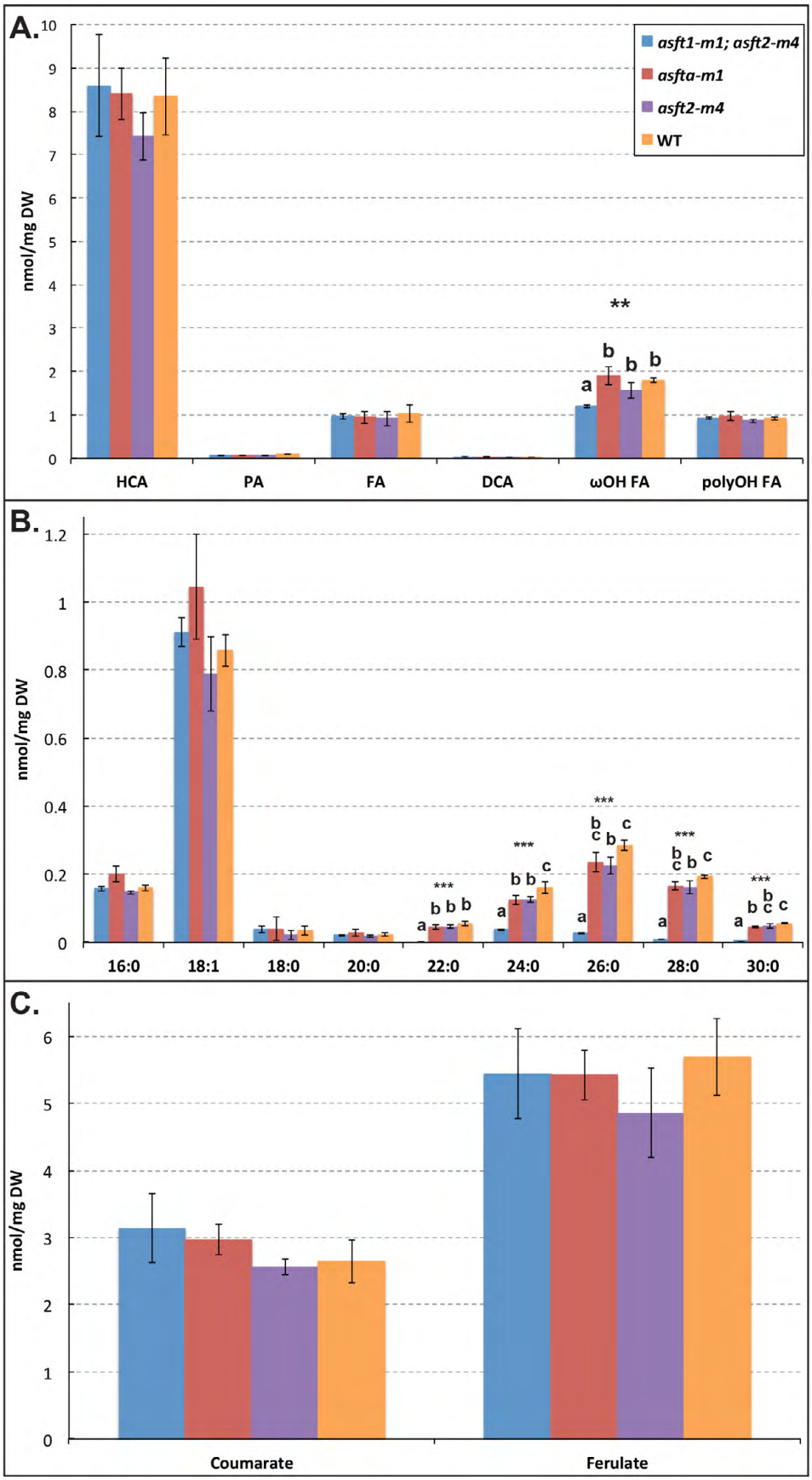
A.
asft1-m1; asft2-m4
asfta-m1
asft2-m4
WT
nmol/mg DW
HCA
PA
FA
DCA
ωOH FA
polyOH FA
B.
nmol/mg DW
16:0
18:1
18:0
20:0
22:0
24:0
26:0
28:0
30:0
C.
nmol/mg DW
Coumarate
Ferulate

Figure 3.6. The aliphatic defect is present in other double mutant combinations .

A. Overview of the major monomer classes present in fully expanded third leaf laminae. Blue bars denote double mutants, red and purple bars denote *asft1* and *asft2* single mutants, respectively, and orange bars denote WT. Monomers were quantified by total GC-FID peak area normalized to ω-pentadecalactone and methyl heptadecanoate as internal standards, and are presented as nmoles per mg dry weight. Inset: Higher resolution view of the low abundance primary alcohol (PA) and α,ω-dicarboxylic acid (DCA) compounds. Asterisks denote significant differences between genotypes determined by a one-way ANOVA (***, $p < 0.001$) with a Tukey-Kramer post-hoc comparison (different letters denote significant differences at $p < 0.05$). Values are averages with standard deviations of three biological replicates. HCA, hydroxycinnamic acid; PA, primary alcohol; FA, fatty acid; DCA: α,ω-dicarboxylic acids; ωOH FA, omega-hydroxy fatty acids; polyOH FA, poly-hydroxy fatty acids.
B. Analysis of the hydroxycinnamic acids *p*-coumaric and ferulic acid. The aromatic monomers presented in this panel and the aliphatic species presented in Figure 3.6C were evaluated for significant differences in accumulation between genotypes with a one-way ANOVA, and *p*-values were corrected with a Holm-Bonferroni adjustment for multiple testing. Monomer classes with a significant F statistic were evaluated with a Tukey-Kramer post-hoc analysis as described in Figure 3.6A (*, $p < 0.05$; letters denote significant differences between genotypes at $p < 0.05$). *p*-Coumaric acid varied significantly between genotypes, but ferulic acid did not.
C. Analysis of aliphatic monomer content. Monomer classes were analyzed as described in Figure 3.6B. Horizontal axis labels denote chain lengths of individual monomers grouped by compound class (labels as described in Figure 3.5A).

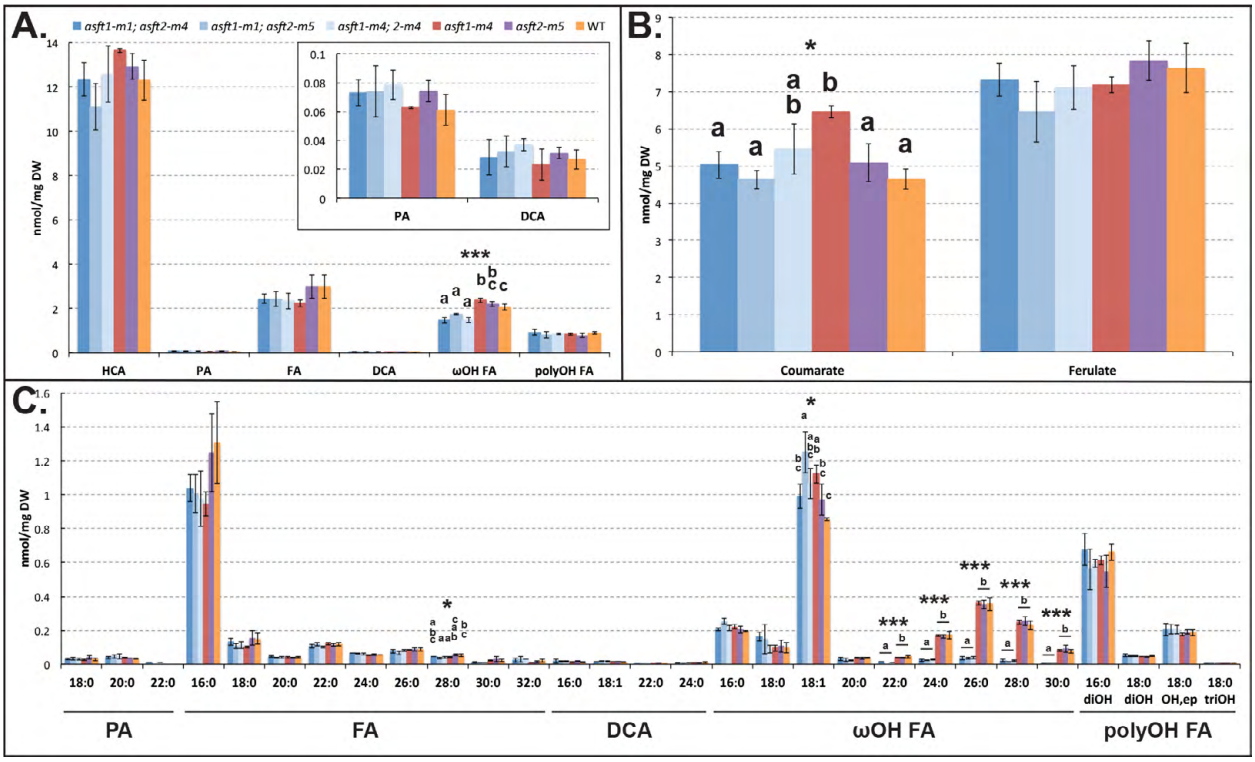
A.
asft1-m1; asft2-m4
asft1-m1; asft2-m5
asft1-m4; 2-m4
asft1-m4
asft2-m5
WT
nmol/mg DW
HCA
PA
FA
DCA
ωOH FA
polyOH FA
B.
Coumarate
Ferulate
C.
18:0
20:0
22:0
16:0
18:0
20:0
22:0
24:0
26:0
28:0
30:0
32:0
16:0
18:1
22:0
24:0
16:0
18:0
18:1
20:0
22:0
24:0
26:0
28:0
30:0
16:0 diOH
18:0 diOH
18:0 OH,ep
18:0 triOH
PA
FA
DCA
ωOH FA
polyOH FA

amounts of caffeic acid were recovered (less than 10 pmol/mg dry weight), and it was concluded that caffeic acid was not sufficiently abundant to couple with ω-OH VLCFA in the expected 1:1 stoichiometry. Although both *p*-coumaric and ferulic acid were sufficiently abundant (Figure 3.5C), all biochemically characterized ASFT orthologues strongly prefer ferulic acid (reviewed in Molina and Kosma, 2015). Thus, the percent reduction in ferulic acid was estimated assuming that 670 pmol/mg DW of the total cell wall ferulate was esterified to ω-OH VLCFA *in muro*. A reduction of approximately 11% in total leaf ferulic acid in was expected in double mutants. This degree of change was approximately equal to the sample standard deviations for double mutant and WT and was too small to measure. Thus, a fractionation protocol was developed to enrich the proportion of HCA associated with leaf polyesters in the samples.

Suberized regions of ten-day-old third leaf laminae distal to the point of emergence were harvested, and the tissue was macerated with a liquid homogenizer. This fractionation procedure eliminated the mesophyll cells and yielded a mixture of mechanically recalcitrant walls from suberized BS strands, the cutinized outer wall of the epidermis, and guard cells. HCA and hydroxylated fatty acids were significantly enriched relative to whole leaf preparations by this protocol (one-way ANOVA, $p < 0.001$; Figure 3.7A). Omega- and poly-hydroxy fatty acids of all chain lengths were approximately two-fold more abundant in fractionated samples relative to whole leaves (Figure 3.7C). In contrast to fully expanded third leaf laminae, total ω-OH FA content was slightly enriched in *asft1-m1* single mutants and indistinguishable between the other genotypes in developing leaves (Figure 3.5A; Figure 3.7A). Thus, the 33% reduction in ω-OH FA that was observed in fully expanded laminae may result from later synthesis or remodeling of polyesters.

Figure 3.7. Polyester composition of whole and mechanically fractionated leaves of *asft* mutants and wild type siblings.

A. Overview of the major monomer classes present in entire (Whole Leaf; solid bars) and mechanically fractionated (Fraction; hatched bars) 10-day-old third leaf laminae. Developing leaf tissue proximal to the point of emergence was discarded. Asterisks denote significant differences in monomer class abundance between entire and fractionated cell wall preparations (one-way ANOVA; ***, $p < 0.001$). Values are average with standard deviations of four biological replicates.
B. Hydroxycinnamic acid content of whole leaves. Letters denote significant differences in ferulate content between genotypes determined by a Tukey-Kramer post-hoc test ($p < 0.05$) following a significant one-way ANOVA ($p < 0.05$).
C. Chain length distribution of hydroxylated fatty acids. Asterisks denote significant differences as described in Figure 3.7A. Inset: Higher resolution image of $C_{20:0}$-$C_{30:0}$ ω-OH VLCFA monomers with Tukey-Kramer post-hoc test statistics ($p < 0.05$). ω-OH VLCFA are specifically attenuated in double mutants in whole and fractionated samples.

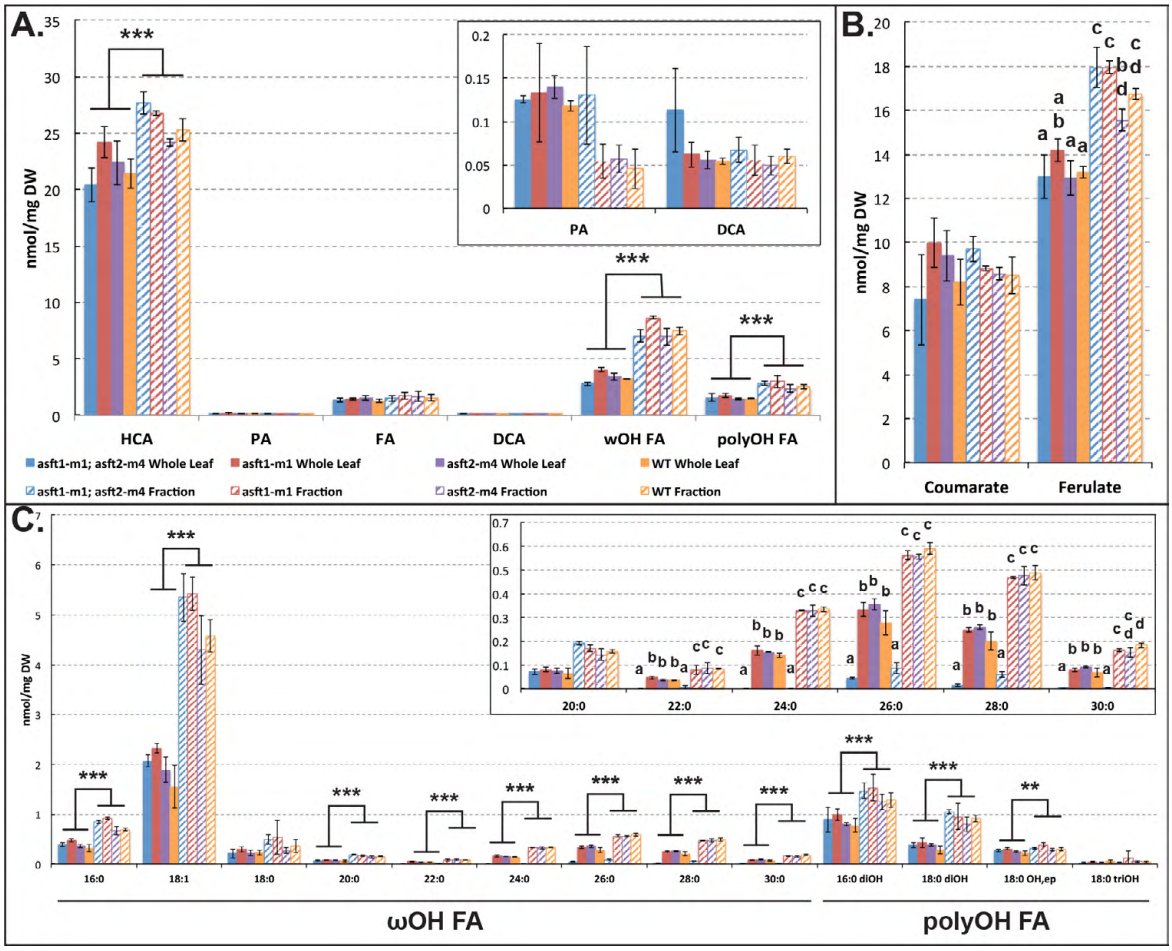
A.
nmol/mg DW
HCA
PA
FA
DCA
wOH FA
polyOH FA
asft1-m1; asft2-m4 Whole Leaf
asft1-m1 Whole Leaf
asft2-m4 Whole Leaf
WT Whole Leaf
asft1-m1; asft2-m4 Fraction
asft1-m1 Fraction
asft2-m4 Fraction
WT Fraction
B.
nmol/mg DW
Coumarate
Ferulate
C.
nmol/mg DW
16:0
18:1
18:0
20:0
22:0
24:0
26:0
28:0
30:0
16:0 diOH
18:0 diOH
18:0 OH,ep
18:0 triOH
ωOH FA
polyOH FA

The enrichment of HCA in fractionated samples was attributed to a significant increase in ferulic acid (one-way ANOVA with Tukey's HSD; $p < 0.05$; Figure 3.7B). Although the fractionation protocol successfully enriched for both ω-OH VLCFA and ferulic acid, there was no detectable HCA deficiency in double mutants relative to WT (Figure 3.7A-B). As observed in fully expanded laminae, double mutants were significantly deficient in $C_{22:0}$-$C_{30:0}$ ω-OH VLCFA without a corresponding stoichiometric decrease in *p*-coumaric, ferulic, or caffeic acid (one-way ANOVA, $p < 0.001$ for all VLCFA; Figure 3.7B-C). Similar results were observed for samples containing purified bundle sheath strands devoid of cutin (Figure 3.8).

Three explanations were proposed for the absence of an HCA deficiency in leaf polyesters. First, the ZmAsft proteins may not be genuine ω-hydroxyacid:hydroxycinnamoyl-CoA acyltransferases, despite their homology to AtASFT. Alternatively, the total amount of HCA esterified to polyesters may be a very small fraction of the total cell wall HCA content. If so, the HCA deficiency in double mutants may be present but too small to measure or masked by reallocation of HCAs to another cell wall polymer, potentially GAX.

GAX feruloylation is not impacted in the *asft* double mutant

In order to investigate the latter hypothesis, it was necessary to measure the quantity of HCA esterified to GAX in the primary cell wall. Both the ASFT proteins and the putative α-L-arabinofuranose-5-O-hydroxycinnamoyl transferases of the Mitchell Clade are likely cytosolic enzymes (Rautengarten *et al*., 2012; Boher *et al*., 2013; Hatfield *et al*., 2009). Therefore, putative reallocation of HCAs to GAX in *asft* mutants was assumed to occur cell autonomously in either the BS or epidermis. Fractionated samples were prepared to maximize the contribution of bundle sheath and epidermal cell walls to the total ester-linked HCA content. A dilute acid solution (50

Figure 3.8. Polyester composition of purified bundle sheath strands.

A. Overview of the major monomer classes present in wild type WT *and asft1-m1; asft2-m4* (ab) 14-day-old third leaf laminae. Values are averages with standard deviations of three biological replicates.
B. Hydroxycinnamic acid content of purified bundle sheath strands.
C. Chain length distributions of aliphatic suberin monomers.

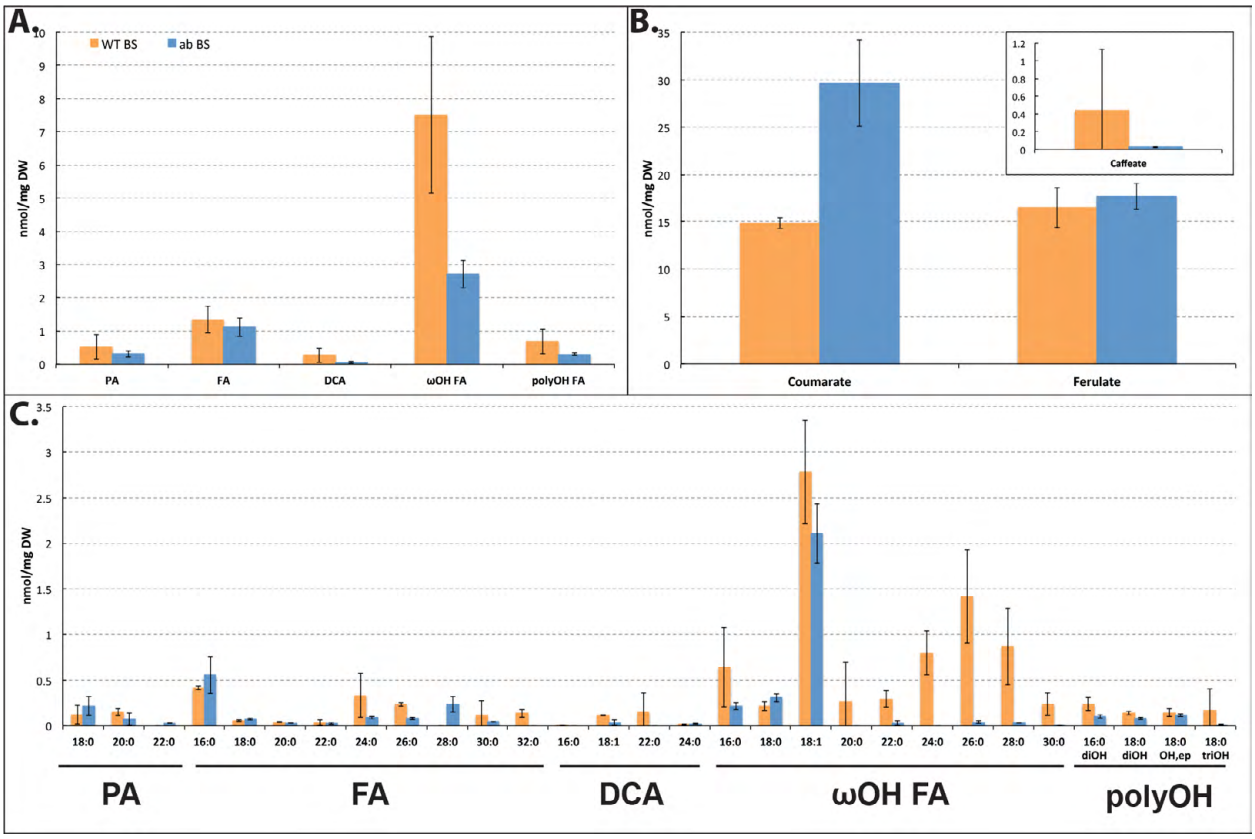
A.
WT BS
ab BS
nmol/mg DW
PA
FA
DCA
ωOH FA
polyOH FA
B.
nmol/mg DW
Caffeate
Coumarate
Ferulate
C.
nmol/mg DW
18:0
20:0
22:0
16:0
18:0
20:0
22:0
24:0
26:0
28:0
30:0
32:0
16:0
18:1
22:0
24:0
16:0
18:0
18:1
20:0
22:0
24:0
26:0
28:0
30:0
16:0 diOH
18:0 diOH
18:0 OH,ep
18:0 triOH
PA
FA
DCA
ωOH FA
polyOH

mM TFA) was utilized to selectively hydrolyze the relatively weak α-L-arabinosyl (1→3)-β-D-xylosyl bonds from the xylan backbone, liberating 5-O-hydroxycinnamoyl-L-arabinose dimers that were resolved by HPLC and quantified by UV absorbance (Saulnier *et al*., 1995; Bartley *et al*., 2013). This treatment released four major acid labile compounds, two of which were identified as monomeric *p*-coumaric and ferulic acids by comparing their UV absorption maxima and retention times to authentic standards (Figure 3.9A and data not shown). Two unknown peaks with similar UV absorption maxima to *p*-coumaric and ferulic acid, respectively, eluted immediately prior to their corresponding HCAs (Figure 3.9A, blue trace). These peaks were eliminated by saponification, suggesting that the underlying compounds contained alkali-labile ester linkages (Figure 3.9A, red trace). The molecular weights of the two unknowns were confirmed to be identical to *p*-coumarate-pentose and ferulate-pentose dimers by HPLC coupled to ESI-MS (data not shown). There is extensive support for HCA esterification to L-arabinose, but not to its isomer D-xylose (Bartley *et al*., 2013, and references therein), and so these peaks were identified as 5-O-*p*-coumaroyl-L-arabinose and 5-O-feruloyl-L-arabinose dimers, respectively.

To determine the correct incubation time for maximum dimer release, double mutant and WT samples were incubated in 50 mM TFA for 0.5h, 1h, 2h, 4h, and 6h at 100˚C and the total acid-labile HCA content was evaluated by HPLC. A 2-hour TFA incubation yielded the maximum release of HCA (Figure 3.9B, top panel) with lower degradation of HCA-arabinose dimers than at longer incubation times (Figure 3.9B, bottom panel). Total HCA release was similar between WT and double mutant samples. As there was a generalized but statistically insignificant trend toward greater HCA release in double mutants relative to WT (Figure 3.9B, top panel), the experiment was repeated with an independent set of samples. Neither dimer

Figure 3.9. The majority of acid-labile ferulic acid in leaves is associated with glucuronoarabinoxylan.

A. Representative UV-absorbance traces before and after saponification. UV absorbance (mAU) of TFA-soluble hydroxycinnamic acid (HCA) was analyzed by HPLC directly (blue trace) or after saponification to cleave alkali-labile ester linkages (red trace). Feruloyl arabinose (F-Ara) and *p*-coumaroyl arabinose (C-Ara) were converted to ferulic acid (FA) and p-coumaric acid (CA) by saponification. 100 μM 3,4,5-trimethoxy-*trans*-cinnamic acid (3,4,5-TCA) was introduced as an internal standard.
B. Time course of HCA solubilization by TFA incubation. Lyophilized cell wall residues of wild type (WT, orange bars) and *asft1-m1*; *asft2-m4* double mutants (Dbl Mut, blue bars) were incubated in 50 mM TFA at 100°C for the indicated time (0h, 0.5h, 1h, 2h, 4h or 6h). Top panel: total ferulic acid (solid) and *p*-coumaric acid (hatched) were determined by normalizing UV absorbance to 3,4,5-TCA. Bottom panel: ratio of total dimers (feruloyl/coumaroyl arabinose) to monomers (ferulic/coumaric acid). Different letters indicate significant differences between treatments according to a Tukey-Kramer post-hoc test ($p < 0.05$) following a significant F-test (two-way ANOVA treatment x genotype, treatment effect $p < 0.001$). There was no genotype effect. Values are averages plus standard deviations of three biological replicates per treatment.
C. Acid-labile ferulic acid derivatives from fractionated (BS+Epi) and whole leaves incubated at 100°C for 2h in 50 mM TFA or water. There was no significant difference in feruloyl arabinose dimers or ferulic acid monomers between genotypes for either cell wall preparation (one-way ANOVA, $p > 0.05$). Values are averages plus standard deviations of six biological replicates.
D. Acid-labile p-coumaric acid derivatives from fractionated (BS+Epi) and whole leaves. Sample preparation and statistical analysis are identical to Figure 3.9C.
E. Linkage-methylation analysis of monosaccharide linkage groups from glucuronoarabinoxylan. The polymer consists of a linear β-(1→4)-D-xylose backbone (4-xyl) decorated with terminal (5-O-feruloyl/coumaroyl) α-L-arabinofuranose-(1→3)-β-D-xylose branches (*t*-araf, 3,4-xyl). The polymer also contains a small number of terminal α-D-glucuronic acid-(1→2)-β-D-xylose branches (*t*-glcA, 2,4-xyl). None of the linkages are significantly different between genotypes for either cell wall preparation (one-way ANOVA, $p > 0.05$). Values are averages with standard deviations for two biological replicates with two technical replicates each.

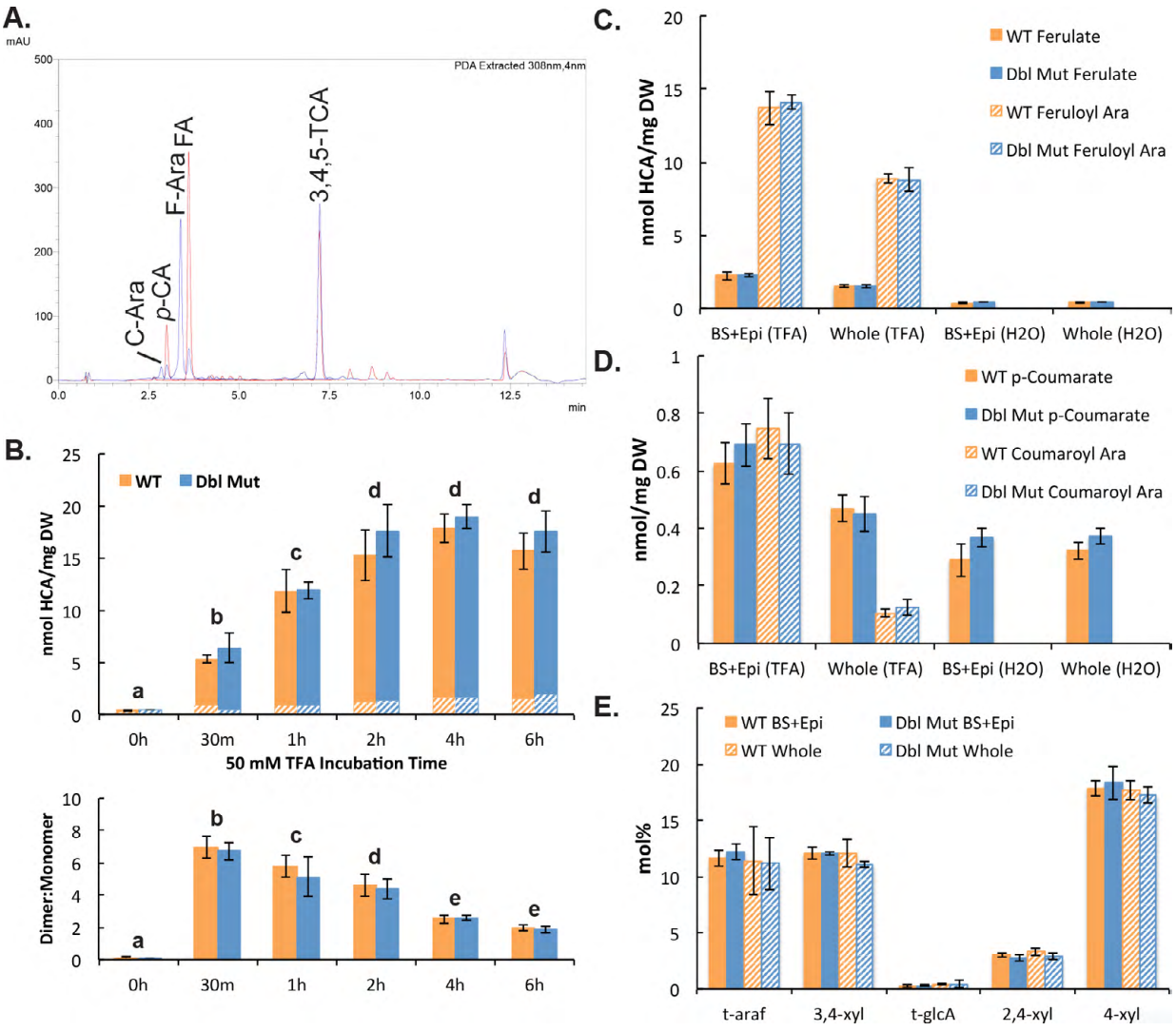
A.
mAU
PDA Extracted 308nm,4nm
C-Ara
p-CA
F-Ara FA
3,4,5-TCA
min
B.
WT
Dbl Mut
nmol HCA/mg DW
50 mM TFA Incubation Time
Dimer:Monomer
0h
30m
1h
2h
4h
6h
C.
WT Ferulate
Dbl Mut Ferulate
WT Feruloyl Ara
Dbl Mut Feruloyl Ara
nmol HCA/mg DW
BS+Epi (TFA)
Whole (TFA)
BS+Epi (H2O)
Whole (H2O)
D.
WT p-Coumarate
Dbl Mut p-Coumarate
WT Coumaroyl Ara
Dbl Mut Coumaroyl Ara
nmol/mg DW
E.
WT BS+Epi
Dbl Mut BS+Epi
WT Whole
Dbl Mut Whole
mol%
t-araf
3,4-xyl
t-glcA
2,4-xyl
4-xyl

differed significantly between double mutant and WT in an independent set of fractionated samples or in whole second leaf laminae from the same plants used in the initial experiment (Student's t-test $p \geq 0.05$; Figure 3.9C-D). Likewise, there was no genotype effect on arabinose side chain abundance or xylan branching for either sample type as determined by a linkage-methylation analysis (Figure 3.9E). Taken together, these data provide no evidence for significant re-allocation of HCAs from polyesters onto GAX in double mutants.

The total proportion of alkali-labile ferulic acid esterified to GAX was estimated for fractionated samples. For WT and double mutants, a 2-hour TFA incubation solubilized 94% and 91% respectively, of the average ferulic acid released by transmethylation (Figure 3.7B; Figure 3.8C). For both genotypes, approximately 86% of TFA-soluble leaf ferulate was recovered as feruloyl arabinose dimers (Figure 3.9C). Thus, the majority of ester-linked ferulic acid is associated with GAX rather than suberin or cutin, even in samples enriched for polyesters. As the average dimer:monomer ratios declined by 34% after a 2-hour incubation compared to their maxima at 30 minutes (Figure 3.9B, lower panel), there was likely some degree of dimer degradation. Therefore, the true proportion of ferulic acid associated with GAX could reach 90%. The previous estimate that approximately 11% of ferulic acid is associated with polyesters based on the proportion of ω-OH VLCFA missing from double mutants is in good agreement with this figure (Figure 3.5B-C). If 11% represents an upper bound, even a complete reduction in the double mutant may be too small to measure accurately with the methodology used in this study.

Bundle sheath suberin ultrastructure is compromised in *asft* double mutants

During the preparation of fractionated cell walls, *asft1-m1*; *asft2-m4* double mutant samples appeared lighter in color than single mutant or WT siblings following homogenization (Figure 3.10A). When the preparations were compared under a light microscope, WT and single mutant samples were comprised of sheared segments of BS strands with predominately intact cells containing abundant chloroplasts. Conversely, nearly all of the cells attached to double mutant BS strands were broken along the outer tangential walls and devoid of plastids (Figure 3.10B). Thus, the outer tangential walls of double mutant BS cells appear to be less recalcitrant to mechanical shearing than WT. As the outer tangential walls are the major sites of suberization in maize BS cells (Evert *et al*., 1996), the apparent fragility of double mutant BS strands could be attributed to changes in the ultrastructure of the suberin lamellae (SL). Thus, leaf ultrastructures of single and double *asft* mutants were compared to WT using transmission electron microscopy (TEM). As expected for maize BS cells, SL spanned the entire outer tangential wall plus the centrifugal portion of each radial wall (Figure 3.11A). In WT and both single mutants, the SL had a classical "tramline" appearance comprised of a central electron lucent region bounded by two electron opaque bands at the interface of the SL with the primary and tertiary cell walls (Figure 3.11B). The SL was thickened and polylamellate in the vicinity of plasmodesmata in all genotypes (Figure 3.11C). In contrast to the other genotypes, the double mutant SL had a severely compromised ultrastructure. The SL appeared entirely electron lucent at all cell wall positions, and the osmiophilic tramlines delimiting WT lamellae were abolished (Figure 3.11B). This phenotype was completely penetrant and affected all BS cells equally in the minor veins that were observed. Although the double mutant SL thickened in the presence of plasmodesmata, these regions were also deficient in osmiophilic material except for a faint signal perpendicular to some pores traversing the wall (Figure 3.11C). The SL often appeared swollen or distorted,

Figure 3.10. Double mutant bundle sheath cell walls are fragile relative to wild type.

A. Homogenate of bundle sheath strands and epidermal cells from mechanically fractionated 10-day-old leaf third leaf laminae of wild type (WT) and *asft* mutants. The double mutant sample appears lighter in color than WT and *asft* single mutants.
B. Bright field microscope images of sheared bundle sheath strands. Nearly all of the bundle sheath cells of the double mutant are broken, and the chlorophyll has leaked out during sample preparation. Single mutant and WT bundle sheath strands retain many intact cells with abundant chlorophyll. A segment of intact epidermis with pavement cells and stomata is visible in the *asft2-m4* image. 200x magnification. Scale bars denote 100 μm.

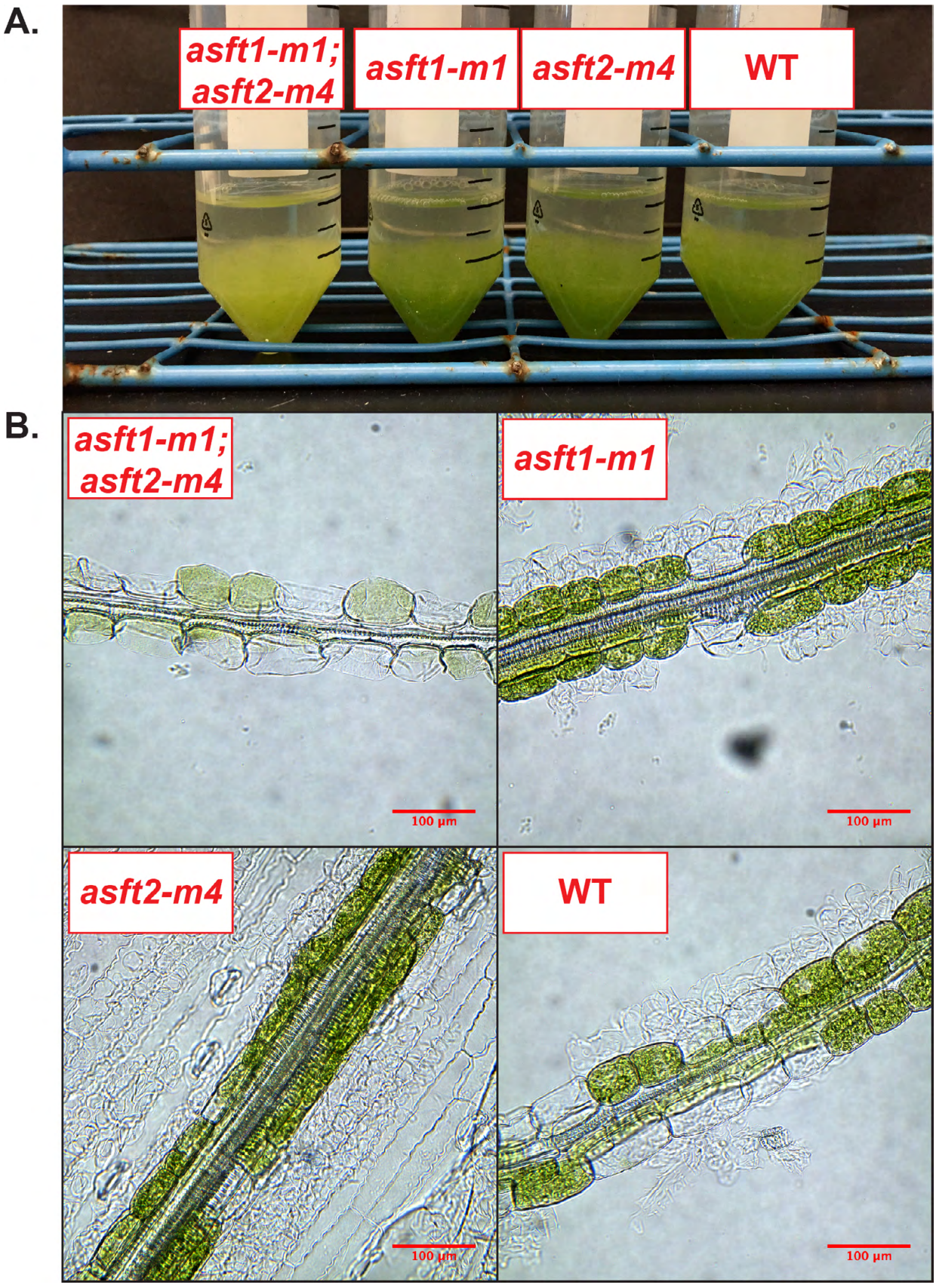
A.
asft1-m1; asft2-m4
asft1-m1
asft2-m4
WT
B.
asft1-m1; asft2-m4
asft1-m1
asft2-m4
WT
100 µm
100 µm
100 µm
100 µm

Figure 3.11. Bundle sheath cell wall ultrastructure is compromised in *asft1-m1*; *asft2-m4* double mutants.

A. Transmission electron micrographs of outer tangential cell walls of wild type (WT) and double mutant (*asft1-m1; asft2-m4*) bundle sheath cells (BS) adjacent to mesophyll (Me). Although suberin lamellae (SL) are present between the primary cell wall (PCW) and tertiary cell wall (TCW) in both genotypes, the SL of the double mutant are devoid of electron-opaque material and irregular in thickness. All samples were prepared by glutaraldehyde fixation. 16,000x magnification. Scale bars denote 200 nm.
B. Comparison of cell-cell interfaces of WT to *asft* single and double mutants. In all genotypes except for the double mutant, SL (red arrows) have a typical "tramline" appearance consisting of a central electron lucent region bounded by two electron opaque bands. The double mutant appears entirely electron lucent and irregular in thickness, particularly near cell corners. Magnifications are 16,000x (*asft1-m1; asft2-m4*), 20,000x (*asft1-m1* and *asft2-m4*), and 10,000x (WT). Double mutant and WT samples are glutaraldehyde-fixed; single mutants were fixed by high-pressure freeze substitution. All scale bars denote 200 nm.
C. SL thicken in the presence of plasmodesmatal pit fields in all genotypes. As observed above, double mutant SL are strongly deficient in electron opaque material. Arrows point toward mesophyll cell-specific caps on individual plasmodesmata at the BS/Me interface. The structure is generally present in double mutants but occluded in the image presented. Magnifications are 25,000x (*asft1-m1; asft2-m4* and WT), 40,000x (*asft1-m1*), and 31,500x (*asft2-m4*). All samples were fixed by high-pressure freeze substitution. Scale bars denote 200 nm.
D. Overview of minor veins in wild type and double mutants. Representative cells of the BS, Me, and vasculature (V) are labeled. Chloroplasts within the bundle sheath are centrifugally positioned adjacent to the BS/Me interface in both WT and double mutants (denoted by asterisks). Magnifications are 800x for WT and 1600x for double mutant. All samples were prepared by glutaraldehyde fixation. Scale bars denote 20 μm.

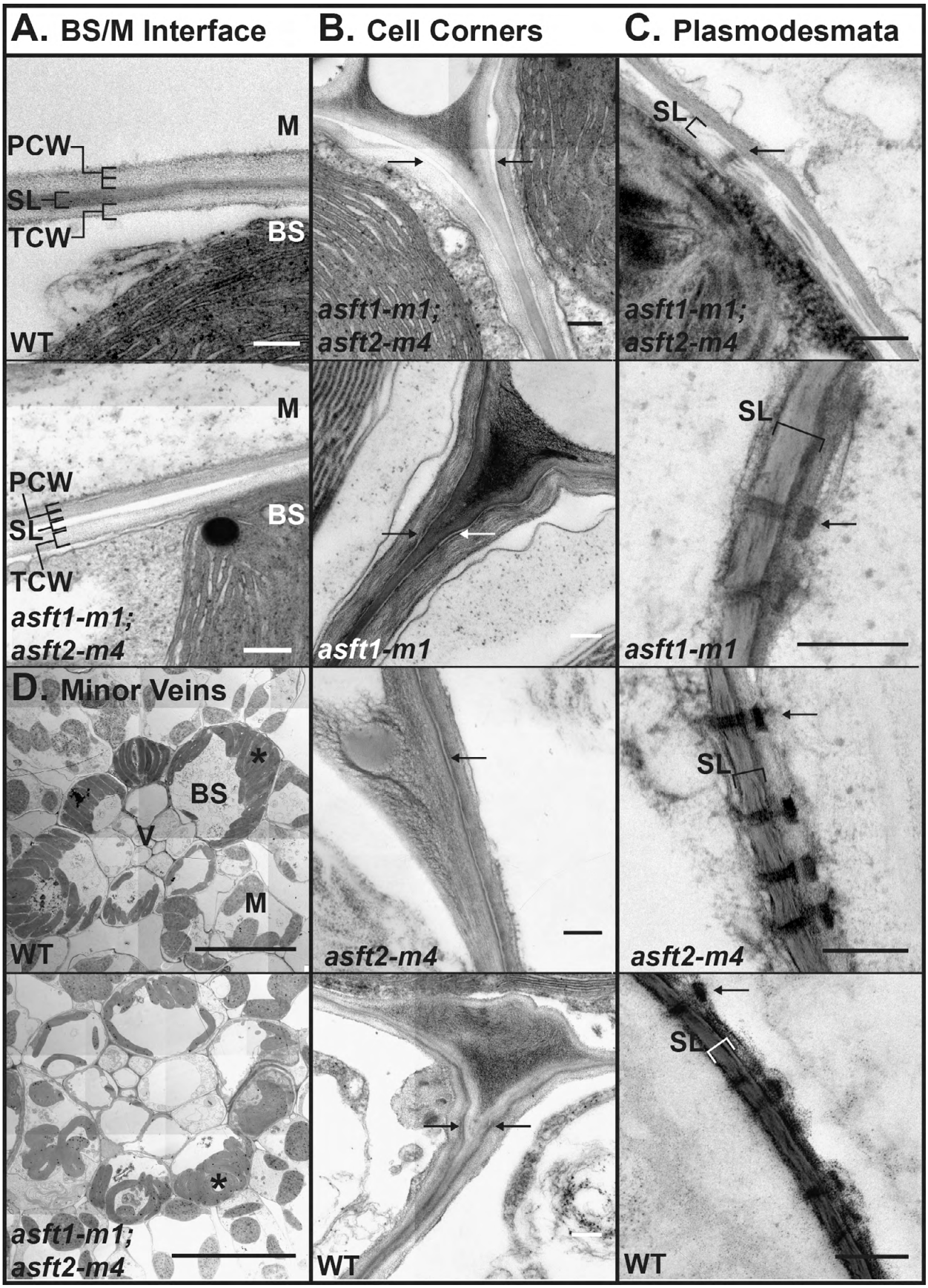
A. BS/M Interface
B. Cell Corners
C. Plasmodesmata
PCW
SL
TCW
M
BS
WT
asft1-m1;
asft2-m4
asft1-m1
asft2-m4
D. Minor Veins
V
*

especially near cell corners (Figure 3.11B). Despite these alterations, no change was observed in the centrifugal orientation of chloroplasts in double mutants relative to WT, nor were there obvious changes in plastid abundance or morphology (Figure 3.11D).

Two possible explanations for the distorted, highly electron lucent double mutant SL were evaluated. Osmium tetroxide generates electron opaque precipitates via the oxidation of unsaturated alkene groups. Thus, the thickened, electron lucent SL might result from increased deposition of saturated aliphatic material that would not react with osmium tetroxide, possibly as a compensatory mechanism. Many of the aliphatic monomers measured in leaves were saturated fatty acid or alcohol derivatives that could potentially meet this requirement. However, there was no evidence for increased aliphatic monomer deposition in double mutants in any of the chemical profiling experiments discussed above (Figures 3.5-3.8). Thus, the ultrastructural defect is not caused by ectopic deposition of insoluble aliphatic polyesters. However, increased deposition of wax or unincorporated monomers cannot be ruled out, as these compounds dissolve in organic solvents and are lost during sample preparation.

A second possibility is that the electron lucent regions are comprised primarily of negative space produced by tearing of the cell wall in the vicinity of the SL, likely during sample preparation. This theory is consistent with the reduced recalcitrance of the double mutant cell wall to breaking during homogenization (Figure 3.10). The fractionated samples and TEM data are consistent, as the distorted SL occur only in the double mutant (Figure 3.11B-C). Chromium trioxide was tested as an alternative fixative for TEM, as this reagent was utilized successfully with bacterial samples to differentiate between aliphatic material and negative space between structural features (Berg, 1994). WT leaf samples fixed in chromium trioxide had SL with typical "tramline" ultrastructures comparable to samples fixed with osmium tetroxide (Figure 3.12A).

Figure 3.12. The ultrastructural defect in double mutants is localized to the suberin lamella-polysaccharide cell wall interface.

A. Transmission electron micrograph of outer tangential cell wall of wild type (WT) bundle sheath (BS) cell adjacent to mesophyll cells (M) and an intercellular air space (*). Positions of primary and tertiary cell walls relative to the suberin lamella (SL) are as described in Figure 3.11. SL are indicated by arrows. All samples were fixed and stained with chromium trioxide prior to electron microscopy. 16,000x magnification.
B. Outer tangential wall of wild type BS cell showing a slight distortion of the tertiary cell wall (arrowhead). 20,000x magnification.
C. Outer tangential cell wall of *asft1-m1; asft2-m4* double mutant BS cell. The SL has torn away from the adjoining primary and tertiary cell walls as a discrete band. 25,000x magnification.
D. Outer tangential cell wall of *asft1-m1; asft2-m4* double mutant BS cell near a cell corner. The suberin lamella has torn away from the adjoining polysaccharide cell wall layers as a discrete band, and the majority of the electron lucent region is negative space. 31,500x magnification.
E. Radial cell walls of two adjacent BS cells in an *asft1-m1; asft2-m4* double mutant. The SL are parallel "tramlines" with no evidence of distortion or shearing. 31,500x magnification. All scale bars are 200 nm.

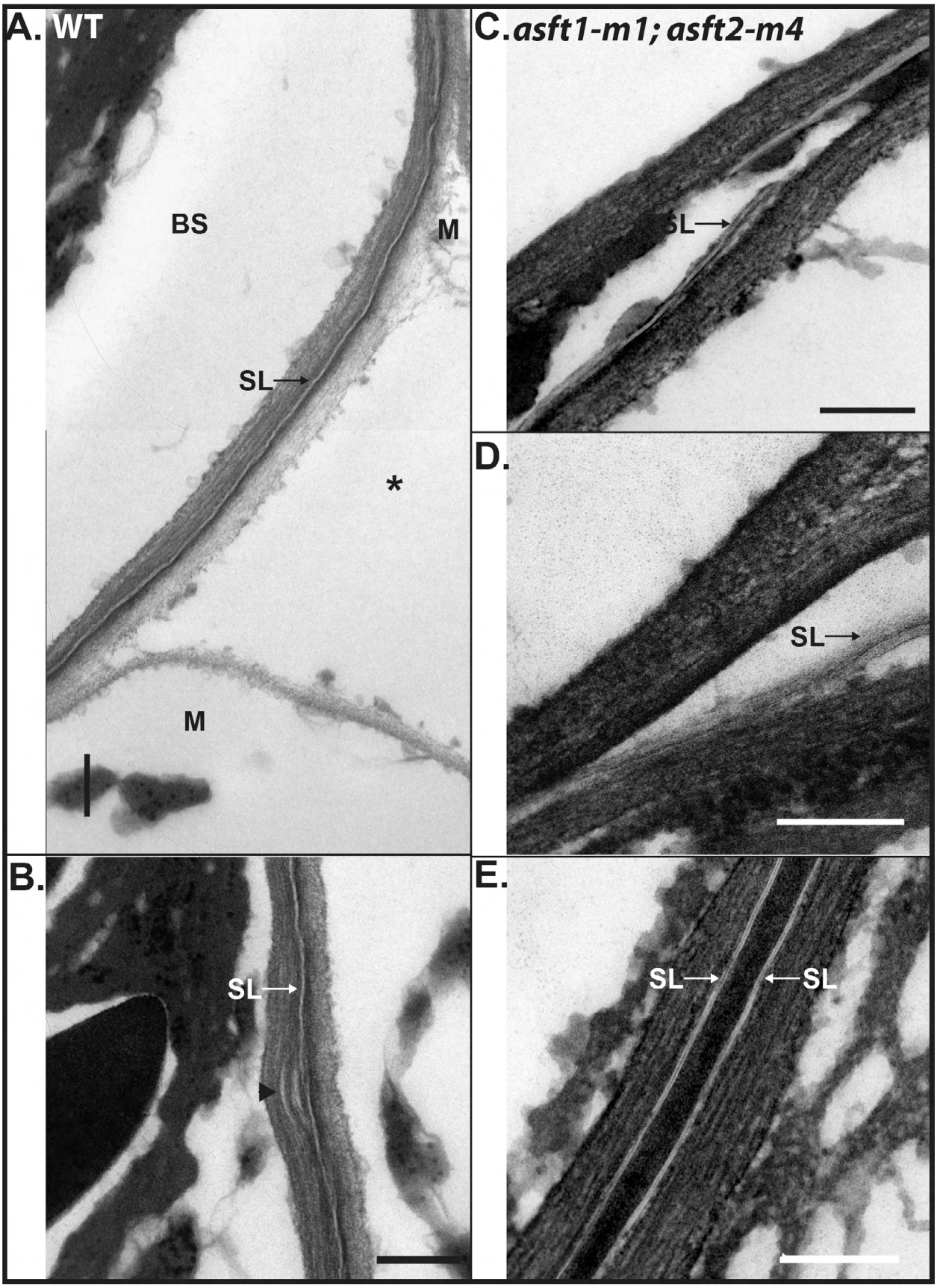
A. WT
BS
M
SL
*
M
C. asft1-m1; asft2-m4
SL
D.
SL
B.
SL
E.
SL
SL

Distortion or shearing of the BS cell wall was limited to occasional puckering of the tertiary cell wall along the outer tangential face of the cell (Figure 3.12B). Conversely, chromium trioxide-fixed leaf sections of the double mutant exhibited significant tearing of both the primary and tertiary cell walls immediately adjacent to the SL (Figure 3.12C-D). Interestingly, the double mutant SL separated from the polysaccharide cell walls as discrete units, and the internal electron lucent region of the lamella was largely indistinguishable from WT (Figure 3.12C-D). In contrast to double mutant samples fixed with osmium tetroxide, distinct "tramline"-patterned SL were apparent, particularly in radial cell walls of adjacent bundle sheath cells (Figure 3.12E). Thus, the ultrastructural defect of double mutants specifically compromises the interface between the SL and adjoining polysaccharide cell walls, and the *ZmAsft* genes have little effect on the internal patterning of the SL.

The ultrastructure and barrier properties of the mutant cuticle are indistinguishable from wild type

In maize leaves, the suberized BS cells of minor veins are separated from the epidermal cuticle by a single layer of mesophyll cells. As the cuticle is the primary apoplastic barrier to non-stomatal water loss (reviewed in Yeats and Rose 2013), it would be difficult to attribute a change in leaf gas exchange to the ultrastructural defect in the BS if the cuticle was also compromised. Thus, the ultrastructure and barrier properties of the leaf epidermal cuticle were compared between WT and *asft* mutants. In contrast to the substantially altered SL ultrastructure of double mutant BS cells, both the cuticle proper and the adjoining polysaccharide cell wall were indistinguishable between mutants and WT (Figure 3.13A). Toluidine Blue staining and chlorophyll leaching assays were utilized to assess barrier function. Cuticular permeability was

Figure 3.13. The ultrastructure and barrier properties of the double mutant leaf cuticle are indistinguishable from wild type.

A. Transmission electron micrographs of the epidermal outer tangential wall in wild type and *asft* mutants. The ultrastructure of the cuticle proper (CP), cuticular layer (CL), and polysaccharide primary cell wall (PCW) are indistinguishable between genotypes. Magnifications are 16,000x except for *asft1-m1* (20,000x). Scale bars denote 200 nm.
B. Toluidine Blue permeability is indistinguishable between genotypes. Toluidine Blue O stains the base of excised leaf laminae near the cut site in all genotypes (left panels), but is excluded from the transition zone (middle panels) and mature source tissue (right panels). Whole third leaf laminae were immersed in aqueous 0.05% (w/v) Toluidine Blue O and observed under bright-field illumination using a dissecting microscope. Adaxial and abaxial (not pictured) surfaces gave identical results. Ink dots on leaves in middle and right panels denote the point of emergence from the whorl and the midpoint of the exposed lamina, respectively. Scale bar denotes 50 mm.
C. Chlorophyll leaching kinetics are indistinguishable between genotypes. Whole third leaf laminae of 10-day-old wild type and *asft* mutant seedlings were excised at the base and immersed in 80% ethanol. Total Chlorophyll a and Chlorophyll b absorbance (A_{664} and A_{647}) of the supernatant was determined spectrophotometrically at the indicated time points and converted to µmoles of chlorophyll according to Lolle *et al*. (1997). Data are presented as average µmoles of chlorophyll per mg fresh weight with standard deviations for 10 biological replicates per genotype.

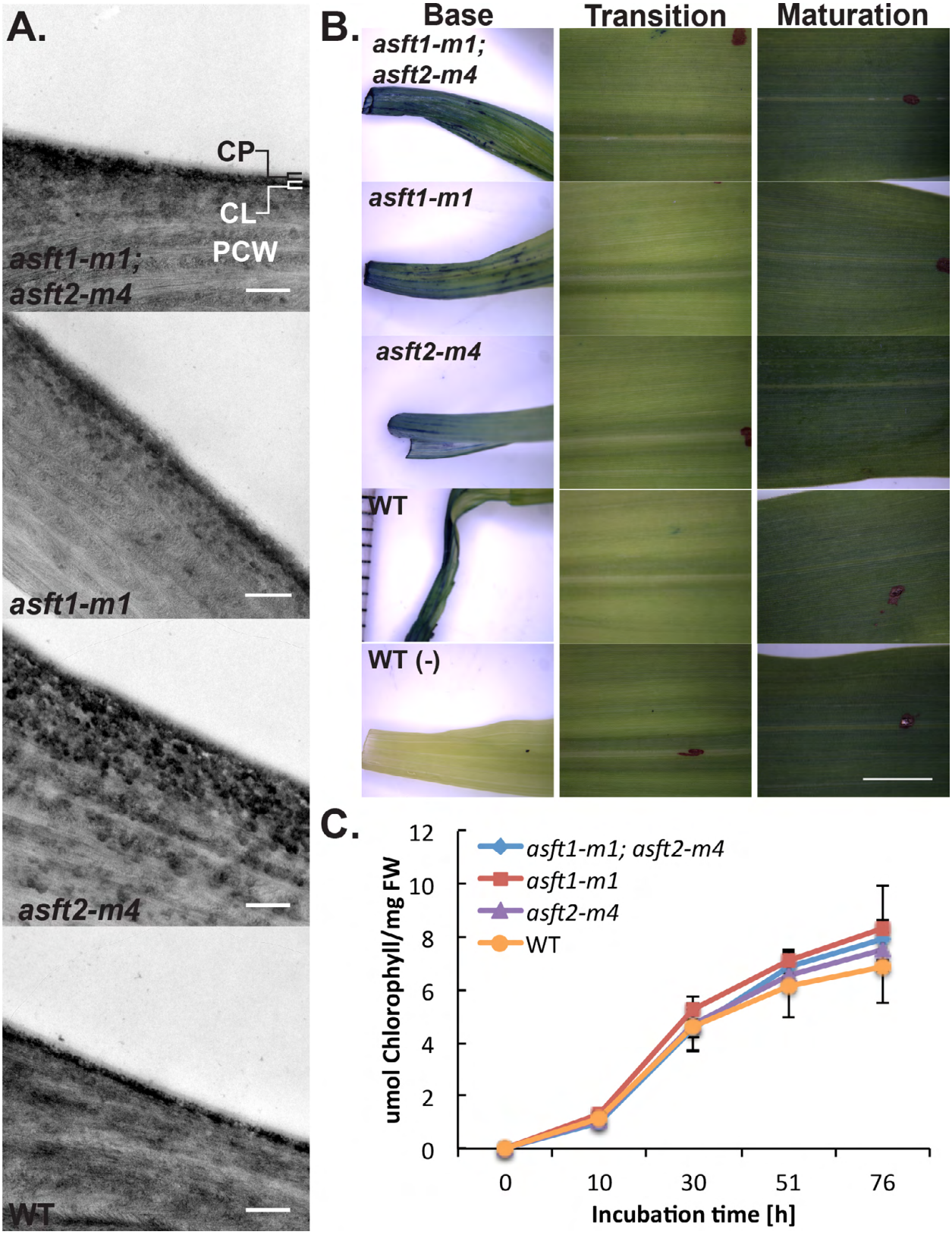
A.
CP
CL
PCW
asft1-m1;
asft2-m4
asft1-m1
asft2-m4
WT
B.
Base
Transition
Maturation
asft1-m1;
asft2-m4
asft1-m1
asft2-m4
WT
WT (-)
C.
asft1-m1; asft2-m4
asft1-m1
asft2-m4
WT
umol Chlorophyll/mg FW
0
2
4
6
8
10
12
0
10
30
51
76
Incubation time [h]

both qualitatively and quantitatively indistinguishable between genotypes. In both WT and *Zmasft* mutants, Toluidine Blue staining was limited to basal portions of excised 10-day old third leaves adjacent to the cut site, with no staining observed in the transition zone or in mature source tissue midway between the point of emergence and the leaf tip (Figure 3.13B). Likewise, the chlorophyll leaching kinetics for whole third leaf laminae were indistinguishable between genotypes at all time points evaluated (Figure 3.13C; one-way ANOVA, all $p > 0.1$). Thus, the *ZmAsft* genes are redundantly essential for normal BS cell wall ultrastructure but dispensable for normal cuticular ultrastructure and barrier function.

The *Asft* genes are not required for normal CO_2 concentration in leaves

To evaluate whether the chemical and ultrastructural defects described above compromise the C_4 carbon concentrating mechanism, CO_2 assimilation curves were generated and online ^{13}C isotope discrimination was measured on WT and *asft1-m1*; *asft2-m4* double mutant plants grown under ambient atmospheric CO_2 concentration. In theory, increased BS permeability due to defective SL would reduce the net CO_2 assimilation rate (A_{net}) in double mutants relative to WT, particularly at low intercellular CO_2 concentrations (C_i) where photosynthesis is CO_2-limited (linear phase of the A-C_i curve in Figure 3.14A; Farquhar *et al*., 1980). However, there was no significant difference in A_{net} in double mutants relative to WT at any measured C_i (Figure 3.14A). Thus, the A-C_i curves suggest that the *Asft* genes are dispensable for normal rates of CO_2 capture.

In C_4 plants, ribulose-1,5- *bis*-phosphate carboxylase/oxygenase (Rubisco) is sequestered within the BS cells, and phosphoenol pyruvate carboxylase (PEPC) carries out the initial carboxylation reaction required for CO_2 capture (reviewed in Sage, 2004). PEPC exhibits a lower

Figure 3.14. The Zm*Asft* genes are not required for normal gas exchange during C_4 photosynthesis.

A. A-C_i curve of net CO_2 assimilation rate (A_{net}) versus intracellular CO_2 concentration (C_i). Net CO_2 assimilation does not differ between wild type (WT, black) and *asft1-m1*; *asft2-m4* double mutants (Dbl Mut, red) at any measured CO_2 concentration (one-way repeated measures ANOVA, $p > 0.05$).
B. Online carbon isotope discrimination measurements for carbon-13 versus carbon-12 ($^{13}CO_2$ isotope discrimination ‰) plotted against the ratio of intercellular to ambient CO_2 concentration (C_i/C_a). There is no significant difference in isotopic discrimination or intercellular CO_2 concentration between double mutant and WT (one-way repeated measures ANOVA, $p > 0.05$). The line indicates the theoretical inverse linear relationship between percent isotope discrimination and C_i/C_a.

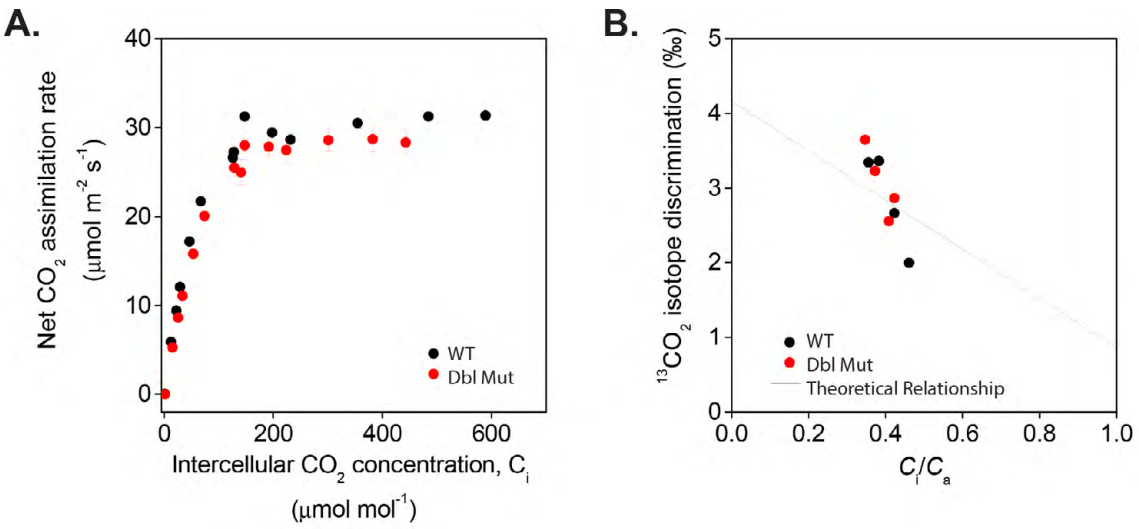
A.
Net CO_2 assimilation rate (μmol m^{-2} s^{-1})
Intercellular CO_2 concentration, C_i (μmol mol^{-1})
WT
Dbl Mut
B.
$^{13}CO_2$ isotope discrimination (‰)
C_i/C_a
WT
Dbl Mut
Theoretical Relationship

degree of ^{13}C isotope discrimination relative to Rubisco, leading to a reduced rate of ^{13}C isotope discrimination in C_4 plants relative to C_3 species (Farquhar *et al*., 1989). Increased bundle sheath permeability would theoretically permit direct diffusion of atmospheric CO_2 to Rubisco, increasing fractionation of the heavy isotopologue $^{13}CO_2$ relative to $^{12}CO_2$ (elevated $^{13}CO_2$ isotope discrimination %) while reducing the ratio of intercellular to ambient CO_2 concentration due to back-diffusion of captured CO_2 to the mesophyll (C_i/C_a; theoretical linear relationship depicted in Figure 3.14B; Henderson *et al*., 1992). However, there was no genotype effect on isotopic discrimination for double mutants relative to WT (Figure 3.14B). Taken together, these gas exchange measurements provide no evidence that the ultrastructural defect in double mutant SL compromises the integrity of the apoplastic diffusion barrier. It was concluded that *Asft1* and *Asft2* are not needed to establish a functional CO_2 concentrating mechanism.

Double mutant roots have a similar aliphatic monomer defect to leaves, but normal ultrastructure and barrier properties.

Although the absence of a carbon-concentrating defect suggests that BS suberization may be dispensable for normal C_4 gas exchange, it is equally plausible to suggest that the *Zmasft* double mutant is a weak mutation that doesn't compromise the SL sufficiently to affect barrier function. To investigate the latter hypothesis, the monomer composition, ultrastructure, and barrier properties of *asft1-m1*; *asft2-m4* double mutant root suberin were evaluated relative to WT.

The root suberin monomer content was quantified using the same methodology as described for leaves. The basal two thirds of 14-day-old soil-grown primary roots were sampled to ensure that all endodermal and hypodermal tissues had fully suberized cell walls. As observed

in leaves, ω-OH FA were the predominant aliphatic monomer class, and were significantly reduced by 48% in double mutants relative to WT (Student's *t* test, $p < 0.01$; Figure 3.15A). This deficiency was predominately attributable to 33.0-83.8% reductions in $C_{22:0}$-$C_{28:0}$ ω-OH VLCFA content ($p < 0.05$; Figure 3.15C), which were not accompanied by a stoichiometric decrease in HCA (Figure 3.15B). The chemical phenotype was specific to double mutants (Figure 3.16). Thus, *Asft1* and *Asft2* are redundantly essential for normal aliphatic suberin composition in both leaves and roots. Although the endo- and hypodermal layers were not separated prior to analysis, previous reports from maize primary roots suggest that ω-OH VLCFA are major components of SL in both layers (Zeier *et al.*, 1999). Thus, it is likely that the *asfta-m1*; *asftb-m4* double mutant affects both tissues.

Given the similar chemical phenotypes of leaf and root polyesters, it was anticipated that the endo- and hypodermis would show similar ultrastructural defects to the BS. However, double mutant cell wall ultrastructure was largely indistinguishable from WT in the endodermis (Figure 3.17A-B). Endodermal SL were continuous on the tangential and radial cell walls, except immediately adjacent to the Casparian Strip (CS). The SL were thickened and globular in the radial wall centripetal to the CS, discontinuous parallel to the CS, and continuous in the centrifugal two thirds of the radial wall (Figure 3.17A-B). As observed in the BS, the distribution of SL around the cell periphery was identical between double mutants and WT. In contrast to the BS, double mutant endodermal SL maintained a uniform thickness in cell corners, were not visibly separated from adjoining cell wall layers, and stained similarly with electron opaque material compared to WT (Figure 3.17A-B). Conversely, the hypodermis had a similar ultrastructural defect to the BS. The double mutant SL had an electron lucent appearance around the entire periphery of the cell, and occasionally exhibited amorphous lamellae with irregular

Figure 3.15. Root and leaf polyesters exhibit similar aliphatic monomer defects.

A. Overview of the major monomer classes present in the basal two thirds of 10-day-old wild type (WT; orange bars) and double mutant (*asfta-m1*; *asft2-m4*; blue bars) seedling primary roots. Asterisks denote significant differences in monomer class abundance between genotypes (Student's t-test; **, $p < 0.01$). Values are averages with standard deviations of three biological replicates.
B. Hydroxycinnamic acid content of seedling primary roots. No significant differences between genotypes were observed for *p*-coumaric acid, ferulic acid, or caffeic acid (inset).
C. Chain length distributions of aliphatic suberin monomers. Asterisks denote significant differences as described in Figure 3.15A (*, $p < 0.05$).

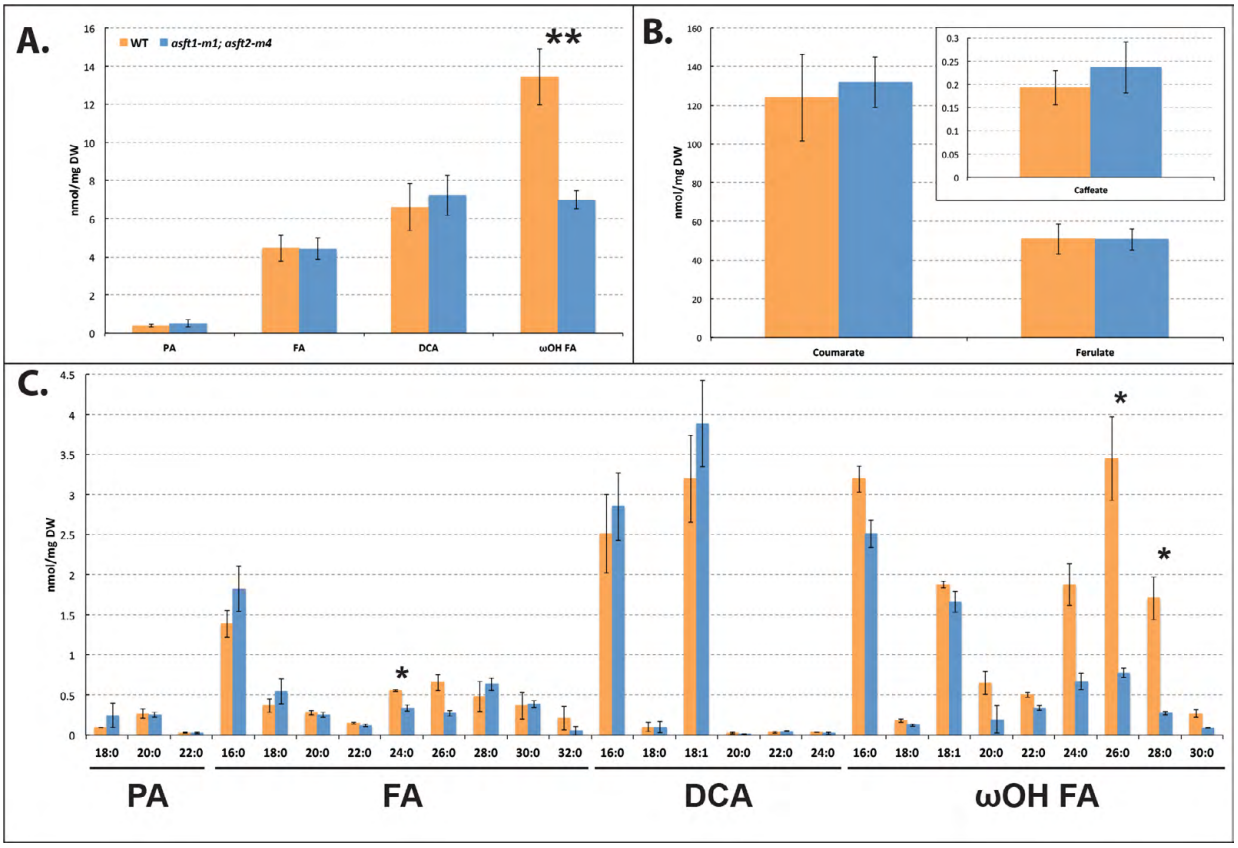
A.
WT
asft1-m1; asft2-m4
nmol/mg DW
**
PA
FA
DCA
ωOH FA
B.
nmol/mg DW
Caffeate
Coumarate
Ferulate
C.
nmol/mg DW
18:0 20:0 22:0 16:0 18:0 20:0 22:0 24:0 26:0 28:0 30:0 32:0 16:0 18:0 18:1 20:0 22:0 24:0 16:0 18:0 18:1 20:0 22:0 24:0 26:0 28:0 30:0
PA
FA
DCA
ωOH FA

Figure 3.16. The root aliphatic monomer defect is specific to double mutants.

A. Overview of the major monomer classes present in seedling primary roots. Monomers were quantified by total GC-FID peak area normalized to ω-pentadecalactone and methyl heptadecanoate as internal standards, and are presented as nmoles per mg dry weight. Values are averages with standard deviations of three biological replicates. HCA, hydroxycinnamic acid; PA, primary alcohol; FA, fatty acid; DCA: α,ω-dicarboxylic acids; ωOH FA, omega-hydroxy fatty acids; polyOH FA, poly-hydroxy fatty acids.
B. Quantities of the hydroxycinnamic acids *p*-coumaric, ferulic and caffeic acid are not significantly different between genotypes. Statistical significance was evaluated as described in Figure 3.6B-C.
C. Analysis of aliphatic monomer content. Monomer classes were analyzed as described in Figure 3.6B-C. Horizontal axis labels denote chain lengths of individual monomers grouped by compound class (labels as described in Figure 3.16A).

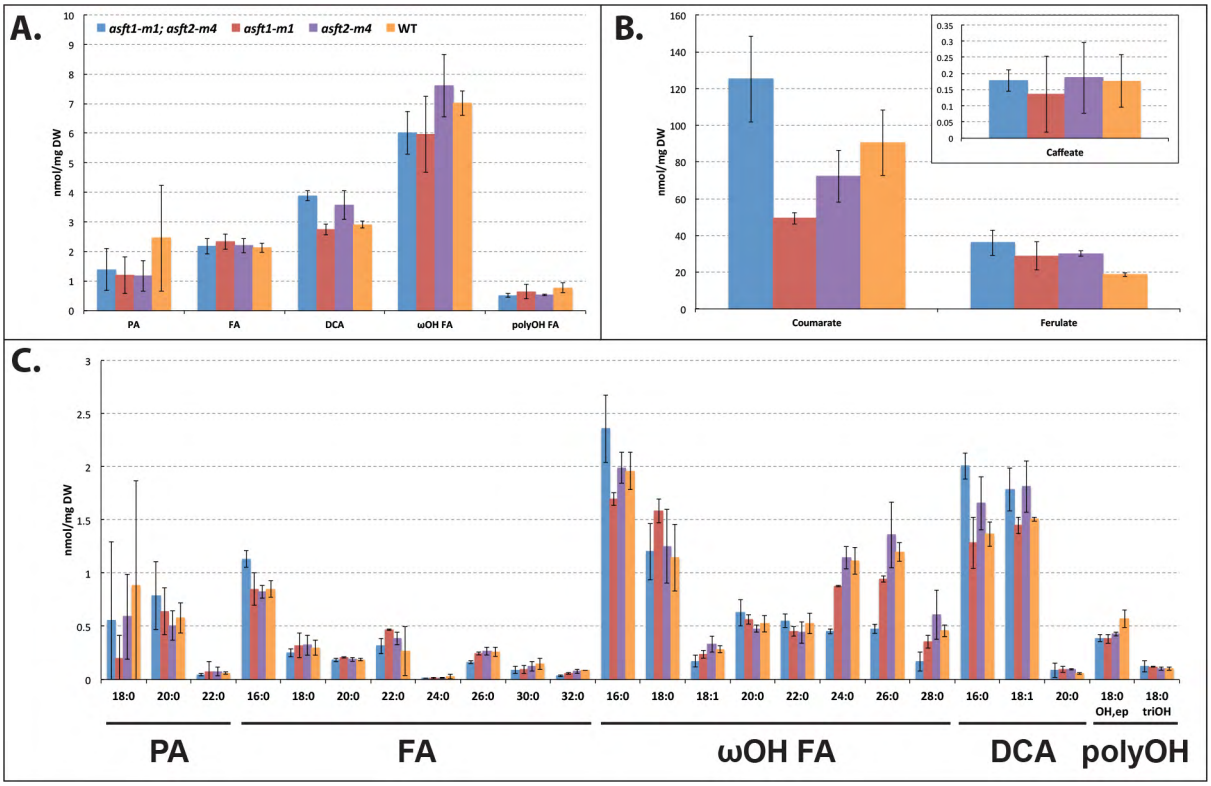
A.
asft1-m1; asft2-m4
asft1-m1
asft2-m4
WT
nmol/mg DW
PA
FA
DCA
ωOH FA
polyOH FA
B.
nmol/mg DW
Caffeate
Coumarate
Ferulate
C.
nmol/mg DW
18:0
20:0
22:0
16:0
18:0
20:0
22:0
24:0
26:0
30:0
32:0
16:0
18:0
18:1
20:0
22:0
24:0
26:0
28:0
16:0
18:1
20:0
18:0 OH,ep
18:0 triOH
PA
FA
ωOH FA
DCA
polyOH

inclusions of electron opaque material between electron lucent bands (Figure 3.17D). However, the polysaccharide cell wall did not appear to separate from the SL as it did in the leaf BS. The wild type SL exhibited conventional tramline architecture as observed in aerial tissues (Figure 3.17C). Therefore, double mutants ultrastructural defect is not conserved between suberized tissues despite similar alterations to the chemical composition of the suberin polyester.

During periods of hypoxic stress experienced by maize roots growing in a stagnant medium, the exodermal cell wall is the primary apoplastic gas exchange barrier against radial oxygen loss (Enstone and Peterson, 2005; Abiko *et al.*, 2012). If *ZmAsft1* and *ZmAsft2* were generally required to form functional suberized gas exchange barriers, plant growth in stagnant medium was expected to be more severely attenuated in double mutants relative to WT. If so, this would imply that a normal suberin lamella is dispensable for the C_4 carbon concentrating mechanism, as the root exodermis and leaf BS have similar ultrastructural defects. 28-day old soil-grown WT and double mutant plants were exposed to a 2-week waterlogging treatment by submerging the pots in stagnant water to a depth of 2 cm above the soil line. Multiple growth parameters were measured, including plant height, leaf dimensions, and dry biomass of shoots and roots. There was no treatment effect between groups prior to the onset of waterlogging stress (two-way ANOVA genotype x treatment, $p > 0.05$). Leaf width at the midpoint of the youngest fully expanded leaf was slightly lower in double mutants relative to WT (Tukey's HSD $p < 0.01$), but growth parameters were otherwise indistinguishable (Table 3.2). After a 2-week period of waterlogging stress, there was a significant treatment effect observed for all growth parameters; stem height, leaf number and dimensions, and total biomass were all strongly attenuated by the waterlogging treatment (two-way ANOVA; all $p < 0.01$). However, there was no genotype effect within treatment groups for any measured parameter except for leaf width in

Figure 3.17. The Zm*Asft* genes are required for normal suberin lamella ultrastructure in the hypodermis.

A. Transmission electron micrograph of inner tangential and radial cell walls of the wild type endodermis near a cell corner. Suberin lamellae (SL) and Casparian Strips (CS) are denoted by arrows. The SL are discontinuous in the cell wall parallel to the CS. 25,000x magnification. Scale bar denotes 200 nm.
B. Inner tangential and radial cell walls of the double mutant endodermis near a cell corner. The distribution, staining, and cohesion of the SL with the primary and tertiary cell walls are indistinguishable from wild type. 25,000x magnification. Scale bar denotes 200 nm.
C. Suberized radial cell walls of two adjacent hypodermal cells from wild type. The SL exhibit a uniform "tramline" architecture. 16,000x magnification. Scale bar denotes 200 nm.
D. Suberized outer tangential cell wall of the double mutant hypodermis adjacent to an epidermal cell. The SL are electron lucent and irregular in thickness compared to WT. Occasional inclusions of electron material of comparable texture to the adjacent polysaccharide cell wall are apparent (arrowhead). 20,000x magnification. Scale bar denotes 200 nm.

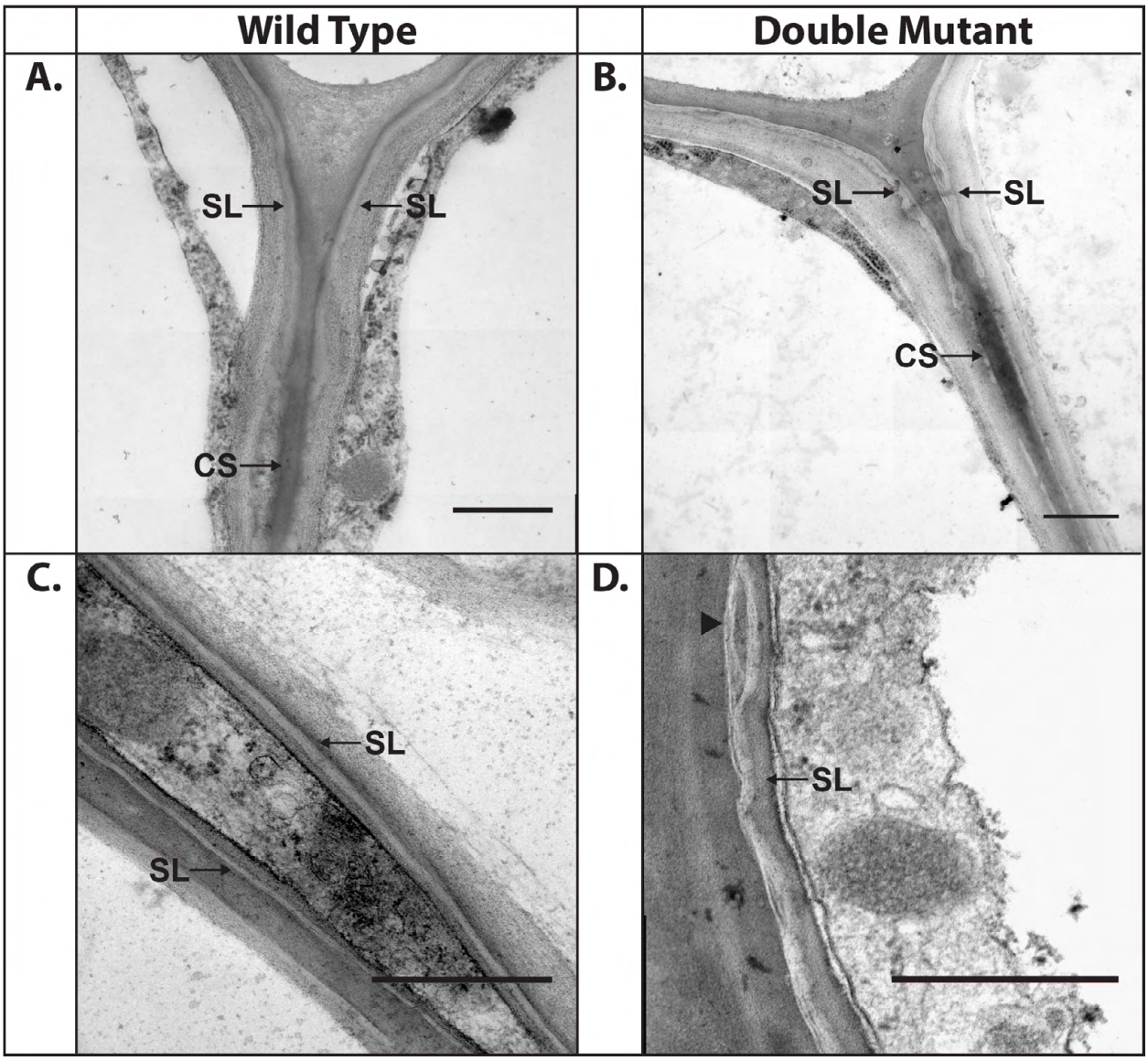
Wild Type
Double Mutant
A.
B.
C.
D.
SL
SL
CS
SL
SL
CS
SL
SL
SL

control plants (Table 3.2). Thus, the ultrastructural defect in *asft1-m1*; *asft2-m4* double mutant roots does not attenuate plant growth relative to wild type under stagnant growth conditions. This implies that mutating the Zm*Asft* genes does not cause sufficient damage to the SL to evaluate whether these structures regulate gas exchange in either roots or leaves. Stronger mutants must be identified to evaluate whether the suberized bundle sheath is an essential component of the carbon concentrating mechanism in maize and other NADP-ME C_4 grasses.

Water flux and stomatal conductance are enhanced in *asft* double mutants.

The lack of a gas exchange defect in double mutants does not preclude the involvement of *ZmAsft1* and *ZmAsft2* in other proposed functions of suberized bundle sheaths. Serra and colleagues (2010) observed a significant increase in water permeability of the tuber periderm in *StFHT* RNAi lines. The cell wall ultrastructure and total aliphatic suberin content were broadly similar to WT, and so the authors proposed that altered cohesion between the SL and cell wall polysaccharides could potentially explain the mutant phenotype (Serra *et al*., 2010a). As the *asft1-m1*; *asft2-m4* double mutant compromises the interface of the SL and the polysaccharide cell wall (Figure 3.12C-E), the mutation may affect leaf water movement. WT and double mutant plants were cultivated under two irradiance regimes, and pressure-volume curves were generated from excised leaves (Tyree and Hamel, 1972). Under both high (1200 µmol quanta/m^2/s) and low (300 µmol quanta/m^2/s) irradiance, double mutants had lower relative water content at the leaf turgor loss point (RWC@ψ_{TLC}; 2-way ANOVA PAR x genotype $p < 0.05$; Figure 3.18A). The absolute leaf capacitance at full turgor (c_{ft}) was also elevated in the double mutant (Figure 3.18C). Thus, it appears that double mutant leaves lose significantly more water than wild type before losing physiological function at the turgor loss point. Under high

Table 3.2 Growth of wild type and double mutant plants during waterlogging stress.

	Outset of waterlogging treatment				2 week waterlogging treatment			
	Controls		Waterlogged		Controls		Waterlogged	
Growth Parameter	**WT**	**Dbl Mut**	**WT**	**Dbl Mut**	**WT**	**Dbl Mut**	**WT**	**Dbl Mut**
Stem Height [cm]	30.17 ± 1.50	31.50 ± 2.16	30.17 ± 1.50	31.50 ± 2.16	93.17 ± 7.86^{a}	97.88 ± 7.17^{a}	57.68 ± 14.30^{b}	60.84 ± 13.68^{b}
Total Leaves (Total Expanded)	11.90 ± 0.32 (7.00 ± 0.00)	12.00 ± 0.00 (7.00 ± 0.00)	11.90 ± 0.32 (7.00 ± 0.00)	12.00 ± 0.00 (7.00 ± 0.00)	20.00 ± 0.47^{a} (13.20 ± 0.48^{a})	19.60 ± 0.70^{a} (13.00 ± 0.00^{a})	17.10 ± 1.85^{b} (11.00 ± 1.25^{b})	17.30 ± 1.85^{b} (11.00 ±1.25^{b})
Leaf 7 Length [cm]	72.56 ± 13.67	74.86 ± 14.64	72.56 ± 13.67	74.86 ± 14.64	ND	ND	ND	ND
Leaf 7 Width [cm]	5.28 ± 0.23^{a}	5.01 ± 0.13^{b}	5.28 ± 0.23^{a}	5.01 ± 0.13^{b}	ND	ND	ND	ND
Leaf 11 Length [cm]	N/A	N/A	N/A	N/A	85.87 ± 3.09^{a}	87.47 ± 3.29^{a}	77.76 ± 4.37^{b}	84.03 ± 4.84^{a}
Leaf 11 Width [cm]	N/A	N/A	N/A	N/A	8.54 ± 0.32^{a}	7.90 ± 0.46^{b}	8.03 ± 0.39^{b}	7.53 ± 0.39^{b}
Stem Dry Mass [cm]	ND	ND	ND	ND	53.20 ± 8.31^{a}	53.41 ± 9.57^{a}	33.28 ± 9.72^{b}	31.44 ± 6.62^{b}
Root Dry Mass [cm]	ND	ND	ND	ND	32.27 ± 18.00^{a}	16.05 ± 2.05^{b}	8.77 ± 4.25^{b}	10.78 ± 5.59^{b}

Figure 3.18. Capacitance and cell wall elasticity are altered in double mutants.

A. Relative water content at the leaf turgor loss point (RWC@Ψ_{TLP}) of *asf1-m1; asft2-m4* double mutants (SM) and isogenic wild types (WT) cultivated under high irradiance (1200 μmol photons/m^2/s) or low irradiance (300 μmol photons/m^2/s). The double mutant has significantly lower relative water content at turgor loss than WT under both irradiance regimes (two-way repeated measures ANOVA PAR x genotype, $p < 0.05$).
B. Bulk elastic modulus (ε) of WT and double mutant. Significantly greater pressure is required to deform the cell wall in double mutant grown under high irradiance relative to WT (two-way repeated measures ANOVA PAR x genotype, $p < 0.05$). There is no genotype effect under low irradiance.
C. Absolute capacitance at full turgor (c_{ft}) is significantly higher in double mutants relative to WT under both irradiance regimes (two-way repeated measures ANOVA PAR x genotype, $p < 0.05$).

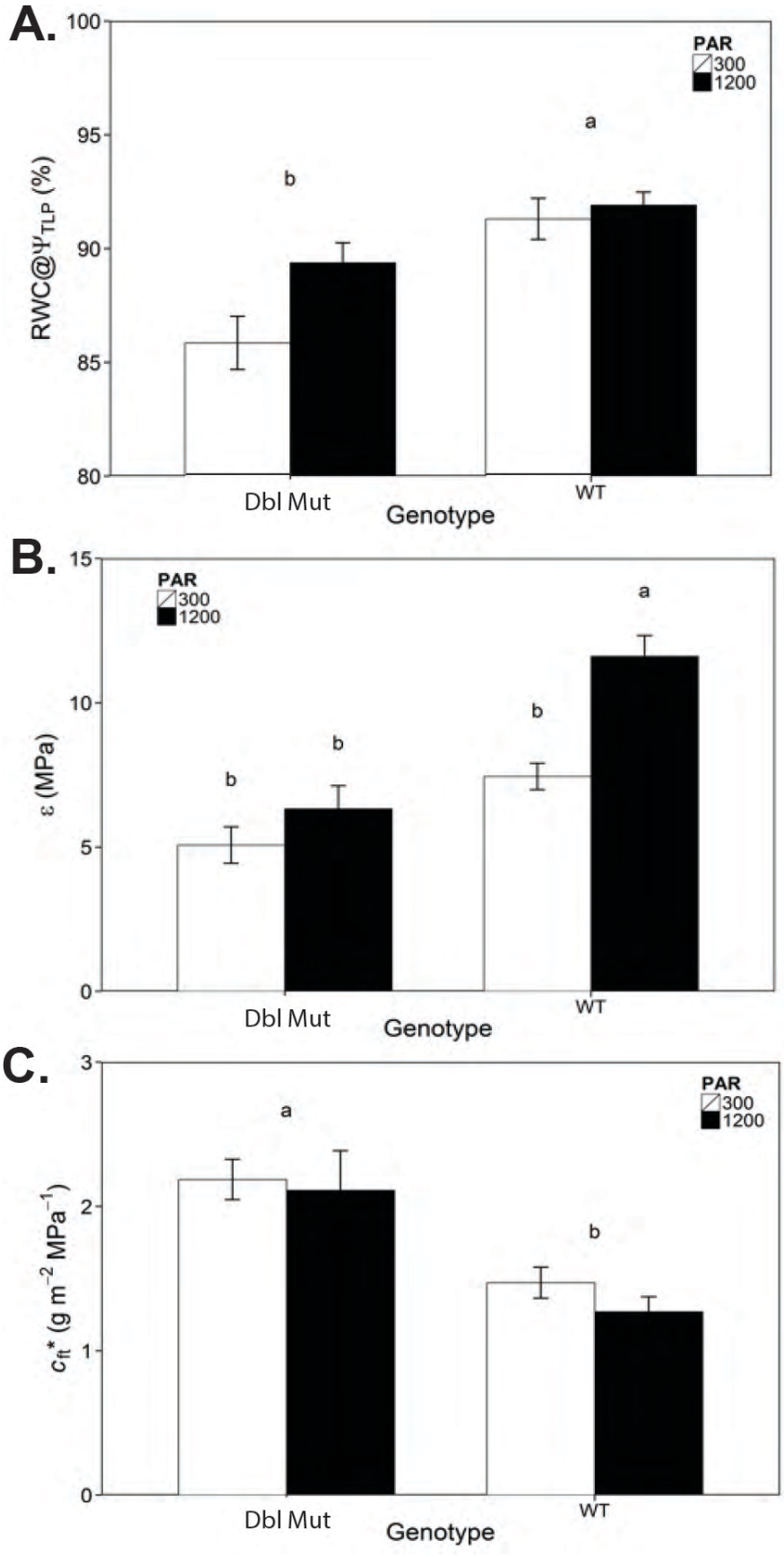
A.
100
95
90
85
80
RWC@Ψ_{TLP} (%)
PAR
300
1200
a
b
Dbl Mut
WT
Genotype
B.
15
10
5
0
ε (MPa)
PAR
300
1200
a
b
b
b
Dbl Mut
WT
Genotype
C.
3
2
1
0
c_{ft}^* (g m^{-2} MPa^{-1})
PAR
300
1200
a
b
Dbl Mut
WT
Genotype

irradiance, the bulk modulus of elasticity (ε) was significantly elevated in double mutants relative to WT (Figure 3.18B). The bulk modulus estimates the average cell wall rigidity across the leaf (Koide *et al*., 2000). Thus, some portion of the cell walls within the double mutant leaf lamina are significantly less flexible than in WT.

An independent set of wild type and double mutant plants were cultivated under the irradiance regimes described above plus two relative humidity levels (50% RH and 80% RH) to evaluate leaf transpiration. For both humidity regimes, transpirational flux (*E*) and stomatal conductance per unit stomata (g_s/stomata) were elevated in double mutants relative to wild type at high irradiance (3-way ANOVA PAR x RH x Genotype, $p < 0.05$; Figure 3.19A-B). Taken together, these results suggest that the resistance to water movement in double mutant cell wall is reduced relative to WT. As the ultrastructure and barrier properties of the leaf cuticle were unaffected in the double mutant (Figure 3.13), the ultrastructural perturbations to the BS cell wall may underlie this phenotype.

DISCUSSION

Aliphatic monomer content differs between root and leaf tissues

In order to functionally dissect bundle sheath suberization in an NADP-ME-type C_4 grass, two paralogously duplicated maize homologues of Arabidopsis *ALIPHATIC SUBERIN FERULOYL TRANSFERASE*, *ZmAsft1* and *ZmAsft2*, were identified, and an allelic series of double mutants was generated using *Dissociation* transposons. Double mutants developed normally under ambient conditions, and so the leaf polyesters were profiled to confirm the mutant phenotype. Several monomer classes typical of aliphatic suberin and cutin were released, including fatty acids, primary alcohols, α,ω-dicarboxylic acids, and saturated, unsaturated, and

Figure 3.19. Transpirational flux and stomatal conductance are elevated in double mutants.

A. Under high irradiance, transpirational flux (*E*) is elevated in double mutants relative to wild type at both 50% and 80% relative humidity (three-way repeated measures ANOVA PAR x RH x genotype, $p < 0.05$). There is no genotype effect for either humidity regime at low irradiance.
B. Stomatal conductance normalized by stomatal number (g_s/stomata) is elevated in double mutants relative to WT under high irradiance at both 50% and 80% relative humidity (three-way repeated measures ANOVA PAR x RH x genotype, $p < 0.05$). There is no genotype effect for either humidity regime at low irradiance.

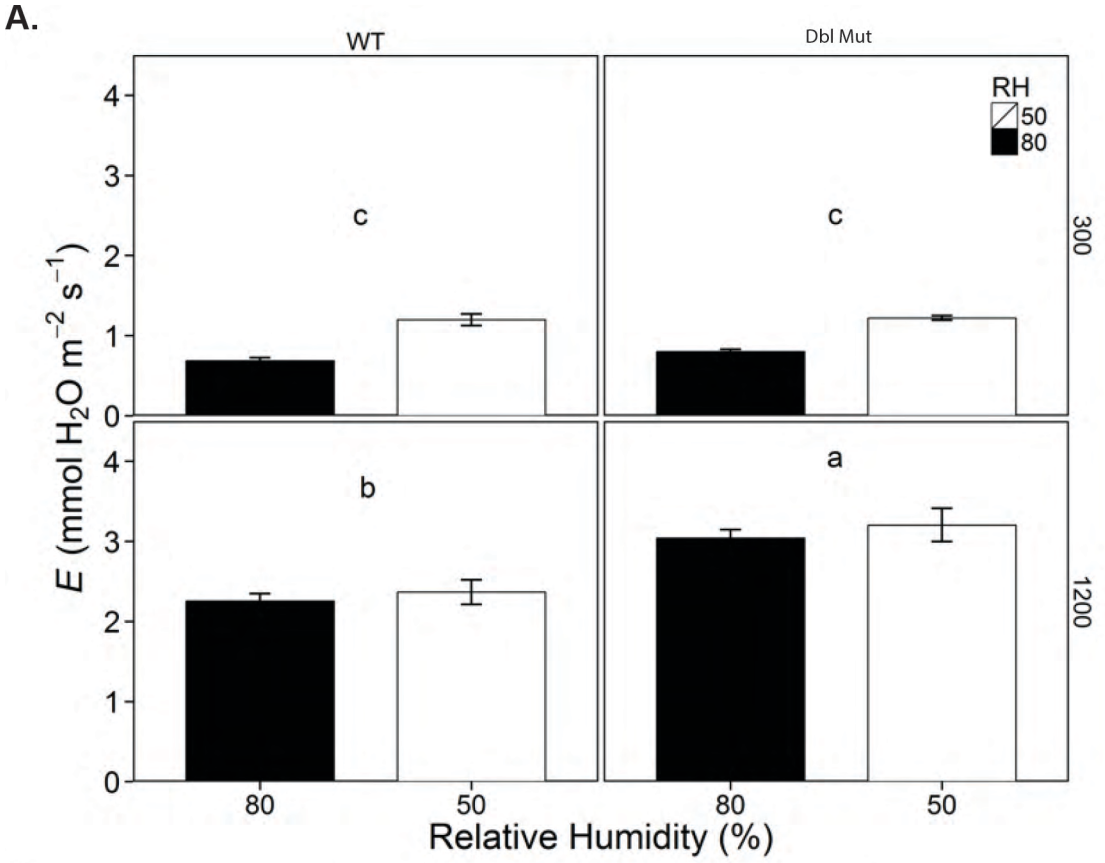
A.
WT
Dbl Mut
RH
50
80
300
1200
c
c
b
a
E (mmol H2O m−2 s−1)
0
1
2
3
4
80
50
80
50
Relative Humidity (%)

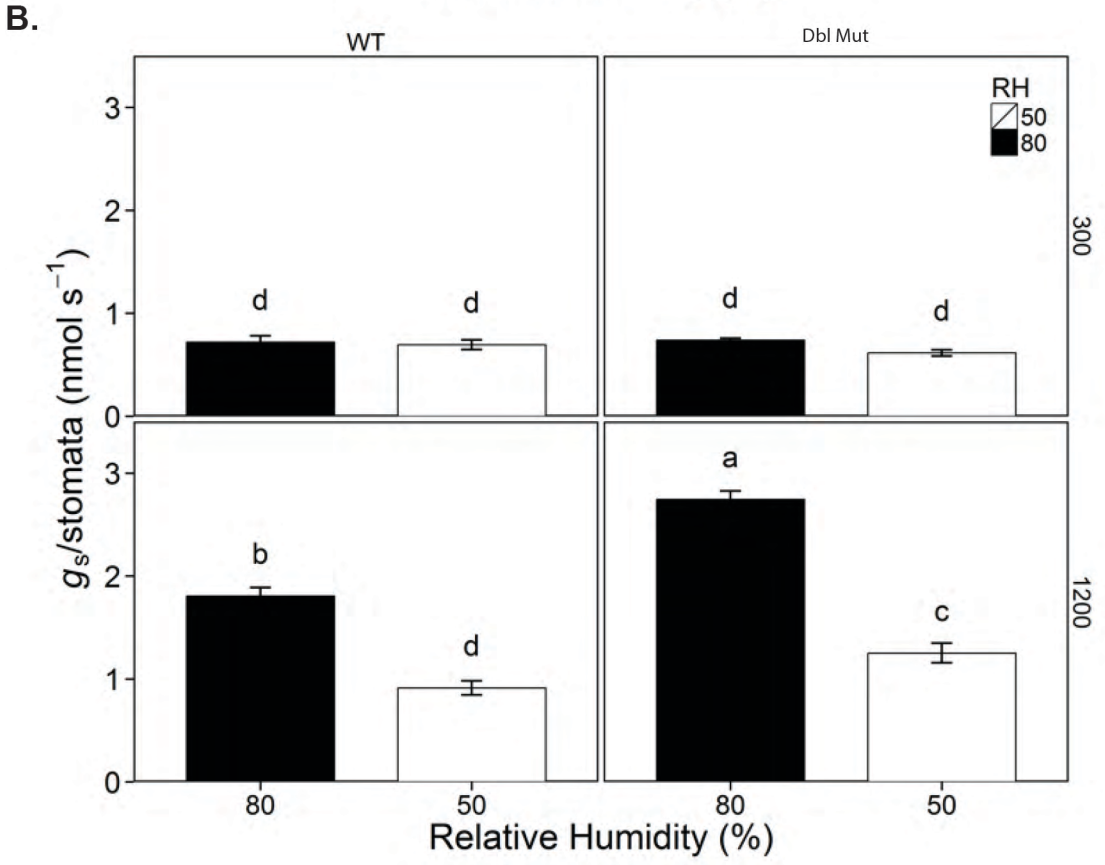
B.
WT
Dbl Mut
RH
50
80
300
1200
d
d
d
d
b
d
a
c
gs/stomata (nmol s−1)
0
1
2
3
80
50
80
50
Relative Humidity (%)

mid-chain oxidized ω-hydroxy fatty acids (Figure 3.5-3.8). The predominant aliphatic monomer class was ω-OH FA, comprising 46-54% of the aliphatic species extracted from entire laminae and 60-64% of mechanically fractionated samples. These results were comparable to the averages of 50-60% and 45-50% reported for suberized endo- and hypodermal root cells, respectively (Zeier et al., 1999), but were significantly higher than the reported values for leaf BS (23.1%) and cuticle (32.4%; Espelie and Kolattukudy, 1979). This discrepancy was attributed to two factors: first, a larger proportion of mid-chain oxidized ω-OH FA was reported for both leaf tissues (30.2% and 34.9%, respectively) than was observed in this study (21-25% for all samples). This discrepancy may result from intrinsic differences in genetic background or developmental stage, or from the greater proportion of ω-OH VLCFA identified in this study. Second, Espelie and Kolattukudy (1979) recovered significant quantities of C_{17} and C_{19} odd-chain fatty alcohols in the BS. C_{17} fatty alcohols were also reported as a major component of the root hypodermal suberin by Pozuelo and colleagues (1984). In both cases, the polyester was depolymerized by reductive hydrogenolysis with $LiAlD_4$; conversely, odd-chain monomers were not reported for any study in which the polyester was depolymerized by acid- or base-catalyzed transmethylation. No putative biosynthesis pathway or candidate genes have been reported for odd-chain fatty acids, and their prevalence in maize suberin remains to be elucidated.

Although ω-OH FA accumulate to comparable levels in all maize polyesters, significant discrepancies were observed in the abundance of α,ω-DCA and mid-chain oxidized ω-OH FA between roots and leaves (Figure 3.5-3.8; Figure 3.15-3.16). Wild type primary root preparations, which contained a mixture of endo- and hypodermal suberin monomers, contained 37% DCA and 54% ω-OH FA (Figure 3.15A). Although the relative proportion of DCA reported in the literature varied considerably between root tissues and experimental conditions, these

monomers comprised at least 10% of the total in all experiments (Pozuelo *et al*., 1984; Zeier *et al*., 1999; Zimmermann *et al*., 2000; Schreiber *et al*., 2005a). Conversely, α,ω-DCA comprised an extremely minor fraction of whole leaf (0.2-0.9%) and fractionated (0.4-0.5%) monomers (Figure 3.5-3.8). Some of this disparity could be attributed to the mixture of cutin and suberin polyesters within these samples, as cutin is deficient in α,ω-DCA relative to suberin across broad taxa, including maize (Espelie and Kolattukudy, 1979; Pollard *et al*., 2008). However, α,ω-DCA were also a minor component of the suberin from purified bundle sheath strands (2.6%; Figure 3.8A,C). Conversely, maize root suberin contains minor quantities of mid-chain hydroxylated ω-OH FAs (9.4% and 2%, respectively, for endo- and hypodermis; Pozuelo *et al*., 1984) relative to epidermal cutin (34.9%; Espelie and Kolattukudy, 1979). Mid-chain hydroxylated ω-OH FAs were not detected in seedling primary roots (Figure 3.15-3.16), were a minor component of purified BS strands (6.5%, Figure 3.8A,C). Taken together with the gene expression data presented in Chapter 2, these results suggest that maize BS suberin is intermediate in character between root suberin and epidermal cutin.

Zmasft1; Zmasft2 **double mutants are deficient in aliphatic suberin monomers**

Zmasft1-m1; *Zmasft2-m4* double mutant polyesters were strongly and specifically deficient in $C_{22:0}$-$C_{30:0}$ ω-OH VLCFA relative to both single mutants and WT in leaves and roots (Figure 3.5-3.8). Purified cuticle samples could not be recovered for analysis, and so a pleiotropic leaf cutin defect cannot be ruled out. However, maize suberin is enriched in VLCFA relative to cutin (Espelie and Kolattukudy, 1979), and ω-OH VLCFA are strongly attenuated in purified BS samples (Figure 3.8). This aliphatic suberin deficiency was qualitatively similar to *Atasft* mutant seed coat polyesters, which exhibited a slight reduction in $C_{22:0}$-$C_{24:0}$ ω-OH

VLCFA, the longest chain ω-OH FA present in Arabidopsis suberin (Molina *et al*., 2010). Conversely, *StFHT*-RNAi lines were strongly deficient in $C_{18:1}$ monounsaturated ω-OH LCFA (Serra *et al*., 2010a), potentially reflecting variation in substrate specificity between ASFT proteins. The ω-OH VLCFA deficiency is hypothesized to reflect the *in vivo* substrate preference of ZmAsft1 and ZmAsft2 for two reasons: first, *ZmAsft1* and *ZmAsft2* are co-expressed with a group of genes specifically involved in VLCFA modification, whereas the majority of putative LCFA-related genes are expressed at the leaf base (Li *et al*., 2009; Wang *et al*., 2014). Second, there is a precedent for esterification of ferulic acid to 26- and 28-carbon ω-OH VLCFA in other grasses; these oligomers were reported as a wax component of oat caryopses, although the causal enzyme has not been purified (Daniels and Martin, 1968).

It is not clear whether the deficiency in ω-OH VLCFA results from a failure to export these species to the apoplast or a failure to esterify them stably into the suberin polyester *in muro*. In both cases, the ω-OH VLCFA would be solubilized by chloroform during sample preparation. Although several groups have successfully analyzed the aliphatic composition of these extracts (Vishwanath *et al*., 2013; Waßmann, 2014), doing so would not clarify whether the monomers originated from an intracellular or apoplastic location. Interestingly, alkyl hydroxycinnamates are severely attenuated in the root wax of Arabidopsis *abcg2*; *abcg6*; *abcg20* triple mutants, suggesting that HCA-fatty alcohol dimers may be a substrate of ABCG transporters (Yadav *et al*., 2014).

Total esterified ferulic acid in mutant Arabidopsis and potato suberin was reduced by 50-90% (Gou *et al*., 2009; Molina *et al*., 2009; Serra *et al*., 2010a). Although the aliphatic defect of the *Zmasft* double mutant was consistent with model dicots, the absence of any stoichiometric reduction in HCA was unexpected (Figure 3.5-3.8; Figure 3.15-3.16). In maize leaves, both *p*-

coumaric and ferulic acids were sufficiently abundant to couple to the depleted ω-OH VLCFA in a 1:1 stoichiometry (Molina et al., 2009). *p*-Coumaric and ferulic acid esters of ω-OH FA have been identified by partial depolymerization of potato periderm suberin and tomato (*Solanum lycopersicum*) fruit cutin (Graça and Santos, 2007; Graça and Lamosa, 2011), but fraction of HCA associated with suberin within the type II cell wall of maize was unknown at the outset of this study. Dilute acid fractionation of the cell wall indicated that 86-90% of total cell wall ferulate in developing leaves is associated with GAX rather than suberin (Figure 3.9C). The estimated quantity of suberin-associated ferulate, 10-14% (1.7-2.3 nmol/mg DW) is in good agreement with the reduction in ω-OH VLCFA (1.5 nmol/mg DW) in double mutants. Interestingly, mutants of Arabidopsis *CYP861*, which is required for ω-OH VLCFA biosynthesis, are deficient in ferulic acid, but the rice *cyp86b3* mutant exhibits no reduction in ferulate despite a complete absence of ω-OH VLCFA in root suberin (Waßmann, 2014). Although a direct covalent linkage between HCA and ω-OH VLCFA remains to be demonstrated for grass suberin, these results indicate that changes in suberin-associated HCA content may be challenging to quantify in grass mutants.

A very small fraction of the total ester-linked *p*-coumarate in our samples was associated with GAX (8.8%; Figure 3.9D). Unlike ferulic acid, *p*-coumarate is extensively esterified to maize lignin as a pendant side-chain, and so the majority of *p*-coumarate is likely associated with lignin (Mueller-Harvey et al., 1986; Ralph et al., 1994). In maize roots, *p*-coumarate accumulation continues throughout tertiary cell wall development after suberization has ceased (Zeier *et al*., 1999). Likewise, *p*-coumarate abundance positively correlates with lignification during maize stem development (Hatfield *et al*., 2008a). An estimation of the *p*-coumarate fraction specifically associated with lignin would require a sophisticated linkage analysis using

Derivatization Followed by Reductive Cleavage (DFRC; Lu and Ralph, 1999; Petrik *et al*., 2014), and is beyond the scope of this study.

The ultrastructural defect of *Zmasft* double mutants is inconsistent with model dicots

The implications of the variable monomer content within maize tissues and genotypes described above on polymer architecture are unclear. Models of the suberin polyester proposed prior to the characterization of Arabidopsis *ASFT* frequently included ferulic acid as an essential structural component of the electron-opaque lamellar bands and the interface with the polysaccharide cell wall (Kolattukudy, 1980; Bernards, 2002; Graça and Santos, 2007). However, both lamellar ultrastructure and cell wall cohesion were unaffected in Arabidopsis roots and potato tuber periderm of *Atasft* and *Stfht* mutants (Molina *et al*., 2009; Serra *et al*., 2010a). Conversely, the BS cell wall ultrastructure of the *Zmasft1-m1*; *Zmasft2*-m4 double mutant is consistent with earlier structural models. BS cells rupture during mechanical shearing, and the SL tear away from adjoining polysaccharides as discrete units during preparation for TEM (Figure 3.10-3.12). Although double mutants exhibited a significant reduction in ω-OH VLCFAs without a detectable stoichiometric reduction in HCAs (Figure 3.5-3.8), it is likely that an aromatic monomer deficiency underlies the ultrastructural defect. Separation of the wall into discrete layers at interfaces between cellulose microfibrils and electron-translucent suberin lamellae was also reported for secondary walls of green cotton fibers treated with aminoindan-2-phosphonic acid (AIP), an inhibitor of phenylalanine ammonia lyase (Figure 4 of Schmutz *et al*., 1993). The authors attributed the ultrastructural defect to a deficiency in caffeic acid, which was esterified to the ω-OH FA side chains of acyl-glycerol oligomers (Schmutz *et al*., 1993). The predominant aliphatic monomer of green cotton suberin is 22-OH docosanoic acid; thus,

VLCFA-HCA oligomers are a crucial structural component of the suberin polyester in this cultivar (Ryser *et al*., 1983; Yatsu *et al*., 1983). Caffeic acid is present predominately as alkyl caffeate wax esters in taproots, and is a minor component of the periderm and seed coat suberin polyester in Arabidopsis (Kosma *et al*., 2012), but was not previously reported as a component of grass suberin. However, most studies published to date, including this study, involved base-catalyzed transmethylation or aqueous washes of extracted monomers (Materials and Methods), both of which attenuate the recovery of caffeate (Kosma *et al*., 2012). Although caffeate content was likely underestimated, the ZmAsft proteins are orthologous to AtASFT (Figure 3.1), which exhibits a strong *in vitro* substrate preference for feruloyl- and *p*-coumaroyl-CoA over caffeoyl-CoA (Molina and Kosma 2015). Of these two HCAs, acyl *p*-coumarate esters are less likely than acyl ferulates to contribute directly to a cell wall adhesion defect. In lignified walls, *p*-coumarate is thought to act as a nucleation site for phenylpropanoid polymerization via radical transfer from its phenol ring, but does not radically couple *in muro* (Ralph *et al*., 1994; Hatfield *et al*., 2008b). Conversely, ferulate esters of GAX readily dimerize *in muro* and are major contributors to cell wall adhesion and biomass recalcitrance in grasses (Ralph *et al*., 1995; Grabber *et al*., 1998 & 2000; Jung and Phillips, 2010; Jones *et al*., 2013). Pending a detailed biochemical characterization of ZmAsft1 and ZmAsft2, they are thought to be ω-OH VLCFA:feruloyl-CoA acyltransferases required for cohesion between SL and feruloylated cell wall polysaccharides in the BS.

In contrast to the BS ultrastructural defect, the root endodermal and hypodermal layers showed little to no change in cell wall cohesion, consistent with the phenotypes of previously characterized *asft* mutants (Figure 3.17). This variation in suberin ultrastructure between tissues was unexpected, and an explanation was sought. The cohesion defect of AIP-treated green cotton

was of particular interest, as the secondary cell walls of cotton fibers are comprised predominately of cellulose (95% by dry weight) plus a very small proportion (~2.6%) of HCAs and lignin-like polymers (Timpa and Triplett, 1992; Fan *et al*., 2009). The BS cells from several grasses, including maize, fluoresce green rather than blue in the presence of 100 mM ammonium hydroxide (pH 10.3), suggesting that this tissue also contains HCAs but not lignin (Harris and Hartley, 1976). The root endo- and exodermis, as well as major vein BS cells, fluoresced blue and reacted positively with phloroglucinol-HCl and Maulë Reagent, but BS cells surrounding minor and intermediate veins did not (data not shown). Thus, lignification of adjoining cell walls may stabilize the double mutant SL in roots, although it remains to be determined whether this involves a direct covalent interaction or a general reinforcement of the entire wall against mechanical disruption. Available data suggests the latter; the BS SL of adjoining radial walls did not separate from adjoining walls and were largely indistinguishable from WT despite a negative stain for lignin (Figure 3.12E and data not shown). BS cells surrounding major veins were not imaged by TEM in this study, and it will be interesting to determine whether the cell wall cohesion defect extends to these cells.

The hypodermis of maize seedling primary roots contains roughly half the thioacidolysis-labile lignin of the endodermis (Zeier *et al*., 1999). Thus, an absence of lignin is not sufficient to explain the mildly disorganized structure of the hypodermal SL (Figure 3.17D). In tissues such as the Arabidopsis endodermis and potato tuber periderm, where the predominant ω-OH FAs are long chain species, mutating *CYP86A1* sub-clade members (Chapter 2, Figure 2.4A) disrupts the SL (Hofer *et al*., 2008; Serra *et al*., 2009a). In particular, periderm SL from *StCYP86A33*-RNAi lines were disorganized and had electron-opaque inclusions within the electron-translucent lamellae (compare Figure 3D of Serra *et al*., 2009a to Figure 3.16D). Whereas ω-OH LCFA are

the major aliphatic monomers of maize endodermal suberin, ω-OH VLCFA predominate in the hypodermis (Zeier *et al*., 1999; Schreiber et al., 2005a). These data seem to indicate a threshold effect whereby the interior ultrastructure of the SL is compromised when a significant proportion of the major aliphatic monomer is attenuated. However, this theory fails to explain the ultrastructure of the BS SL, which separates from the polysaccharide cell wall as a cohesive unit despite a 97% drop in ω-OH VLCFA, which constitute roughly 65% of WT ω-OH FA monomers (Figure 3.8; Figure 3.12C-D). Thus, although *ZmAsft1 and ZmAsft2* are redundantly essential for cell wall cohesion in the BS, the precise contribution to the ultrastructure of suberin and its interface with the cell wall remains ambiguous. As covalent interactions with lignin and feruloylated GAX may be involved, it would be of interest to generate triple mutants of *Zmasft1*; *Zmasft2* and existing *brown midrib* (Marita *et al*., 2003; Méchin *et al*., 2014) or *seedling ferulate ester* (Jung and Phillips, 2010) mutants to test for synergistic interactions.

The *Zmasft* double mutant has a subtle effect on leaf water movement

Altered apoplastic permeability is one of the most prevalent phenotypes reported for suberin mutants. Disruptions to VLCFA elongation by β-ketoacyl-CoA synthases (*StKCS6*; Serra et al., 2009b), LCFA ω-hydroxylation (*AtCYP86A1* and *StCYP86A33*; Hofer *et al*., 2009; Serra *et al*. 2009), and suberin feruloylation (*StFHT*; Serra et al., 2010a) are all sufficient to increase peridermal water permeance. Root pressure probe experiments with *Atcyp86a1* suggest that both hydrostatic and osmotic hydraulic conductivity are elevated, indicating greater flux through both apoplastic and cell-to-cell pathways (Ranathunge *et al*., 2011). As reported for epidermal cuticles, suberin-associated wax is the major barrier to peridermal transpiration; extraction of wax from potato tubers increased the water permeance 10-100 fold (Schreiber *et al*., 2005b;

Schreiber, 2010). However, the composition of the suberin polyester is also critical, as the *StFHT*-RNAi line exhibited 15-fold higher permeance despite WT levels of total suberin and elevated wax deposition (Serra *et al*., 2010a). The latter study also implies that suberin feruloylation is critical for to restrict uncontrolled diffusion of water, even if the ultrastructure of *StFHT*-RNAi lines appears indistinguishable from WT (Serra *et al*., 2010a).

Pressure-volume curves generated from wild type and double mutant leaves implicate the *ZmAsft* genes in the control of leaf water movement (Canny, 1986). Relative water content at the leaf turgor loss point was reduced in double mutants, and capacitance at full turgor increased, irrespective of irradiance regime (Figure 3.18A,C). These results suggest that the double mutant leaves are more permissive to water movement than WT. At least under high irradiance, decreased elasticity of the cell wall correlates with the observed phenotype (Figure 3.18B). Apoplastic tracer studies indicate that the middle lamellae of radial walls between adjoining bundle and mestome sheath cells form an uninterrupted path for the diffusion of water and solutes out of the leaf vasculature (Evert *et al*., 1985; Botha and Evert, 1986; Eastman *et al*., 1988b). Thus, it is plausible that ultrastructural changes at the interface of the SL and primary cell wall facilitate apoplastic water movement in double mutants (Figure 3.12). The elevated transpirational flux and stomatal conductivity of double mutants are consistent with these data (Figure 3.19).

However, there are several caveats associated with the above speculations. First, the *ZmAsft* genes are expressed in both epidermal and BS cells, and the potato orthologue *StFHT* is strongly expressed in lenticels (Boher et al., 2013). Thus, an undetected change to the cuticle or guard cells cannot be ruled out despite the similar ultrastructure, barrier properties, and stomatal number between WT and double mutants (Figure 3.13, Figure 3.19B). Second, the bulk elastic

modulus was estimated at the organ level, and cannot be specifically attributed to the BS cell walls. The reduction in elasticity is consistent with a recent solid-state ^{13}C NMR study of isolated periderm suberin from *StFHT*-RNAi lines (Serra *et al*., 2014). The authors attributed the reduced peridermal elasticity to increased incorporation of recalcitrant polyphenolic material into the cell wall (Serra *et al*., 2014). It remains to be determined whether a similar compensatory effect occurs in *Zmasft* double mutants, and whether the BS cell walls in particular are responsible for the reduction in leaf elasticity. Finally, although stomatal conductance was elevated in double mutants under high irradiance, no significant genotype effects were observed on intercellular CO_2 concentration or net CO_2 assimilation under any experimental conditions (Figure 3.14 and data not shown). Thus, although slight effects on leaf water movement can be measured experimentally, the physiological relevance of these alterations remains to be elucidated.

It is clear that quantitative monomer profiling is not sufficient to fully elucidate the *Zmasft* double mutant cell wall defect. Existing models of aromatic suberin structure (Cottle and Kolattukudy, 1982; Bernards *et al*., 1995; Lapierre *et al*., 1996) are based on potato periderm. It is unknown whether the HCA-rich polyphenolic compound described for tubers is also present in grass vascular sheaths. Purification of milligram quantities of BS outer tangential cell walls for structural studies using solid-state NMR (Serra *et al*., 2014) or FTIR (Arrieta-Baez and Stark, 2006) would be challenging. However, the BS strand purification protocol presented in this study (Figure 3.8; Materials and Methods) could generate sufficient quantities of reasonably pure material for a pilot study.

ZmAsft1 and *ZmAsft2* do not compromise BS suberization sufficiently to assess its role in gas exchange

Although the leaf CO_2 assimilation and online carbon isotope discrimination data strongly indicate *ZmAsft1* and *ZmAsft2* are not required to establish a normal CO_2 concentrating mechanism in the maize BS (Figure 3.14), the disruption to the SL ultrastructure is subtle and apparently limited to the cell wall interface (Figure 3.12). Thus, it is possible that *Zmasft1*; *Zmasft2* is a weak mutant, and that stronger mutations will be required to be determine whether suberin itself is involved in gas exchange. Interestingly, the hypodermal layer, which functions as the primary apoplastic diffusion barrier during hypoxia stress, is enriched in VLCFA relative to the endodermis in several monocot species (Zeier *et al*., 1998; Zeier *et al*., 1999; Schreiber *et al*., 2005a). However, there is little evidence for a specific functional role of VLCFA derivatives in the architecture or barrier properties of polyester cell walls. Specifically attenuating ω-OH VLCFA has no effect on barrier properties in Arabidopsis roots (Compagnon et al., 2009). Likewise, cuticles are largely devoid of these molecules across diverse taxa (reviewed in Pollard et al., 2008).

Molecular genetic data from the first suberin biosynthesis mutants characterized in rice provide compelling evidence that SL, and aliphatic suberin in particular, are required to form diffusion barriers to O_2, at least in roots. The *reduced culm number1 (rcn1/Osabcg5)* mutant was recently demonstrated to encode an ABCG half transporter essential for elongation of rice roots in stagnant, deoxygenated medium (Yasuno *et al*., 2009; Shiono *et al*. 2014a). *RCN1*/*OsABCG5* expression is strongly and specifically induced by hypoxia treatment in the endo- and hypodermal layers of nodal roots, and total aliphatic suberin content is halved in the mutant (Shiono *et al*., 2014a). Intriguingly, neither enhanced lignification of the subtending sclerenchyma proximal to the cortex nor elevated HCA deposition was sufficient to prevent the penetration of the apoplastic tracers periodic acid and berberine hemisulfate into the cortex

(Shiono *et al*., 2014a). Although diffusional permeability of O_2 was not measured directly, these data suggest a specific role for aliphatic suberin in the formation of diffusion barriers in roots. The recent characterization of the rice VLCFA ω-hydroxylase CYP86B3 supports this conclusion. Roots of *Oscyp86b3* are entirely deficient in ω-OH VLCFA derivatives, and establishment of a tight barrier to radial O_2 loss is significantly delayed relative to WT in roots cultivated in well-aerated medium (Waßmann, 2014). An uncharacterized compensatory mechanism reverses this effect under hypoxia, and is there is no genotype effect on biomass accumulation after an 18d stagnant medium treatment (Waßmann, 2014). The ω-OH VLCFA defect and normal biomass accumulation of *Oscyp86b3* under waterlogging stress are highly reminiscent of the *Zmasft1*; *Zmasft2* double mutant. Biomass differences after a period of waterlogging stress correlate with differences in radial O_2 loss between *Hordeum* and *Zea* species with and without strong constitutive exodermal gas exchange barriers (Malik *et al*., 2011; Abiko *et al*., 2012). Taken together, these data suggest that the significant attenuation of ω-OH VLCFA in these mutants is not sufficient to abolish barrier function, and that stronger mutants are necessary to functionally dissect suberization. In particular, the *rcn1*/*Osagcg5* mutant suggests that interfering with export of aliphatic suberin to the apoplast may be a viable approach, though it remains to be determined whether the pleiotropic morphological phenotypes of this mutant are caused directly by its suberization defect (Shiono et al., 2014a).

CONCLUSION

Although the suberin biosynthesis pathway is broadly conserved between model dicots and maize, the selection of suitable candidate genes to disrupt barrier function is limited by the availability of *Dissociation* transposons in sufficiently tight linkage to generate targeted

insertional mutants at high frequency. Two functionally redundant paralogues of Arabidopsis *ALIPHATIC SUBERIN FERULOYL TRANSFERASE*, *ZmAsft1* and *ZmAsft2*, were mutated using *Ds* elements and found to be essential for normal accumulation of omega-hydroxy very long chain fatty acids in bundle sheath suberin. Double mutants exhibited a cohesion defect between bundle sheath suberin lamellae and cell wall polysaccharides indicative of cryptic changes to cell wall architecture. However, the defect was found to be insufficiently strong to characterize the role of bundle sheath suberization in the C_4 carbon concentrating mechanism. A recently published functional dissection of a rice exodermal suberin mutant suggests that a more severe disruption to the aliphatic suberin polymer is necessary to compromise the gas exchange barrier.

Future work will focus on the targeted mutagenesis of candidate genes involved in suberin polymerization. In Chapter 2, a small clade of GDSL lipase/acylhydrolases were identified and proposed to function as suberin synthases. *ZmGDSL1* lacks tightly linked donor *Ds* elements and is not a suitable candidate for mutagenesis. Thus, *Setaria viridis*, a developing model system for NADP-ME-type C_4 Panicoid grasses, will be presented in Chapter 4 as an appropriate model system for bundle sheath suberization in maize. Ongoing efforts to disrupt *SvGDSL1* expression using monocot-optimized RNAi vectors will be discussed.

MATERIALS AND METHODS

Phylogenetic analysis of candidate *Asft* genes

Phylogenetic analysis of the ASFT sub-clade was carried out as described in Chapter 2. Briefly, the *Arabidopsis thaliana* ALIPHATIC SUBERIN FERULOYL TRANSFERASE amino acid sequence was queried against the maize (*Zea mays*; B73 RefGen_v3), sorghum (*Sorghum bicolor* v3.1), switchgrass (*Panicum virgatum* AP13 v1.0), foxtail millet (*Setaria italica* v2.2),

green millet (*Setaria viridis* A10.1 v1.1), rice (*Oryza sativa* Nipponbare/*japonica* v7.0), and Brachypodium (*Brachypodium distachyon* Bd21 v3.1) reference proteomes using BLAST-P searches under the default parameters at Phytozome 11 (http://www.phytozome.net; Goodstein *et al*., 2012). Previously characterized amino acid sequences from model dicots (AtASFT, AtDCF, AtFACT, PtHHT, and StFHT) were retrieved from Phytozome 11, and all amino acid sequences were aligned within the MEGA environment using MUSCLE under the default parameters. A Neighbor-Joining tree was generated from the alignments using a Jones-Taylor-Thornton model assuming uniform substitution rates, and pairwise deletion of gaps. Branch support was estimated with 1000 bootstrap replications. The ASFT sub-clade formed a monophyletic group within Clade V of the BAHD acyltransferases (Tuominen *et al*., 2011).

Plant Growth Conditions

Unless otherwise indicated, seedlings were germinated in flats (5 columns by 10 rows, 10 cm soil depth) filled with 3:1 (v/v) Metromix 360 (Hummert 10-0356-1):Turface (Hummert 10-2400). At 12-14 days after sowing, seedlings were transplanted into Classic 1000 pots (25.7 cm x 23.2 cm x 20.6 cm) filled with ProMix-BRK 20 potting mix (Hummert 10-2018-1) supplemented with 10 mL fertilizer mix (Osmocote [15-9-12], Tomato Maker, Sprint, $FeSO_4$; 1:1: 0.083: 0.06). Beginning 10 days after sowing, plants were watered weekly with a 200 ppm solution of 15-5-15 fertilizer (Calcium-Magnesium LX; Hummert 07-5902-1).

Seedlings were cultivated in a Conviron BDW growth room with a daily irradiance regime of 550 μmol photons/m^2/s, a photoperiod of 12h L:D, day/night temperatures of 31°C/22°C, and 50% relative humidity. From transplantation to maturity, plants were cultivated in a greenhouse (300 μmol/m^2/s irradiance, 12h/12h photoperiod, day/night temperature and

relative humidity 28 °C/24 °C and 30%/50%) at the Donald Danforth Plant Science Center in Saint Louis, MO.

Reverse genetic screen using *Ds* transposons

Testcross populations were generated as described in Studer *et al.* (2014). *Ds* donor lines carrying an immobilized *Activator* transposon (*Ac-im*) were crossed as the male parent to T43, a W22 derivative carrying a *Ds* insertion in the *R* locus that serves as a colorimetric marker of transposase activity (Conrad and Brutnell, 2005). *Ac-im* positive progeny were identified by a mottled pattern of anthocyanin accumulation in the aleurone layer of kernels, and a total of 450 spotted and solid purple kernels were planted per screen. When the first leaf was fully expanded (7-8 days after sowing), a 1/8 inch tissue punch was collected near the leaf margin at the midpoint of the first leaf. The tissue of 15 individual plants was pooled, for a total of 30 pools per screen, and gDNA was extracted using the cetyl-trimethyl-ammonium bromide protocol (available at http://www.brutnelllab.org/#!molecular-tools/cs6e). Pools were screened by polymerase chain reaction using a target gene-specific primer paired with a *Ds*-specific primer (Table 3.4). Two PCR reactions were conducted per gene-specific primer to account for *Ds* insertions in both forward and reverse orientations relative to the gene of interest. All screens were conducted using Platinum Taq HF (Invitrogen) to facilitate long-distance screening of insertions distal to the target gene coding sequence. Pools containing putative germinal insertions were de-convoluted by re-sampling the 15 individual seedlings. To differentiate germinal *Ds* insertions from large somatic sectors, tissue was sampled near the leaf margin at the midpoint of the second fully expanded leaf, as these tissues do not share a clonal lineage with the margin of leaf 1 (Esau, 1965). Germinal *Ds* insertions were confirmed by amplifying the flanking sequence

using the same primers that were used in the initial screen and Sanger sequencing of the purified PCR product. Individuals containing germinal insertions were backcrossed to T43, and single mutants were cross-pollinated to generate double mutants, which were validated by PCR genotyping (Table 3.4).

Transcript expression analysis by qRT-PCR

For each biological replicate, fifty seeds of approximately uniform size and mass were sown in flats as described above. To promote uniform growth, seedlings were cultivated in a Conviron BDW growth room as described above. Ten days after sowing, third leaves of 16 ± 1 cm average length were marked at the point of emergence from the second leaf ligule and harvested two hours after the beginning of the photoperiod as described previously (Li *et al*., 2010; Wang *et al*., 2014). Leaves were divided into 1 cm increments and immediately frozen in liquid nitrogen. Eight plants were pooled per biological replicate, and three to four replicates were collected per genotype.

For root samples, 20 seeds per biological replicate were sown in individual Deepot D40L containers (Steuwe and Sons) filled with 1:1 (v/v) Sand (Hummert 10-2210-1):Profile (Hummert 10-2390-1) to facilitate vertical root growth. Seedlings were cultivated for ten days under standard greenhouse conditions. Roots were removed from the sand mixture under a gentle steam of water, and the seedling primary root was excised at the kernel. Roots of 20 cm ± 5 cm total length were divided into 4 cm increments from the root tip and immediately pooled and frozen as described above. In addition, leaf 3 was sampled as described above to confirm that greenhouse and growth chamber-grown plants were at comparable developmental stages.

Frozen samples were macerated in a tissue homogenizer, and total RNA was extracted

using TriPure Isolation Reagent (Roche; 11 667 165 001) according to the manufacturer's instructions. Total RNA was suspended in RNASecure Resuspension Solution (Ambion; AM7010) and RNA integrity was verified via agarose gel electrophoresis before proceeding. 10 µg total RNA (quantified by NanoDrop) was treated with a TURBO DNA-free Kit (Roche; AM1907), and a 1 µg aliquot was used for cDNA synthesis via the anchored Oligo$(dT)_{18}$ method using a Transcriptor First Strand cDNA Synthesis Kit according to the manufacturer's instructions for a 1h reverse transcription reaction at 50°C (Roche; 04 897 030 001). Two duplicate cDNA preparations and a negative control without reverse transcriptase were prepared for each biological replicate.

For all qPCR reactions, each cDNA preparation was analyzed in technical triplicate in a 10 µL reaction of LightCycler 480 SYBR Green I Master Mix (Roche; 04 887 352 001) with all primer concentrations at 0.4 µM and 4 µL of [1:160] diluted cDNA aliquoted per reaction. All primers utilized are described in Table 3.3 and Table3.4. The reference gene primers were previously validated for stable expression in developing leaves (Wang *et al*., 2014). The *ZmAsft* primers were targeted to unique regions of the 3'UTR and evaluated for transcript specificity by BLAST searches against the maize reference genome (B73 RefGen_v2, accessed via http://www.maizegdb.org). All qPCR reactions were carried out on a LightCycler 480 Multiwell Plate 384 (Roche) using the following thermocycler protocol: 1 pre-incubation cycle at 95°C for 5 min (ramp rate 4.8°C /s); 45 amplification cycles, each with denaturing at 95°C for 10 s (ramp rate 4.8°C/s), annealing at 50°C for 10s (ramp rate 2.5°C/s), and extension at 72°C for 10s (ramp rate 4.8°C/s); and a melt curve starting at 95°C for 5 s (ramp rate 4.8°C/s), cooling to 65°C for 1 min (ramp rate 2.5°C/s), and continuous signal acquisition at 97°C (10 acquisitions/s). Threshold cycle values were obtained from the LightCycler software using the Absolute Quantification/2nd

Table 3.3. Primers used in this study.

Name	Target Locus	Target GRMZM	Function	Sequence (5'→3')
FT1 qF1	*Asft1* 3'UTR	GRMZM2G034360	qPCR Primer	GGGTGCTTATACATTCTTCAA
FT1 qR1	*Asft1* 3'UTR	GRMZM2G034360	qPCR Primer	ACATAGATCGAGTATTAACACGG
FT2 qF1	*Asft2* 3'UTR	AC155610.2_FG007	qPCR Primer	GCCTGCTTTGGTTTATGTACGA
FT2 qR1	*Asft2* 3'UTR	AC155610.2_FG007	qPCR Primer	TATGCGTGTACCATCTCAGAAC
FT3 qF1	*Asft3* 3'UTR	GRMZM2G168499	qPCR Primer	ATCGAGGCCGCAATCCCGTCT
FT3 qR1	*Asft3* 3'UTR	GRMZM2G168499	qPCR Primer	ATGGAAGGCAATCCGGCACCCAA
TUB qF1	*Tub1* Exon 14	GRMZM2G157598	qPCR Primer	TTGTGGCCTCTGATAAGCTG
TUB qR1	*Tub1* Exon 15	GRMZM2G157598	qPCR Primer	TCCAGTGCCAATCCAAGAAT
18S qF1	*18S1* Exon 2	GRMZM2G114613	qPCR Primer	CAATGGAGATGGCTCGACTT
18S qR1	*18S1* Exon 2	GRMZM2G114613	qPCR Primer	GTTGCACTGCGAGCATACAT
UBQ qF1	*Ubq2* Exon2	GRMZM2G419891	qPCR Primer	GCAAGACCATAACCCTGGAG
UBQ qR1	*Ubq2* Exon2	GRMZM2G419891	qPCR Primer	ATCTTCGCCTTCACGTTGTC
JSR01	*Ds* 5' end	N/A	*Ds* Screen	GTTCGAAATCGATCGGGATA
JSR05	*Ds* 3' end	N/A	*Ds* Screen	CGTCCCGCAAGTTAAATATGA
FT1 F1	*Asft1* 5'UTR	GRMZM2G034360	*Ds* Screen	TCAAGTCACAACAAACACCAC
FT1 R1	*Asft1* Exon 3	GRMZM2G034360	*Ds* Screen	GTGCGCCAGGAACAGGATGACTTC
FT2 F1	*Asft2* Exon 1	AC155610.2_FG007	*Ds* Screen	AAATCACAAACCCCGCTACCT
FT2 F2	*Asft2* Promoter	AC155610.2_FG007	*Ds* Screen	ATCAGCCTCTCCTACCTTGTC
FT2 F3	*Asft2* Intron 1	AC155610.2_FG007	*Ds* Screen	GCTTATAGTTGCTAGCCATGC
FT2 R1	*Asft2* Exon 3	AC155610.2_FG007	*Ds* Screen	CGTTGATGCTCTTCCTCTCTTTGCCGTGTG
FT2 R2	*Asft2* 5'UTR	AC155610.2_FG007	*Ds* Screen	GGTTGACGACGTGGGTCTGAG
TBp34	*Ac-im* 3' end	N/A	Genotyping	ACCTCGGGTTCGAAATCGATCGG
Ac-im Fl.3	*Ac-im* flanking	N/A	Genotyping	TCTCACACATATGATGACTCATGG
JGp3	*Ds* 3' end	N/A	Genotyping	ACCCGACCGGATCGTATCGG
I.S07.2991	*Ds* Donor	N/A	Genotyping	GGCATCGCGGTCAAAAGAGG
B.W06.0682	*Ds* Donor	N/A	Genotyping	CTCCAAGGAAGAGTATGACGA
I.S07.1288	*Ds* Donor	N/A	Genotyping	TCGCCTATAGGACGGTTTACTCT
FT1 F2	*Asft1* Promoter	GRMZM2G034360	Genotyping	TGAAGAAGCTTCCAGGGGCTCCACT
FT1 F3	*Asft1* Intron 2	GRMZM2G034360	Genotyping	TGGCAGGTGACGAGGTTCAAGTGTG
FT1 R2	*Asft1* Promoter	GRMZM2G034360	Genotyping	GTGCCTTGGTGTTGTACTTCTTG
FT1 R3	*Asft1* Intron 2	GRMZM2G034360	Genotyping	AGCTCCCAGCTGAGAATTCGTCAATCCA
FT2 F3	*Asft2* Exon 2	AC155610.2_FG007	Genotyping	CGTAAGCCCGGAGATGAA
FT2 F4	*Asft2* Exon 2	AC155610.2_FG007	Genotyping	GACAAGGTTCAAGTGTGG
FT2 R3	*Asft2* Exon 2	AC155610.2_FG007	Genotyping	GAGGCATCTCGAGGATGT

Table 3.4. Quality control metrics for qPCR primers.

Primer Pair	Amplicon [bp]	Location	Splice Variants[a]	Min. Efficiency[b]	Min. r^2	LOD
FT1 qF1/R1	65	3'UTR	N/A	1.926	0.975	[1:10240]
FT2 qF1/R1	118	3'UTR	N/A	2.002	0.9930	[1:10240]
TUB qF1/R1	70	Exon14/15	N/A	1.937	0.980	[1:640]
UBQ qF1/R1	61	Exon 2	4/5	1.946	0.989	[1:40960]
18S qF1/R1	67	Exon 2	4/5	1.932	0.981	[1:640]

a. "N/A" indicates that the gene model has no reported splice variants at the time of publication (B73 RefGen_v3; http://www.maizegdb.org). UBQ qF1/R1 and 18S qF1/R1 amplify 4 of 5 possible alternative transcripts, including the primary transcript at their locus (GRMZM2G419891_T05 and GRMZM2G114613_T02, respectively).
b. Min. Efficiency, y=mx+b, and Min. r^2 report the lowest efficiency and r^2 value and its regression equation observed for a given primer set across all dilution curve experiments.
c. Reports the minimum relative cDNA concentration yielding reliable quantification values ($C_p \geq 35$) for each amplicon over a twofold dilution curve from [1:5] to [1:81,920].

derivative maximum method. Normalized relative quantities were calculated using the $E^{\Delta CT}$ method as described in Hellemans *et al*. (2007). Statistical significance was determined by a one-way ANOVA followed by a Tukey-Kramer post-hoc test for values giving significant F-statistics ($p < 0.05$).

Prior to each transcript quantification experiment, equal aliquots of all wild type cDNA samples were pooled and a twofold dilution series spanning 6 logs was created using the reaction conditions described above. This pooled sample was used as the calibrator in all subsequent qPCR experiments. An identical negative control curve was constructed using pooled cDNA synthesized as described above with reverse transcriptase omitted from the reaction. No amplification was observed from these samples. Dilution curve results are summarized in Table 3.3.

Harvesting leaf tissue for cell wall compositional analyses

For the whole leaf monomer profiling experiments (Figure 3.5-3.6), fully expanded third leaf laminae of *asft1; asft2* single and double mutants and isogenic WT siblings were measured 28 days after sowing and excised at the auricle. Approximately 500 mg fresh weight of tissue were collected from the central portion of the lamina by discarding the apical and basal 4-6 cm. Leaves were immediately flash frozen in liquid nitrogen and stored at -80°C. For the purified bundle sheath samples (Figure 3.8), the same harvesting procedure was conducted with fully expanded third leaves of *asft1-m1; asft2-m4* double mutants and WT 14 days after sowing, and leaf macerates were prepared as described below.

For all experiments conducted on 10-day-old plants (Figure 3.7; Figure 3.9), third leaves of individual plants were measured from the soil line to the leaf tip. Equally sized leaf laminae

were harvested by excising the entire shoot at the soil line and gently removing the first, second, and fourth leaves by hand. Developing regions of the third leaf proximal to the point of emergence were discarded, and 8 maize leaves were pooled per biological replicate to yield a total fresh weight per sample of 300-450 mg. Pooled leaves were cut into 3 mm square pieces and immediately immersed in 15 mL cold (4°C) grinding buffer 1 (330 mM sorbitol, 300 mM NaCl, 100 mM $MgCl_2$, 10 mM EGTA, 10 mM DTT, and 0.5 mM DETC in 200 mM Tris buffer, pH 9.0). Leaf suspensions were macerated for 30 s using a polytron liquid homogenizer (speed 6), filtered through 60 μm mesh to remove mesophyll protoplasts and cell wall fragments, and re-suspended in 15 mL grinding buffer 2 (350 mM sorbitol, 50 mM EDTA, and 0.1% [v/v] β-mercaptoethanol in 50 mM Tris buffer, pH 8.0). Leaf suspensions were homogenized for 1 minute, filtered, and re-suspended a total of 3 times. Pellets were immediately wrapped in aluminum foil, flash frozen in liquid nitrogen, and stored at -80°C.

For purified bundle sheath strand preparations (Figure 3.8), pellets were prepared as described above and filtered through a stainless steel no. 35 mesh (500 μm) sieve with several washes of MILLI-Q grade water. The eluent, containing isolated bundle sheath strands, was captured by decanting onto a 60 μm mesh. The residual pellet, containing a mixture of cuticle strips and residual bundle sheath strands that did not pass through the sieve, was collected on a separate 60 μm mesh, and both tissues were collected and frozen as described above.

Leaf Polyester Analysis

Alcohol insoluble cell wall residues were isolated and chemically derivatized according to the protocol of Beisson and colleagues (Li-Beisson *et al.*, 2013). Frozen samples were boiled for 10 minutes in pre-weighed, Teflon-capped 40 mL glass tubes containing 20 mL isopropanol

with 0.1% (w/v) *bis*-hydroxytoluene. The tubes were cooled and macerated three times for 1 minute each using a Polytron liquid homogenizer at speed setting 6. Samples were washed on a rocking agitator for at least 2 hours, centrifuged at 1500g for 10 minutes to pellet insoluble material, and the supernatant was discarded. The washing step was repeated once more with isopropanol, and then twice each with chloroform:methanol (2:1, v/v), chloroform:methanol (1:2, v/v) and methanol. Samples were air-dried and stored in a desiccator containing Drierite for five days until a stable dry weight was achieved.

Fresh standard solutions of omega-pentadecalactone (10 μg/μL) and methyl heptadecanoate (10 μg/μL) in methanol were prepared. 5 μL of each standard was injected into each sample immediately prior to transmethylation. The transmethylation solution contained 4 mL per reaction of 6.25% (v/v) sodium methoxide and 15% (v/v) methyl acetate in methanol. Transmethylation reactions were heated for 2 hours at 60°C, cooled, and then acidified with 1 mL glacial acetic acid, solubilized with 8mL dichloromethane, and washed with 2 mL 0.9% (w/v) NaCl in Tris, pH 8.0. Samples were vortexed for 30s to wash and extract fatty acid methyl esters and centrifuged for 2 minutes at 1500g for phase separation. The organic phase was transferred to a fresh 40 mL glass vial and washed a second time with 4 mL 0.9% (w/v) NaCl in deionized water. The organic phase was transferred to a fresh 8 mL glass vial and dried over anhydrous $NaSO_4$, and then dried in 2.5 mL conical reaction vials on a 33°C heat block under a gentle stream of N_2. Dried samples were re-suspended in 10 μL each of pyridine and N,O-Bis(trimethylsilyl) trifluoroacetamide (BSTFA) and heated to 100°C for 10 minutes. Samples were dried as described above, re-suspended in 50 μL chloroform, and transferred to autosampler vials.

Monomers were quantified by GC-FID. Samples (2 μL) were injected onto a TRACE TR-5MS GC column (30 m length x 250 μm ID x 0.25 μm film thickness) using a 1:10 split injection ratio at 320°C. The oven was programmed to hold at 140°C for 2 minutes, ramp to 320°C at 5°C/minute, and hold for 10 minutes. Helium carrier gas was supplied at a flow rate of 1.5 mL/min. Monomers were normalized by area ratios using methyl heptadecanoate as an internal standard for fatty acid methyl esters, and omega-pentadecalactone for silylated species as described in (Jenkin and Molina, 2015). Monomer identities were determined by GC-MS. Samples were injected onto an identical TR-5MS GC columns using an automated splitless injection with an inlet temperature of 320°C. The oven temperature was held at 120°C for 1 minute, then ramped to 320°C at 5°C/minute, followed by a 15 minute hold. Helium carrier gas was supplied at a 1 mL/minute flow rate. Fragmentation spectra were obtained using an Agilent quadrupole detector operating in electron impact mode with an accelerating voltage of 2500, scanning from 35-750 at a rate of 0.3 s/scan with a 0.1 s interscan delay and a 5 minute solvent delay at the beginning of each run.

Cell wall HCA fractionation

Extractive free alcohol insoluble cell wall residues were prepared as described above. To remove soluble starch, samples were incubated overnight in 90% DMSO on a rocking agitator following the final methanol wash step (Carpita, 1983). Samples were transferred to 15 mL falcon tubes, pelleted at 2500g for 10 minutes, and washed twice with MilliQ-grade water. Samples were re-suspended in water, flash frozen in liquid nitrogen, and lyophilized for 48 hours.

For HCA fractionation, the method of Saulnier *et al*. (1995) was utilized. For the pilot

time course experiment, 20 mg portions of lyophilized material were transferred to 4 mL conical reaction vials with Teflon caps. 3 mL aliquots of 50 mM TFA or water (negative control) were added immediately prior to incubation on a heat block at 100°C. After the designated incubation period (0.5, 1, 2, 4, or 6 hours), residual solid material was pelleted for 5 minutes at 3000g, and the supernatant was divided equally between two 1-dram glass reaction vials with Teflon caps. Both aliquots were mixed with 0.5 mL *tert*-butanol and dried overnight under a gentle stream of air. The first aliquot was solubilized with 50% (v/v) methanol containing 100μM 3,4,5 trimethoxy-*trans*-cinnamic acid (3,4,5-TCA) as an internal standard and analyzed immediately by reverse-phase HPLC as described below. The second aliquot was saponified with 1 mL of 1M NaOH containing 100 μM 3,4,5-TCA for 30 minutes in a 42 °C water bath, acidified with 1 mL of 3M HCl, and extracted three times with ethyl acetate. The combined ethyl acetate extracts were evaporated to dryness under N_2 and re-solubilized in 50% methanol for HPLC analysis. For the replicate experiment, fractionation was carried out as described above with 100μM 3,4,5-TCA added prior to TFA hydrolysis.

HPLC was carried out on a Dionex Ultimate 3000 HPLC system (Thermo Scientific-Dionex) with UV detection (320 nm) using an SPD-M20A photodiode array detector (Shimadzu). Samples were partitioned on a reverse-phase C18 (Shimadzu Shim-pack XR-ODS, 3 mm i.d. x 0.75 mm length 2.2 μm bead diameter) column maintained at 40°C. Solvents A (0.1% v/v formic acid) and B (100% acetonitrile) were supplied at a flow rate of 0.7 mL/min according to the following program: 0 to 0:30, 5% B isocratic; 0:30 to 0:40 5% to 10% B linear; 0:40 to 11:00, 10% to 25% B linear; 11:00 to 11:20, 25% B to 95% B linear; 11:20 to 12:20, 95% B isocratic; 12:20 to 13:10, 95% to 5% B linear; 13:10 to 14:00, 5% B isocratic.

Linkage-methylation analysis

Linkage-methylation analyses were carried out as described in Mertz *et al*. (2012). Duplicate samples from two biological replicates were prepared for mechanically fractionated and whole leaf samples of WT and *asft1-m1*; *asft2-m4* double mutants. Approximately 10 mg of extractive-free, lyophilized residue per sample was carboxyl-reduced with $NaBD_4$ in the presence of a water-soluble diimide as described in Kim and Carpita (1992) and Carpita and McCann (1996). The reaction was terminated with glacial acetic acid and samples were dialyzed against running water for 48 hours, frozen, and lyophilized. Pellets were partitioned into three 1-2 mg samples; the first sample was prepared for monosaccharide compositional analysis using the alditol acetates protocol as described in Gibeaut and Carpita (1991). A linkage-methylation analysis was conducted from the second and third sample as technical duplicates according to Gibeaut and Carpita (1991).

Electron microscopy

Marginal leaf sections were harvested from the midpoint of fully expanded fourth and fifth leaf laminae of 28d old mutant and WT plants. For roots, seedling primary roots of 10 day old soil grown seedlings were gently exhumed from the soil, and 1 cm sections were collected 0.5 cm behind the root tip, in the region of first lateral root emergence (8-12 cm from tip), and 2 cm from the root base. Samples were collected in biological triplicate.

For samples post-fixed in osmium tetroxide, two sample fixation protocols were employed, with comparable results. Unless otherwise noted, tissues were hand sectioned into 1 mm fragments in 2 mL of freshly prepared 100mM PIPES buffer (pH 6.8) containing 2% (v/v) glutaraldehyde solution. A drop of Aerosol OT was applied as a surfactant, and samples were

vacuum infiltrated in 15-30s intervals until tissues sank to the bottom of the vial. Samples were incubated for 2 hours at room temperature, and then rinsed 3 times for 5 minutes each with fresh 100 mM PIPES. Samples were post-fixed for 1.5 hours in 100 mM PIPES containing 2% (w/v) osmium tetroxide and rinsed 3 times for 5 minutes each with water. Samples were sequentially dehydrated in an ethanol/acetone series (5%, 10%, 20%, 30%, 50%, 75%, 95%, and 100% ethanol, followed by 100% acetone) for 15 minutes each, and then incubated in a fresh aliquot of acetone for 45 minutes prior to infiltration with Spurr's resin. Infiltration was carried out in 12 hour intervals with 5% and 10% (v/v) Spurr's resin diluted in acetone, and then in 24 hour intervals with 25%, 50%, 75%, and 100% Spurr's resin. Samples were transferred to fresh aliquots of 100% Spurr's resin in labeled embedding molds and polymerized for 48 hours at 60°C. Ultrathin sections were prepared with a diamond knife and stained with uranyl acetate prior to imaging. Leaf samples presented in Figure 3.11B (*asft1-m1* and *asft2-m4*) and Figure 3.12C (all genotypes) were prepared by high-pressure freeze substitution. Leaf discs were collected from marginal samples using a Harris Uni-Core 1.20. Individual discs were transferred into 100 μm sample planchettes filled with packing buffer (0.15 M sucrose in 50 mM PIPES, pH 6.8) and capped with a second planchette coated with hexadecane. Samples were flash frozen in a grid plunge freezer, uncapped, and stored in a dueur at -80°C. Samples were freeze-substituted for 3-5 days at -80°C in a dry acetone solvent containing 2% (w/v) osmium tetroxide and 0.1% (w/v) uranyl acetate, and then slowly warmed to room temperature. Thawed samples were gently removed from the planchette well and embedded in a Spurr's resin series as described above.

Chromium trioxide preparations were carried out as described in Berg (1994). Leaf tissues were hand sectioned into 1 mm fragments in water, and then transferred into a 10% (v/v) chromium trioxide solution for simultaneous fixation and staining for 1 hour at room

temperature. The samples were washed with repeated aliquots of water until the rinse solution became clear, and then dehydrated and embedded as described above.

Cuticular Permeability Assays

The Toluidine Blue O permeability assay was carried out as originally described in Tanaka *et al*. (2004) with an extended incubation time for monocot leaves as described in Wu *et al*. (2011). Seedlings of 10-day old soil grown wild type, *asft1-m1*, *asft2-m4*, and *asft1-m1*; *asft2-m4* mutants were excised at the base, and whole third leaf laminae were carefully separated the whorl. Immediately prior to separation, the point of emergence and the midpoint of the exposed third leaf lamina were gently marked with a waterproof marker. Leaves were immersed in a 0.05% (w/v) solution of Toluidine Blue O dissolved in distilled water for 10 minutes, and then removed, immersed in distilled water to remove residual stain, and blotted dry. Negative controls were prepared as described above, with a 10-minute incubation in distilled water instead of Toluidine Blue O solution. Leaves were imaged and photographed using a Nikon Dissecting Microscope with bright-field illumination. The experiment was repeated twice with identical results.

The chlorophyll leaching assay was carried out according to Lolle *et al*. (1997). Whole third leaf laminae from seedlings of 10-day old soil grown wild type, and *asft* mutants were isolated as described above. Ten individual leaves per genotype were weighed and placed into 50 mL conical tubes containing 30 mL of 80% (v/v) ethanol. Tubes were covered with aluminum foil to protect extracted chlorophyll from degradation and placed on a rocking agitator at room temperature for 3 days. At the indicated time-points, a 100 µL aliquot of chlorophyll was taken and absorbance values (A_{664} and A_{647}) were measured using a spectrophotometer. Absorbance

values were converted to μmoles of chlorophyll by the following equation: μmol Chl = $7.93(A_{644}) + 19.53(A_{647})$ (Lolle *et al*., 1997). Chlorophyll content was normalized per unit fresh weight.

Waterlogging Stress Experiment

The waterlogging stress experiment was modeled after Abiko *et al*. (2012). Fifty kernels per genotype of *asft1-m1*; *asft2-m4* double mutants and isogenic wild types were sown in flats of soil and transplanted into 2.5 gallon pots at 2 weeks after sowing as described above. Seedlings were cultivated under ambient greenhouse conditions for 2 weeks following transplantation (28 days after sowing), and then divided into control and treatment groups (n = 10 plants per genotype per treatment; 20 total plants per genotype). Plant height, length and width of the youngest fully expanded leaf, and total number of leaves per plant were recorded and compared to confirm that there were no pre-existing treatment effects between groups (two-way ANOVA [treatment x genotype] with a Bonferroni-Holm multiple testing correction; all $p > 0.05$ and no interaction between factors). Plants assigned to the waterlogging treatment group were submerged in a hydroponic box (8’ L x 4’ W x 1.5’ H) containing stagnant water maintained at a depth of 2 cm above the soil line. WT and double mutant plants were arranged in an alternating pattern around the periphery of the box to minimize shading and positional effects. Control plants were arranged in randomized blocks adjacent to the submergence box. After two weeks, plant height, total leaves, and dimensions of the youngest fully expanded leaf common to both treatment groups were recorded. Shoot and root tissue for each plant were harvested and dried at 60˚C until a stable dry weight was achieved, and dry weights were measured and recorded. Genotype and treatment effects were evaluated as described above with a Tukey’s HSD post-hoc test conducted at a 95% significance level following a significant ANOVA result.

Physiological experiments

All CO_2 assimilation, online ^{13}C isotope discrimination, pressure-volume curve, and leaf transpiration experiments were carried out by Mr. Lwanga Nsubuga, Dr. Susanne von Caemmerer, and Dr. Patricia Ellsworth, respectively, in the laboratory of Dr. Asaph Cousins at Washington State University. For the CO_2 assimilation and online ^{13}C isotope discrimination experiments (Figure 3.15), twenty kernels each of *asft1-m1*; *asft2-m4* double mutants and isogenic wild type were cultivated in soil in a Conviron BDW growth chamber under the default parameters described above. At four weeks post-sowing, four biological replicates per genotype were selected, and CO_2 response ($A\text{-}C_i$) curves were generated for the uppermost fully expanded leaf using an LI6400XT (LI-COR Biosciences) with a LI6400-22 leaf chamber and a LI6400-18 light source as described in Studer *et al*. (2014). Online isotope discrimination experiments were performed on the same plants using an LI6400XT coupled to a tunable diode laser absorption spectroscope (TDL-AS, TGA 100A; Campbell Scientific) as described by Ubierna *et al*. (2013).

For the pressure-volume curve experiments (Figure 3.17), plants were cultivated as described above, with the following modifications. Plants were cultivated in a Conviron BDW growth chamber with a photoperiod 16h programmed with a 1 hour ramp for light reaching 1000 μmol quanta m^{-2} s^{-1} at canopy level and 1 hour ramp for temperature to mimic sun up and sun set. Day and night temperatures were 28°C and 20°C, respectively, and relative humidity was maintained at 70%. All plants were grown simultaneously in the same growth chamber with the height of the pots adjusted to maintain the desired light treatments at canopy level from germination until the conclusion of the experiment. Plants in the high light (HL) group were

irradiated with 1000 μmol quanta m^{-2} s^{-1} at canopy level, and the low light (LL) group was irradiated with 300 μmol quanta m^{-2} s^{-1} at canopy level. On the morning of the experiment, two to three leaves fully expanded leaves (one leaf per treatment per experimental batch; five biological replicates in total for each genotype) were collected simultaneously before the onset of the photoperiod and immediately sealed in individual plastic bags. Samples were equilibrated for 2 hours at 4˚C prior to measurements. Pressure-volume curves were generated using a pressure bomb apparatus as described in Tyree and Hammel (1972). The bulk elastic modulus was inferred from the pressure-volume curve by plotting the pressure potential versus the relative water content and calculating the slope of the regression line.

For the leaf transpiration experiment, plants were cultivated as described above for the pressure-volume experiment, but with two relative humidity levels (50% and 80%) maintained in separate chambers. Gas exchange measurements and online oxygen isotope discrimination were measured on the youngest fully expanded leaf using an LI6400XT with the appropriate modifications as described above.

REFERENCES

Abiko T, Kotula L, Shiono K, Malik AI, Colmer TD, & Nakazono M. (2012) Enhanced formation of aerenchyma and induction of a barrier to radial oxygen loss in adventitious roots of *Zea nicaraguensis* contribute to its waterlogging tolerance as compared with maize (*Zea mays* ssp. *mays*). *Plant, Cell, and Environment* **35**: 1618-1630.

Ahern KR, Deewatthanawong P,Schares J, Muszynski M, Weeks R, Vollbrecht E, Duvik J, Brendel VP, & Brutnell TP. (2009) Regional mutagenesis using *Dissociation* in maize. *Methods* **49**: 248-254.

Arrieta-Baez D & Stark RE. (2006) Using trifluoroacetic acid to augment studies of potato suberin molecular structure. Journal of Agricultural and Food Chemistry 54: 9636-9641.

Bartley LE, Peck ML, Kim S-R, *et al*. (2013) Overexpression of a BAHD acyltransferase, *OsAt10*, alters rice cell wall hydroxycinnamic acid content and saccharification. *Plant Physiology* **161**: 1615-1633.

Berg RH. (1994) Symbiotic vesicle ultrastructure in high pressure-frozen, freeze-substituted actinorhizae. *Protoplasma* **183**: 37-48.

Bernards MA, Lopez ML, Zajicek J, & Lewis NG. (1995) Hydroxycinnamic acid-derived polymers constitute the polyaromatic domain of suberin. *Journal of Biological Chemistry* **270**(13): 7382-7386.

Bernards, MA. (2002) Demystifying suberin. *Canadian Journal of Botany* **80**: 227-240.

Beisson F, Li Y, Bonaventure G, Pollard M, &. **Ohlrogge JB**. (2007) The acyltransferase GPAT5 is required for the synthesis of suberin in seed coat and root of Arabidopsis. *The Plant Cell* **19**: 351-368.

Boher P, Serra O, Soler M, Molinas M, & Figueras M. (2013) The potato suberin feruloyl transferase FHT which accumulates in the phellogen is induced by wounding and regulated by abscisic and salicyclic acids. *Journal of Experimental Botany* **64**(11): 3225-3236.

Botha CEJ & Evert RF. (1986) Free space marker studies on the leaves of *Saccharum officinarum* and *Bromus unioloides*. *South African Journal Of Botany* **52**: 335-342.

Canny MJ. (1986) Water pathways in wheat leaves. III. The passage of the mestome sheath and the function of the suberised lamellae. *Physiologia plantarum* 66: 637-647.

Carpita NC. (1983) Hemicellulosic polymers of cell walls of *Zea* coleoptiles. *Plant Physiology* **72**: 515-521.

Carpita NC & Gibeaut DM. (1993) Structural models of primary cell walls in flowering plants: consistency of molecular structure with the physical properties of the walls during growth. *The Plant Journal* **3**(1): 1-30.

Carpita NC & McCann MC. (1996) Some new methods to study plant polyuronic acids and their esters. In R. Townsend & A. Hotchkiss (Eds.) *Progress in Glycobiology* New York Marcell Dekker. pp 595-611.

Compagnon V, Diehl P, Benveniste I, Meyer D, Schaller H, Schreiber L, Franke R, & Pinot F. (2009) *CYP86B1* is required for very long chain ω-hydroxyacid and α,ω-dicarboxylic acid synthesis in root and seed suberin polyester. *Plant Physiology* **150**: 1831-1843.

Conrad LJ & Brutnell TP. (2005) *Ac-immobilized*, a stable source of Activator transposase that mediates sporophytic and gametophytic excision of *Ds* elements in maize. *Genetics* **171**(4): 1999-2012.

Cottle W & Kolattukudy PE. (1982) Biosynthesis, deposition, and partial characterization of potato suberin phenolics. *Plant Physiology* 69: 393-399.

Daniels DGH & Martin HF. (1968) Antioxidants in oats: glyceryl esters of caffeic and ferulic acids. *Journal of the Science of Food and Agriculture* **19**: 710-712.

D'Auria JC. (2006). Acyltransferases in plants: a good time to be BAHD. *Current Opinion in Plant Biology* **9**: 331-340.

Eastman PAK, Dengler NG, Peterson CA. (1988a) Suberized Bundle Sheaths in Grasses (Poaceae) of Different Photosynthetic Types .1. Anatomy, Ultrastructure and Histochemistry. *Protoplasma* **142**: 92-111.

Eastman PAK, Peterson CA, Dengler NG. (1988b) Suberized bundle sheaths in grasses (Poaceae) of different photosynthetic types. 2. Apoplastic permeability. *Protoplasma* **142**: 112-126.

Enstone DE, Peterson CA. (2005) Suberin lamella development in maize seedling roots grown in aerated and stagnant conditions. *Plant Cell and Environment* **28**: 444-455.

Esau K. 1965. *Plant Anatomy*: New York, Wiley.

Espelie KE & Kolattukudy PE. (1979) Composition of the aliphatic components of 'suberin' from the bundle sheaths of *Zea mays* leaves. *Plant Science Letters* **15**: 225-230.

Evert RF, Botha CEJ, Mierzwa RJ. (1985) Free-space marker studies on the leaf of *Zea-mays*-L. *Protoplasma* 126, 62-73.

Evert RF, Russin WA, & Bosabalidis AM. (1996). Anatomical and ultrastructural changes associated with the sink-to-source transition in developing maize leaves. *International Journal of Plant Sciences* **157(3)**: 247-251.

Fan L, Shi W-J, Hu W-R, Hao X-Y, Wang D-M, Yuan H, & Yan H-Y. (2009) Molecular and biochemical evidence for phenylpropanoid synthesis and presence of wall-linked phenolics in cotton fibers. *Journal of Integrative Plant Biology* **51**(7): 626-637.

Farquhar GD, von Caemmerer S, & Berry JA. (1980) A biochemical model of photosynthetic CO_2 assimilation in leaves of C_3 species. *Planta* **149**(1): 78-90.

Farquhar, GD, Ehleringer, JR, and Hubick, KT. (1989) Carbon isotope discrimination and photosynthesis. *Annual Review of Plant Physiology and Plant Molecular Biology* **40**: 503-537.

Felsenstein J. (1985) Confidence limits on phylogenies: An approach using the bootstrap. *Evolution* **39**:783-791.

Furbank RT. (2011) Evolution of the C_4 photosynthetic mechanism: are there really three C4 acid decarboxylation types? *Journal of Experimental Botany* **62**(9): 3103–3108.

Gibeaut, DM & Carpita, NC. (1991) Tracing cell-wall biogenesis in intact cells and plants. Selective turnover and alteration of soluble and cell-wall polysaccharides in grasses. *Plant Physiology* **97**: 551–561.

Goodstein DM, Shu S, Howson R, *et al*. (2012) Phytozome: a comparative platform for green plant genomics. Nucleic Acids Research 40 (D1): D1178-D1186.

Gou JY, Yu XH, Liu CJ. (2009). A hydroxycinnamoyltransferase responsible for synthesizing suberin aromatics in Arabidopsis. *Proceedings of the National Academy of Sciences of the United States of America* **106**: 18855-18860.

Graça J & Santos S. (2007) Suberin: a biopolyester of plants' skin. *Macromolecular Bioscience* **7**: 128-135.

Graça J & Lamosa P. (2011) Linear and branched poly(ω-hydroxyacid) esters in plant cutins. *Journal of Agricultural and Food Chemistry* **58**: 9666–9674.

Grabber JH, Hatfield RD, & J. (1998) Diferulate cross-links impede the enzymatic degradation of non-lignified maize walls. *Journal of the Science of Food and Agriculture* **77**:193-200.

Grabber JH, Ralph J, & Hatfield RD. (2000) Cross-linking of maize walls by ferulate dimerization and incorporation into lignin. *Journal of Agricultural and Food Chemistry* **48**: 6106-6113.

Harris PJ & Hartley RD. (1976) Detection of bound ferulic acid in cell walls of the Graminae by ultraviolet fluorescence microscopy. *Nature* **259**: 508-510.

Hatfield RD, Marita JM, & Frost K. (2008a) Characterization of *p*-coumarate accumulation, *p*-coumaroyl transferase, and cell wall changes during the development of corn stems. *Journal of the Science of Food and Agriculture* **88**: 2529-2537.

Hatfield RD, Ralph J, & Grabber JH. (2008b) A potential role for sinapyl *p*-coumarate as a radical transfer mechanism in grass lignin formation. *Planta* **228** (6): 919-928.

Hatfield RD, Marita JM, Frost K, Grabber J, Ralph J, Lu F, Kim H. (2009) Grass lignin acylation: p-coumaroyl transferase activity and cell wall characteristics of C_3 and C_4 grasses. *Planta* **229**: 1253-1267.

Hattersley PW, Browning AJ. (1981) Occurrence of the suberized lamella in leaves of grasses of different photosynthetic types.1. In parenchymatous bundle sheaths and PCR (Kranz) sheaths. *Protoplasma* **109**: 371-401.

Hellemans J, Mortier G, De Paepe A, Speleman F, & Vandesompele J. (2007) qBase relative quantification framework and software for management and automated analysis of real-time quantitative PCR data. *Genome Biology* **8**(2): R19.

Henderson SA, von Caemmerer S, & Farquhar GD. (1992) Short-term measurements of carbon isotope discrimination in several C4 species. *Australian Journal of Plant Physiology* **19**: 263-285.

Hofer R, Briesen I, Beck M, Pinot F, Schreiber L, & Franke R. (2008). The *Arabidopsis* cytochrome P450 CYP86A1 encodes a fatty acid ω-hydroxylase involved in suberin monomer synthesis. *Journal of Experimental Botany* **59**: 2347-2360.

Jenkin S & Molina I. (2015) Isolation and analysis of plant cuticle lipid polyester monomers. *Journal of Visualized Experiments* **105**: e53386 **doi: 10.3791/53386**

Jones AMP, Shukla M, Chattopadhyay A, Zoń J, & Saxena P. (2013) Investigating the role of phenylpropanoids in the growth and development of Zea mays L. *In Vitro Cellular and Developmental Biology* – **Plant** 49: 765-772.

Jung HG & Phillips RL. (2010) Putative Seedling ferulate ester (*sfe*) maize mutant: morphology, biomass yield, and stover cell wall composition and rumen degradability. *Crop Science* **50**: 403-418.

Kato Y & Nevins DJ. (1985) Isolation and identification of O-(5-O-feruloyl-α-L-arabinosyl)-(1→3)-O-β-D-xylopyranosyl-(1→4)-D-xylopyranose as a component of *Zea* shoot cell walls. *Carbohydrate Research* **137**: 139-150.

Kim J-B & Carpita NC. (1992) Changes in esterification of the uronic acid groups of cell wall polysaccharides during elongation of maize coleoptiles. *Plant Physiology* **98**: 646-653.

Kolattukudy PE. (1980) Biopolyester membranes of plants: cutin and suberin. *Science* **208**(4447): 990-1000.

Koide RT, Robichaux RH, Morse SR & Smith CM. (2000) Plant water status, hydraulic resistance and capacitance. In: *Plant Physiological Ecology: Field Methods and Instrumentation* Pearcy RW, Ehleringer JR, Mooney HA, & Rundel PW, eds. Kluwer, Dordrecht, the Netherlands. pp. 161-183.

Kosma DK, Molina I, Ohlrogge JB, & Pollard M. (2012) Identification of an Arabidopsis Fatty Alcohol: Caffeoyl-Coenzyme A Acyltransferase required for the synthesis of alkyl hydroxycinnamates in root waxes. *Plant Physiology* **160**: 237-248.

Kromdijik J, Ubierna N, Cousins AB, & Griffiths H. (2014) Bundle-sheath leakiness in C4 photosynthesis: a careful balancing act between CO2 concentration and assimilation. *Journal of Experimental Botany* **65**(13): 3443-3457.

Laetsch WM. (1971) Chloroplast structural relationships in leaves of C_4 plants. In: Hatch MD, Osmond CB, Slayter CO, eds. *Photosynthesis and photorespiration*. New York: Wiley Interscience, 323-349.

Langdale J. (2011) C4 cycles: past, present, and future research on C4 photosynthesis. *The Plant Cell* **23**: 3879-3892.

Lapierre C, Pollet B, & Négrel J. (1996) The phenolic domain of potato suberin: structural comparison with lignins. *Phytochemistry* **42**(4): 949-953.

Li P, Ponnala L, Gandotra N, *et al*. (2010) The developmental dynamics of the maize leaf transcriptome. *Nature Genetics* **42**: 1060-1067.

Li-Beisson Y, Shorrosh B, Beisson F, *et al*. (2013) Acyl-Lipid Metabolism. *The Arabidopsis Book* 11:e0161. doi:10.1199/tab.0161

Lolle SJ, Berlyn GP, Engstrom EM, Krolikowski KA, Reiter W-D, & Pruitt RE. (1997) Developmental regulation of cell interactions in the *Arabidopsis fiddlehead-1* mutant: a role for the epidermal cell wall and cuticle. *Developmental Biology* **189**: 311-321.

Lu F & Ralph J. (1999) Detection and determination of *p*-coumaroylated units in lignins. *Journal of Agricultural and Food Chemistry* **47**: 1988–1992.

Malik AI, Islam AKMR, & Colmer TD (2011) Transfer of the barrier to radial oxygen loss in roots of *Hordeum marinum* to wheat (*Triticum aestivum*): evaluation of four *H. marinum*–wheat amphiploids. *New Phytologist* **190**: 499–508.

Marita JM, Vermerris W, Ralph J, & Hatfield RD. (2003) Variations in the cell wall composition of maize *brown midrib* mutants. *Journal of Agricultural and Food Chemistry* **51**(5): 1313–1321.

Méchin V, Laluc A, Legée F, Cézard L, Denoue D, Barrière Y, & Lapierre C. (2014) Impact of the *Brown-Midrib bm5* mutation on maize lignins. *Journal of Agricultural and Food Chemistry* **62**: 5102−5107.

Mertz RA, Olek AT, & Carpita NC. (2012) Alterations of cell-wall glycosyl linkage structure of Arabidopsis *murus* mutants. *Carbohydrate Polymers* **89**: 331-339.

Mitchell PL & Sheehy JE. (2006) Supercharging rice photosynthesis to increase yield. *New Phytologist* **171**(4): 688-693.

Mitchell RAC, Dupree P, & Shewry PR. (2007) A novel bioinformatics approach identifies candidate genes for the synthesis and feruloylation of arabinoxylan. *Plant Physiology* **144**: 43-53.

Molina I, Li-Beisson Y, Beisson F, Ohlrogge JB, Pollard, M. (2009). Identification of an Arabidopsis Feruloyl-Coenzyme A transferase required for suberin synthesis. *Plant Physiology* **151**: 1317-1328.

Molina I & Kosma DK. (2015) Role of HXXXD-motif/BAHD acyltransferases in the biosynthesis of extracellular lipids. *Plant Cell Reports* **34**: 587-601.

Mueller-Harvey I & Hartley RD. (1986) Linkage of *p*-coumaroyl and feruloyl groups to cell-wall polysaccharides of barley straw. *Carbohydrate Research* **148**: 71-85.

Nelson T. (2011) Development of leaves in C_4 plants: anatomical features that support C_4 metabolism. In: Raghavendra AS & Sage RF (Eds.). *C_4 Photosynthesis and Related CO_2 Concentrating Mechanisms*. Springer Science+Business Media B.V. pp. 147–159

Petrik DL, Karlen SD, Cass CL *et al*. (2014) *p*-Coumaroyl-CoA:monolignol transferase (PMT) acts specifically in the lignin biosynthetic pathway in *Brachypodium distachyon*. *The Plant Journal* **77**: 713–726

Pollard M, Beisson F, Li Y, Ohlrogge JB. (2008) Building lipid barriers: biosynthesis of cutin and suberin. *Trends in Plant Science* **13**: 236-246.

Pozuelo JM, Espelie KE, Kolattukudy PE. (1984) Magnesium-deficiency results in increased suberization in endodermis and hypodermis of corn roots. *Plant Physiology* **74**: 256-260.

Ray DK, Mueller ND, West PC, & Foley JA. (2013) Yield trends are insufficient to double global crop production by 2050. PLoS One 8(6): e66428. doi:10.1371/journal.pone.0066428.

Ralph J, Hatfield RD, Quideau S, Helm RF, Grabber JH, & Jung H-JG. (1994) Pathway of *p*-coumaric acid incorporation into maize lignin as revealed by NMR. *Journal of the American Chemical Society* **116**: 9448-9456.

Ralph J, Quideau S, Grabber JH, & Hatfield RD. (1995) Identification and synthesis of new ferulic acid dehydromers present in grass cell walls. *Journal of the Chemical Society, Perkin Transactions 1***23**: 3485-3498.

Ranathunge K & Schreiber L. (2011) Water and solute permeabilities of Arabidopsis roots in relation to the amount and composition of aliphatic suberin. *Journal of Experimental Botany* **62**(6): 1961–1974.

Rautengarten C, Ebert B, Ouellet M, Nafisi M, Baidoo EEK, Benke P, Stranne M, Mukhopadhyay A, Keasling JD, Sakuragi Y, & Scheller HK. (2012) Arabidopsis Deficient in Cutin Ferulate encodes a transferase required for feruloylation of ω-hydroxy fatty acids in cutin polyester. *Plant Physiology* **158**: 654-665.

Reeves TG, Thomas G, Ramsay G. (2015) *Save and grow in practice: maize, rice wheat. A guide to sustainable cereal production*. Rome, Food and Agriculture Organization of the United Nations.

Ryser U, Meier H, & Holloway PJ. (1983) Identification and localization of suberin in the cell walls of green cotton fibres (*Gossipym hirsutum* L., var. green lint). *Protoplasma* **117**: 196-205.

Sage, RF. (2004) The evolution of C_4 photosynthesis. *New Phytologist* **161**: 341–370.

Saitou N & Nei M. (1987) The neighbor-joining method: A new method for reconstructing phylogenetic trees. *Molecular Biology and Evolution* **4**:406-425.

Saulnier L, Vigouroux J, & Thibault J-F. (1995) Isolation and partial characterization of feruloylated oligosaccharides from maize bran. *Carbohydrate Research* **272**: 241-253.

Schnable PS, Ware D, Fultron RS, *et al*. (2009) The B73 maize genome: complexity, diversity, and dynamics. *Science* **326**: 1112-1115.

Schmutz A, Jenny T, Amrhein N, & Ryser U. (1993) Caffeic acid and glycerol are components of the suberin layers in green cotton fibers. *Planta* **189**: 453-460.

Schreiber L, Franke R, Hartmann KD, Ranathunge K, Steudle E. (2005a) The chemical composition of suberin in apoplastic barriers affects radial hydraulic conductivity differently in the roots of rice (*Oryza sativa* L. cv. IR64) and corn (*Zea mays* L. cv. Helix). *Journal of Experimental Botany* **56**: 1427-1436.

Schreiber L, Franke R, & Hartmann K. (2005) Wax and suberin development of native and wound periderm of potato (*Solanum tuberosum* L.) and its relation to peridermal transpiration**.** *Planta* **220**: 520–530.

Schreiber L. (2010) Transport barriers made of cutin, suberin and associated waxes. *Trends in Plant Science* **15**(10): 546-553.

Sekhon RS, Lin HN, Childs KL, Hansey CN, Buell CR, de Leon N, Kaeppler SM. (2011) Genome-wide atlas of transcription during maize development. *The Plant Journal* **66**: 553-563.

Serra O, Soler M, Hohn C, Sauveplane V, Pinot F, Franke R, Schreiber L, Prat S, Molinas M, & Figueras M. (2009a) *CYP86A33*-targeted gene silencing in potato tuber alters suberin composition, distorts suberin lamellae, and impairs the periderm's water barrier function. *Plant Physiology* **149**: 1050-1060.

Serra O, Soler M, Hohn C, Franke F, Schreiber L, Prat S, Molinas M, & Figueras M. (2009b) Silencing of *StKCS6* in potato periderm leads to reduced chain lengths of suberin and wax compounds and increased peridermal transpiration. *Journal of Experimental Botany*, **60**(2): 697–707.

Serra O, Hohn C, Franke R, Prat S, Molinas M, & Figueras M. (2010) A feruloyl transferase involved in the biosynthesis of suberin and suberin-associated wax is required for maturation and sealing properties of potato periderm. *The Plant Journal* **62**: 277-290.

Serra O, Chatterjee S, Figueras M, Molinas M, & Stark RE. (2014) Deconstructing a plant macromolecular assembly: chemical architecture, molecular flexibility, and mechanical performance of natural and engineered potato suberins. *Biomacromolecules* **15**: 799−811.

Shiono K, Ando M, Nishiuchi S, *et al*. (2014a) RCN1/OsABCG5, an ATP-binding cassete (ABC) transporter, is required for hypodermal suberization of roots in rice. *The Plant Journal* **80**: 40-51.

Stelpflug SC, Sekhon RS, Vaillancourt B, Hirsch CN, Buell CR, de Leon N, & Kaeppler SM. (2015) An expanded maize gene expression atlas based on RNA-sequencing and its use to explore root development. *The Plant Genome* doi:10.3835/plantgenome2015.04.0025.

Studer AJS, Gandin A, Kolbe AR, Wang L, Cousins AB and Brutnell TP. (2014) A limited role for carbonic anhydrase in C_4 photosynthesis as revealed by a *ca1ca2* double mutant in maize. Plant Physiology **165**: 608-617.

Tanaka T, Tanaka H, Machida C, Watanabe M, & Machida Y. (2004) A new method for rapid visualization of defects in leaf cuticle reveals five intrinsic patterns of surface defects in *Arabidopsis*. *The Plant Journal* **37**: 139-146.

Taylor SH, Hulme SP, Rees M, Ripley BS, Woodward FI, Osborne CP. (2010) Ecophysiological traits in C-3 and C-4 grasses: a phylogenetically controlled screening experiment. *New Phytologist* **185**: 780-791.

Tillman D, Balzer T, Hill J, & Befort BL. (2011) Global food demand and the sustainable intensification of agriculture. *Proceedings of the National Academy of Sciences, USA* **108**(50): 20260-20264.

Timpa JD & Triplett BA. (1993) Analysis of cell-wall polymers during cotton fiber development. *Planta* **189**: 101-108.

Tuominen LK, Johnson VE, &Tsai C-J. (2011) Differential phylogenetic expansions in BAHD acyltransferases across five angiosperm taxa and evidence of divergent expression among Populus paralogues. *BMC Genomics* **12**: 36.

Tyree MT & Hammel HT. (1972) The measurement of turgor pressure and the water relations of plants by the pressure-bomb technique. *Journal of Experimental Botany* **23**(74): 267-282.

Ubierna N, Sun W, Kramer DM, & Cousins AB. (2013) The efficiency of C_4 photosynthesis under low light conditions in *Zea mays*, *Miscanthus x giganteus* and *Flaveria bidentis*. *Plant, Cell, and Environment* **36**: 365–381.

Vishwanath SJ, Kosma DK, Pulsifer IP, *et al*. (2013) Suberin-associated fatty alcohols in Arabidopsis: distributions in roots and contributions to seed coat barrier properties. *Plant Physiology* **163**: 1118-1132.

Vollbrecht E, Duvik J, Schares JP, *et al*. (2010) Genome-wide distribution of transposed *Dissociation* elements in maize. *The Plant Cell* **22**: 1667-1685.

von Caemmerer S, Quick WP, & Furbank RT. (2012) The development of C_4 rice: current progress and future challenges. *Science* **336**: 1671-1672.

von Caemmerer S, Ghannoum O, Pengelly JJL, & Cousins AB. (2014) Carbon isotope discrimination as a tool to explore C_4 photosynthesis. *Journal of Experimental Botany* **65**(13): 3459-3470.

Wang L, Czedik-Eysenberg A, Mertz RA, *et al*. (2014) Comparative analysis of C4 and C3 photosynthesis in developing leaves of maize and rice. *Nature Biotechnology* **32(11)**: 1158-1165.

Waßmann FFM. (2014) Suberin biosynthesis in *O. sativa*: Characterisation of a cytochrome P450 monooxygenase. PhD Dissertation, University of Bonn.

Wu R, Li S, He S, Waßmann R, Yu C, Qin G, Schreiber L, Qu L-J, & Gu G. (2011) CFL1, a WW domain protein, regulates cuticle development by modulating the function of

HDG1, a Class IV Homeodomain Transcription Factor, in Rice and *Arabidopsis*. *The Plant Cell* **23**: 3392-3411.

Yadav V, Molina I, Ranathunge K, Castillo IQ, Rothstein SJ, & Reed JW. (2014) ABCG transporters are required for suberin and pollen wall extracellular barriers in *Arabidopsis*. *The Plant Cell* **26**: 3569-3588.

Yasuno N, Takamure, I, Kidou S, Tokuji Y, Ureshi A, Funabiki A, Ashikaga K, Yamanouchi U, Yano M and Kato K. (2009) Rice shoot branching requires an ATP-binding cassette subfamily G protein. *New Phytologist* **182**: 91–101.

Yatsu LY, Espelie KE, & Kolattukudy PE. (1983) Ultrastructural and chemical evidence that the cell wall of green cotton fiber is suberized. *Plant Physiology* **73**: 521-524.

Yeats TH & Rose JKC. (2013) The formation and function of plant cuticles. *Plant Physiology* **163**: 5-20.

Zeier J, Schreiber L. (1998) Comparative investigation of primary and tertiary endodermal cell walls isolated from the roots of five monocotyledoneous species: chemical composition in relation to fine structure. *Planta* **206**: 349-361.

Zeier J, Ruel K, Ryser U, & Schreiber L. (1999) Chemical analysis and immunolocalisation of lignin and suberin in endodermal and hypodermal/rhizodermal cell walls of developing maize (*Zea mays* L.) primary roots. *Planta* **209**, 1-12.

Zimmermann HM, Hartmann K, Schreiber L, Steudle E. (2000) Chemical composition of apoplastic transport barriers in relation to radial hydraulic conductivity of corn roots (*Zea mays* L.). *Planta* **210**: 302-311.

Zuckerkandl E & Pauling L. (1965) Evolutionary divergence and convergence in proteins. Edited in *Evolving Genes and Proteins* by V. Bryson and H.J. Vogel, pp. 97-166. Academic Press, New York.

CHAPTER FOUR

DEVELOPMENT OF *SETARIA VIRIDIS* AS A MODEL SYSTEM FOR MOLECULAR GENETIC DISSECTION OF SUBERIN SYNTHESIS

ABSTRACT

The rate-limiting step in the characterization of *ZmAsft1* and *ZmAsft2* in the preceding chapter was the slow, labor-intensive process of disrupting two paralogously duplicated genes by targeted mutagenesis with *Dissociation* elements. Thus, a rapid-cycling model C_4 plant with robust reverse genetic resources would relieve a major bottleneck in the molecular genetic dissection of bundle sheath suberization. The Panicoid grass green millet (*Setaria viridis*) was evaluated as a potential model system for maize bundle sheath suberization. The spatiotemporal pattern of sheath suberization was comparable between maize and *Setaria viridis*, as were the polyester monomers released from developing leaves by transesterification. *Setaria* orthologues of maize suberin biosynthesis candidates were identified and a method to isolate RNA Interference lines containing single copy transgene insertions was developed using the candidate suberin synthase *SvGDSL1* as a pilot. *Setaria viridis* was determined to be a promising model for functional characterization of bundle sheath suberization in Panicoid grasses.

INTRODUCTION

As discussed in the preceding chapters, vascular sheath suberization has multiple putative barrier functions, and a thorough functional dissection of these structures in maize may be necessary to successfully engineer NADP-ME-type C_4 photosynthesis into C_3 cereal crops.

Although the initial characterization of the C_4 bundle sheath suberin biosynthesis pathway was carried out in maize, it has several disadvantages as a model system for rapid genetic dissection of complex traits. The plants are large and long-lived, which constrains the number of plants that can be reared under controlled experimental conditions and limits the maximum number of generations per year to approximately four cycles. Maize is an ancestral autotetraploid with a large, 1.6 GB genome that retains numerous paralogous gene duplications, which complicate efforts to generate strong mutant phenotypes via targeted reverse genetic mutagenesis of single genes (Schnable *et al.*, 2009; Studer *et al*., 2009; Ahern et al., unpublished observations).

Transgenic plants expressing RNAi constructs targeted to conserved sequences of redundant paralogues could ameliorate this issue. This approach has been utilized to generate double mutants of tandemly arrayed suberin biosynthetic genes in Arabidopsis (Vishwanath *et al*., 2013), and to evaluate multiple candidate arabinoxylan feruloyl transferase genes simultaneously in rice (Piston *et al*., 2010). Although robust *Agrobacterium tumefaciens*-mediated transformation protocols have been developed for maize, eight to twelve months are required to acquire T_0 seed from a transformation event (Frame *et al*., 2002). Furthermore, neither the B73 inbred, the source of the reference genome (Schnable *et al*., 2009), nor the recently sequenced inbred W22, the genetic background of *Ac/Ds* mutant collection (Ahern *et al*., 2009, Vollbrecht *et al*., 2010) is used for transformation. Thus, multiple generations of backcrossing are required to introduce a novel transgene into the desired inbred background, prolonging the required time between construct design and mutant analysis. Therefore, a compact, rapid-cycling model grass is desirable to facilitate rapid dissection of bundle sheath suberization.

The first rapid-cycling grass species developed as a model system, *Brachypodium distachyon*, is a diploid Pooid species closely related to temperate cereal crops such as wheat (*Hordeum vulgare*; Draper *et al*., 2001). *Brachypodium distachyon* has a sequenced 272 MB genome, and considerable resources for gene characterization, including an indexed collection of T-DNA insertion mutants, a robust transformation protocol, and a large collection of accessions suitable for population genetics (Vogel and Hill, 2008; Filiz *et al*., 2009; Vogel *et al*., 2010; Bragg *et al*., 2013). However, like all members of the BEP (Bambusoideae, Erhartoideae, Pooideae) Clade, *Brachypodium* is a classical C_3 grass with a non-photosynthetic, suberized internal mestome sheath and an unsuberized, parenchymatous external bundle sheath containing few chloroplasts (Hattersley and Browning, 1981; Grass Phylogeny Working Group II, 2012). Thus, it is not a suitable model system with which to assess the role of bundle sheath suberization in C_4 gas exchange. A compact Panicoid grass utilizing NADP-ME-type C_4 photosynthesis would an ideal complementary model system for functional dissection of suberin synthesis.

Green millet (*Setaria viridis*) was recently proposed as a small model grass for functional dissection of C_4 traits (Brutnell *et al*., 2010). Like *Brachypodium distachyon*, *Setaria viridis* has a compact stature, a rapid-cycling growth habit, and a small, sequenced genome (510 MB), which was recently released to the public (*Setaria viridis* v1.1, DOE-JGI, http://phytozome.jgi.doe.gov/). Considerable progress has been made toward efficient *Agrobacterium*-mediated transformation of seed callus, and a refined transformation protocol was recently published (Van Eck and Smartwood, 2015). Unlike maize, the principal accession used for transformation, A10.1, is also the source of the reference genome.

The objective of this study was to evaluate *Setaria viridis* as a model system for rapid molecular genetic dissection of candidate suberin biosynthesis genes. The spatiotemporal pattern of bundle sheath suberization was confirmed to occur within a similar developmental window in both maize and *Setaria viridis*. This spatiotemporal pattern correlated with the expression of a small set of genes putatively involved in very long chain fatty acid modification orthologous to suberin biosynthesis candidates from maize and rice (Chapter 2). Broad similarities in gene expression between maize and *Setaria viridis* suggested that suberin monomer composition might also be similar. Thus, leaf polyester content was profiled for both species, and it was confirmed that total aliphatic material and the monomeric chain length distributions were comparable. To specifically disrupt suberin biosynthesis, RNAi constructs targeting unique regions of four candidate genes were introduced into *Setaria viridis* (A10.1) seed callus via *Agrobacterium tumefaciens*-mediated transformation. Although the majority of T_0 transformation events recovered were clonal and contained multiple transgene insertions, lines containing two unlinked copies were successfully segregated into single copy lines by a TaqMan-based copy number assay of segregating progeny. The utility of *Setaria viridis* as a model for Panicoid cell wall development and prospective future directions for targeted mutagenesis are discussed.

RESULTS

Bundle sheath suberization proceeds similarly in *Setaria viridis* and maize juvenile leaves.

As discussed in Chapter 2, a developing grass leaf matures basipetally and encompasses a complete sink-to-source gradient if sampled at the proper time point (Evert *et al*., 1996; Li *et al*., 2010). A subset of putative suberin biosynthesis candidates involved in very long chain fatty acid

(VLCFA) modification and their putative transcriptional regulators were co-expressed within a tightly delimited spatiotemporal region of leaf development in maize, rice, and *Setaria viridis* (Chapter 2, Figure 2.5). A series of electron micrographs spanning the *Setaria viridis* developmental gradient were evaluated to determine whether bundle sheath (BS) suberization proceeds similarly in both species (Figure 4.1). As observed for maize, the BS cell wall was in an undifferentiated primary state in the section immediately proximal to the leaf base (Figure 4.1A; 0-0.5 cm). Suberin lamellae (SL) were not apparent in the region of maximum candidate gene expression (0.5-1.0 cm; data not shown). No data was available for the section immediately distal to the region of maximum expression (1.0-1.5 cm), and by the section immediately distal to the point of emergence (2.0 -2.5 cm), SL were established along the BS/mesophyll interface (Figure 4.1B). SL were ubiquitous in the outer tangential walls of all BS cells distal to the point of emergence (Figure 4.1C). Thus, BS suberization occurs prior to the point of leaf emergence in both maize and *Setaria viridis*, but maximum expression of the VLCFA-modifying suberin candidates is associated with the first appearance of the SL in maize only.

***Setaria viridis* has a similar leaf polyester composition to maize.**

The similar vein anatomy and developmental trajectory of BS suberization in maize and *Setaria viridis* indicates that that the latter is potentially an effective model system for the former. However, ultrastructural similarities do not preclude significant differences in the underlying suberin composition. For example, although the maize and rice root endodermis have similar developmental trajectories and cell wall ultrastructure, the composition of the suberin polyester itself is markedly different both qualitatively and quantitatively (Haas and Carothers, 1975; Clark & Harris, 1981; Schreiber *et al.*, 2005). Thus, a pilot study was designed to compare the

Figure 4.1. Suberization of *Setaria viridis* bundle sheaths along leaf spatiotemporal gradient.

A. The cell wall is in an undifferentiated primary state proximal to the leaf base (0-0.5 cm).
B. Suberin lamellae are fully established immediately distal to the point of emergence (2.0-2.5 cm).
C. Suberin lamellae are ubiquitous in mature tissue distal to the point of emergence (3.5-4.0 cm). Scale bar, 500 nm. TEMs courtesy of Richard Medville (Electron Microscopy Services).

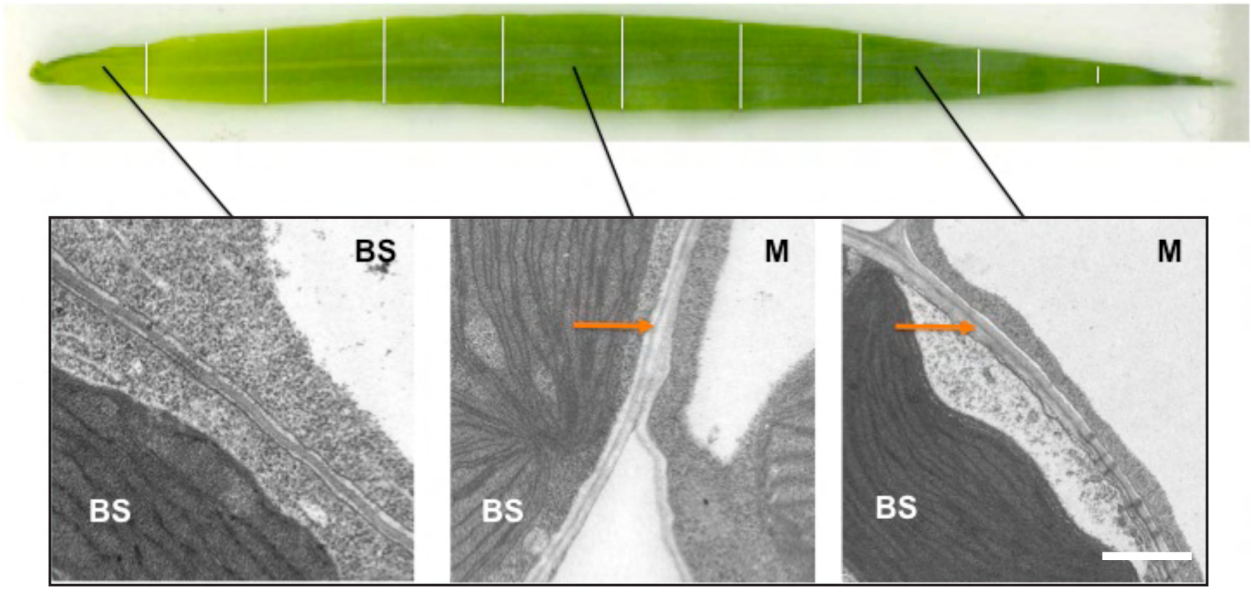
BS
BS
M
BS
M
BS

quantity and composition of leaf polyesters in ten-day-old third leaves of maize (B73) and *Setaria viridis* (A10.1). Entire third leaf laminae were harvested and exhaustively delipidated cell wall residues were prepared as described in Chapter 3. Leaf polyesters were depolymerized by base-catalyzed transmethylation, derivatized to produce trimethylsilyl ethers, and quantified by GC-FID. All monomer amounts were normalized on a nmoles per leaf surface area basis rather than by dry weight, as the latter can generate misleading results for interspecies comparisons of suberin quantity between disparately sized tissues (Schreiber *et al.*, 2005). The same classes of monomer species as described in Chapter 3 were recovered from whole leaf laminae for both maize and *Setaria viridis* (Chapter 3, Figure 3.5). The total nmoles of monomers recovered were significantly different between maize and *Setaria viridis* (Figure 4.2A; 12.79 nmol/cm^2 versus 6.98 nmol/cm^2; Student's t-test with Bonferroni-Holm multiple testing correction, $p < 0.03$). To identify the specific monomers underlying this disparity, chain length distributions of individual monomers from both species were quantified and grouped into aromatic or aliphatic components. *Setaria viridis* leaves were specifically deficient in ester-linked aromatic monomers, particularly *p*-coumaric acid, relative to maize (Figure 4.2B; $p < 0.03$). Although the total amount of the other major aromatic monomer, ferulic acid, was also lower in *Setaria viridis*, the ratio of ferulic to *p*-coumaric acid was significantly greater than observed for maize (Figure 4.2B; $p < 0.007$). Conversely, both the total quantity and the chain length distribution of aliphatic monomers were largely identical between maize and *Setaria viridis* (Figure 4.2C; 4.37 nmol/cm^2 versus 3.95 nmol/cm^2; $p = 0.50$). Both aliphatic distributions were dominated by the same three monomer species: octadec-9-enoic acid, 18-hydroxy octadec-9-enoic acid, and 9/10,16-dihydroxyhexadecanoic acid (Figure 4.2C). Omega-hydroxy fatty acids (ω-OH FA) were the

Figure 4.2. Leaf polyester analysis of maize and *Setaria viridis*.

A. Overview of ester-labile aliphatic and aromatic monomers from cell walls of 10-day-old maize (B73) and *Setaria viridis* (A10.1) leaves. Asterisks denote significant differences between species (Student's t-test with Bonferroni-Holm multiple testing correction, $p < 0.05$). HCA, hydroxycinnamic acid; PA, primary alcohol, DCA, α,ω-dicarboxylic acid; ωOH FA, omega-hydroxy fatty acid; polyOH FA, mid-chain oxidized omega-hydroxy fatty acid.
B. Hydroxycinnamic acid content of developing leaves.
C. Aliphatic monomer content of developing leaves. Monomer classes labeled as in Figure 4.2A.

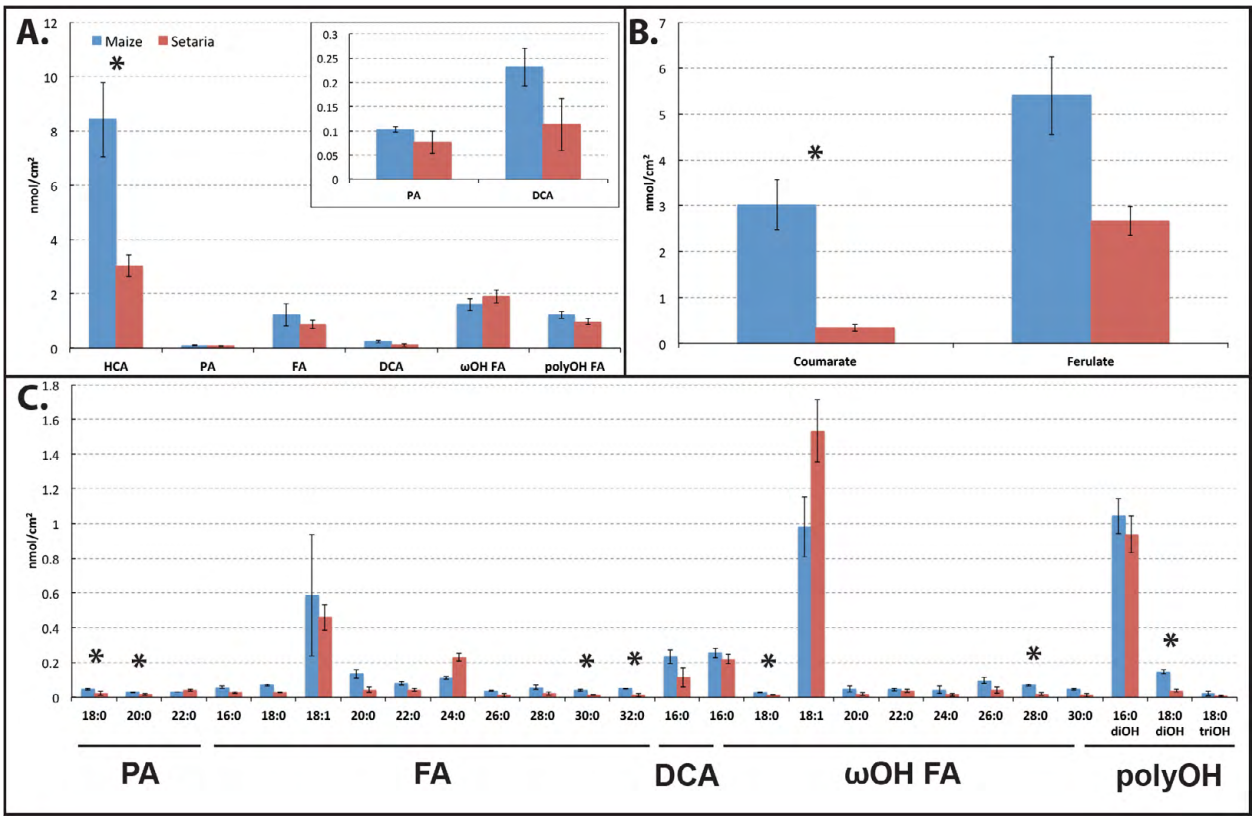
A.
Maize
Setaria
nmol/cm²
HCA
PA
FA
DCA
ωOH FA
polyOH FA
B.
Coumarate
Ferulate
C.
18:0
20:0
22:0
16:0
18:1
24:0
26:0
28:0
30:0
32:0
18:0
18:1
20:0
22:0
24:0
26:0
28:0
30:0
16:0 diOH
18:0 diOH
18:0 triOH
PA
FA
DCA
ωOH FA
polyOH

major aliphatic monomer class for both species (Figure 4.2A). Long chain omega-hydroxy fatty acids (ω-OH LCFA; $<C_{20}$) predominate over very long chain (ω-OH VLCFA; $\geq C_{20}$) species in both maize and *Setaria viridis* (Figure 4.2C). ω-OH VLCFA are specifically enriched in suberin relative to cutin across broad taxa, as are α,ω-dicarboxylic acids (α,ω-DCA) of all chain lengths (reviewed in Pollard *et al.*, 2008). Both maize and *Setaria viridis* contained a comparable quantity of hexadecane-1,16-dioic acid in addition to the ω-OH VLCFA acids discussed above (Figure 4.2C). Taken together, these results suggest that maize and *Setaria viridis* bundle sheaths contain a comparable quantity and chain length distribution of conventional aliphatic suberin. Thus, *Setaria viridis* is an appropriate complementary model to maize for bundle sheath suberization of NADP-ME C_4 Panicoid grasses.

Suberin biosynthesis candidates were targeted using RNA Interference

Taken together, the similarities in polyester composition and spatiotemporal expression patterns of candidate genes indicate that the suberin biosynthesis pathway is largely conserved between maize and *Setaria viridis*. Thus, the VLCFA-modifying genes identified as high priority mutagenesis candidates for maize should yield similar polyester defects when disrupted in *Setaria viridis*. Whereas the *ZmAsft* genes were the only practical mutagenesis targets in maize due to a lack of *Dissociation* elements in sufficiently tight linkage to the other candidates (Chapter 3), *Setaria viridis* orthologues of all four VLCFA-modifying genes could be targeted using *Agrobacterium*-mediated transformation of seed callus with RNA Interference (RNAi) constructs.

In order to disrupt suberin biosynthesis in *Setaria viridis*, amplicons from *SvCYP86B16*, *SvGPAT5*, *SvASFT*, and *SvGDSL1* were cloned from accession A10.1 and sub-cloned into the

Table 4.1. RNAi construct design for *Setaria viridis* suberin candidates.

Target Gene	*S. viridis* GeneID	*S. italica* GeneID	Fwd and Rev Primers [5'→3']	Amplicon Length [bp]
SvASFT (5')	Sevir.8G135900	Si026351m.g	F: CACCACCCCCATCCTCTCTTGTCT R: CAGTACACCGTCTGCACGAT	312
SvCYP86B16 (5')	Sevir.9G213400	Si034638m.g	F: ACCTCCTGACTGTGTTCACCAAGA R: AGGTAATCCATCCGCTTCACCTCA	277
SvCYP86B16 (3')			F: TTACAGTGTACCATGCACTTGGGC R: GCAGGGCTTGAAGTTGAACAACCA	271
SvGPAT5 (5')	ND	Si021782m.g	F: TGCCCAAGTTCATGGCCGA R: TTGCAGAATGGCAAGAAGGAGCG	316
SvGPAT5 (3')			F: GTTCCTGCTCCACTAACCACACTA R: TGATGAGGGAGCAACGCTGATCTT	253
SvGDSL1 (5')	Sevir.2G436600	Si030233m.g	F: CACCTCGGAGATCTTGATCCG GAGC R: CGCCCAACCCATGCTTGCTTC	199
SvGDSL1 (3')			F: CACCAGACAGCAAGTACATCTCGCC R: ACTGGCTCACAAATTACATAC	210

Table 4.2. Validation of *Setaria viridis* UTRs by RACE.

Gene Name	Predicted *S. italica* UTR length [bp][a]	Number of *S. viridis* isoforms (length [bp])	Total SNPs	Contains amplicon?[b]
SvASFT (5'UTR)	119	1 (126)	0	Yes
SvASFT (3'UTR)	277	1 (277)	0	N/A
SvCYP86B16 (5'UTR)	62	1 (71)	0	Yes
SvCYP86B16 (3'UTR)	738	0	ND	ND
SvGPAT5 (5'UTR)	ND	0	ND	ND
SvGPAT5 (3'UTR)	250	0	ND	ND
SvGDSL1 (5'UTR)	208	2 (342, 229)	1, 0	Yes
SvGDSL1 (3'UTR)	171	2 (202, 177)	2, 0	Yes

a. Based on gene models from *Setaria italica* v2.1 (http://www.phytozome.net)
b. If "Yes", contains entire amplicon sequence with no predicted SNPs in the primer sequences. N/A, an amplicon was not designed to this sequence. ND, not determined.

inverted repeat cassette of the rice-optimized RNAi vector pANDA using Gateway cloning (Miki and Shimamoto, 2004). The inverted repeat construct was driven by a constitutive maize *Ubiquitin* promoter, so unique regions of the putative 5'UTR and 3'UTR sequences were selected for each gene to minimize the risk of off-target silencing of related cutin biosynthesis candidates (Table 4.1). However, no transgenic seedlings were successfully regenerated from any of the pANDA::*Sv*Suberin RNAi constructs. The probable cause was the single 35S promoter driving the antibiotic selection cassette, which did not yield sufficiently strong hygromycin phosphotransferase expression in *Setaria viridis* to regenerate transgenic plantlets on selective media (J. van Eck, personal communication). All five amplicons described in Table 4.1 were regenerated from entry clones and sub-cloned into the Panicoid grass-optimized RNAi vector pANIC12A (Mann *et al*., 2012).

The *Setaria viridis* reference genome was not yet available at the time of construct design, and so the amplicons were designed using the gene models of the putative *Setaria italica* orthologues (Bennetzen *et al*., 2012). In order to confirm that the UTR sequences were conserved in *S. viridis*, RACE was carried out. No alternative splice isoforms affecting the predicted coding sequence were identified in *Setaria viridis* leaf cDNA, and no SNPs affecting the primer binding sites were identified. *SvASFT* was present as a single splice isoform with comparable UTR lengths to its *Setaria italica* orthologue (Table 4.2). *SvGDSL1* encoded two isoforms of each UTR, one of comparable length to the *Setaria italica* gene model, and a second, slightly longer isoform. No 3'UTR sequence could be amplified from *SvCYP86B16*, and no sequences matching either UTR could be amplified from *SvGPAT5*. A putative *Setaria viridis* homologue of *SiGPAT5* co-expressed with other suberin biosynthesis candidates was identified

by RNA-Sequencing (Chapter 2, Figure 2.5). However, a BLAST-P search against the *Setaria viridis* reference proteome (v1.1) using SiGPAT5 as a query did not yield an orthologous gene model with the diagnostic mutated phosphatase motifs described in Chapter 2. Canonical GPAT5 proteins appear to be conserved across all extant vascular plants (Yang *et al*., 2012), and it would be highly unusual if an SvGPAT5 orthologue did not exist. However, these data were obtained concurrently with the discovery that the *Zmasft1*; *Zmasft2* double mutant did not disrupt BS suberization sufficiently to evaluate its role in the C_4 carbon concentrating mechanism (Chapter 3, Figure 3.14). The putative suberin synthase *SvGDSL1* was hypothesized to be the candidate *Setaria viridis* gene most likely to severely disrupt BS suberization, and was prioritized for all subsequent experiments. No further efforts were made to characterize the transcripts of *SvASFT*, *SvCYP86B16*, or *SvGPAT5*.

Single copy *SvGDSL1*-RNAi lines were identified using a TaqMan-based protocol

Transgenic plants were received from the Boyce Thompson Institute Center for Biotechnology Research as T_1 seeds. The first batch of seeds received contained *SvGPAT5*-RNAi lines. An initial assessment of the segregation ratios was made by PCR genotyping of 10-15 T_1 seedlings per line. With few exceptions, all T_1 progeny of T_0 plants originating from the same seed callus had comparable segregation ratios, indicating a likely clonal origin. To recapitulate the T_0 genotype for Southern Blotting, T_1 progeny of each selfed T_0 parent were pooled. The pilot Southern Blotting results were consistent with the predictions made based on the segregation ratios. The majority of plants regenerated from common calli (Multiple Shoot Calli; Table 4.3) were clonal. Likewise, the majority of unique transformation events contained two or more transgene copies, and the few events that segregated 3:1 by PCR were single copy

lines (Table 4.3). Single copy lines were desirable to mitigate the risk of transgene silencing (Rajeevkumar *et al*., 2015), and so a protocol was developed to identify unlinked two copy lines with which to generate additional single copy lines by segregation.

A TaqMan-based protocol was developed to identify single copy homozygotes from *SvGDSL1*-RNAi lines segregating two unlinked transgene events. For the panic12A-*SvGDSL1* (5') RNAi construct presented in Table 4.3 (orange row), seven clonal T_0 lines were regenerated from the event that contained two independent transgenes. Twelve T_1 progeny were cultivated from each of these lines and genotyped to determine the segregation ratio. 6 out of 69 (8.6%) of these progeny were wild type. Thus, approximately 1/16 (6.25%) of all progeny were wild type, suggesting that the two transgenes were segregating independently. A similar experiment was conducted with T_1 progeny of the eight clonal T_0 lines originating from the single transgene event (Table 4.3). 28 of 98 (28.57%) of these progeny were wild type, consistent with a single transgene insertion segregating 3:1.

Copy numbers for all transgenic T_1 progeny from the single and double transgene lines described above were quantified using a TaqMan hydrolysis probe assay. For the two copy line, the T_1 individuals segregated in reasonable agreement with the expected 1:4:6:4:1 ratio for 0, 1, 2, 3, or 4 total transgene copies, respectively (Figure 4.3A). The 27 two copy individuals, which were comprised of fixed homozygous single copy lines (25% expected for each transgene) and double heterozygotes (50% expected), were evaluated by Southern Blotting. 3 and 5 clonal single copy lines, respectively, were identified for each independently segregating transgene.

The TaqMan procedure was repeated with the transgenic T_1 individuals from the single copy event, and the 0, 2, and 1 copy individuals were found to segregate in roughly a 1:2:1 ratio (Figure 4.3B). In total, 22 individuals were identified as clonal single copy homozygotes. Thus,

Table 4.3. Copy Number Verification of *Sv*Suberin-RNAi lines by Southern Blotting.

pANIC12A-Target	Total Calli	MSC (Unique/Clonal)[a]	Unique Events[b]	1 Copy	2 Copies	3+ Copies
SvASFT (5')	4	1 (1/0)	5 (-1)	2	1	1
SvGPAT5 (5')	3	3 (1/2)	4 (-2)	1	0	1
SvGPAT5 (3')	10	6 (1/5)	11	2	4	5
SvGDSL1 (5')	4	3 (0/3)	4 (-1)	1	1	1
SvGDSL1 (3')	1	1	1	0	0	1
Empty	3	2 (1/1)	3 (-2)	0	0	1

a. MSC, "Multiple Shoot Calli". Lists the number of calli out of the total in the preceding column that produced multiple regenerated T_0 plants. The values in parentheses indicate the number of MSC that produced unique T_0 events versus the number from which all T_0 plants were clonal. All Unique MSC evaluated in this study produced exactly two independent events.

b. "Unique Events" is the sum of all unique transgene events observed for a given construct (Equal to Total Calli, except in lines where an MSC gave two unique events, in which case Unique Events = Total Calli + 1). The negative values in parentheses denote escapes that survived hygromycin selection but could not be validated as transgenic by either Southern Blot or genotyping PCR.

multiple clonal individuals suitable for seed bulking were identified for each of three independent, single copy transgene insertion events.

DISCUSSION

Setaria viridis is a promising model for Panicoid grass suberin synthesis

Although relatively few species have been profiled to date, it is clear that vascular sheath suberin content varies qualitatively and quantitatively between grass taxa (Chapter 1). Thus, it was not a foregone conclusion that *Setaria viridis* would be an effective model for maize BS suberization despite the relatively recent evolutionary divergence of the Paniceae and Andropogoneae tribes (~27 million years ago; Vicentini *et al*., 2008; Christin *et al*., 2009; Zhang *et al*., 2012). This is especially true if independent origins of NADP-ME-type C_4 photosynthesis involve differential recruitment of suberin biosynthesis genes or regulatory elements to the BS cell wall program, although this remains to be tested.

Leaf polyesters released a similar suite of monomer constituents upon transesterification in both species (Figure 4.2). The largest interspecies disparity was in HCA content, particularly *p*-coumaric acid, which was nearly ten times more abundant in maize than in *Setaria viridis* (Figure 4.2A-B). Maize and sorghum are known to contain substantially higher levels of ester-labile *p*-coumaric acid relative to other Panicoid grasses, including switchgrass, the closest relative of *Setaria* surveyed (Hatfield et al., 2009). As discussed in the preceding chapter, the majority of ester-labile *p*-coumaric acid is associated with lignin, and this disparity is not expected to reflect differences in suberization between maize and *Setaria viridis*.

Figure 4.3. Identification of segregating homozygous single copy insertion events using TaqMan hydrolysis probes.

A. Copy number estimation for two unlinked, segregating transgenes. Estimates based on the expression ratio of TaqMan probes for the *Hpt* selectable marker and the native *SvPCK* gene. User-predicted copy numbers (red lines 1-4) vary slightly from the software (y-axis). Putative 2-copy lines are marked with asterisks. 1/2(+), one- and two-copy calibration controls. (-), A10.1 WT.
B. Copy number estimation for one segregating transgenes. Annotations are as described in Figure 4.3A. Putative single copy homozygotes are marked with an asterisk.

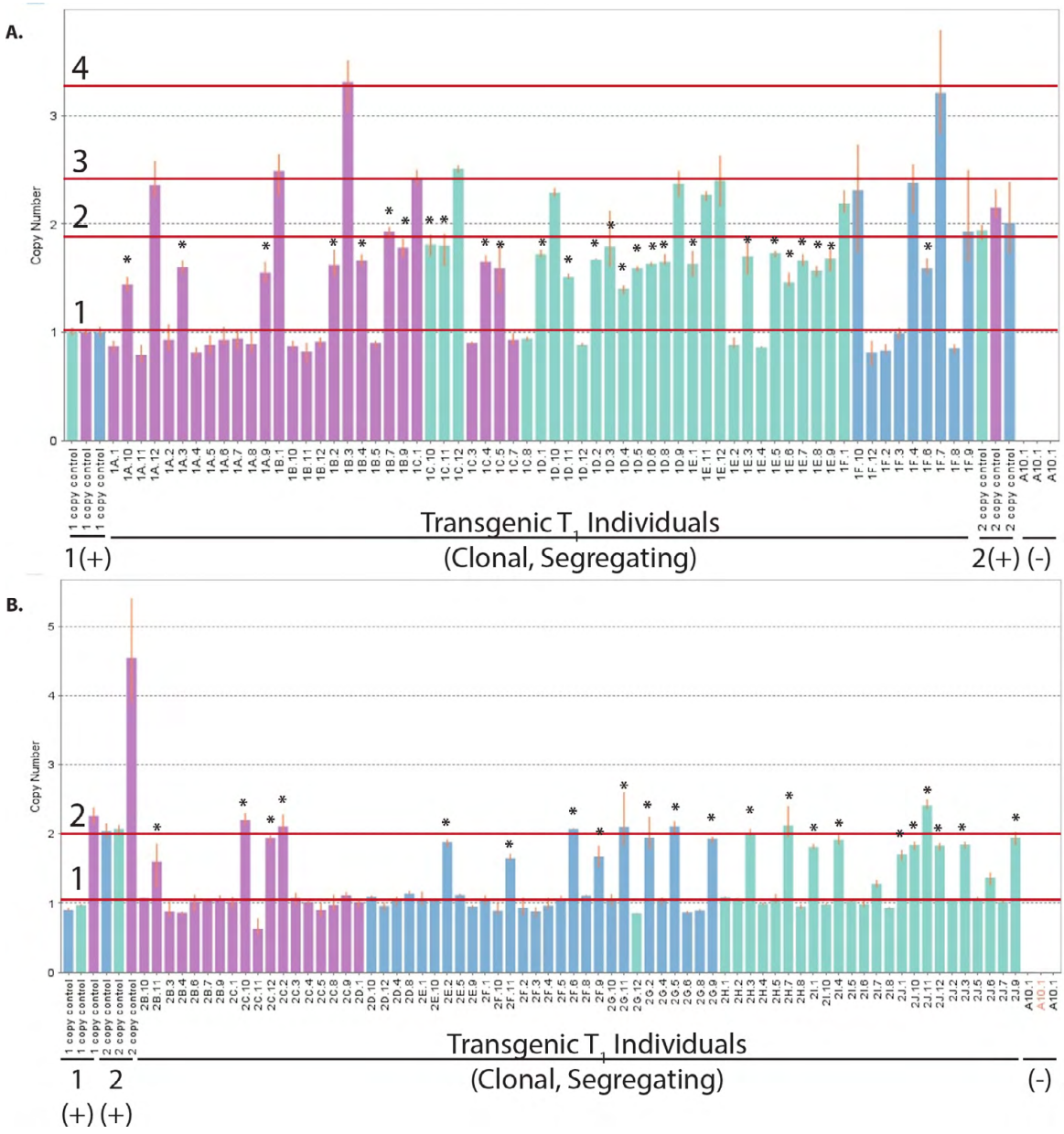
A.
Copy Number
4
3
2
1
0
1 copy control
1 copy control
1 copy control
2 copy control
2 copy control
2 copy control
Transgenic T1 Individuals
(Clonal, Segregating)
1(+)
2(+)
(-)
B.
Copy Number
5
4
3
2
1
0
1 copy control
2 copy control
Transgenic T1 Individuals
(Clonal, Segregating)
1
(+)
2
(+)
(-)

Aliphatic monomers were qualitatively and quantitative similar between the two grasses. The major aliphatic species recovered were 18-hydroxy ocatadec-9-enoic acid and (9)10,16-dihydroxy hexadecanoic acid (Figure 4.2C). Taken together with the monomer profile of purified maize BS strands presented in the previous chapter (Chapter 3, Figure 3.8), this suggests that the majority of aliphatic material recovered originated from the epidermal cuticle. The mechanical fractionation protocol utilized to purify maize BS strands is also effective on *Setaria viridis* leaves (S. Weissmann, personal communication), and it will be informative to generate a suberin-specific polymer profile for Setaria BS strands in the future. The general trend toward lower ω-OH VLCFA content in *Setaria* leaves may indicate lower levels of BS suberization (Figure 3.C). However, monomer quantities were normalized to total leaf surface area, and underlying differences in BS area or vein density were not accounted for. The relatively simple concentric arrangement of suberized root tissues facilitates accurate estimations of suberized surface area (Schreiber et al., 2005), but the variation in vein density, vein size, and BS cell size within leaves makes accurate area normalization considerably more challenging. A more sophisticated model of suberized and cutinized surface areas within leaves is needed to resolve fine differences in suberin content between different genotypes and species.

Taken together with previous studies of polysaccharide and lignin composition (Pettit *et al*., 2013) the broad similarities in polyester content between maize and *Setaria viridis* suggest that the latter is an excellent model system for functional dissection of cell wall biosynthesis in Panicoid grasses. A recent study of biomass feedstocks in Pooid (wheat [*Triticum aestivum*] and *Brachypodium distachyon*) and Panicoid (maize and *Miscanthus x giganteus*) grasses indicated that ethanol production and phylogenetic relationship were correlated between maize and *Miscanthus x giganteus* but not between Panicoids and Pooids (Meinkeke *et al*., 2014). Likewise,

in a second study, members of the BEP Clade showed significant intergroup variation in neutral sugar content, whereas monosaccharide content was less variable between C_4 Panicoids (Hatfield *et al*., 2009). Thus, as a model Panicoid grass, *Setaria viridis* may be a superior option to *Brachypodium distachyon* for functional dissection of cell wall traits in bioenergy feedstocks.

A refined protocol was developed for *Setaria viridis* transgene validation

At the outset of the experiment, *Setaria viridis* was a nascent model system with a draft genome in progress and a pilot transformation protocol under development (Brutnell *et al*., 2010). The *Sv*Suberin RNAi constructs were among the first plasmids created and introduced into the *Setaria viridis* transformation pipeline at the Boyce Thompson Institute. Although a detailed characterization of *SvGDSL1*-RNAi was not completed within the time frame of this dissertation project, the data generated during the validation of transgenic lines streamlined the protocol for subsequent experiments. In particular, the selection of multiple shoots from the same callus was eliminated following the completion of the Southern Blot experiments described in Table 4.3. Likewise, the *SvGDSL1*-RNAi lines were among the first samples tested to validate the TaqMan protocol as a robust method for identification of single copy lines from segregating populations. Bulked T_2 seed stocks of four independent, single copy lines of *SvGDSL1*-RNAi are currently available, and could be evaluated for leaf polyester defects within a month if desired.

CONCLUSION

Since the beginning of this dissertation project in 2010, considerable progress has been made toward functional dissection of bundle sheath suberization in model grasses. At the outset of the project, candidate gene selection was based entirely on homology to functionally

characterized Arabidopsis suberin genes that were essential for barrier function. It was not clear whether the phenotypes observed in model dicots could be recapitulated in model grasses by targeted disruption of orthologous genes. At least for the core genes of the very long chain fatty acid biosynthetic pathway, the answer appears to be no. Functional characterization of the *ZmAsft* genes in this study, as well as complementary work with *OsCYP86B3* in Dr. Lukas Schreiber's lab (Waßmann, 2014), indicates that grasses can tolerate significant attenuations in ω-hydroxyacid content and compromised ultrastructure with only minor effects on leaf water movement and radial oxygen loss, respectively. Thus, a major focus of future suberin research in model grasses must be the identification of candidate genes that will yield a stronger disruption to the lamellar ultrastructure in both vascular sheaths and roots. In recent years, GDSL lipase/acylhydrolases (Yeats *et al*., 2012; Girard *et al*. 2012), ABCG transporters (Yadav *et al*., 2014; Shiono *et al*., 2014), and transcriptional regulators (Kosma *et al*., 2014) have emerged as particularly promising candidates.

Over the same time frame, the resources for functional dissection of suberization in *Setaria viridis* have matured considerably. Reverse genetic resources for many of the gene candidates described above remain limiting in maize, and so *Setaria viridis* will likely play a crucial role in their functional dissection. A robust transformation protocol for *Setaria seed* callus has been developed (van Eck and Smartwood, 2015), and a promising method for floral dip transformation was recently published (Saha and Blumwald, 2016), which should significantly reduce the cost and difficulty of generating transgenic plants. Efforts are currently underway to supplement the existing RNAi resources described in this study with the emerging CRiSPR-Cas9 technology (Miao *et al*., 2013; Zhou *et al*., 2014; Bortesi and Fischer, 2015). The

stage is set for considerable advancement in our understanding of suberin biosynthesis in the coming years.

MATERIALS AND METHODS

Plant growth conditions

Seeds of maize (B73 inbred) and *Setaria viridis* (A10.1 accession) were sown in flats containing 3:1 (v/v) Metromix 360:Turface (for maize) or Metromix 360 (*Setaria viridis*). Maize seeds were sown in 56-well 1.5”w x 8”h cylindrical plug trays at a planting density of one seed per plug. *Setaria viridis* seeds were sown in 4”x 4” square plug trays at a planting density of five seeds per square. Trays were hydrated to soil capacity with RO water and cultivated for ten days in Seedlings were cultivated in a Conviron BDW growth room with a daily irradiance regime of 550 μmol photons/m^2/s, a photoperiod of 12h L:D, day/night temperatures of 31°C/22°C, and 50% relative humidity.

Harvesting leaf tissue for polyester analysis

Ten days after sowing, third leaves of individual plants were measured from the soil line to the leaf tip. Maize third leaf laminae measuring 15 cm ± 0.5 cm and *Setaria viridis* leaves measuring 5 cm ± 0.5 cm were harvested by excising the entire shoot at the soil line and gently removing the first, second, and fourth leaves by hand. Three maize leaves or 16-20 *Setaria viridis* leaves were pooled per biological replicate to yield a total fresh weight per sample of 300-450 mg. Pooled leaves were weighed to determine the total fresh weight, and then immediately flash frozen in liquid nitrogen and stored at -80°C.

When interspecies comparisons are made between plants with suberized tissues of unequal areas, normalizing polyester quantities by total dry weight can produce misleading results (Schreiber *et al.*, 2005). We decided to normalize by total leaf surface area because our samples were homogenates of entire leaves containing both suberin and epidermal cutin polyesters. To generate a ratio of average leaf surface area per unit fresh weight, we selected ten leaves per species, weighed and recorded the fresh weight of each, and then flattened the laminae between two sheets of clear tape and scanned them. Images were converted to 8-bit black and white images using ImageJ software and leaf areas were calculated. Leaf areas were multiplied by two to approximate the total leaf surface area.

Leaf Polyester Analysis Protocol

Alcohol insoluble cell wall residues were isolated and chemically derivatized according to the protocol of Beisson and colleagues (Beisson *et al*., 2010). Frozen samples were boiled for 10 minutes in pre-weighed, Teflon-capped 40 mL glass tubes containing 20 mL isopropanol with 0.1% bis-hydroxytoluene. The tubes were cooled and macerated three times for 1 minute each using a Polytron liquid homogenizer at speed setting 6. Samples were washed in a room temperature shaker with 200 rpm agitation for at least 2 hours, centrifuged at 1500g for 10 minutes to pellet insoluble material, and the supernatant was discarded. The washing step was repeated once more with isopropanol, and then twice each with chloroform:methanol (2:1, v/v), chloroform:methanol (1:2, v/v) and methanol. Samples were air-dried and stored in a desiccator containing Drierite for five days until a stable dry weight was achieved.

Fresh standard solutions of omega-pentadecalactone (10 μg/μL) and methyl heptadecanoate (10 μg/μL) in methanol were prepared. 10 μL of each standard was injected into

each sample immediately prior to transmethylation. The transmethylation solution contained 4 mL per reaction of 6.25% (v/v) sodium methoxide and 15% (v/v) methyl acetate in methanol. Transmethylation reactions were heated for 2 hours at 60°C, cooled, and then acidified with 1 mL glacial acetic acid, solubilized with 8mL dichloromethane, and washed with 2 mL 0.9% (w/v) NaCl in Tris, pH 8.0. Samples were vortexed for 30s to wash and extract fatty acid methyl esters and centrifuged for 2 minutes at 1500g for phase separation. The organic phase was transferred to a fresh 40 mL glass vial and washed a second time with 4 mL 0.9% (w/v) NaCl in deionized water. The organic phase was transferred to a fresh 8 mL glass vial and dried over anhydrous $NaSO_4$, and then dried in 2.5 mL conical reaction vials on a 33°C heat block under a gentle stream of N_2. Dried samples were re-suspended in 10 μL each of pyridine and N,O-Bis(trimethylsilyl) trifluoroacetamide (BSTFA) and heated to 100°C for 10 minutes. Samples were dried as described above, re-suspended in 50 μL chloroform, and transferred to autosampler vials.

Monomers were quantified by GC-FID. Samples were injected onto a DB-1 column (30 m x 320 μm x 0.1 μm) using an automated on-column injection at 50°C. The oven was programmed to hold at 50°C for 2 minutes, ramp to 120°C at 40°C/minute, hold for 2 minutes, ramp to 320°C at 10°C/minute and hold for 15 minutes. Helium carrier gas was supplied at a flow rate of 1.4 mL/min. Monomer identities were determined by GC-MS. Samples were injected onto a DB-5 column (30 m x 250 μm x 0.25 μm) using an automated splitless injection with an inlet temperature of 320°C. The oven temperature was held at 120°C for 1 minute, then ramped to 320°C at 5°C/minute, followed by a 15 minute hold. Helium carrier gas was supplied at a 1 mL/minute flow rate. Fragmentation spectra were obtained using a JEOL GC-Mate quadrupole detector operating in electron Impact mode with an accelerating voltage of 2500,

scanning from 35-750 at a rate of 0.3 s/scan with a 0.1 s interscan delay and a 5 minute solvent delay at the beginning of each run.

Genotyping and transgene copy number assays

gDNA extraction from Setaria viridis leaves was carried out according to the CTAB protocol as described in Chapter 3. The PCR-based genotyping assay to identify transgenic plants was a single tube PCR reaction targeting a native *Setaria viridis* control gene (primers SvF/SvR: 5' CAGCAAGCCGCCTATATGGAG/5' TCGTCTCAGGAGTGGCCAAGT) and the hygromycin phosphotransferase gene of the T-DNA insert (hptF/hptR: 5'AGGCTCTCGATGAGCTGATGC TTT/ 5'AGCTGCATCATCGAAATTGCCGTC). Samples were analyzed using GoTaq Flexi DNA polymerase (Promega). PCR was conducted according to the manufacturer's recommendations with a 57°C annealing temperature and a 1:00 extension at 72°C. Samples were resolved on a 1.5% w/v agarose gel containing 1% v/v ethidium bromide. The Southern Blotting and TaqMan assays were carried out according to the protocols available online at http://www.brutnelllab.org/#!molecular-tools/cs6e.

REFERENCES

Ahern KR, Deewatthanawong P,Schares J, Muszynski M, Weeks R, Vollbrecht E, Duvik J, Brendel VP, & Brutnell TP. (2009) Regional mutagenesis using *Dissociation* in maize. *Methods* **49**: 248-254.

Bennetzen JL, Schmutz J, Wang H, *et al*. (2012) Reference genome sequence of the model plant *Setaria*. *Nature Biotechnology* **30**: 555–561.

Bortesi L & Fischer R. (2015) The CRISPR/Cas9 system for plant genome editing and beyond. *Biotechnology Advances*, **33**: 41-52.

Bragg JN, Wu J, Gordon SP, Guttman MA, Thilmony RL, Lazo GR, Gu YQ, & Vogel JP. (2012) Generation and characterization of the Western Regional Research Center Brachypodium T-DNA Insertional Mutant Collection. *PLoS One* **7**(9): art. no. e41916.

Brutnell TP, Wang L, Smartwood K, Goldschmidt A, Jackson D, Zhu X-G, Kellogg E, & Van Eck, J. (2010) *Setaria viridis*: A model for C_4 photosynthesis. *The Plant Cell* **22**: 2537-2544.

Christin PA, Salamin N, Kellogg EA, Vicentini A, and Besnard G. (2009) Integrating phylogeny into studies of c4 variation in the grasses. *Plant Physiolology* **149**: 82–87.

Clark LH, Harris WH. (1981) Observations on the root anatomy of rice (*Oryza-sativa*-L). *American Journal of Botany* **68**: 154-161.

Draper J, Mur LAJ, Jenkins G, Ghosh-Biwas GC, Bablak P, Hasterok R, & Routledge APM. (2001) *Brachypodium distachyon*. A new model system for functional genomics in grasses. *Plant Physiology* **127**: 1539-1555.

Evert RF, Russin WA, & Bosabalidis AM. (1996). Anatomical and ultrastructural changes associated with the sink-to-source transition in developing maize leaves. *International Journal of Plant Sciences* **157(3)**: 247-251.

Filiz E, Ozdemir BS, Budak F, Vogel JP, Tuna M, & Budak H. (2009) Molecular, morphological, and cytological analysis of diverse Brachypodium distachyon inbred lines. *Genome* **52**: 876-890.

Frame BR, Shou H, Chikwamba R, *et al*. (2002) *Agrobacterium tumefaciens*-mediated transformation of maize embryos using a standard binary vector system. *Plant Physiology* **129**: 13-22.

Girard A-L, Mounet F, Lemaire-Chamley M, *et al*. (2012) Tomato GDSL1 Is Required for Cutin Deposition in the Fruit Cuticle. *The Plant Cell* **24**: 3106–3121.

Grass Phylogeny Working Group II. (2012) New grass phylogeny resolves deep evolutionary relationships and discovers C_4 origins. *New Phytologist* **193**: 304–312

Haas DL & Carothers ZB. (1975) Some Ultrastructural Observations on Endodermal Cell Development in *Zea Mays* Roots. *American Journal of Botany* **62**(4): 336-348.

Hatfield RD, Marita JM, Frost K, Grabber J, Ralph J, Lu F, Kim H. (2009) Grass lignin acylation: p-coumaroyl transferase activity and cell wall characteristics of C_3 and C_4 grasses. *Planta* **229**: 1253-1267.

Hattersley PW, Browning AJ. (1981) Occurrence of the suberized lamella in leaves of grasses of different photosynthetic types.1. In parenchymatous bundle sheaths and PCR (Kranz) sheaths. *Protoplasma* **109**: 371-401.

Kosma DK, Murmu J, Razeq FM, Santos P, Borgault R, Molina I, & Rowland O. AtMYB41 activates ectopic suberin synthesis and assembly in multiple plant species and cell types. *The Plant Journal* **80**: 216-229.

Mann DGJ, LaFayette PR, Abercrombie LL, e*t al.* (2012) Gateway-compatible vectors for high-throughput gene functional analysis in switchgrass (*Panicum virgatum* L.) and other monocot species. *Plant Biotechnology Journal* 10: 226–236.

Meineke T, Manisseri C, & Voigt CA. (2014) Phylogeny in Defining Model Plants for Lignocellulosic Ethanol Production: A Comparative Study of *Brachypodium distachyon*, Wheat, Maize, and *Miscanthus x giganteus* Leaf and Stem Biomass. *PLoS One* **9**(8): e103580.

Miao J, Guo D, Zhang J, Huang Q, Qin G, Zhang X, Wan J, Gu H, & Qu L-J. (2013) Targeted mutagenesis in rice using CRISPR-Cas system. *Cell Research* **23**:1233–1236.

Miki D and Shimamoto K. (2004) Simple RNAi vectors for stable and transient suppression of gene function in rice. *Plant and Cell Physiology* **45**(4): 490-495.

Petti C, Shearer A, Tateno M, Ruwaya M, Nokes S, Brutnell T, & DeBolt S. (2013) Comparative feedstock analysis in *Setaria viridis* L. as a model for C_4 bioenergy grasses and panicoid crop species. *Frontiers in Plant Science* 4.181 doi:10.3389/fpls.2013.00181.

Piston F, Uauy C, Fu L, Langston J, Labavitch J, & Dubcovsky J. (2010) Down-regulation of four putative arabinoxylan feruloyl transferase genes from family PF02458 reduces ester-linked ferulate content in rice cell walls. *Planta* **231**: 677–691.

Pollard M, Beisson F, Li Y, Ohlrogge JB. (2008) Building lipid barriers: biosynthesis of cutin and suberin. *Trends in Plant Science* **13**: 236-246.

Rajeevkumar S, Anunanthini P, & Sathishkumar R. (2015) Epigenetic silencing in transgenic plants. *Frontiers in Plant Science* **6**:693. doi:10.3389/fpls.2015.00693.

Saha P & Blumwald E. (2016) Spike dip transformation of *Setaria viridis*. The Plant Journal, Accepted Article. doi: 10.1111/tpj.13148.

Schreiber L, Franke R, Hartmann KD, Ranathunge K, Steudle E. (2005) The chemical composition of suberin in apoplastic barriers affects radial hydraulic conductivity differently in the roots of rice (*Oryza sativa* L. cv. IR64) and corn (*Zea mays* L. cv. Helix). *Journal of Experimental Botany* **56**: 1427-1436.

Schnable PS, Ware D, Fultron RS, *et al*. (2009) The B73 maize genome: complexity, diversity, and dynamics. *Science* **326**: 1112-1115.

Shiono K, Ando M, Nishiuchi S, *et al*. (2014) RCN1/OsABCG5, an ATP-binding cassete (ABC) transporter, is required for hypodermal suberization of roots in rice. *The Plant Journal* **80**: 40-51.

Studer AJS, Gandin A, Kolbe AR, Wang L, Cousins AB and Brutnell TP. (2014) A limited role for carbonic anhydrase in C_4 photosynthesis as revealed by a *ca1ca2* double mutant in maize. Plant Physiology **165**: 608-617.

Van Eck, J & Smartwood, K. (2015) *Setaria viridis*. *Methods in Molecular Biology* **1223**: 57-67.

Vicentini A, Barber JC, Aliscioni, SA, Giussani, LM, and Kellogg, EA. (2008) The age of the grasses and clusters of origins of C_4 photosynthesis. *Global Change Biology* **14**: 1–15.

Vishwanath SJ, Kosma DK, Pulsifer IP, Scandola S, Pascal S, Joubès J, Dittrich-Domergue F, Lessire R, Rowland O, & Domergue F. (2013) Suberin-associated fatty alcohols in Arabidopsis: distributions in roots and contributions to seed coat barrier properties. *Plant Physiology* **163**: 1118-1132.

Vogel J & Hill T. (2008) High-efficiency *Agrobacterium*-mediated transformation of *Brachypodium distachyon* inbred line Bd21-3. *Plant Cell Reports* **27**: 471-478.

Vogel JP, Garvin DF, Mockler TC, *et al*. (2010) Genome sequencing and analysis of the model grass *Brachypodium distachyon*. *Nature* **463**: 763-768.

Vollbrecht E, Duvik J, Schares JP, *et al*. (2010) Genome-wide distribution of transposed *Dissociation* elements in maize. *The Plant Cell* **22**: 1667-1685.

Waßmann FFM. (2014) Suberin biosynthesis in *O. sativa*: Characterisation of a cytochrome P450 monooxygenase. PhD Dissertation, University of Bonn.

Yadav V, Molina I, Ranathunge K, Castillo IQ, Rothstein SJ, & Reed JW. (2014) ABCG transporters are required for suberin and pollen wall extracellular barriers in *Arabidopsis*. *The Plant Cell* **26**: 3569-3588.

Yang W, Simpson JP, Li-Beisson Y, Beisson F, Pollard MR, Ohlrogge JB. (2012) A Land Plant-Specific Glycerol-3-Phosphate Acyltransferase Family in Arabidopsis: Substrate Specificity, *sn*-2 Preference and Evolution. *Plant Physiology* **160**: 638-652.

Yeats TH, Martin LBB, Viart HMF, Isaacson T, He Y, Zhao L, Matas AJ, Buda GJ, Domozych, DS, Clausen MH, Rose JKC. (2012) The identification of cutin synthase: formation of the plant polyester cutin. *Nature Chemical Biology* **8**, 609-611.

Zhang G, Liu X, Quan Z *et al*. (2012) Genome sequence of foxtail millet (*Setaria italica*) provides insights into grass evolution and biofuel potential. *Nature Biotechnology* **30**: 549–554.

Zhou H, Liu B, Weeks DP, Spalding MH, & Yang B. (2014) Large chromosomal deletions and heritable small genetic changes induced by CRISPR/Cas9 in rice. *Nucleic Acids Research*, **42**: 10903-10914.

CHAPTER FIVE

A PLAN TO GENERATE STRONGER SUBERIN MUTANTS USING CRISPR-CAS9 TECHNOLOGY IN *SETARIA VIRIDIS*

INTRODUCTION

At the outset of the experiment, the only experimental approach available to disrupt candidate suberin biosynthesis genes in green millet (*Setaria viridis*) was RNA interference (RNAi) using a rice (*Oryza sativa*)-optimized RNAi vector (Miki & Shimamoto, 2004). Even after the release of Panicoid-optimized RNAi and overexpression vectors (Mann *et al*., 2012), the reverse genetics strategy described in Chapter 4 was beset with numerous obstacles. In particular, the validation of transgene copy number and target expression level were extremely time-consuming and labor intensive (Table 4.3; Figure 4.3). A targeted approach to generate stable null alleles that could be rapidly validated would have greatly expedited the search for stronger suberin mutants.

Recently, the type II CRISPR-Cas9 (Clustered, regularly interspersed, short palindromic repeats-CRISPR-associated endonuclease 9) adaptive immune system from the bacterium *Streptococcus pyogenes* was adapted as a genome editing tool for eukaryotic organisms, including plants (reviewed in Kumar and Jain, 2015). In the native bacterial system, the Cas9 endonuclease is directed to cleave non-native DNA molecules by two guide RNAs: a target-specific CRISPR RNA (crRNA), and a *trans*-encoded CRISPR RNA (tracrRNA) that binds the crRNA to the nuclease enzyme via homologous base pairing (Jinek *et al*., 2012; Karvelis *et al*., 2013). By synthesizing a single small guide RNA (sgRNA) containing the tracrRNA and a crRNA homologous to a target gene of interest, the Cas9 endonuclease can be directed to any

candidate gene sequence containing a suitable protospacer adjacent motif (PAM; NGG in the case of *S. pyogenes* Cas9; Jinek *et al*., 2012). Following DNA cleavage, single nucleotide polymorphisms (SNPs) and small insertion/deletion events (indels) are introduced into the target gene sequence via imprecise DNA damage repair by non-homologous end joining (NHEJ) machinery (Jinek *et al*., 2012). Targeted genome editing using CRISPR-Cas9 technology has been successfully applied in numerous crop and model plant species, including maize (*Zea mays*; Liang et al., 2014) and green millet (*Setaria viridis*; C. Coelho, personal communication).

As discussed in the preceding chapters, the mutants generated during the course of this project were insufficiently severe to assess the role of bundle sheath suberization in the C_4 carbon concentrating mechanism. To rapidly evaluate candidate genes for stronger mutant phenotypes, a targeted mutagenesis and overexpression approach using CRISPR-Cas9 technology is presented here for two high priority candidate genes, the GDSL lipase/acylhydrolase *SvGDSL1* (Chapter 2; Chapter 4) and the transcription factor candidate *SvMYB48* (Chapter 2). A transgenic suberin esterase construct containing *AtCDEF1* (Takahashi *et al*., 2010; Naseer *et al*., 2012; Chapter 2) is described as an alternative approach to depolymerize wild type suberin *in muro*. Although the transgenic approaches presented in this section would also be feasible in maize (*Zea mays*), a plan is presented for *Setaria viridis* due to its shorter generation time and rapid spike dipping transformation protocol (Saha and Blumwald, 2016).

EXPERIMENTAL DESIGN

Targeted mutagenesis of *SvGDSL1* using CRISPR-Cas9

To evaluate *SvGDSL1* for suitable sequences from which to synthesize sgRNA, the complete genetic sequence of the foxtail millet (*Setaria italica*) orthologue Si30233m.g was submitted to the CRISPOR program (http://crispor.tefor.net/crispor.cgi). The *Setaria viridis* genomic sequence was unavailable on the CRISPOR interface at the time, but has since become available. Multiple candidate sgRNA sequences 5'-proximal to an *S. pyogenes* PAM were identified using the default parameters. Candidate sgRNA homologous to the first exon of *SvGDSL1* (the site of the catalytic GDSL motif) that contained restriction sites for rapid validation were prioritized. The next step will be to order a series of sgRNA targeting *SvGDSL1*, prioritizing candidates with high specificity and cutting efficiency scores in CRISPOR, and where possible, selecting candidates with restriction sites for easy validation of mutagenesis. To minimize the risk of off-target mutations, candidates with three or fewer mismatches to off-target gene sequences within 12 bp of the PAM should not be considered. Cloning of sgRNA oligonucleotides into entry and destination vectors will be conducted using GoldenGate technology (Engler *et al*., 2008; Weber *et al*., 2011). To avoid internal sgRNA cleavage during GoldenGate cloning, *SvGDSL1* was evaluated for internal Esp3I, BsmBI, and BsaI restriction sites and none were present; this step will need to be repeated for all future target genes. Following cloning into a Level 0 entry vector, sgRNA modules will be subcloned into the level 1 vector pJG310, sequenced to validate the correct insertion, and subcloned into the level 2 expression vector pTC278, which contains insertion sites for the Level 1 sgRNA module and a codon-optimized Cas9 expression cassette (vectors courtesy of D. Voytas lab). Validated level 2 vectors can be utilized for *Agrobacterium tumefaciens*-mediated transformation into *Setaria viridis* using either the conventional seed callus inoculation protocol (van Eck and Smartwood, 2015) or the rapid spike dipping method (Saha and Blumwald, 2016).

Utilizing CRISPRi and CRISPRa to modulate expression levels

Although neither tomato cutin synthase mutants nor transgenic Arabidopsis plants devoid of detectable endodermal suberin lamellae exhibited a vegetative phenotype under ambient conditions (Girard *et al*., 2012; Naseer *et al*., 2012), the possibility that *Svgdsl1* null mutants could be severely deleterious or even lethal cannot be ruled out. In this case, a CRISPR-interference (CRISPRi) approach using catalytically inactive Cas9 (dCas9) fused to the SRDX repression domain could complement existing *SvGDSL1*-RNAi lines (Chapter 4; Piatek *et al*., 2015). Optimization will be needed to achieve efficient transcriptional repression using CRISPRi. At least in human cell lines, CRISPRi is most effective within a narrow region of the proximal promoter adjacent to the transcription start site (Gilbert *et al*., 2014). In plants, the efficacy of CRISPRi is enhanced by introducing multiple sgRNA targeting the same promoter (Piatek *et al*., 2015). Thus, a tiling array canvassing the proximal promoter of *SvGDSL1* will likely be needed to identify the most effective target sites. Likewise, a GoldenGate destination vector that can incorporate multiple sgRNA cassettes may yield better results than the single cassette pTC278 vector described above. Although the spike dip transformation protocol discussed above would expedite the production of transgenic *Setaria* lines, *SvGDSL1*-CRISPRi lines would require the same labor-intensive copy number validation protocol as did conventional *SvGDSL1*-RNAi lines. It remains to be determined whether CRISPRi transgenes predominately insert as single or multiple copies during *Setaria viridis* transformation.

When fused to an EDLL or TAL transcriptional activator, dCas9 can also be utilized for CRISPR-activation (CRISPRa) overexpression experiments (Piatek *et al*., 2014). This is a

promising approach to characterize the putative *Setaria viridis* orthologue of *AtMYB41*, *SvMYB48*, as the Arabidopsis gene was characterized exclusively as an overexpression line and exhibited no phenotype when targeted with conventional RNAi constructs (Kosma *et al*., 2014). CRISPRa is a complementary approach to the existing pANIC vector technology that facilitates ubiquitous overexpression of cDNA in *Setaria viridis* (Mann *et al*., 2012; L. Tausta, personal communication). However, as described above for CRISPRi of *SvGDSL1*, identifying the optimal regions of the *SvMYB48* promoter for sgRNA targeting would be required for effective CRISPRa (Piatek *et al*., 2014). In the short term, conventional Gateway cloning of the *SvMYB48* cDNA into the pANIC10A vector is likely the most expedient method to assess whether this candidate gene is the functional orthologue of *AtMYB41*.

Cell type-specific expression of a transgenic esterase construct

Depolymerization of wild type suberin lamellae *in muro* is a promising alternative approach to generate a strong disruption to the apoplastic diffusion barriers in bundle sheaths. Naseer and colleagues (2012) successfully eliminated detectable polymeric suberin from Arabidopsis endodermal cell walls using an esterase cDNA, *Arabidopsis CUTICLE DESTRUCTING FACTOR 1* (*AtCDEF1*), driven by a cell type-specific promoter. A Gateway-compatible entry vector containing *AtCDEF1* available in the lab, but a suitable cell type-specific promoter for Panicoid bundle sheaths was not identified during this project. A search was conducted for a promoter candidate with strong bundle sheath-enriched expression relative to mesophyll cells and minimal root expression using existing gene expression atlas data (Sekhon *et al*., 2010; S. Weissmann, personal communication). The proximal promoters plus 5'UTR sequences of two candidate genes, maize *Fructose bisphosphate aldolase1* (GRMZM2G046284)

and *Rubisco activase1* (GRMZM2G162200) were delimited using CoGe (https://genomevolution.org/coge/), and cloned into a GUS reporter construct (D-Y. Lee, personal communication). Although the *pZmFba1*::GUS reporter construct yielded sporadic vascular strand-specific staining in T_1 *Setaria viridis* leaves (data not shown), neither reporter yielded the strong, reproducible tissue-specific expression needed to drive the *AtCDEF1* construct. It is plausible that additional regulatory elements present in the distal promoter or introns could enhance the strength of the cloned *ZmFba1* promoter. To evaluate this possibility, GoldenGate technology could be utilized to clone the promoter, UTRs, and introns into separate level 0 modules to create customized combinations of promoter elements (Weber *et al*., 2011). However, it would likely be more efficient to acquire an existing promoter with reliable vascular strand-specific expression. Relatively few cell type-specific promoters have been characterized in Panicoid grasses, but the promoters of maize of *Short-root1* (*ZmShr1*) and *Scarecrow1* (*ZmScr1)* as well as the auxin efflux transporter *ZmPIN1* (Galavotti *et al*., 2008; Slewinski *et al*. 2012; 2014) are promising candidates. Although these promoters are expressed early in vascular development prior to the onset of bundle sheath suberization, they may be sufficient to induce suberin depolymerization if AtCDEF1 persists in the apoplast during later developmental stages. As all three candidates are also expressed in maize roots, the possibility of a confounding endodermal phenotype would have to be considered when characterizing the phenotypes of these lines.

REFERENCES

Galavotti A, Yang Y, Schmidt RJ, & Jackson D. (2008) The relationship between auxin transport and maize branching. *Plant Physiology* **147**: 1913-1923.

Gilbert LA, Horlbeck MA, Adamson B, *et al*. (2014) Genome-scale CRISPR-mediated control of gene repression and activation. *Cell* **159**: 647-661.

Girard A-L, Mounet F, Lemaire-Chamley M, *et al*. (2012) Tomato GDSL1 Is Required for Cutin Deposition in the Fruit Cuticle. *The Plant Cell* **24**: 3106–3121.

Engler C, Kandzia R, & Marillonnet S. (2008) A one pot, one step, precision cloning method with high throughput capability. *PLoS One* **3**(11): e3647.

Jinek M, Chylinski K, Fonfara I, Hauer M, Doudna JA, Charpentier EA. (2012) A programmable dual RNA guided DNA endonuclease in adaptive bacterial immunity. *Science* **337**: 816–821.

Karvelis T, Gasiunas G, Miksys A, Barrangou R, Horvath P, Siksnys V. (2013) crRNA and tracrRNA guide Cas9-mediated DNA interference in Streptococcus thermophilus. *RNA Biology* **10**: 841–851.

Kosma DK, Murmu J, Razeq FM, Santos P, Borgault R, Molina I, & Rowland O. (2014) AtMYB41 activates ectopic suberin synthesis and assembly in multiple plant species and cell types. *The Plant Journal* **80**: 216-229.

Kumar V & Jain M. (2015) The CRISPR-Cas system for plant genome editing: advances and opportunities. *Journal of Experimental Botany* **66**(1): 47-57.

Liang Z, Zhang K, Chen K, & Gao C. (2014) Targeted mutagenesis in maize using TALENs and the CRISPR/Cas system. *Journal of Genetics and Genomics* **41**: 63-68.

Mann DGJ, LaFayette PR, Abercrombie LL, e*t al.* (2012) Gateway-compatible vectors for high-throughput gene functional analysis in switchgrass (*Panicum virgatum* L.) and other monocot species. *Plant Biotechnology Journal* 10: 226–236.

Miki D and Shimamoto K. (2004) Simple RNAi vectors for stable and transient suppression of gene function in rice. *Plant and Cell Physiology* **45**(4): 490-495.

Naseer, S., Lee, Y., Lapierre, C., Franke, R., Nawrath, C., and Geldner, N. (2012). Casparian strip diffusion barrier in Arabidopsis is made of a lignin polymer without suberin. *Proceedings of the National Academy of Sciences, USA* **109**: 10101-10106.

Piatek A, Ali Z, Baazim H, Li L, Abulfaraj A, Al-Shareef S, Aouida M, & Mahfouz MM. (2015) RNA-guided transcriptional regulation *in planta* via synthetic dCas9-based transcription factors. *Plant Biotechnology Journal* **13**: 578-589.

Slewinski TL, Anderson AA, Zhang CK, Turgeon R. (2012) Scarecrow Plays a Role in Establishing Kranz Anatomy in Maize Leaves. *Plant and Cell Physiology* **53**: 2030-2037.

Slewinski TL, Anderson AA, Price S, Withee JR, Gallagher K, and Turgeon R. (2014) Short-Root1 plays a role in the development of vascular tissue and Kranz anatomy in maize leaves. *Molecular Plant* **7**(8): 1388-1392.

Saha P & Blumwald E. (2016) Spike dip transformation of *Setaria viridis*. The Plant Journal, Accepted Article. doi: 10.1111/tpj.13148.

Takahashi K, Shimada T, Kondo M, Tamai A, Mori M, Nishimura M, & Hara-Nishimura I. (2010) Ectopic expression of an esterase, which is a candidate for the unidentified plant cutinase, causes cuticular defects in *Arabidopsis thaliana*. *Plant and Cell Physiology* **51**(1): 123-131.

Van Eck J & Smartwood K. (2015) *Setaria viridis*. *Methods in Molecular Biology* **1223**: 57-67.

Weber E, Engler C, Gruetzner R, Werner S, & Marillonnet S. (2011) A modular cloning system for standardized assembly of multigene constructs. *PLoS One* **6**(2): e16765.